



ALMA MATER STUDIORUM  
UNIVERSITÀ DI BOLOGNA

**DOTTORATO DI RICERCA IN**  
**SCIENZE BIOTECNOLOGICHE, BIOCOMPUTAZIONALI,**  
**FARMACEUTICHE E FARMACOLOGICHE**

**Ciclo XXXVII**

**Settore Concorsuale: 03/D1** - Chimica e tecnologie farmaceutiche, tossicologiche e nutraceutico-alimentari

**Settore Scientifico Disciplinare: CHIM/08** – Chimica farmaceutica

**DESIGN AND SYNTHESIS OF RAD51/RAD52 INHIBITORS TO ACHIEVE  
SYNTHETIC LETHALITY IN COMBINATION WITH PARP INHIBITORS  
IN PANCREATIC CANCER**

**Presentata da:** Giovanni Ferrandi

**Coordinatore Dottorato**

Maria Laura Bolognesi

**Supervisore**

Andrea Cavalli

**Co-supervisore**

Marinella Roberti

Esame finale anno 2025

<b>Abstract.....</b>	<b>3</b>
<b>1. INTRODUCTION.....</b>	<b>4</b>
<b>1.1 Cancer overview .....</b>	<b>4</b>
<b>1.2 Precision oncology overview.....</b>	<b>5</b>
1.2.1 Synthetic Lethality (SL) in DDR as an approach in precision oncology .....	8
<b>1.3 Overview of DNA damage repair (DDR) mechanisms.....</b>	<b>11</b>
<b>1.4 PARP/BRCA2: targeting SL in DDR .....</b>	<b>18</b>
1.4.1 PARP1 protein: structure and involvement in cancer .....	18
1.4.2 PARP inhibitors: overview .....	21
1.4.3 BRCA2 protein: structure and functional domains .....	26
<b>1.5 Mimicking “BRCAness”: new SL targets in DDR .....</b>	<b>28</b>
<b>1.5.1 RAD51 protein: structure and functions.....</b>	<b>30</b>
1.5.1.1 RAD51 inhibitors .....	32
<b>1.5.2 RAD51-BRCA2 protein-protein interaction: functions and inhibition .....</b>	<b>33</b>
<b>1.5.3 RAD52 protein: structure and functions.....</b>	<b>39</b>
1.5.3.1 RAD52 inhibitors .....	41
 <b>2. AIM OF THE THESIS .....</b>	 <b>45</b>
 <b>3. Part I: STRUCTURE-BASED DESIGN APPROACH TO THE IDENTIFICATION OF RAD51-BRCA2 PPI DISRUPTORS.....</b>	 <b>48</b>
3.1 Hit identification and optimization targeting Zone II .....	48
3.2 Chemistry .....	51
3.3 SAR studies and biological evaluation.....	58
3.4 Future perspectives.....	70
3.5 Conclusions .....	71
 <b>4. Part II: SYNTHESIS AND EVALUATION OF A COMPUTATIONAL DESIGNED PEPTIDIC LIBRARY TO INHIBIT RAD52 .....</b>	 <b>73</b>
4.1 Search for RAD52 potential pockets.....	74
4.2 Peptide library creation and Virtual Screening .....	75

4.3 Solid-phase peptide synthesis.....	77
4.4 Binding affinity evaluation.....	85
4.5 Conclusions .....	86
<b>5. Concluding remarks and future perspectives .....</b>	<b>88</b>
<b>6. Experimental section .....</b>	<b>90</b>
6.1 Experimental section: Part I .....	90
6.1.1 Material and methods .....	90
6.1.2 General procedure A for the synthesis intermediates <b>25, 27, 17, 55</b> .....	91
6.1.3 Doebner trials with TEA for the synthesis of intermediates <b>62, 27, 64</b> .....	93
6.1.4 Doebner trials with Cp <sub>2</sub> ZrCl <sub>2</sub> for the synthesis of intermediates <b>67b, 63</b> .....	94
6.1.5 General procedure B for the synthesis of intermediates <b>62-65, 18, 78</b> . ....	97
6.1.6 General procedure C for the synthesis of intermediates <b>28b, 29b, 66b-69b</b> .....	100
6.1.7 General procedure D for the synthesis of intermediates <b>28c, 29c, 66c-69c</b> . ....	102
6.1.8 General procedure E for the synthesis of intermediates <b>40-51, 70-73, 20</b> . ....	104
6.1.9 General procedure F for the synthesis of derivatives <b>1-16</b> . ....	112
6.1.10 Procedure G for the synthesis of derivative <b>19</b> .....	120
6.1.11 Procedure H for the synthesis of compound <b>79</b> .....	121
6.1.12 Procedure I for the synthesis of compound <b>54</b> .....	121
6.1.13 Procedure L for synthesis of compound <b>75</b> .....	122
6.2 Experimental section: Part II.....	123
6.2.1 Material and methods .....	123
6.2.2 HMBA resin loading and N-Allyloxy carbonyl substitution trial .....	124
6.2.3 N-Tert-butyloxycarbonyl deprotection screening .....	125
6.2.4 HMBA resin loading trials .....	125
6.2.5 General procedure for CTC resin loading .....	126
6.2.6 General procedures of solid-phase peptide synthesis .....	127
6.2.7 General procedure for HPLC purification .....	128
6.2.8 Synthesis of Dipeptides <b>1-10</b> and <b>1B-10B</b> .....	129
<b>Appendix.....</b>	<b>146</b>
<b>Abbreviations and acronyms .....</b>	<b>153</b>
<b>References .....</b>	<b>157</b>

## Abstract

My main PhD research project, described in the first part of the thesis, has been in collaboration with the Italian Institute of Technology (IIT) and focused on the discovery of potential disruptors of the RAD51-BRCA2 protein-protein interaction (PPI), with the goal of triggering synthetic lethality (SL) in BRCA2-proficient pancreatic cancer, in combination with PARPi olaparib or talazoparib. SL has been clinically validated as a therapeutic approach for cancer due to the efficacy of olaparib in BRCA2-deficient patients. In this scenario, we suggested to trigger a “fully small-molecule-induced SL” by combining a RAD51-BRCA2 PPI disruptor with PARPi to target pancreatic cancer cells. The interaction between RAD51 and BRCA2 is crucial in DNA damage repair by homologous recombination (HR) and is mediated by two key “hotspots” on RAD51 surface, identified as Zone I and Zone II, which have been previously confirmed as ideal sites to design small molecule inhibitors.

Initially, a virtual screening (VS) campaign on Zone II was exploited as *hit* identification strategy, followed by chemical modifications that led to the creation of a library of analogues with a phenyl-furan-quinoline core structure. Derivative **14** (**ARN26912**) proved to be a promising lead compound inhibiting RAD51-BRCA2 interaction, reducing HR and inducing cell death in combination with olaparib in BRCA2-proficient pancreatic cancer cell lines, fully reproducing the paradigm of SL.

The second part of the thesis concerned the experience I carried out during the six-month secondment at EPFL in Lausanne in Professor Heinis' Laboratory. The project focused on the synthesis of dipeptides aimed at inhibiting the monomer-monomer interaction of RAD52. RAD52 inhibition proved to induce SL in cancer cells with defective DNA repair-related proteins, such as BRCA1/2 proteins. After a VS on an identified RAD52 monomer-monomer interaction pocket, the best 10 dipeptides had been selected and synthesized. Preliminary biophysical assays have been carried out to evaluate their efficacy in binding RAD52. The final goal will be triggering a three-pathways SL by a PARPi, a RAD51-BRCA2 PPI disruptor and a potential RAD52i in BRCA2-proficient pancreatic cancer cells.

## 1. INTRODUCTION

### 1.1 Cancer overview

“A neoplasm is an abnormal mass of tissue, the growth of which exceeds and is uncoordinated with that of the normal tissues and persists in the same excessive manner after cessation of the stimulus which evoked the change”. Almost 100 years have passed since one of the first definitions of cancer was postulated by the Australian oncologist Rupert Allan Willis (The Spread of Tumors in the Human Body, London, Butterworth, 1935). In 2022, as reported by the World Cancer Research Fund International, 18.7 million cancer cases occurred worldwide. Of these, 9.5 million cases involved men and 9.2 million women. Figure 1 shows the age-standardized cancer incidence rate in 2022, for both sexes, on a global scale. Areas with the highest rates (dark blue) include North America, Europe and Australia, while the lowest rates (light blue and grey) are found in many parts of Africa and Asia.<sup>1</sup> In addition, Covid-19 has caused tremendous effects on cancer patients, with a huge number of diagnoses and treatments delayed due to the constraints that Covid-19 has imposed on healthcare systems.<sup>2</sup>

Age-Standardized Rate (World) per 100 000, Incidence, Both sexes, in 2022  
All cancers

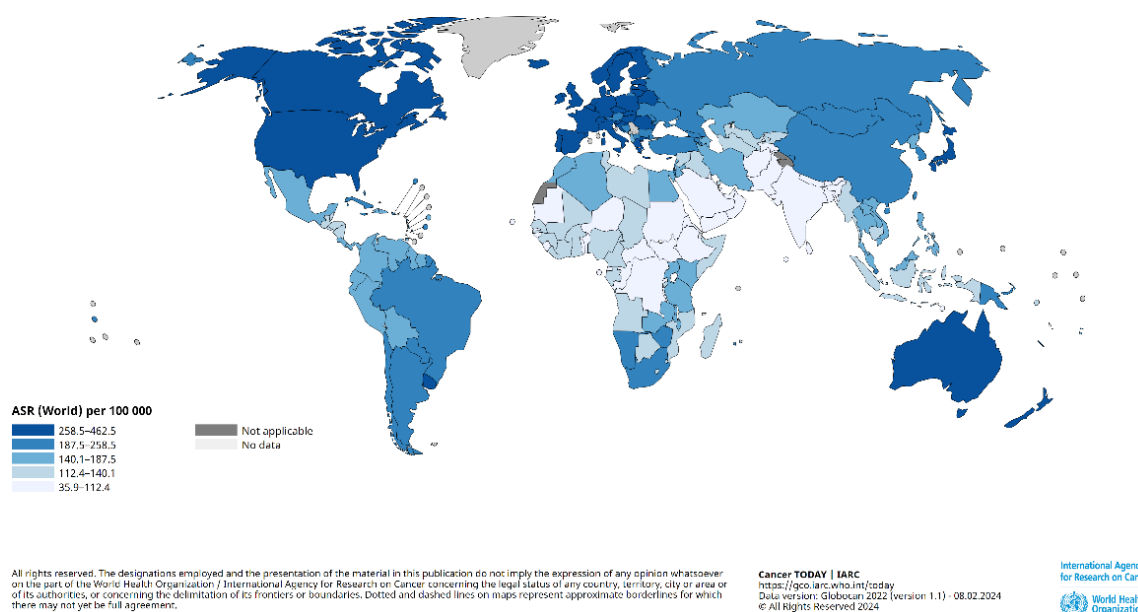


Figure 1. Estimated age-standardized incidence rates (World) in 2022, all cancers, both sexes, all ages. Adapted from <https://gco.iarc.fr><sup>3</sup>

In recent years new technologies such as single-cell profiling by sequencing to characterize cancer heterogeneity, precision genome editing by CRISPR to identify and manipulate random cancer genes, and cancer genomics on an increasing scale have revealed new targets, mechanisms and approaches for better early diagnosis, development of new cancer therapies and cancer prevention.<sup>4</sup> The following chapter deals with the advantages and limitations of the development of precision oncology techniques in recent years by reporting on the most interesting data and innovations.

## **1.2 Precision oncology overview**

Precision oncology encompasses a range of rapidly evolving approaches to cancer therapy that exploit the growing knowledge provided by molecular biomarker profiling.<sup>5</sup> Efforts in recent years have focused on genomic screening of cancer cells. Tumors accumulate somatic aberrations such as gene mutations that are the actual main cause of oncogenesis. The number of mutations found in any tumor can vary up to hundreds of thousands. Through genome screening, oncologists are identifying different mutations that contribute to each person's cancer. They are like fingerprints at a crime scene.<sup>6</sup> Genomic tests look at all the genes in the tumor itself to analyze how active they are and whether they exhibit mutations. The ability to profile complex molecular features of patients' tumors, such as DNA sequence data, has been driven by the evolution of increasingly sophisticated omics methods, which are now showing potential to become an integral part of clinical practice.<sup>7, 8</sup> Figure 2 compares the traditional and customized approaches in treating patients. In the traditional approach, patients receive the same treatment, which can have variable results. The personalized approach, on the other hand, uses detailed analysis (genomics, proteomics, etc.) to create tailored therapies, optimizing efficacy and reducing toxicity. Nutritional and environmental data are also integrated, with the use of artificial intelligence to make targeted therapeutic decisions. The result is a more effective and safer health promotion for each patient.<sup>9</sup>

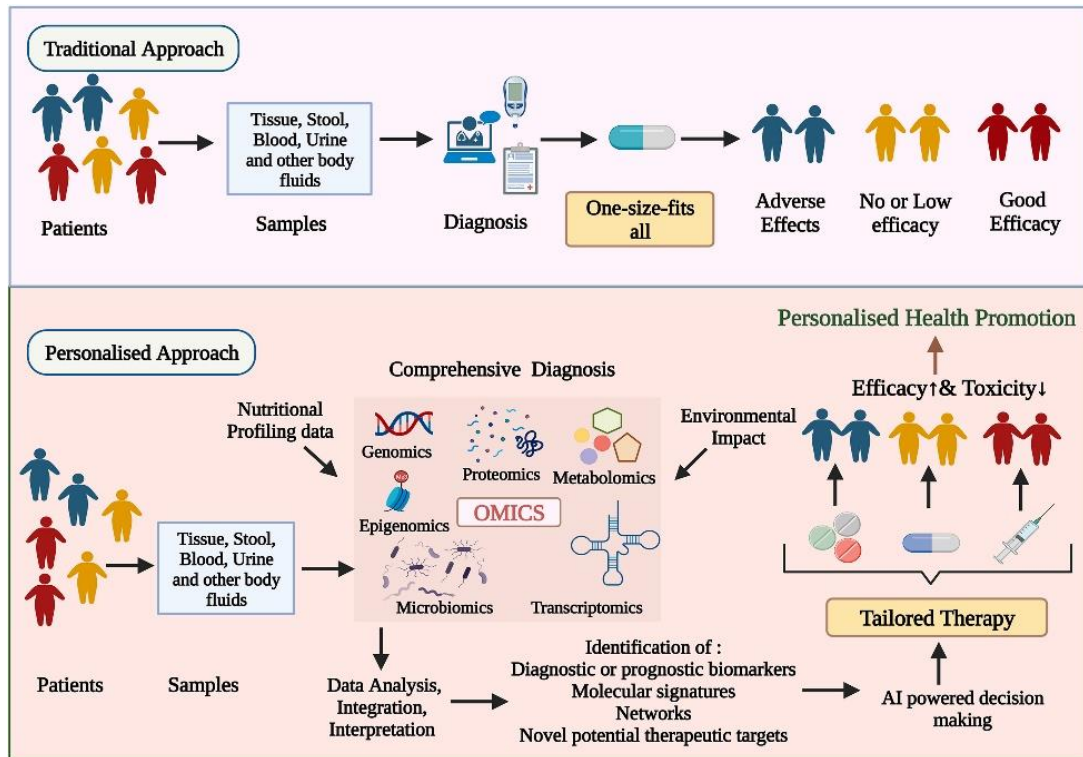
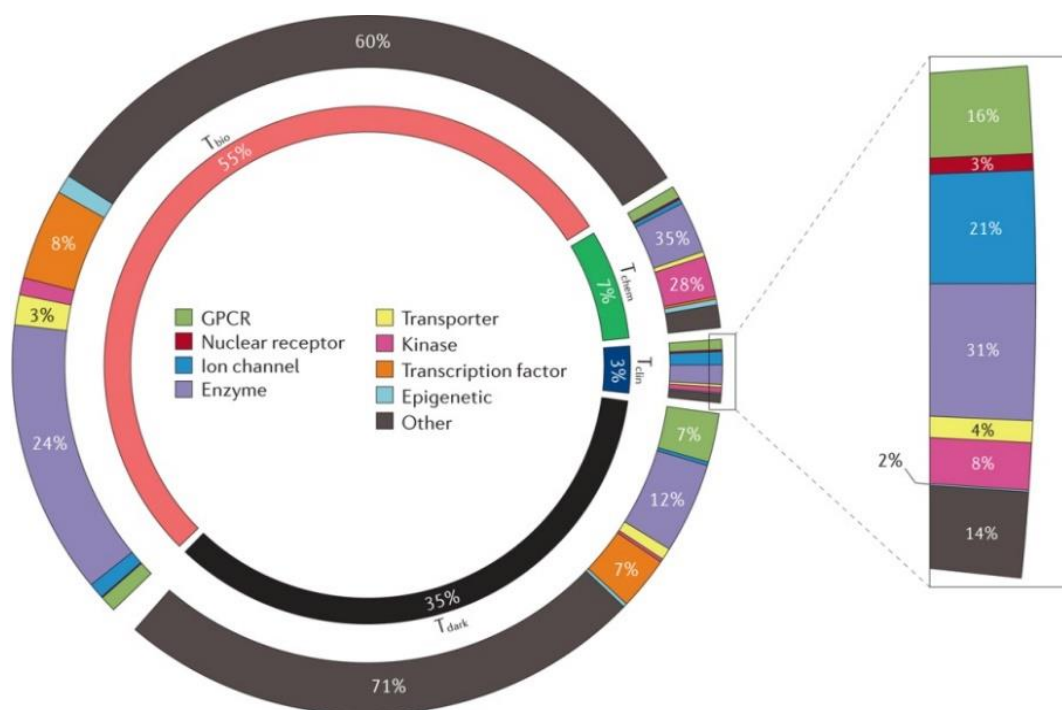


Figure 2. Tailored personalized medicine approach employing omics techniques and physiological measurements coupled with machine learning and AI techniques to enable early identification and prevention of disease in clinical decision-making. Adapted from Singh et al. (2023) <sup>9</sup>

In 2006, the Cancer Genome Atlas project was launched with the ambitious aim of cataloguing all the mutations and genomic alterations responsible for different forms of cancer. Thanks to the project, of the approximately 23,000 genes that make up the human genome, scientists are beginning to know which ones are involved in the different malignancies.<sup>10</sup> Genomic tests can help an oncologist decide what kind of targeted therapies might work for a specific type of cancer. These tests can also predict the likelihood of cancer recurrence over time. In 2018, contributors to the Illuminating the Druggable Genome initiative, funded by the US National Institutes of Health, reported that one-third of all human proteins had yet to be studied in detail and that only 3% were targets of at least one approved drug with a known mechanism of action (Figure 3).<sup>11</sup> Despite significant advances<sup>12</sup>, precision medicine is currently unavailable for many patients. This is an immense amount of work, which will still take many years, but it is beginning to bear fruit and is leading to the development of drugs that are effective against certain subtypes of cancers.

Unfortunately, many proteins that are potential targets for precision oncology, such as DNA damage response and repair proteins, are currently not druggable by such means.<sup>13</sup>



*Figure 3. Target development level categories applied to the human proteome. Percentages of the whole proteome are shown in the inner ring. Percentages of each target development level (TDL) category for selected major protein families are shown in the outer ring, with the  $T_{clin}$  category expanded.  $T_{clin}$  (blue) = drug targets with at least one approved drug by mechanism of action (MoA);  $T_{bio}$  (red) = proteins without MoA-related drug targets;  $T_{chem}$  (green) = proteins without MoA-based approved drugs but that bind to small molecules with high potency;  $T_{dark}$  (black) = remaining proteins that do not meet any of the criteria for the other  $T$ s. Adapted from Oprea et al. (2018)<sup>11</sup>*

Several innovative approaches have been developed to address current limitations in cancer treatment. Artificial intelligence (AI) and advanced machine learning can help design targeted therapies by selecting specific mutational profiles.<sup>14</sup> One example is an AI model developed at MIT that predicts the risk of developing lung cancer up to six years earlier.<sup>15</sup> Another innovation is CAR-T therapy, which genetically modifies the T-cells of the immune system to recognize and destroy cancer cells.<sup>16</sup> Immunotherapy has also made progress, with monoclonal antibodies that block abnormal tumor proteins or inhibit immune checkpoints to strengthen the immune system response.<sup>17</sup>



Regarding drug development, there have been various examples of precision oncology in tumors with “oncogene dependence”, where a tumor relies excessively on a particular oncogene for survival. Therefore, inhibition of this oncogene through small molecules or antibodies results in selected cell death. Examples are imatinib, a BCR-ABL inhibitor, for chronic myeloid leukemia or the BRAF inhibitor, vemurafenib, for the treatment of melanoma, which led to a clinically significant response to a previously difficult-to-treat disease.<sup>18, 19</sup>

Unfortunately, not all tumors show a simple dependence on oncogenes and their survival mechanisms are much more complex and not yet characterized; moreover, some oncogenes have proved to be indestructible by small molecules and antibodies.<sup>20</sup> Additionally, resistance problems have led to the result that oncology still relies on radiotherapy and non-specific chemotherapeutics. However, a variety of oncogenic mutations, some of which confer treatment resistance and loss of function (as seen in HRD tumors with homologous recombination deficiency), may pose a challenge to selective inhibition by molecular drugs. In these cases, new approaches to drug development may be effective, such as multifunctional drugs, gene silencing, target degradation or synthetic lethality (SL).<sup>21</sup> SL represents an innovative approach in medicinal chemistry for oncology, based on interactions between mutated genes that, when combined, lead to selective cancer cell death. This mechanism makes it possible to develop targeted therapies that exploit specific genetic vulnerabilities of cancer cells, minimizing the impact on normal cells and increasing therapeutic efficacy.<sup>22</sup>

### **1.2.1 Synthetic Lethality (SL) in DDR as an approach in precision oncology**

SL is a phenotypic condition in which cells do not survive due to the combination of two genetic perturbations that, taken individually, do not induce cell death. This concept comes from genetic studies on organisms like fruit flies<sup>23</sup> and yeasts<sup>24</sup> and it highlights the critical roles two genes can play in keeping the cell alive. If one of these two genes is mutated, the non-mutated gene can compensate for the loss of the mutated one and vice versa, whereas if both genes are impaired, cell death is triggered (Figure 4A).<sup>25</sup> SL can be exploited in drug combinations simultaneously inhibiting two synthetically lethal partners to induce tumor cell death (Figure 4B).<sup>26, 27</sup> The SL concept may also apply to proteins encoded by synthetic lethal genes that mediate two cellular

pathways essential to the cell. Inhibition of one pathway is not lethal as it is compensated by the alternative pathway, while combined inhibition is lethal.<sup>28</sup>

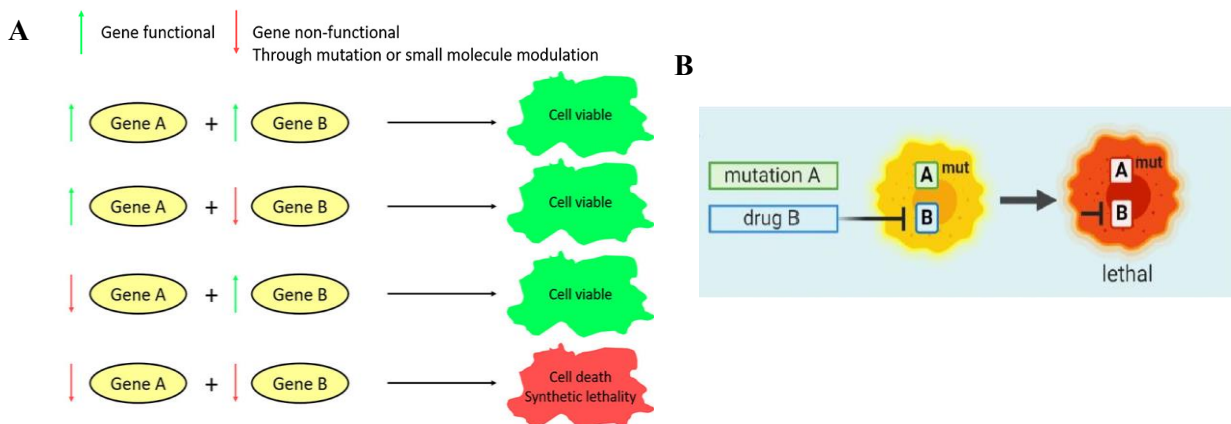


Figure 4. A) Concept of synthetic lethal interactions; B) SL in anticancer therapy where a molecule inhibiting a lethal gene B with a mutated gene A leads to cell death. Adapted from Myers et al. (2020)<sup>28</sup>

Targeted inhibition of synthetic lethal partners of mutated tumor suppressor genes can offer significant efficacy combined with improved safety profiles compared to chemotherapeutic alternatives.<sup>21</sup> For instance, poly ADP-ribose polymerase 1 (PARP1) inhibitors have proved efficacy in the targeted treatment of a variety of HRD tumor types<sup>29</sup>, but efforts are ongoing to identify new synthetic lethal gene pairs to expand the pool of potential synthetic lethal targets and tumor biomarkers to predict sensitivity to synthetic lethal agents.<sup>30</sup> In cases of acquired resistance to PARP inhibitors, SL could be exploited to identify synergistic drug combinations to reduce the risk of resistance.<sup>31</sup>

Screening for clinically relevant synthetic lethal interactions poses three main challenges: i) lethal genetic interactions make the recovery and identification of mutants difficult; ii) many synthetic lethal interactions are condition-dependent and are not conserved in all genetic backgrounds; iii) synthetic lethal interactions are rare and it is necessary to study a large number of combinations of mutant gene pairs.<sup>32</sup> Advances in RNA interference (RNAi) have made it possible to perform large-scale synthetic lethal screening directly in human cell culture. Initiatives such as the Cancer Dependency Map<sup>33</sup> integrate data from a large number of genetic and drug screenings, together with genomic profiles of cellular models to identify new therapeutic targets. At the same time,

analysis of large-scale parallel datasets based on CRISPR-Cas9 is used to estimate the prevalence of mutations conferring sensitivity or resistance to such therapies in patients.<sup>34, 35</sup>

SL approaches could be extended beyond targeting mutations with loss of function or reduction of function in tumors:

*Synthetic dosage lethality* (SDL) is a genetic interaction in which overexpression of one gene combined with reduced function of a second gene results in lethality. Cancer cells often exhibit gene overexpression, derived from somatic copy number alterations<sup>36</sup> or epigenetic changes that increase gene transcription. Genes overexpressed in tumors can be targeted by identifying interaction partners that determine SDL. For example, CKS1B, frequently overexpressed in breast, lung and liver cancer, shows SDL with inhibition or knockdown of PLK1.<sup>37</sup> SDL has the potential to open new avenues for SL-mediated cancer therapies by indirectly targeting genes commonly overexpressed in tumors.

*Conditional synthetic lethality.* Cancer cells are heterogeneous and are in environments that influence genetic interactions, being dependent on intrinsic (genetic background and metabolic state) or extrinsic (cellular microenvironment and exposure to therapeutic agents) conditions. Conditional SL may explain why some genetic interactions are specific to a cell line; these interactions are often referred to as “context-specific” synthetic lethal interactions, whereas interactions that are common to many cell lines are known as “core” synthetic lethal interactions.

The genetic background can have both positive and negative effects on synthetic lethal interactions. Some genetic interactions require the disruption of three or more genes to generate a phenotype.<sup>38</sup> On the other hand, background mutations can suppress synthetic lethal interactions, resulting in synthetic viability (Figure 5B). For example, loss of 53BP1 can suppress the synthetic lethal interaction between PARP1 and the breast cancer susceptibility gene BRCA1.<sup>39</sup> Therefore, the genetic background of a tumor, such as loss of p53 or activation of an oncogene, could uncover or suppress synthetic lethal interactions. Conditional SL is also exploited under extrinsic tumor conditions (hypoxia, altered metabolism and exposure to standard therapies) often poorly addressed by the classical combination strategies based on SL pairs.<sup>40</sup> For instance, hypoxia reduces the efficacy of homologous recombination,<sup>41</sup> resulting in an impaired DNA repair state that sensitizes cells to PARP1 inhibition (Figure 5Aa). Conditional synthetic lethal interactions may also increase the cytotoxicity of existing therapeutic agents. Ionizing radiation or cytotoxic

drugs change the tumor environment compared to untreated cells. PARP inhibitors can indeed increase the sensitivity of tumor cells to DNA-damaging agents<sup>42</sup> through a mechanism of *synthetic cytotoxicity* (Figure 5Ab). For example, in glioblastoma cell lines containing mutations in the cohesin component STAG2, PARP inhibition resulted in synthetic cytotoxicity in response to the DNA-damaging chemotherapeutic agent temozolomide.<sup>43</sup>

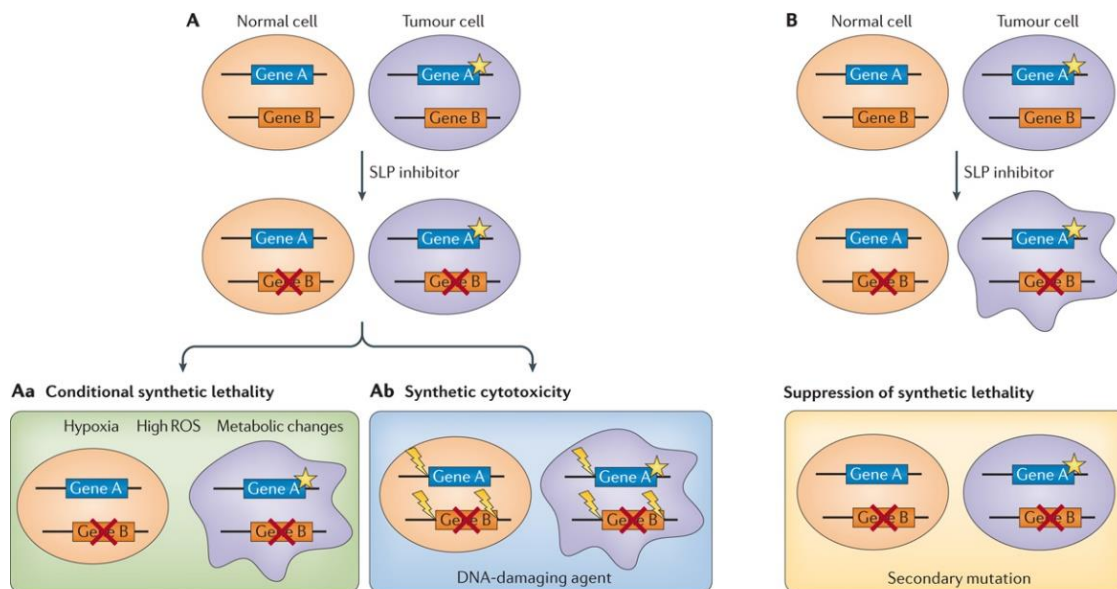


Figure 5. Synthetic lethal interactions may be dependent on certain intrinsic conditions such as genetic background, hypoxia or metabolic changes (part **Aa**), or extrinsic conditions such as treatment with DNA-damaging agents, which results in synthetic cytotoxicity (part **Ab**). Conversely, synthetic lethal interactions may be suppressed by conditions such as genetic background mutations (part **B**). Star = mutation, red cross = pharmacological inhibition, lightning bolt = DNA damage; viable cells as ovals, non-viable cells as random shapes. ROS, reactive oxygen species; SLP, synthetic lethal partner. Adapted from O'Neil et al. (2017)<sup>32</sup>

### 1.3 Overview of DNA damage repair (DDR) mechanisms

Showing increased endogenous DNA damage, cancer cells have one or more inactive DNA damage repair (DDR) pathways. These deficiencies are of interest for the development of anticancer treatments based on SL; indeed, most SL interactions regard proteins involved in DDR pathways. The exploitation of DNA damage and the resulting DDR response have contributed to SL-based therapeutic approaches,<sup>44</sup> identifying new drug targets, overcoming the genetic

heterogeneity of tumor cells<sup>22</sup> and showing selectivity on tumor cells rather than normal cells not having a specific genotype.<sup>32</sup>

Genomic instability and metabolic reprogramming contribute to the robust and evasive nature of cancer especially when cancer cells are exposed to chemotherapeutic agents. Genomic instability is defined as the increased frequency of mutations within the genome, while metabolic reprogramming is the alteration of metabolic pathways that cancer cells undergo to adapt to increased bioenergetic demand.<sup>45</sup> The cause of mutations is the product of DNA damage and a defective repair pathway, both of which result in the expansion of genomic lesions. Genomic instability and defects in the DDR pathway can promote uncontrolled proliferation and survival of cancer cells by inducing de novo driver mutations, generating tumor heterogeneity and evading apoptosis. Furthermore, DNA repair mechanisms can be utilized by tumor cells to repair damage caused by drugs or other therapies.<sup>46</sup>

DNA is subject to damage that occurs endogenously or exogenously on DNA residues damaged by replication errors, X-rays, UV light, IR but also alkylating agents, ROS, and inflammation. ROS-induced DNA damage is believed to play a role in the development of cancer, ageing and neurodegeneration. Oxidative DNA stress can cause mutations that activate or deactivate tumor suppressor genes.<sup>47</sup> Various DNA repair mechanisms and other cellular stress response pathways, such as cell cycle arrest and apoptosis, increase the likelihood of genetic changes leading to neoplastic events.

There are different types of DNA damage, such as single-strand DNA breaks (SSB), double-strand DNA breaks (DSB), DNA protein cross-linking (DPC), bulky adducts and base mismatches. The activation of DDR promotes a cellular repair mechanism involving numerous proteins depending on the type of damage.<sup>48</sup> SSBs can be repaired directly or indirectly by base excision repair (BER). DSBs can be repaired using two types of mechanisms: non-homologous or error-prone end-joining (NHEJ) and homologous or less error-prone recombination (HR). Non-homologous end-joining (NHEJ) repair is the simplest and most frequent way to repair DSBs although it modifies the DNA sequence as the broken ends are joined by DNA ligation resulting in the loss of nucleotides at the joining site. Homologous recombination (HR) repair is a much more accurate way to repair DSBs than NHEJ since it accurately restores the original DNA sequence by sister chromatids as templates for the repair of the original sequence. Other types of damage, such as DNA adducts, cross-links and oxidized bases, can be repaired using the nucleotide excision repair (NER). Nucleotide

excision repair (NER) pathway addresses DNA damage caused by UV radiation and platinum salts and acts on mutated nucleotides that distort the structure of the double helix.<sup>49</sup> When a DNA mutation occurs, such as an insertion, deletion or base mismatch, mismatch repair (MMR) is activated (Figure 6).<sup>50</sup>

Numerous types of DNA damage have been strongly linked to tumor development and the mechanisms where the proteins of interest are most involved are analyzed below.

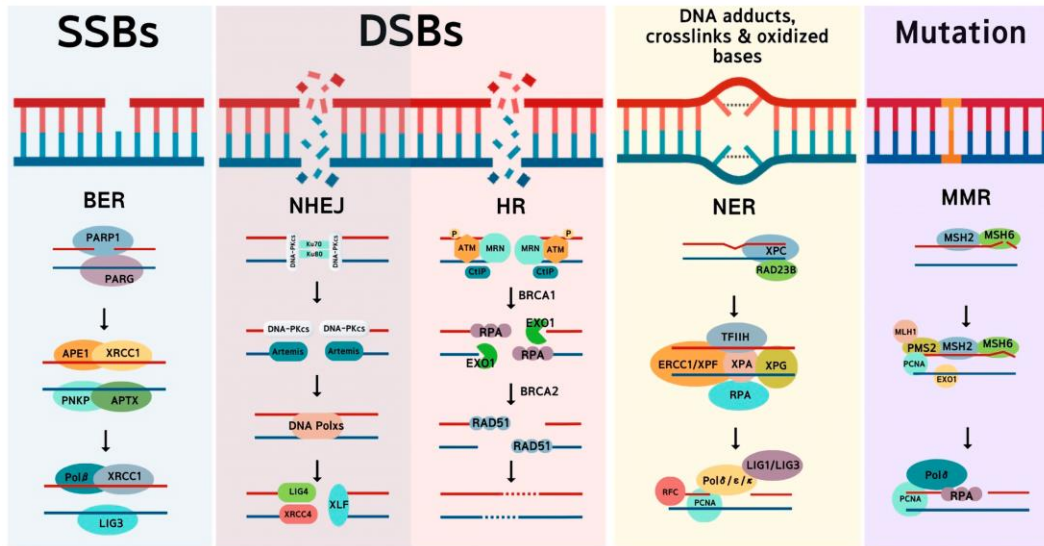


Figure 6. Types of DNA damage and their repair systems. Exogenous or endogenous insults cause strand breaks and base modification and mutation and activate specific repair pathways corresponding to the types of DNA damage. Adapted from Moon et al. (2023)<sup>50</sup>

### Base excision repair

Base excision repair (BER) pathway is responsible for the repair of DNA SSBs that do not distort the helix and are caused by modified bases, abasic sites and their frequent processing in the cell. The stages of BER are excision, incision, final processing, repair synthesis and base lesion. After the first steps<sup>51</sup>, poly (ADP-ribose) polymerase 1 (PARP1) and X-ray repair cross-complementing protein 1 (XRCC1) promote the assembly of repair factors. DNA synthase I and DNA ligase I finish the job; however, this repair may result in structural distortions or ground-level issues.<sup>52</sup>

BER pathway repairs residues damaged by ROS, IR and alkylating agents and could be of crucial importance for cancer prevention. Altering the amount of BER proteins may be a viable gene

therapy strategy to kill cancer cells.<sup>53</sup> Analyses of BER gene mutations in tumors could be useful for understanding the genesis of neoplasms in a specific organ and the potential function of BER in metastasis. Furthermore, BER enzymes are crucial targets for anti-cancer drugs, as they prevent cell sensitivity to various chemicals and ionizing radiation.

#### *DNA double-strand breaks repairs*

DNA double-strand breaks (DSBs) are the most damaging type of DNA damage. DSBs can result from exposure to ionizing radiation, chemicals or reactive oxygen species or arise from natural cellular processes such as DNA replication. Unrepaired DSBs compromise genetic integrity and stability, eventually leading to cell death or carcinogenesis. In the presence of DSBs, DDR mechanisms act by activating cell cycle checkpoints to halt the cell cycle and allow time to restore genome integrity. G1/S checkpoints, intra-S transitions and G2/M checkpoints are those activated by DDR. In particular, the G1/S checkpoint is the most sensitive to DNA damage and is defective in many human cancers.<sup>54</sup> Several DSB repair mechanisms have evolved to maintain the integrity of the genome, and the ones concerned in our research project are detailed below.

#### *Single strand annealing repair*

Single strand annealing (SSA) repair is an error-prone mechanism used when DSBs occur in highly repeated regions of DNA and relies on long stretches of homology to stitch together two 3'-ssDNA protrusions.<sup>55</sup> This mechanism therefore requires neither a template donor from a sister chromatid nor strand invasion.<sup>56</sup> SSA begins with the resection of DNA ends and the creation of 3' overhangs due to the nuclease activity of Mre11/Rad50/Nbs1 (MRN) and C-terminal binding protein 1 interacting protein (CtIP) complexes.<sup>57</sup> The DNA/RNA-binding protein RAD52 is then recruited to promote annealing of the resected DNA ends and recognize the ssDNA homology region (<30 base pairs). After annealing in the homology regions, the Excision Repair Cross-Complementation Group 1 (ERCC1)-Xenoderma Pigmentosum Complementation Group F (XPF) complex binds the N-terminal domain of RAD52 and cleaves the non-homologous 3'-ssDNA flap ends.<sup>58</sup> Then, DNA polymerases fill any gaps and DNA ligase I blends the DNA strands to complete the SSA process (Figure 7B). However, not all polymerases and ligases involved in SSA have yet been identified.<sup>59</sup>

As SSA is itself mutagenic, its normal function to repair DSBs can also cause deletions in genes important for cancer transformation. SSA-specific deletions have been observed between homologous segments of repeats in germline mutations of several tumor suppressor genes.<sup>60</sup> Some studies have suggested that RAD52 and SSA may belong to the main sources of genomic instability, which are vital for cancer induction and development, and may therefore be considered in anticancer strategies.<sup>61,62</sup> SSA could also contribute to cancer-related genomic instability in its canonical form. It seems important when DSBR switches from an error-free pathway to SSA, as this switch usually occurs under non-physiological conditions that favor non-canonical, error-prone SSA, further increasing genomic instability. Interestingly, depending on the different cancer types, RAD52 was found to be up- or down-regulated and RAD52 levels could be correlated with good or bad prognosis for patients. For example, cervical and rectal cancer cells with low expression of RAD52 have been associated with poor response to platinum-based chemotherapeutics and increased resistance.<sup>63, 64</sup> On the other hand, in another study, RECQL4-deficient breast, colon and lung cancer cells with significant upregulation of RAD52 showed increased sensitivity to ionic radiation.<sup>65</sup>

#### *Homologous recombination repair*

In contrast, homologous recombination (HR) repair is a much more accurate way to repair DSBs than NHEJ and SSA. The mechanism accurately restores the original DNA sequence since sister chromatids are used as templates for accurate repair of the original sequence. The damaged DNA must be in close proximity to the template DNA and, for this reason, it occurs mainly in the S and G2 phases of the cell cycle when the two daughter DNA strands are close together. DSBs mostly result from stalled DNA replication forks, independent of external stimuli, but also from radiation or chemical damage. First, 53BP1 is activated and the 53BP1-RIF1-shieldin-CST/ASTE1 complex stabilizes chromatin at the DSB site.<sup>66</sup> The Mre11-RAD50-Nbs1 (MRN) complex detects DSBs by recruiting BLM helicase and EXO1 to the breaks to initiate the resection of the free ends of the 5'-3' double-stranded DNA. The MRN complex also mediates the recruitment and activation of ATM (Ataxia Telangiectasia Mutated) kinase at the damaged sites through its binding to Nbs1.<sup>67</sup> Once activated, ATM recruits additional DDR factors to initiate DDR signal transduction through phosphorylation of several proteins, including histone H2AX and Chk2. The resection process mediated by ATM-MRN, Exo1 and BLM produces long stretches of ssDNA, which are coated by



replication protein A (RPA) preventing further resection. In parallel, ATR is recruited to the RPA-coated ssDNA recruitment platform. As part of DDR signal transduction, ATR kinase activity leads to the phosphorylation of other kinases, such as Chk1, involved in the regulation of cell cycle checkpoints.<sup>68</sup> This results in the arrest of the cell cycle and preserves the cell filament.<sup>69</sup> RPA is a heterotrimeric protein that binds ssDNA thanks to its three subunits RPA70, RPA32 and RPA14,<sup>70</sup> but its most important role is the dynamic exchange with the recombinase RAD51 on ssDNA that facilitates the nucleation of RAD51 to form the nucleoprotein filament.<sup>72</sup> In addition, free RPA has a regulatory effect on the nucleoprotein filament formation of RAD51, as free RPA in solution, resulting from displacement, can inhibit the nucleation of RAD51.<sup>73</sup> The loading of RAD51 onto ssDNA at the DSB site and the subsequent formation of the nucleoprotein strand is a highly regulated process in which numerous proteins participate as mediators. The most important mediator of RAD51 is the breast cancer type 2 susceptibility protein (BRCA2)<sup>74</sup> which binds to RAD51 by recruiting it to the DSB. At this point RAD51 coats the ssDNA substrate, forming helical nucleoprotein filaments, to perform homology research, invading the DNA duplex and finding the undamaged DNA template.<sup>75</sup> Base pairing between RAD51-coated ssDNA and its dsDNA homolog triggers the exchange of DNA strands for genetic recombination. In addition, this generates heteroduplex DNA (hDNA) bound to RAD51 within a displacement loop called a D-loop.<sup>76</sup> The nucleation of RAD51 on ssDNA and the search for homology are highly regulated by the activity of many HR proteins, including RAD52.<sup>77</sup> After dissociation of RAD51 from hDNA, the 3'-invaded end of ssDNA acts as a primer for DNA synthesis, using the complementary strand in hDNA as a template to restore the missed sequence. DNA synthesis can take place via different mechanisms, such as BIR, SDSA or dHJ, in which DNA polymerase and DNA ligase proceed to extend the damaged 3'-end and anneal the strands, resulting in DNA repair (Figure 7A).<sup>78</sup>

Several cancers, including breast, ovarian and pancreatic cancer, involve altered HR genes, such as mutated BRCA1 or BRCA2 (BRCA1/2).<sup>79</sup> Therefore, HR proteins are potential targets for anticancer therapies due to their involvement in tumorigenesis and therapeutic resistance. In general, although defects in the DDR mechanism cause tumor initiation, these defects also provide therapeutic opportunities. Since pharmacological inhibition of the DDR signaling cascade directs tumor cells to rely on compensatory survival pathways, these vulnerabilities have been exploited in SL-based anticancer therapies that will be discussed in more detail in the next chapter.

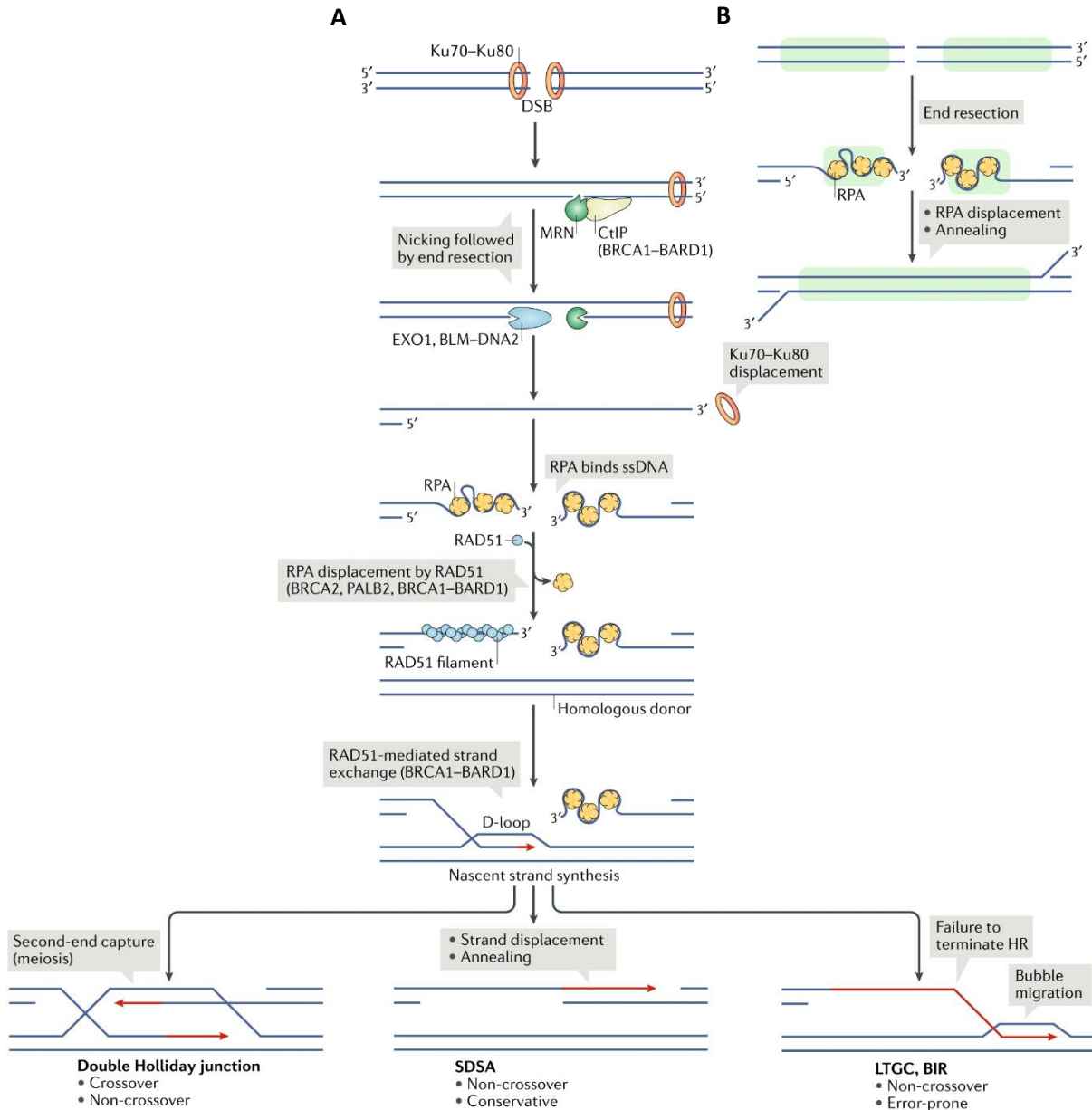


Figure 7. A) The DNA double-strand break HR repair pathway; B) SSA converts sequence repeats (green boxes) into a single copy of the repeats by annealing complementary ssDNA ends from different repeats. Replication protein A (RPA) must be displaced to expose complementary ssDNA for annealing. Adapted from Scully et al. (2019)<sup>80</sup>

## **1.4 PARP/BRCA2: targeting SL in DDR**

The concept of targeting SL in DDR in the clinic is best exemplified using PARP inhibitors to specifically target tumors deficient in the homologous recombination DNA repair factors, such as BRCA1/2 proteins. The use of PARP inhibitors (PARPi) prevents the tumor from repairing single-strand DNA breaks and increases the incidence of DSBs. Therefore, upon administration of PARPi to BRCA1/2 mutated cancer, the tumor cells are unable to survive and die because of SL, while normal cells remain unharmed.<sup>81</sup>

The disclosure of SL in various DNA repair pathways has expanded the clinical strategies of DDR targeting, with various DDR inhibitors in preclinical and clinical development. The encouraging results of PARP inhibitors have led to an increasing amount of research focusing on targeting other components of the DDR pathway as synthetic lethal approaches for cancer treatment. To date, there are numerous examples of synthetically lethal gene pairs. S. Myers *et al.* in their recent perspective<sup>28</sup> select the most prominent examples with pharmaceutical development. The perspective emphasizes that ATR, ATM and DNA-PKcs are promising targets for inhibiting DNA damage repair, as they are all involved in disrupting the cell cycle and initiating the DNA damage repair process.

In this thesis, the PARP/BRCA2 SL pair is treated in more detail since it is in line with the conducted research aimed at strategies to enlarge the therapeutic use of PARPi and to avoid PARPi-acquired resistance.

### **1.4.1 PARP1 protein: structure and involvement in cancer**

PARP1 belongs to the poly (ADP-ribose) polymerase family of proteins, enzymes that catalyze the polymerization of ADP-ribosyl units into target proteins (PARylation), including histones, DNA repair proteins and chromatin modulators using  $\text{NAD}^+$  as a donor of ADP-ribose units.<sup>82</sup> PARylation modulates the conformation, stability or activity of target proteins that have negatively charged branched polymers of approximately 20-30 units. PARP1 is a particularly important protein for DNA damage repair and genome stability. When DNA damage occurs, PARP1 initiates its self-parylation, which activates it and enables PARylation of histones and other DNA damage-associated proteins. Finally, this self- and hetero-modification recruits downstream DNA repair proteins, such as XRCC1 and histones H1 and H2B, to the site of DNA damage, promoting

effective DNA repair. PARP1 acts mainly in basic excision repair (BER), to recognize, process and repair DNA SSBs, through not only its autoregulation but also by reorganizing chromatin around the DNA damage site.<sup>83</sup>

The primary structure of PARP1 (Figure 8) has several domains: a DNA-binding domain, a caspase-cleaved domain, an automodification domain and a catalytic domain. The N-terminus contains three Zn-finger domains, which mediate interaction with DNA and induce a conformational change. Two zinc-binding domains, Zn1 and Zn2, allow PARP1 to recognize DNA structures, while a third zinc-binding domain, Zn3, has a structure and function distinct from those of Zn1 and Zn2. The central region (AD self-regulatory domain) is involved in PARP1's self-regulation, containing BRCT (C-terminus domain of BRCA1) and the self-parylation site (P). Finally, the C-terminal portion contains WGR (tryptophan, glycine and arginine-rich domain), which is responsible for interdomain contacts and DNA damage recognition. The catalytic domain (CAT) is composed of two subdomains, the helix-loop-helix (HD) subdomain and the ART subdomain, which is conserved in other ADP-ribosyl-transferases (ART), and includes the amino acids involved in catalysis and nicotinamide adenine dinucleotide (NAD<sup>+</sup>) binding.<sup>84</sup> In its non-DNA bound state, PARP1 has minimal catalytic activity due to an auto-inhibitory helical domain (HD) interaction with its catalytic domain.<sup>85</sup> When PARP1 binds DNA, via zinc finger domains, a conformational change in the PARP1 protein relieves the autoinhibitory interaction between the HD and the catalytic domain, allowing nicotinamide adenine dinucleotide ( $\beta$ -NAD<sup>+</sup>), the PARP1 co-factor, to bind the active site of the enzyme. PARP1 then uses the hydrolysis of  $\beta$ -NAD<sup>+</sup> to catalyze the transfer of ADP-ribose moieties on to target proteins. This PARylation of proteins in the vicinity of the DNA breaks then likely mediates DNA repair by modifying chromatin structure (e.g. via histone-PARylation) and by localizing DNA repair effectors. PARP1 self-PARylation eventually leads to its own release from the site of DNA damage.

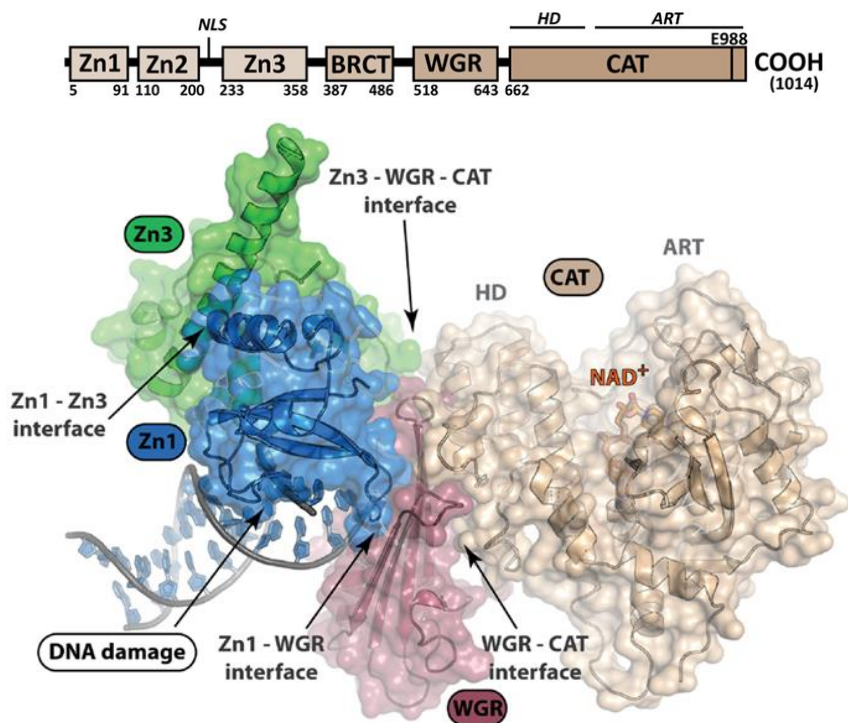


Figure 8. PARP1 sequence, complex formation and protein–protein interactions between domains upon DNA damage recognition (PDB ID: 4DQY). Adapted from Steffen et al. (2013)<sup>86</sup>

Various works have been published showing the involvement of PARP1 in carcinogenesis. Loss of PARP1 causes disorders in DNA repair as well as transcriptional inhibition of genes involved in DNA replication and cell cycle regulation. Decreased expression of PARP1 also contributes to general genome instability.<sup>87</sup> While cases of increased PARP1 expression such as in breast and lung cancers,<sup>88, 89</sup> are associated with an unfavorable survival prognosis,<sup>90</sup> being correlated with a more aggressive tumor phenotype.<sup>91</sup> PARP1 expression may be related to tumor resistance to therapy<sup>92</sup> since PARP1 facilitates the repair of damaged DNA and, thus, the overcoming of tumor genetic instability.

PARP inhibition blocks the DDR processes in which it is involved and leads to the accumulation of single-strand DNA breaks. This leads to the formation of double-strand breaks, which require homologous recombination for repair. Cancer cells harboring mutations in DNA repair genes such as BRCA1, BRCA2, PALB2 or ATM are unable to utilize DNA repair by homologous recombination and accumulate double-strand DNA breaks over time, resulting in cell death.<sup>93</sup> The BRCA2 gene encodes for the protein of the same name, which participates in the homologous

recombination (HR) process to repair DSBs. Loss-of-function mutations in the BRCA2 gene therefore sensitize cancer cells to the inhibition of other pathways and proteins involved in the DNA damage response (DDR) network, including PARP which plays a role in the repair of SSBs through repair by BER.<sup>94</sup> PARP1 inhibition is therefore synthetically lethal in the presence of biallelic defects in the BRCA1/2 genes found in a number of breast and ovarian cancers.<sup>81, 95</sup> In PDAC, it was shown that patients with mutations in BRCA1/2 have a better overall survival (OS) when treated with platinum-based chemotherapy than those treated with non-platinum-based therapies because the BRCA mutation prevents repair of the double-strand DNA breaks generated.<sup>96</sup> Since cancer cells can still exploit the PARP pathway to prolong survival, PARP inhibition leads to cancer cell death in the presence of mutations in the BRCA1/2, PALB2 or ATM genes (Figure 9).<sup>97-99</sup> Several PARP inhibitors have already been approved for the treatment of patients with breast, ovarian, prostate and, more recently, advanced pancreatic cancer with germline or somatic BRCA mutation.<sup>100, 101</sup>

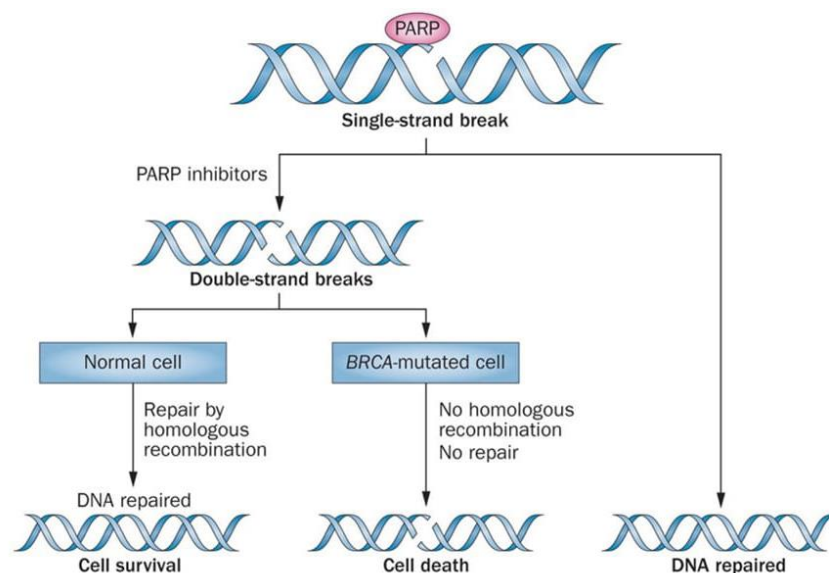


Figure 9. The role of PARP inhibitors in SL-based therapies. Adapted from Sonnenblick (2015)<sup>102</sup>

#### 1.4.2 PARP inhibitors: overview

Between the 1980s and 1990s, two generations of PARP1i were developed. The first started from modifications of nicotinamide to develop a class of 3-aminobenzamides, which showed low

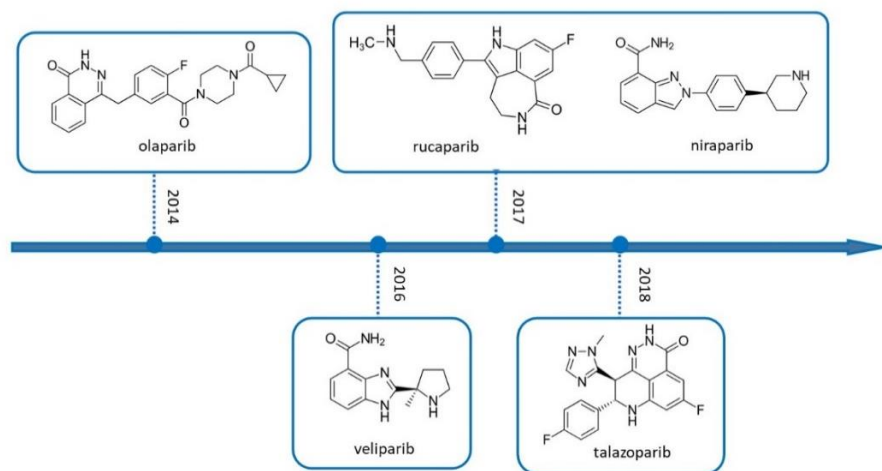
selectivity and cytotoxic effects. The second generation of PARP1 inhibitors based on a class of quinazoline analogues proved to be more effective and target-specific.<sup>103</sup>

In 2014, olaparib (AZD2281)<sup>104</sup> obtained approval from the European Medicines Agency (EMA) in the European Union and the Food and Drug Administration (FDA)<sup>105</sup> of the United States as monotherapy in hereditary ovarian cancer with a deleterious or suspected BRCA germline mutation (gBRCA).<sup>106</sup> From 2017, olaparib (Lynparza ®, 2014) is also used for the maintenance treatment of adult patients with recurrent epithelial, fallopian tube or primary peritoneal ovarian cancer who had a complete or partial response to platinum-based chemotherapy.<sup>107</sup> In 2018, olaparib was the first PARPi to be approved for the treatment of breast cancer, particularly HER2-negative metastatic breast cancer with a gBRCA mutation.<sup>108</sup> Olaparib also received FDA approval in 2019 for the pancreatic cancer indication (NCT02184195). In this study, patients with a gBRCA mutation and metastatic pancreatic cancer that had not progressed during first-line platinum-based chemotherapy had a significantly longer PFS with maintenance olaparib compared to a placebo (Figure 10).<sup>109</sup>

After 2014, other PARP inhibitors, including rucaparib<sup>110</sup>, niraparib<sup>111</sup> and talazoparib<sup>112</sup>, have received approval for their use in various types of cancer. To date, rucaparib (Rubraca ®, 2016) is used for the treatment of advanced, chemotherapy-resistant ovarian and breast cancer in patients with BRCA1/2 deficiency, and niraparib (Zejula ®, GSK, 2017) for platinum-sensitive ovarian, fallopian tube and primary peritoneal cancers.<sup>113</sup> The FDA indications for niraparib as maintenance therapy were subsequently extended to patients with ovarian cancer independently of their HR deficiency status showing significantly longer progression-free survival (PFS) in clinical trials (NCT02655016, Figure 10).<sup>114</sup> Rucaparib on the other hand has been approved for the treatment of patients with metastatic castration-resistant prostate cancer with a deleterious BRCA mutation (NCT02952534, phase II).<sup>115</sup>

Talazoparib (BMN 673/Talzenna; Pfizer) received approval for the treatment of HER2-negative metastatic breast cancer with gBRCA1/2 mutations due to its efficacy and safety (Figure 10).<sup>116</sup> Talazoparib is known to exhibit the most potent PARP trapping capacity. It has a more rigid structure and is the largest in size among the PARP inhibitors.<sup>117</sup> The difference in stereospecificity and size of the chemical structure is thought to determine the difference in PARP trapping capacity. Veliparib (ABT-888; AbbVie) is undergoing phase 3 clinical trials as combination therapy for breast and ovarian cancer. Although veliparib is an effective catalytic PARP inhibitor with low IC<sub>50</sub>

values, its ability to trap PARPs is considered relatively weak. However, veliparib increases sensitivity to treatments with DNA-damaging reagents, such as chemotherapy and radiotherapy.<sup>118</sup> Interestingly, veliparib significantly improved the PFS of ovarian cancer patients independently of the presence or absence of BRCA mutations or HR-deficient status, although the degree of benefit was greater in HR-deficient patients (Figure 10).<sup>119</sup>



drug	approval in cancers	ongoing clinical trials (phase III)
olaparib	gBRCA- mut <b>ovarian</b> cancer	NCT03737643
	early and metastatic gBRCA-mut HER2-negative <b>breast</b> cancer	NCT03150576
	gBRCA-mut metastatic <b>pancreatic adenocarcinoma</b>	NCT02184195
	HRR gene-mut metastatic castration-resistant <b>prostate</b> cancer	NCT03732820
rucaparib	gBRCA- mut metastatic <b>ovarian</b> cancer	NCT03522246/NCT04227522/NCT02855944
	BRCA-mut metastatic castration-resistant <b>prostate</b> cancer	NCT02975934/ NCT04455750
niraparib	platinum-sensitive advanced <b>ovarian</b> cancer with HRD	NCT03705156//NCT05009082/NCT02655016
	<b>breast</b> cancer	NCT04915755
	<b>prostate</b> cancer	NCT04497844/ NCT03748641
talazoparib	<b>non-small cell lung</b> cancer	NCT04475939
	advanced gBRCA mut- HER2-negative <b>breast</b> cancer	
	<b>ovarian</b> cancer	NCT03642132
veliparib	<b>prostate</b> cancer	NCT04821622/ NCT03395197
	<b>breast</b> cancer	NCT02163694
	<b>ovarian</b> cancer	NCT02470585

Figure 10. Timeline of PARPi approved in clinics by FDA and EMA and their clinical progress. Adapted from Kim et al. (2022)<sup>120</sup>



PARPi structurally mimic nicotinamide and have two general effects: (i) catalytic inhibition of PARP1 (i.e. prevention of PARylation) and (ii) blocking or ‘trapping’ of PARP1 on damaged DNA. Two mechanisms have been proposed to explain the trapping of PARP1: (i) PARPi prevents the release of PARP1 from DNA by inhibiting self-PARylation<sup>121</sup>; (ii) PARPi binds the catalytic site causing allosteric changes in the structure of PARP1 by improving DNA avidity.<sup>122</sup> In both cases, trapped PARP1 blocks the progress of replication forks.<sup>123</sup> In cancer cells that lack one of the key HR proteins, such as BRCA2, cells use alternative DNA repair mechanisms such as NHEJ. The use of these error-prone DNA repair pathways leads to genome fragmentation that eventually kills the cell.<sup>124</sup> After being captured, PARP1 is ubiquitinated by the E3 ligase Ubiquitin promoting the removal of trapped PARP1 from chromatin. The high reparability of PARP-DNA complexes is linked to acquired drug resistance.

Indeed, despite the advantageous selectivity of targeting mutations harbored only by cancer cells, the PARP inhibition strategy has shown the occurrence of acquired resistance.<sup>125, 126</sup> While the mechanisms of innate resistance are poorly understood, several mechanisms of acquired resistance to PARPi have been described in accordance with the adaptive nature of cancer. The best described mechanisms are shown in Figure 11 and include:

1. *Restoration of HR by BRCA1/2 reverse mutations*: one of the best described resistance mechanisms developed after exposure to PARP inhibition.<sup>127</sup> The mechanism may occur through: 1. reversion mutations in circulating tumor DNA (occurring in up to 39% of prostate cancer patients with BRCA1/ 2 mutation after progression with rucaparib; up to 24% of ovarian cancer patients after treatment with platinum chemotherapy and PARPi)<sup>128</sup>; 2. loss of methylation of epigenetically silenced BRCA1 and RAD51C promoters (leads to restoration of functional BRCA1/2)<sup>129</sup>; 3. alternative mRNA splicing that can induce hypomorphic BRCA isoforms by restoring HR function.<sup>130</sup>
2. *BRCA1/2-independent HR restoration*: other DDR pathways may be altered in response to PARPi. One of the best studied mechanisms, inactivation of mutations in the *TP53BP1* gene encoding the 53BP1 protein, has been implicated in maintaining genetic stability in the context of BRCA1 loss. 53BP1 in combination with the Shieldin complex promotes NHEJ by counteracting the resection of the DSB end, which creates the DNA substrate

required for HR.<sup>66</sup> In addition to HR and NHEJ, DSBs can also be repaired by alternative end joining (TMEJ), mediated by DNA polymerase theta (Polθ).<sup>131</sup>

3. *DNA replication fork protection*: BRCA1/2 prevent degradation of blocked replication forks by DNA nucleases.<sup>132</sup> In the absence of BRCA1/2, MRE11 and MUS81 erode the ends of the replication fork, resulting in fork collapse.<sup>133</sup> In BRCA2-deficient cell lines, the loss of the MLL3/4 PTIP complex protein was associated with reduced association of MRE11 with chromatin, leading to replication fork stability and resistance to PARPi.<sup>134</sup>

Other mechanisms of PARPi-acquired resistance include the downregulation of PARP1 or its alteration in the DNA binding domains<sup>135</sup> and the increased PARPi efflux by pump MDR1 (P-glycoprotein) (Figure 11).<sup>136</sup>

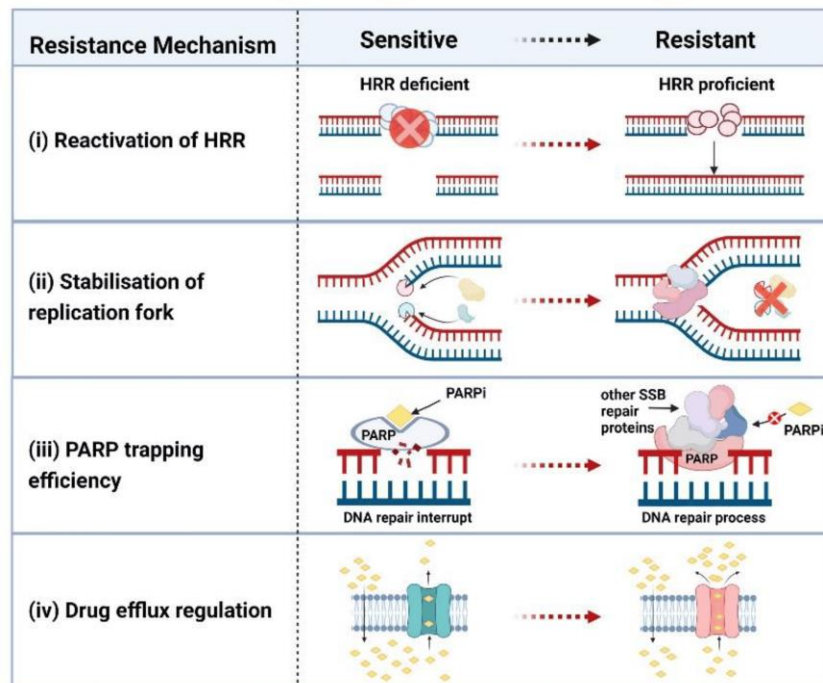


Figure 11. Mechanisms of PARPi-acquired resistance. Adapted from Xie et al. (2022)<sup>137</sup>

Recent research has turned to the exploration of promising combination approaches using PARPi, with the aim of exploiting synergistic effects to improve efficacy and sensitize PARPi-resistant tumors to treatment. In this context, beyond studies combining PARPi with chemotherapeutic agents such as DNA alkylating or platinum-based agents, PARPi have been studied at the

preclinical level in combination with agents inducing a “BRCAness” phenotype.<sup>138</sup> In the next chapter, the BRCA2 protein and its involvement in cancer will be discussed, delving into the concept of BRCAness and its progressive therapeutic potential in recent years.

### **1.4.3 BRCA2 protein: structure and functional domains**

Breast cancer type 2 susceptibility protein (BRCA2) is a tumor suppressor protein involved in maintaining genomic integrity. BRCA2 can prevent the formation of chromosome aberrations during replication stalling by inhibition of the nuclease MRE11.<sup>139</sup> BRCA2 localizes in the nucleus during the S and G2 phases of the cell cycle as part of the process of mitosis and repair of DSBs by HR.<sup>140</sup>

BRCA2 is the main mediator of RAD51 loading on the RPA-ssDNA complex at the DSB site.<sup>74</sup> In turn, BRCA2 is recruited by Partner and Localizer of BRCA2 (PALB2) and the breast cancer susceptibility protein type 1 (BRCA1) to DSB.<sup>141</sup> BRCA2 interacts with both PALB2 and the BRCA1-BARD1 complex, suggesting that all these components are involved in stabilizing the RAD51 nucleoprotein filament during recombination and the filament exchange reaction.

Germline mutations in the BRCA2 gene are associated with hereditary breast and ovarian cancer syndrome (HBOC), which is related to susceptibility to early breast cancer and increased susceptibility to cancers of the ovary, pancreas, stomach, larynx, fallopian tubes and prostate.<sup>142</sup><sup>143</sup> The prevalence of detrimental BRCA gene mutations in the general population is about 0.2%-0.3% (or about 1 in 400). More than 40% of women who inherit a harmful change in BRCA1 or BRCA2 will develop breast cancer during their lifetime, while about 15%-25% of women who inherit a harmful change in BRCA2 will develop ovarian cancer (which includes fallopian tube cancer and primary peritoneal cancer) during their lifetime. Pancreatic cancer, on the other hand, has been diagnosed in 2%-7% of those with detrimental changes in BRCA2. About 15% of those with detrimental changes in BRCA2 will develop prostate cancer by the age of 80 (Figure 12).<sup>144</sup>

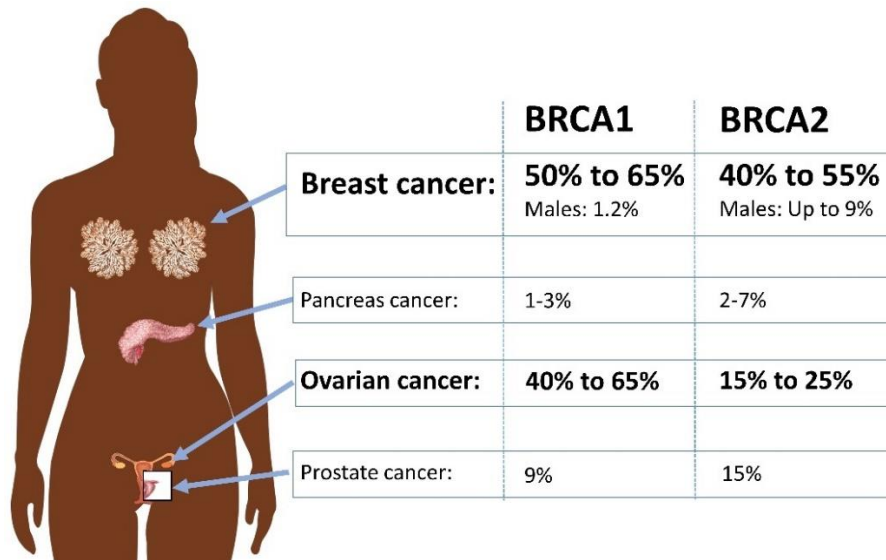


Figure 12. Absolute risk of cancers in BRCA1 or BRCA2 mutation. Adapted from Petrucelli et al. (2023)<sup>142</sup>

BRCA2 contains 3,418 amino acid residues and has several functional domains, mainly described by three available crystal structures of isolated domains and regions, PDB ID 1N0W and 1MJE and EMDB ID 2779.<sup>145, 146</sup> The N-terminal portion of BRCA2 is characterized by a PALB2 binding domain and eight highly conserved motifs of approximately 30 amino acids each, BRC repeats 1-8, which are the primary sites for binding to RAD51 (987-2113 residues) (Figure 13a).<sup>147</sup> In addition, BRCA2 contains a DNA binding domain (DBD), which binds to ssDNA and dsDNA. The DBD domain consists of five portions, an  $\alpha$ -helical domain of 190 amino acids (H), three oligonucleotide binding folds (OB) (OB1, OB2, OB3), which are the binding modules to ssDNA, and a tower domain (TD), which protrudes from OB2 to bind dsDNA (Figure 13b).<sup>148, 149</sup> Finally, at the C terminus, BRCA2 contains a residue Ser3291, a substrate of cyclin-dependent kinase (CDK) phosphorylation, which represents a secondary binding site for RAD51.<sup>140</sup>

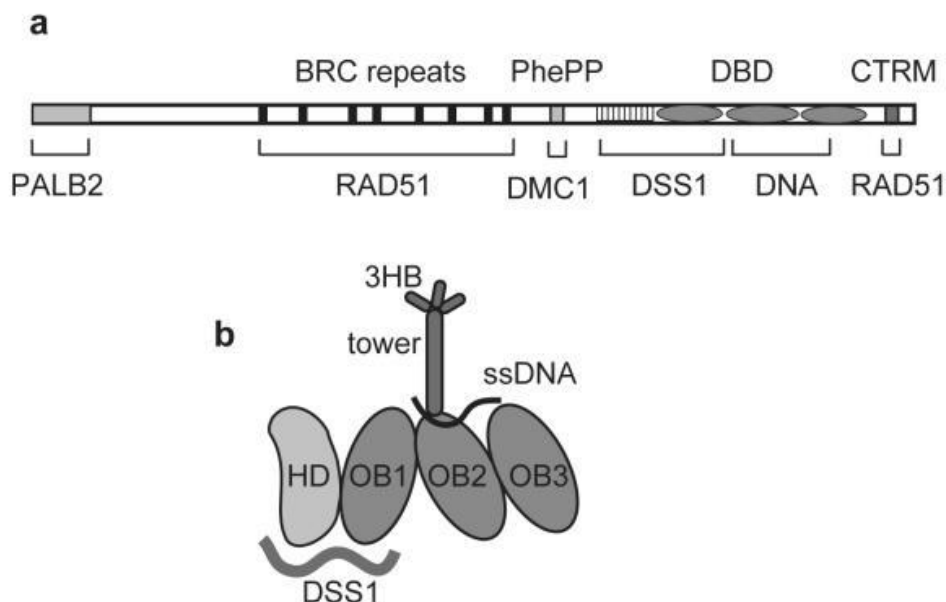


Figure 13. a) BRCA2 primary structure and functional domains; b) scheme of 800 residue DBD domain with the helix-rich domain (HD) followed by the OB folds. Adapted from Holloman W.K. (2011)<sup>149</sup>

### 1.5 Mimicking “BRCAness”: new SL targets in DDR

The canonical definition of “BRCAness” is a defect in homologous recombination repair, mimicking the loss of BRCA1 or BRCA2.<sup>150</sup> Recent work has broadened the mechanistic basis of BRCAness to include regulatory mechanisms causing SL with PARPi.<sup>138</sup> Today, PARPi are studied at the preclinical level in combination with agents that induce a BRCAness or homologous recombination deficiency (HRD) phenotype by directly or indirectly interfering with HR.<sup>28, 151</sup> The goal is to improve efficacy and raise awareness of PARP-resistant tumors and to expand the treatment of PARPi to a much larger subset of BRCA-competent tumors. Many of these emerging mechanisms are now being investigated for inhibition by small molecules, beyond combination with chemotherapy, and the most exemplary studies are being reported.<sup>151</sup>

Combining PARPi with tyrosine kinase receptor inhibitors (e.g. EGFR, VEGFR and FLT3-ITD)<sup>152-154</sup> has been shown to modulate DDR genes via downstream signaling partners such as the RAS/RAF/MEK/ERK and PI3K/mTOR pathways.<sup>155, 156</sup> Furthermore, PARPi have been studied in combination with modulators of epigenetic mechanisms, as they regulate chromatin mobility and thus influence the accessibility of the DDR protein to DNA damage sites, in particular to

DSBs. Indeed, inhibition of certain epigenetic proteins (e.g. BRD4) has been shown to downregulate key DDR proteins.<sup>157</sup> In addition, other combination strategies use inhibitors of alternative DDR pathways, which are relied on due to PARP inhibition. Examples of this approach include the combination of PARPi with ATR inhibitors<sup>158</sup> or with inhibitors of the new Polθ and USP1 targets.<sup>159, 160</sup> Finally, PARPi upregulate PD-L1, as a downstream effect of DDR impairment, and are also correlated with cancer resistance. The upregulation of PD-L1 is positively correlated with the accumulation of DNA breaks. This confirms the therapeutic relevance of combining anti-PD-1/PD-L1 therapies with PARPi (Table 1).<sup>22</sup>

<i>Drug class</i>	<i>Treatment</i>	<i>Cancer population</i>	<i>Phase, Results</i>
<i>Anti-VEGF</i>	Bevacizumab + olaparib <sup>161</sup> /niraparib <sup>162</sup> maintenance	Ovarian cancer responsive to first-line platinum chemotherapy	III/II, PFS: 22/19 months
<i>PI3K/AKT inhibitor</i>	Capivasertib + olaparib <sup>163</sup>	Recurrent endometrial, ovarian, and TNBC	Ib, ORR 19%
<i>EGFR inhibitor</i>	Lapatinib + veliparib <sup>164</sup>	Metastatic TNBC	I, ORR 24%
<i>MEK inhibitor</i>	Selumetinib + olaparib <sup>165</sup>	Advanced solid tumors with RAS pathway alterations	I, ORR 17%
<i>ATR inhibitor</i>	Ceralasertib + olaparib <sup>166</sup>	Recurrent platinum-resistant, PARPi-naïve ovarian cancer	II, ORR 0%
<i>WEE1 inhibitor</i>	Sequential adavosertib + olaparib <sup>167</sup>	Advanced cancer with actionable DDR variants	Ib, ORR 25%
<i>USP1 inhibitor</i>	TNG348 + olaparib <sup>168</sup>	BRCA1 mut. and HRD+ breast and solid tumors	I+II, in progress
	KSQ-4279 + olaparib <sup>169</sup>	Advanced solid tumors	I, in progress
<i>Polθ inhibitor</i>	ART4215 + talazoparib/niraparib <sup>170</sup>	HRD advanced or metastatic solid tumors	I, in progress
<i>Immunotherapy (CTLA-4 or PD-1 inhibitor)</i>	Pembrolizumab + niraparib <sup>171, 172</sup>	Recurrent platinum-resistant ovarian cancer and advanced TNBC	I+II, ORR 18%
	Ipilimumab/nivolumab maintenance + niraparib after platinum chemotherapy <sup>173</sup>	Advanced platinum-sensitive pancreatic cancer	Ib/II, PFS: 60%/21%

*Table 1. Efficacy data for some selected studies evaluating PARP inhibitor combinations to mimic BRCA2 mutation or HRD in tumors.<sup>126, 151</sup> PFS: progression-free survival, ORR: overall response rate, TNBC: triple-negative breast cancer. Adapted from Bhamidipati et al. (2023)<sup>126</sup>*

Among the various therapeutic approaches using small molecules, the therapeutic potential of so-called “fully small molecule-induced SL” is mentioned in our perspective.<sup>151</sup> This paradigm is based on the hypothesis that it might be possible to mimic the effect of germline BRCA2 mutations also by using small organic molecules that disrupt the RAD51-BRCA2 protein-protein interaction (PPI).<sup>174-176</sup>

Indeed, RAD51 impairment was found to be SL with PARPi.<sup>177</sup> Specific miRNAs were found to sensitize cancer cells to olaparib by weakening the expression of RAD51 beyond BRCA deficiency. Regarding pharmacological inhibition of RAD51, several compounds that modulate RAD51 activity in vitro have been identified, most of which modulate its binding to ssDNA. However, the clinical use of RAD51 inhibitors (RAD51i) has been slow, and no clinical studies on any RAD51i have been conducted to date.<sup>178</sup> The mechanism of action of the only putative RAD51i, CYT-0851, currently in clinical trials (NCT03997968), was recently disclosed and attributed to monocarboxylate transporter (MCT) inhibition, thus excluding it as RAD51i.<sup>179</sup>

### **1.5.1 RAD51 protein: structure and functions**

RAD51 is an evolutionarily conserved ATP-dependent recombinase that catalyzes DSB repair through filament exchange reactions during HR. Dynamic RPA exchange facilitates the nucleation of RAD51 to form the nucleoprotein filament. First discovered in yeast, RAD51 is a 43 KDa protein with an  $\alpha$ -helical N-terminal domain (NTD) of approximately 84 amino acids connected by a short helical linker to the C-terminal ATPase domain of 240 amino acids.<sup>67</sup>

NTD has a DNA-binding function by regulating ssDNA and dsDNA recognition. RAD51 has been shown to interact with DNA through its phosphate backbone. Specifically, each monomer of RAD51 binds DNA in triplet clusters by intercalating Arg235 and Val273 extending the DNA length by nearly 1.5 times in comparison to B-DNA. The complex is further stabilized by the interaction of Arg235 with the phosphate backbone of the complementary strand (PDB ID: 5H1B, Figure 14b).<sup>67, 180</sup>

On the other hand, the large C-terminal region includes a Walker A/B motif, responsible for ATP binding and hydrolysis.<sup>181</sup> The presence of ATP promotes the formation of the RAD51 nucleoprotein filament through the interaction of RAD51 monomers, while the hydrolysis of ATP promotes the disassembly of the nucleoprotein.<sup>76</sup> Residues Lys133 and Thr134 from the Walker A motif bind to ATP where loop 315-323 from the adjacent monomer contributes hydrophobic interactions with the adenosine moiety (PDB ID: 5NWL, Figure 14a).<sup>182</sup> The C-terminal region of RAD51 includes residues Met158-Met210 and Met251-Phe259, which form hydrophobic pockets that can accommodate BRCA2 residues to mediate protein-protein interaction (PPI).<sup>145</sup> Finally, the



short bridge connecting the two helical domains, bearing the 86-FTTA-89 motif, appears to play a crucial role in monomer recognition and oligomerization interaction.<sup>180</sup>

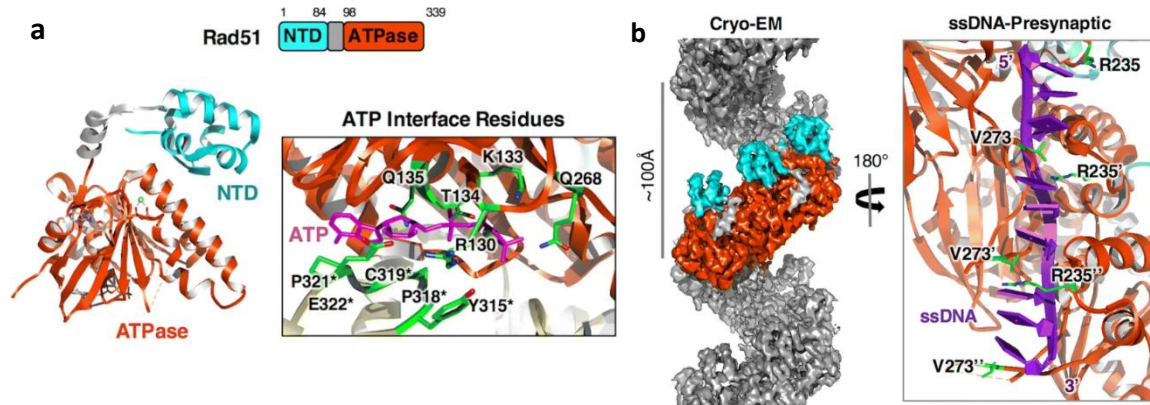


Figure 14. a) Structure of hRad51 in the presence of ATP (PDB ID: 5NWL); b) CryoEM structure of the presynaptic Rad51 filament bound to ssDNA underlying the intercalation of Arg235 and Val273 (PDB ID: 5H1B). Adapted from Sun et al. (2020)<sup>67</sup>

The monomeric RAD51 form is a valuable tool for drug discovery investigations, as it allows for the examination of additional binding sites, interactions with third-party partners or conformational rearrangements. A structure obtained by electron microscopy of the human RAD51 presynaptic complex (PDB ID: 7EJC) was recently published<sup>183</sup> and it contains a larger part of the N-terminal domain than the reference monomeric structure in complex with the BRC4 motif of BRCA2 (PDB ID: 1N0W)<sup>184</sup>. Despite the significantly larger portion of NTD domain shown, it must still be investigated whether the clustered ligand J46, ATP or a portion of RNA present in the reported structure modify the natural structure of the RAD51 monomer and its N-terminal domain, which has been shown to be highly mobile and intrinsically disordered.

RAD51 mediates the repair of DSBs and replication stalling lesions caused by radio- and chemotherapy. Indeed, RAD51 has been found to correlate with poor survival and resistance to chemotherapy and is upregulated in breast cancer, pancreatic cancer, prostate cancer and non-small cell lung cancer.<sup>185-187</sup> Overexpression of RAD51 can cause DNA hyperrecombination, contributing to genomic instability and could turn normal cells into cancerous cells, affecting cancer progression.<sup>188, 189</sup> Targeted inhibition of RAD51 has demonstrated an anticancer effect in several tumors.<sup>190, 191</sup> In addition, reduction of RAD51 expression has been shown to overcome resistance to radio- and chemotherapy. Inhibition of RAD51 activity can be achieved either by



inhibiting the catalytic function of RAD51 or by interfering with the network of interactions established between RAD51 and its partners, including DNA.<sup>190, 192</sup>

#### **1.5.1.1 RAD51 inhibitors**

Several inhibitors have been identified to modulate RAD51 activity in vitro but, despite promising preclinical studies, no clinical studies on any RAD51i have been conducted to date (Figure 15). The natural product halenaquinone is able to inhibit RAD51-dsDNA binding and inhibit the formation of both the D-loop and the ternary complex containing ssDNA, dsDNA and RAD51, which promotes the homologous DNA pairing step.<sup>193</sup> The same results were obtained by Normand *et al.* in 2014 with the compound Chicago Sky Blue (CSB).<sup>194</sup> On the other hand, compound B02 inhibited RAD51 binding to ssDNA, as well as nucleoprotein strand formation and DNA strand exchange activity. B02 had also been shown to increase sensitivity to ionizing radiation and cisplatin in triple-negative breast cancer.<sup>195</sup>

In 2012, chloromaleimide-based RI-1 was shown to form a covalent bond with the thiol group of RAD51's Cys319 leading to irreversible inhibition of RAD51 polymerization during nucleofilament formation.<sup>196</sup> The compound was then optimized to minimize the undesirable side effects of RI-1 by subsequent structure-activity relationship (SAR) studies leading to the RI-2 analogue.<sup>197</sup>

RS-1 had been reported to promote the accumulation of genotoxic nucleoprotein complexes in cancer cells. Stabilization of the RAD51-ssDNA complex caused the accumulation of RAD51 complexes with undamaged chromatin resulting in a toxic effect in tumor cells overexpressing RAD51.<sup>198</sup>

The compounds RI(dl)-1 and RI(dl)-2, on the other hand, had been reported to inhibit the homologous filament exchange activity of RAD51, thereby preventing D-loop formation.<sup>198</sup>

Downregulation of RAD51 protein expression can also be triggered by small molecules: methotrexate had been shown to decrease RAD51 foci formation after irradiation in the human osteosarcoma (HOS) cell line.<sup>199</sup> Abexinostat also showed the same results and reduces the HR response to DNA DSBs caused by chemotherapy in human colorectal cancer (HTC116).<sup>200</sup> Lastly, by downregulating mRNA expression in several breast carcinoma cell lines, prodigiosin showed a downregulatory effect on the level of RAD51 protein.<sup>201</sup>

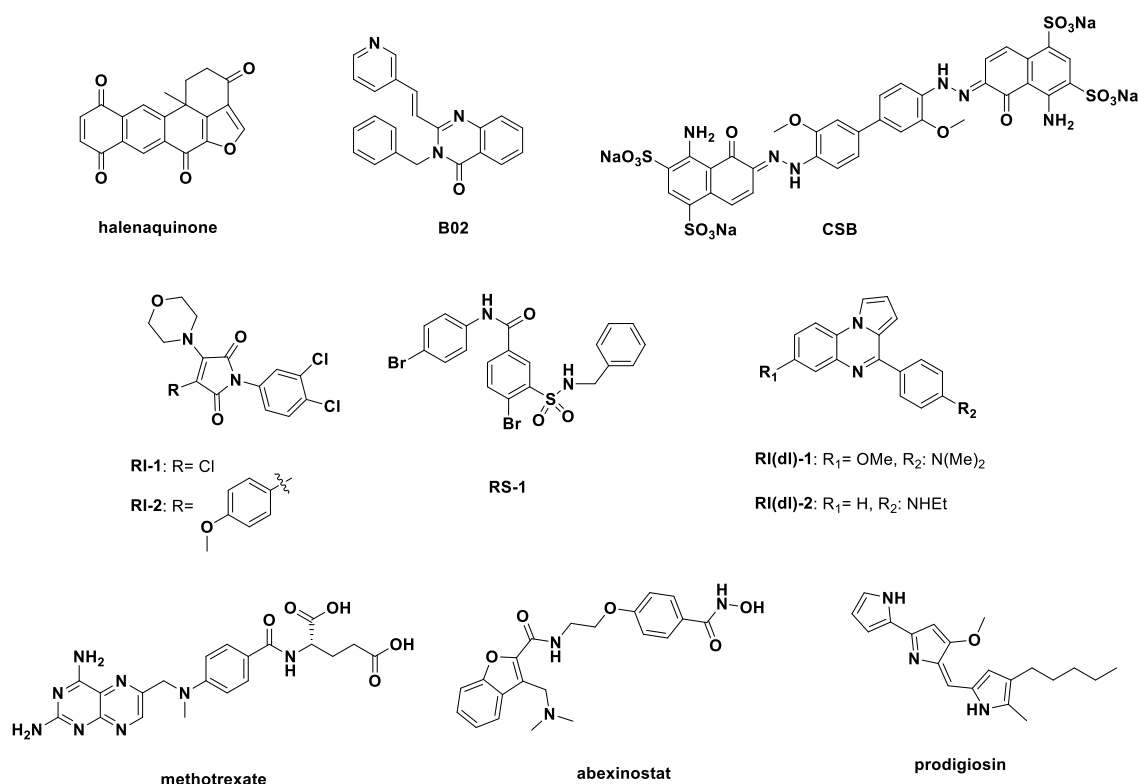


Figure 15. Small molecule inhibitors targeting RAD51.<sup>190, 202</sup>

### 1.5.2 RAD51-BRCA2 protein-protein interaction: functions and inhibition

As previously mentioned, during HR, BRCA2 recruits the recombinase RAD51 to the site of DNA damage and mediates its loading and stabilization on RPA-ssDNA to promote homology searching, strand invasion and strand exchange reactions. Full-length BRCA2 has a binding capacity of at least six monomers of RAD51.<sup>74, 203</sup>

BRCA2 repeats known as BRC1-8 allow it to bind the central region of RAD51. Co-operation between BRCs results in the modulation of RAD51-DNA interaction and RAD51 functions, ensuring the efficiency and regulation of crucial HR steps.<sup>147</sup> The eight BRC domains have different binding affinities for RAD51 and are therefore divided into two distinct classes, the BRC1-4 repeats with the strongest affinity for RAD51 (1:1 binding stoichiometry) and the BRC5-8 repeats with the weakest affinity for RAD51 and no effect on either ATPase activity or RAD51-dsDNA inhibition (1:100 approximate binding stoichiometry).<sup>204</sup> Indeed, BRC1-4s can block RAD51-mediated ATP hydrolysis and inhibit the formation of the RAD51-dsDNA nucleoprotein.

On the other hand, BRC5-8 show significantly higher affinity when RAD51 is in complex with ssDNA and are therefore functional in stabilizing the nucleoprotein strand during HR.<sup>204</sup>

The proposed mechanism shown in Figure 16 is therefore as follows: in the presence of a DSB, after DNA resection, BRCA2 interacts with the free form of RAD51 via BRC1-4s, altering the conformation of RAD51 to enhance binding to ssDNA. Due to their high affinity for RAD51, BRC1-4 kinetically modulate the nucleation of RAD51 on ssDNA, preventing association with dsDNA and inhibiting ATP hydrolysis. After nucleation, BRC5-8 repeats bind and stabilize the RAD51-ssDNA complex, guiding its growth in both directions. During strand growth, RPAs are displaced by ssDNA and BRCA2 dissociates. The nucleofilament of RAD51 grows to form a complex, bound to ATP, and performs the HR.<sup>147, 204</sup>

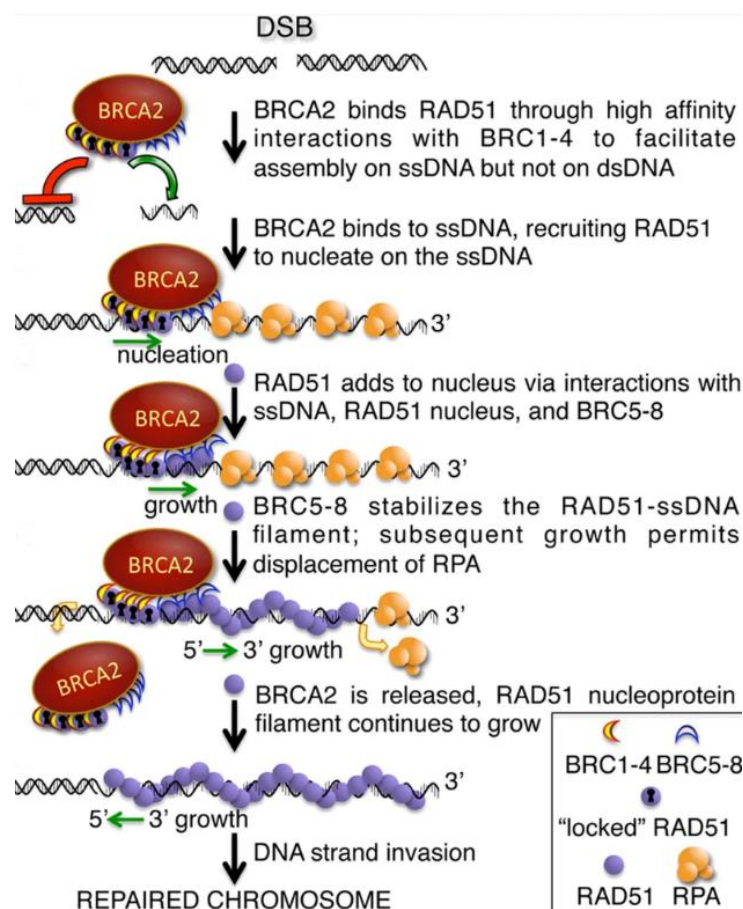


Figure 16. Proposed model for the role of the BRC repeats in the context of the entire BRCA2 protein in DSB repair. Adapted from Carreira et al. (2011)<sup>204</sup>

In a recent study by F. Schipani and colleagues<sup>205</sup>, it was shown that, in the absence of DNA, recombinant RAD51 has an intrinsic tendency to form fibrils with a helical organization and size that depends on protein concentration. After RAD51-BRC4 binding, the peptide reverses the fibrillar self-association of RAD51. Indeed, during cytosolic recruitment of RAD51, BRCA2 can gradually disassemble fibrils from their termini rather than through attachments at random positions along the fibril. Moreover, this interaction is preserved in the absence of DNA.

In a study conducted by my colleague F. Rinaldi *et al.*<sup>206</sup>, SAXS studies on monomeric RAD51 and the RAD51-BRC4 complex suggest that the N-terminal domain of RAD51 is an intrinsically disordered region and that, upon binding of BRC4 to RAD51 fibrils, it shifts and reorganizes into an intrinsically disordered region. This behavior provides a clear explanation for the difficulties in obtaining a full-length 3D structure of RAD51 in complex with BRC4.

Despite these difficulties, in 2002 Pellegrini *et al.*<sup>145</sup> reported the high-resolution crystal structure of the RAD51-BRC4 monomer complex (PDB ID: 1N0W, Figure 17) without RAD51 N-terminal region and 86-FTTA-89 domain of RAD51 required for oligomerization. Among the eight BRC repeats, BRC4 has the highest binding affinity for RAD51, the strongest inhibitory effect on the DNA-dependent ATPase activity of RAD51 and the strongest stimulatory effect on the formation of the RAD51-ssDNA complex.<sup>204</sup>

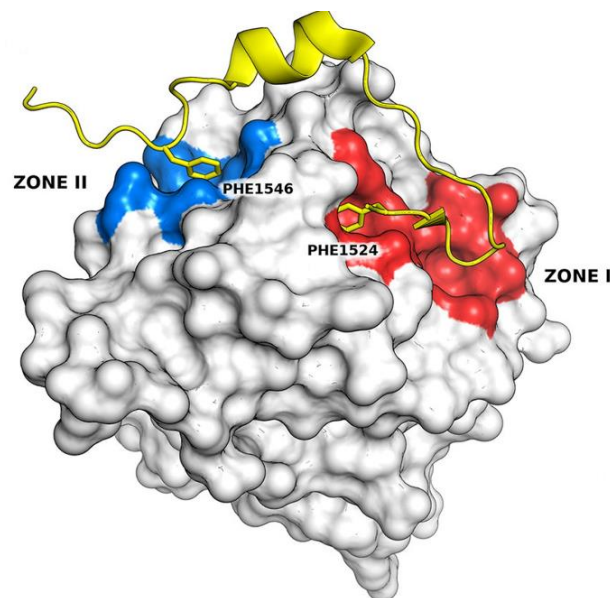


Figure 17. RAD51-BRC4 complex (PDB ID 1N0W). RAD51 is represented as a surface (grey), BRC4 as a cartoon (yellow). The two hot spots of the interaction between the proteins (F1524 and F1546) are highlighted in sticks (zone I in red, zone II in blue). Adapted from Bagnolini *et al.* (2020)<sup>175</sup>

The crystal structure shows two crucial tetrameric clusters of BRC4, FXXA and LFDE, interacting with two distinct hydrophobic pockets of RAD51. The two pockets on RAD51, known as zone I (86-FTTA-89) and zone II (1545-LFDE-1548) respectively, can be defined as hot spots of the RAD51-BRCA2 interaction.<sup>207</sup> In detail, RAD51-BRC4 covers an interface area of 2.026 Å, over a sequence of 28 amino acids, where hydrophobic interactions are prevalent and the amino acids Phe1524, Ala1527, Leu1545 and Phe1546 of BRC4 are mainly involved in the interaction.<sup>145</sup>

Zone I of RAD51 may host the 86-FTTA-89 of another RAD51 molecule and has in fact also been described as a RAD51 oligomerization site. Therefore, the FTHA domain of BRC4 is a molecular mimic of the RAD51 oligomerization sequence and is considered a potential antagonist of RAD51 oligomerization during HR. In the previously cited study by F. Schipani, it was shown that the peptide BRC4myr prevents the nuclear localization of RAD51 in the case of DNA damage, affecting cell proliferation after treatment with DNA-damaging agents. The absence of RAD51 in the nucleus makes cancer cells unable to repair damaged DNA, potentially leading to SL.<sup>205</sup>

As a second PPI hot spot, the 1545-LFDE-1548 motif of the C-terminal domain of BRC4 involves zone II, away from the oligomerization interface. Specifically, residues Leu1545 and Phe1546 insert between helices A4 and A5 of RAD51, buried by residues Leu204, Tyr205, Ser208, Met251, Arg254, Leu255, Glu258 and Phe259. Furthermore, mutation of the LFDE binding pocket was associated with failure to assemble RAD51 foci and cellular lethality.<sup>207</sup>

Since the RAD51-BRCA2 interaction is essential for the recruitment and nucleation of RAD51 at the site of DNA damage during HR, PPI disruption between RAD51 and BRCA2 has been proposed as a strategy to sensitize cancer cells to chemotherapy and to PARPi use in cases of acquired resistance to PARPi by exploiting the SL between BRCA2 and PARP.<sup>174</sup> Moreover, beyond the specific PARP-BRCA2 SL pair, this approach provides the basis for future combination strategies targeting SL pairs involved in DDR.

The first RAD51-BRCA2 PPI disruptors were identified in 2013 by Zhu *et al.*<sup>208</sup> The authors identified two phenyl-sulphonyl indolyl-isoquinoline compounds, IBR-1 and IBR-2, that can disrupt PPI and have promising anti-cancer activity (Figure 18). In addition, IBR-2 has been shown to impair HR and reduce the formation of RAD51 foci in breast cancer cells (MCF-7) after irradiation.<sup>209</sup>

In 2021, Scott *et al.*<sup>210</sup> identified CAM833 (Figure 18) as a potential RAD51-BRCA2 PPI disruptor able to bind the RAD51 oligomerization pocket (zone I) through a structure-led fragment-based approach using an in-house developed humanized RadA-RAD51 construct (HumRadA22F). CAM833 reduced the assembly of RAD51 foci at the DNA damage site and HR was reduced in non-small cell lung carcinoma (NSCLC) cell lines. Finally, CAM833 increased IR-induced cytotoxicity and acted synergistically with PARP1i.<sup>210</sup>

Considering the RAD51-BRC4 complex (PDB ID 1N0W), Virtual Screening (VS) campaigns on both RAD51 zones I and II have recently been conducted by our research group.<sup>174, 175</sup> Following SAR studies of a triazole-based compound identified by VS on zone I, derivative ARN21560 inhibited the RAD51-BRCA2 interaction, increased the formation of DNA double-strand breaks in combination with olaparib, and significantly increased the therapeutic power of olaparib in BRCA2-competent pancreatic cancer cells (BxPC-3). Unfortunately, the SL paradigm with ARN21560 has not been fully reproduced due to its low potency (HRi < 40%) and low solubility that do not allow for a drug-like profile of the molecule of interest.<sup>176</sup> On the other hand, following VS on zone II and SAR optimization, a dihydroquinolone pyrazoline derivative ARN24089 showed inhibition of the RAD51-BRCA2 protein-protein interaction. The compound inhibited HR activity and acted synergistically with olaparib to trigger SL in BxPC-3 cells. However, the low solubility of ARN24089 affected its metabolic and pharmacokinetic (DM/PK) profile, preventing its further study in cancer models *in vivo* (Figure 18).<sup>175</sup>

The recent isolation of a fully human RAD51 monomer<sup>206</sup> has enabled ARN24922 to be validated as a PPI disruptor resulting from a <sup>19</sup>F NMR fragment-based screening on human wild-type RAD51, followed by medicinal chemistry optimization (Figure 18).<sup>211</sup> ARN24922 showed HR inhibition in BxPC-3 cells and its combination with talazoparib also showed efficacy in 3D pancreatic cancer models. Despite the promising results, biophysical studies on ARN24922 could not confirm the proposed binding on one of the RAD51-BRCA2 PPI zones, so further investigations will be conducted to understand the real mechanism of interaction with RAD51 of this promising compound.

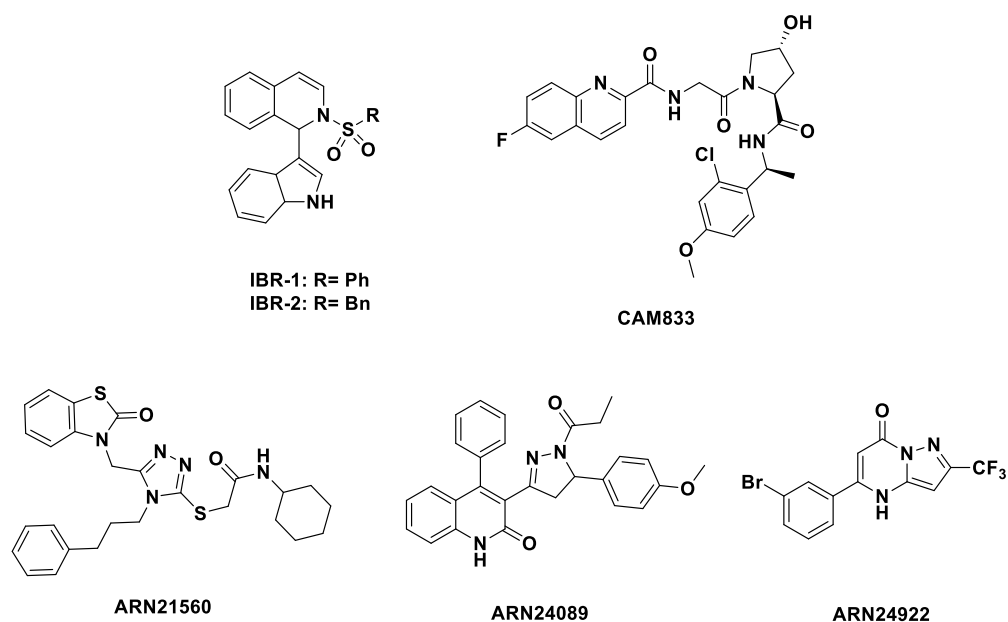


Figure 18. Inhibitors of the RAD51-BRCA2 interaction<sup>151, 176, 208</sup>

Finally, despite promising preclinical results, the therapeutic potential of RAD51-BRCA2 interaction inhibitors and their combination with PARPi in the clinic has been hampered due to the toxicity in normal tissues that may result from systemic inhibition of both RAD51 and PARP1. However, cancer cells are more heavily dependent on DNA repair mechanisms than healthy cells due to their genetic instability. Consequently, the combination of PARPi and RAD51-BRCA2 inhibitors may affect healthy cells far less than cancer cells, offering a possibility of selectivity. In fact, this specific chemically induced SL can be exploited in several scenarios: (i) to treat patients with acquired resistance to PARPi, mainly due to restoration of the mutated BRCA2 gene or overexpression of RAD51; (ii) to treat tumors with mutations that have an SL relationship with BRCA impairment.

### 1.5.3 RAD52 protein: structure and functions

It is well known that cancer cells, due to intrinsic mutations in their genome and the consequent inactivation of many of the canonical DNA repair mechanisms, must rely on alternative DNA repair pathways to survive.<sup>212</sup> In recent years, it has emerged that RAD52, a DNA/RNA-binding protein, has an important oncogenic role since it mediates many of these alternative pathways that can act as backup.<sup>213</sup> Although not normally essential for cell survival, RAD52 is essential in tumor conditions in which other DSB repair-related proteins are mutated.<sup>214</sup> For instance, the inhibition of RAD52 induces SL in many tumor cells deficient in DNA repair-related proteins such as BRCA1/2, PALB2 and paralogues of RAD51.<sup>215</sup> Among these DSB repair mediator proteins, the SL relationship between RAD52 and BRCA1/2 in cells has been extensively studied in recent years.<sup>216</sup> RAD52 has thus become an attractive target for SL-based anticancer therapy to pursue selectivity in tumors lacking BRCA1/2 and in cells mimicking drug-induced “BRCAness”.<sup>151</sup>

As already mentioned, RAD52 is involved in DDR mechanisms essential to cancer cell survival and the main functions are summarized as follows. In HR, RAD52 might be able to lead RAD51 loading by acting as a backup for BRCA2 in mediating RAD51 activity.<sup>217</sup> RAD52 might also play a role in second end capture after D-loop formation.<sup>218</sup>

During SSA however, RAD52 plays a key mediator role as it is recruited to the resected DNA ends to promote their annealing and recognize the ssDNA homology region (<30 base pairs). RAD52 also appears to stimulate the nuclease activity of ERCC1-XPF.<sup>55, 219</sup>

During DNA replication, cells can suffer DNA damage. This damage can occur at the replication fork site, leading to stalling and, if prolonged, fork collapse.<sup>220</sup> RAD52 is involved in fork protection, acting as a gatekeeper for the replicative fork state. This prevents MRE11-mediated unscheduled degradation and ensures that fork-reversal enzymes only charge when necessary.<sup>221</sup> RAD52 also takes part in the fork-break mechanism for fork stalling.<sup>222</sup>

RNA-dependent DNA repair is an HR sub-pathway that uses RNA transcripts as an alternative template for DSB repair and is active during G0 and G1 phases. This mechanism has been described as RAD52-dependent in both yeast and human cells.<sup>223</sup> Teng and colleagues suggested that RAD52 plays a role in transcription-coupled homologous recombination (TC-HR).<sup>224</sup> Here,



RAD52 can be recruited to the R-loop (three-stranded DNA:RNA hybrids) to help load RAD51 onto the DSB site in a BRCA1/BRCA2-independent manner.<sup>224</sup>

RAD52 also appears to play a role in regulating the balance between single-strand break repair (SSBR) and double-strand break repair (DSBR) mechanisms.<sup>225</sup>

### *RAD52 structure*

Human RAD52 is a 47 kDa protein of 418 amino acids that form multimeric, ring-shaped functional units. Its N-terminal domain (1-208 AA) comprises the oligomerization domain and DNA binding domain,<sup>226</sup> while its C-terminal domain contains the RAD51 binding site and the replication protein A (RPA) binding site (Figure 19A).<sup>227</sup> A 3.5 Å cryo-EM structure of full-length (FL) RAD52 has recently been published (PDB ID: 8BJM), suggesting that the oligomerization state of full-length RAD52 is undecameric, as for the truncated N-terminal form of the protein, with, however, a disordered C-terminal domain (Figure 19B).<sup>228</sup>

The FL rings of RAD52 tend to form even higher molecular weight (MW) superstructures that interact with other protein functional units in a stacked or flanking manner. The tendency to form such high MW superstructures increases in the presence of DNA.<sup>56, 229</sup> The crystal structure of the N-terminal domain of RAD52 shows a ring-shaped, mushroom-like undecamer with a ‘stem’ and a ‘domed cap’.<sup>226</sup> There is a negatively charged surface at the top of the flat, domed cap and a positively charged surface at the bottom of the ring, between the stem and the hairpin loop, which is the first DNA binding site of the protein. The DNA coils along the outer part of the undecameric ring of RAD52, fitting into this positive gap (Figure 19C).<sup>230</sup>

Both the RAD52 FL and RAD52 N-terminal domains have high thermal stability.<sup>231</sup> This characteristic is probably related to their oligomeric state and their propensity to form ring complexes with higher PM. In particular, although the RAD52 N-terminal and RAD52 FL domains have a similar ring structure, the propensity to form high MW superstructures is greater in the RAD52 FL domain than in the RAD52 N-terminal domain.<sup>229</sup> This may be due to the fact that the C-terminal portion of the domain favors intermolecular bonds and hydrophilic interactions between different protein functional units.<sup>232</sup>

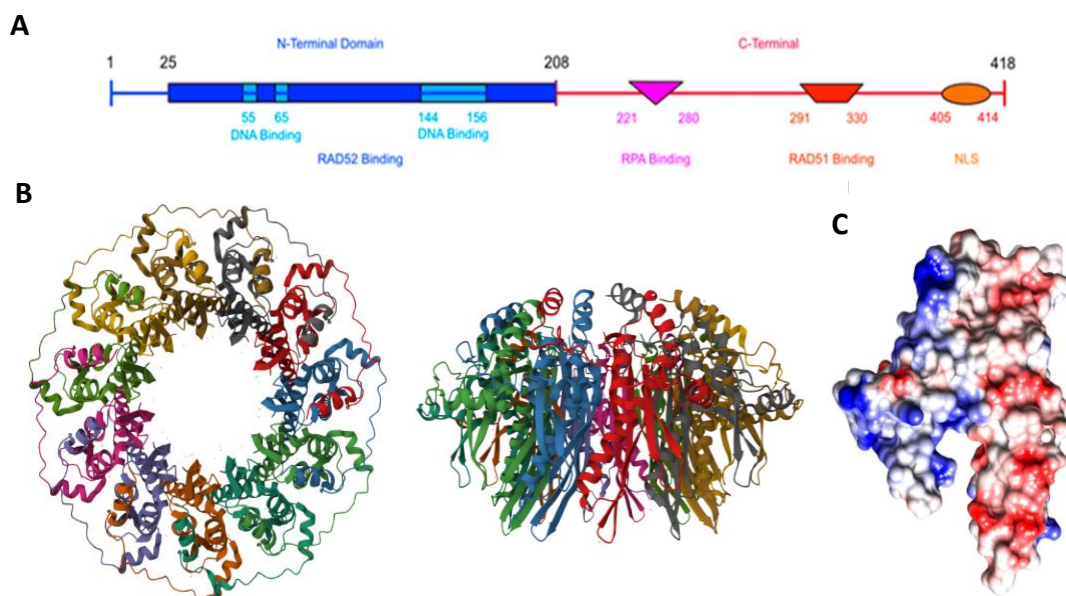


Figure 19. A) Domain map of human RAD52; B) Side and bottom views of the mushroom-like cryo-EM structure of the undecameric ring of FL-RAD52 (PDB ID: 8BJM);<sup>233</sup> C) N-terminal RAD52 monomer surface electrostatic potentials (PDB 1KN0). Adapted from Balboni et al. (2023)<sup>56</sup>

### 1.5.3.1 RAD52 inhibitors

The SL relationship between RAD52 and BRCA1/2 has been extensively studied in cells in recent years.<sup>214, 216</sup> Researchers have devoted considerable effort to identifying and characterizing RAD52 inhibitors for SL strategies in tumors with BRCA1/2 depletion or drug-induced BRCA1/2 depletion. But to date, there are no FDA-approved RAD52i on the market and they are not yet reported to be in clinical development. However, the reported inhibitors suggest that the most druggable regions of the protein are the ssDNA binding domain and the oligomerization interface, which are interconnected.<sup>56</sup> The data collected suggest some general guidelines for the rational design of the RAD52i. In the following, the most recent RAD52i are described, and the main positive and negative features are reported (Figure 20).

#### *F79 peptide aptamer*

In 2013, using computational methods, the Skorski group<sup>234</sup> designed the peptide aptamer F79 containing the 13-amino acid sequence surrounding Phe79 of RAD52, an essential amino acid in RAD52-DNA binding and RAD52 proton-proton hydrophobic interactions. Treatment with F79

resulted in a significant abrogation of RAD52-DNA binding activity. F79 selectively killed BRCA-deficient leukemic cells with a low risk for normal cells ( $EC_{50} < 5 \mu M$ ). Treatment with F79 also induced SL in breast, pancreatic and ovarian cancer cells with BRCA1/2 mutation and exerted synergistic effects with imatinib (approved for BCR-ABL1-positive leukemia) and ATRA (for PML-RAR-positive leukemia).<sup>234</sup> However, there have been no further reports on subsequent development or administration studies with this peptide.

### *6-OH-DOPA*

In 2015, the Chandramouly group<sup>235</sup> discovered 6-OH-DOPA, the first small-molecule RAD52i, through an HTS of a library of drug-like compounds (Sigma Lopac), using the Fluorescence Polarization (FP) method to assess their inhibition of the DNA-RAD52 interaction. 6-OH-DOPA also inhibited SSA with no or little effect on other mechanisms such as HR and NHEJ in BRCA-competent cells. 6-OH-DOPA selectively inhibited cell proliferation in BRCA1-depleted triple negative breast cancer (TNBC) cells and in BRCA-deficient AML and CML patient cells.<sup>235</sup> Despite these promising results, 6-OH-DOPA is not suitable for cancer therapy because it is a dopaminergic toxin that contributes to Parkinson's disease and the degeneration of mitral neurons.<sup>236</sup>

### *D-I03*

In 2016, Huang *et al.*<sup>237</sup> used an HTS with a fluorescence quenching assay and found D-I03 to be a promising RAD52i. The compound showed a high inhibitory effect on D-loop formation *in vitro* on several BRCA1/2-deficient cell lines and on BRCA1-deficient CML cells from patients. In addition, D-I03 inhibited RAD52-mediated SSA foci formation after treatment with cisplatin.<sup>237</sup> The Skorski group subsequently demonstrated the efficacy of D-I03 also *in vivo*: D-I03 was effective in reducing the growth of BRCA1-deficient xenograft tumors in mice, and its effect was even more pronounced in combination with PARP1i talazoparib.<sup>212</sup> Unfortunately, the thiourea scaffold of D-I03 had disadvantages such as poor solubility and metabolic and chemical instability.<sup>238</sup>

### *Z56 e Z99*

In 2016, Hengel *et al.*<sup>239</sup> identified epigallocatechin (EGC), a natural compound that competes with ssDNA to bind to RAD52, by FRET-HTS assays. EGC caused a reduction in cell viability in

cells with BRCA1/2 depletion. Again, despite promising biological results in vitro, EGC and its analogues had poor ADME properties, largely due to low intestinal absorption.<sup>240</sup> Very recently, Bhat *et al.*<sup>241</sup> attempted to overcome the ADME challenges associated with EGC to produce new RAD52i. After careful study of the pharmacophores of EGC, six distinct chemical scaffolds were identified that occupy the same physical space of RAD52 as EGC. The six compounds were all efficient RAD52i, particularly against the RPA-RAD52-ssDNA complex ( $IC_{50} \sim 8-96 \mu M$ ). Among the selected inhibitors, Z56 and Z99 showed enhanced activity in cell viability assays. Z56 was selective for RAD52 compared to RPA in vitro and selectively killed BRCA mutant cells. In contrast, Z99 inhibited both proteins in vitro and showed toxicity towards wild-type BRCA cells. Z99 showed excellent drug-like profile similarity and was selected for scaffold expansion, resulting in potent and selective RAD52i Z58-54 and Z58-87 with  $IC_{50}$  values in the low micromolar range able to discriminate between BRCA1/2-mutated and BRCA-competent cells.<sup>241</sup> Further rounds of chemical exploration could be a promising strategy to obtain more potent and selective RAD52i.

#### *C791-0064*

In 2021, Yang *et al.*<sup>242</sup> conducted a VS campaign with a previously used computational algorithm but selected a new binding pocket (e.g. self-association domain). C791-0064 was the most promising new RAD52 inhibitor of the 66,608 compounds examined. Docking studies suggested that C791-0064 docked to the RAD52 self-associative binding site. BRCA2-deficient cancer cell lines were more sensitive to treatment with C791-0064 in clonogenic and cell viability assays than wild-type BRCA2 cancer cells, also showing more apoptosis and DNA damage. In vitro assays showed that C791-0064 disrupted the oligomeric form of RAD52 and inhibited its ssDNA annealing activity.<sup>242</sup> Further studies will be conducted on this RAD52i.

#### *Quinacrine, mitoxantrone and doxorubicin*

In a different approach to the discovery of RAD52i, a recent study in 2021 targeted the RPA-RAD52 interaction rather than RAD52 oligomerization or DNA binding sites.<sup>243</sup> Using HTS based on FluorIA, the researchers identified quinacrine, mitoxantrone and doxorubicin as the most potent compounds, with an  $EC_{50}$  of  $97.7 \mu M$ ,  $29.7 \mu M$  and  $10.1 \mu M$ , respectively. Using co-immunoprecipitation of RAD52 and RPA, mitoxantrone disrupted the RPA-RAD52 interaction. All three compounds inhibited the cell viability of several HR-deficient ovarian and breast cancer

cell lines, including some PARPi-resistant cell lines, at a higher rate than their HR-competent counterparts.<sup>243</sup> These results indicate that RPA-RAD52 interaction could be a promising therapeutic target for HR-deficient cancer cell lines. Also in this case, further investigations will be conducted.

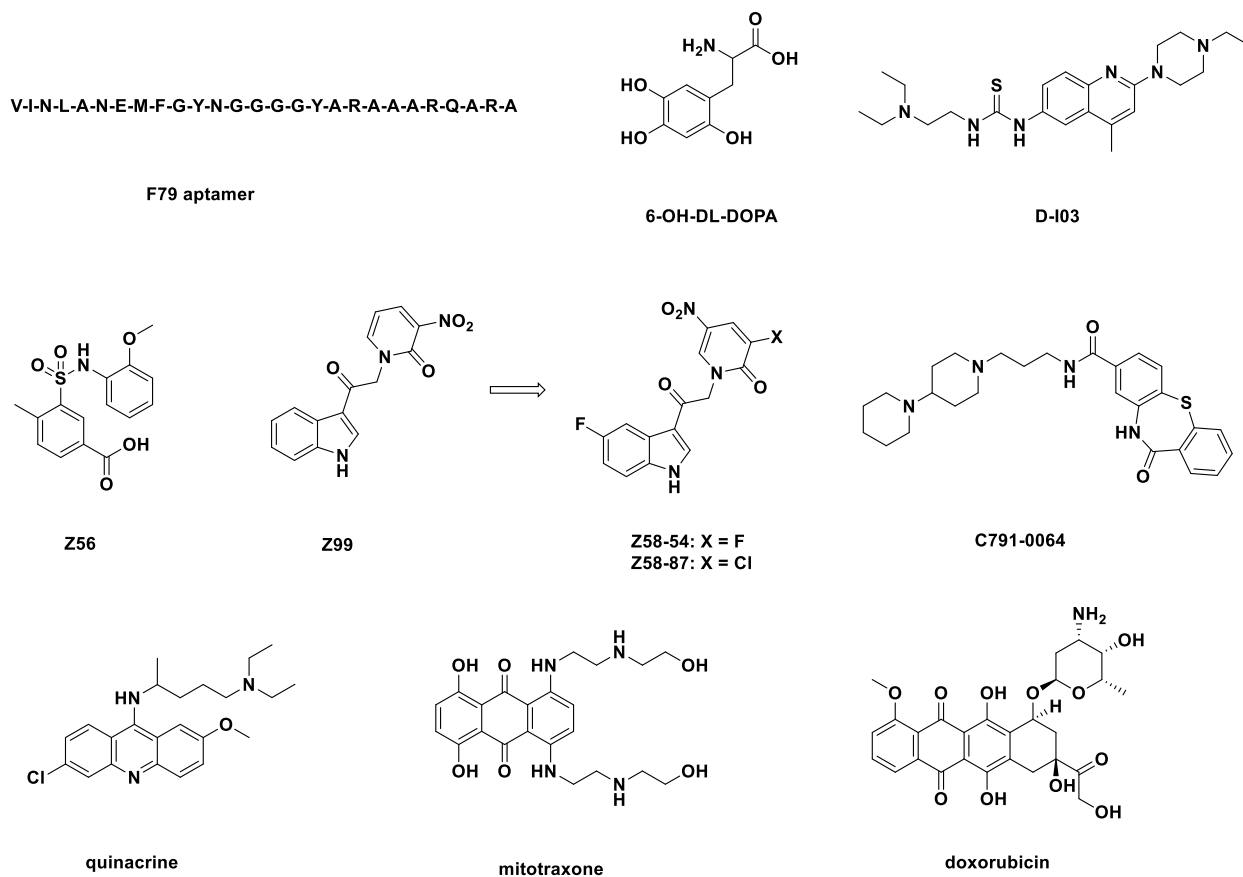


Figure 20. Structures of most recent and relevant RAD52 inhibitors.<sup>56, 151</sup>

## 2. AIM OF THE THESIS

My PhD project in collaboration with the Italian Institute of Technology (IIT) focused on the development of small molecules to pursue a “fully small molecule induced SL” with PARP inhibitors in pancreatic cancer. This concept was introduced by our research group to overcome the PARPi resistance and expand PARPi therapy to BRCA2-competent patients.<sup>174, 176</sup> As mentioned in the introduction, DNA repair pathways offer the opportunity to apply SL in cancer therapy. The best example is the clinical use of PARPi in patients with BRCA1/2 mutations (Figure 21A). PARP is crucial for repairing DNA SSBs, whereas BRCA2 is important for repairing DNA DSBs by HR. The simultaneous impairment of both repair mechanisms results in SL. A key role for BRCA2 in DDR is to recruit RAD51 to initiate HR.<sup>174-176</sup> Our hypothesis was that, by using small molecules to disrupt RAD51-BRCA2 PPI, it could be possible to mimic the effect of BRCA2 germline mutations, in turn inducing a BRCAness-like phenotype. Ultimately, this would widen the population of patients eligible for the treatment with PARPi. Moreover, RAD51-BRCA2 disruptors could also represent a therapeutic option for patients who developed resistance to PARPi. This resistance was mostly due to either restoration of non-mutated BRCA2 protein or overexpression of RAD51, which in turn increased HR. Ultimately, RAD51-BRCA2 inhibitors could be used as a chemosensitizer for radiotherapy and DNA-damaging agents (Figure 21B).

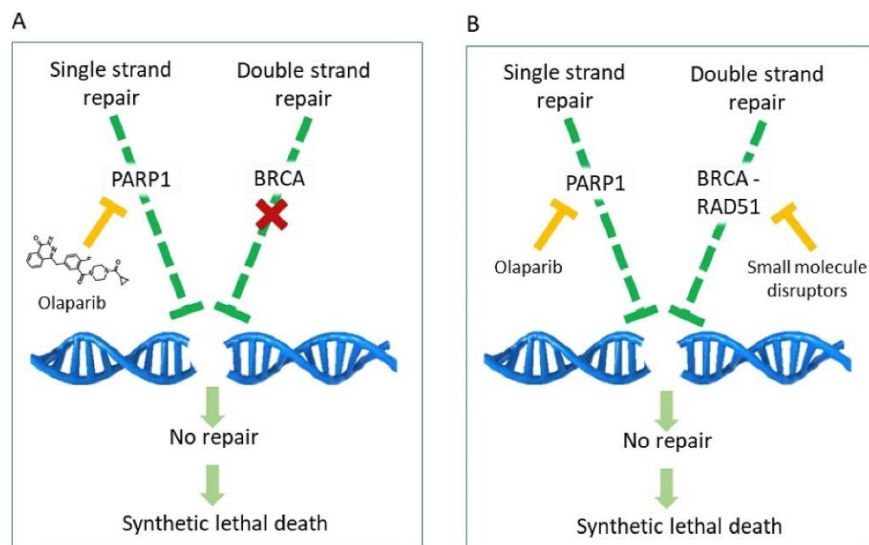


Figure 21. A) SL induced by olaparib in BRCA-defective cancer cells. B) Fully small molecule induced SL by combining olaparib and RAD51-BRCA2 PPI disruptors. Adapted from Roberti et al. (2019)<sup>176</sup>

As a model for cell-based experiments, we used pancreatic adenocarcinoma for its clinical relevance. In the case of pancreatic cancers, germline mutations occur in about 10-20% of patients, with mutations in BRCA1 and BRCA2 genes as the most common ones.<sup>244, 245</sup>

To identify RAD51-BRCA2 inhibitors, we used the available X-ray crystallographic of the fourth BRC repeat (BRC4) in complex with the catalytic domain of RAD51 (PDB ID 1N0W).<sup>145</sup> BRC4/RAD51 interaction is mediated by two critical hot spots, zone I and zone II respectively, considered druggable sites for small molecules. Indeed, both RAD51 pockets were studied by our group for the structure-based design of potential PPI inhibitors.<sup>174-176</sup> The most promising results were observed targeting Zone II with a dihydroquinolone derivative, **ARN24089** (Figure 18). This result supported the hypothesis that one can trigger SL using only small organic molecules. However, the poor drug-like profile of **ARN24089** hampered its advancement to *in vivo* studies. Therefore, the next step was the development of new classes of PPI inhibitors targeting Zone II. In this context, the main part of my PhD project aimed to synthesize and optimize analogs of the quinolinic-based derivative **ARN22142** (named compound **1** in the following Chapters) (Figure 22A), a promising *hit* compound previously identified by our group through a VS campaign on zone II. My aim has been to synthesize a small library of analogs of the *hit* **ARN22142** to conduct structure-activity relationship (SAR) studies by focusing on the most important interactions with RAD51 residues of zone II. The objective was to find a promising lead compound that was able to inhibit the RAD51-BRCA2 interaction, reduce HR and induce cell death in combination with olaparib in BRCA2-proficient pancreatic cancer cell lines, fully replicating the SL paradigm.

To further develop the proposed concept of “fully small molecule induced SL”, we focused on the observation that, in proliferating cells, alternative repair mechanisms can take place when the conventional BRCA2/RAD51 driven HR is inhibited. This includes RAD52-dependent HR pathway and single-strand annealing (SSA), in which RAD52 is the main player. These alternative pathways can protect BRCA1/2 defective tumor cells from SL with PARP inhibition, indicating RAD52 as an attractive target for BRCA defective tumors. For this reason, we hypothesized that the simultaneous inhibition of RAD52, PARP and RAD51-BRCA2 interaction might result in a robust three-pathway SL in tumor cells maintaining BRCA function. Additionally, since deletion of RAD52 (unlike RAD51) does not lead to death of normal cells, SL approaches based on RAD52 inhibition have a higher potential of reduced toxicity.

In this context the second part of my PhD project refers to the six months experience I spent in the laboratory of Therapeutic Proteins and Peptides (LPPT) of Professor Heinis in EPFL of Lausanne, Switzerland. The group focuses on the development of cyclic peptide libraries that are analyzed through high-throughput screening platforms on proteins proven to be undruggable or difficult-to-inhibit targets by considering their PPI interactions.<sup>246-249</sup>

In the LPPT lab, my goal was to synthesize a small library of dipeptides able to disrupt the interaction between monomers of RAD52 that arrange in a ring-shaped undecameric structure<sup>56</sup> Choosing among all the natural and non-natural amino acids (AA) in Professor Heinis' lab, a big library of dipeptides was created by coupling different AA with the specific program DataWarrior. The designed dipeptides were docked in a VS conducted by the computational IIT unit against a previously identified RAD52 protomer-protomer interaction pocket. The VS selected 11 compounds with promising docking scores in binding RAD52. My work aimed to conduct an in-parallel synthesis of the 11 dipeptides selected by VS, optimizing the synthetic strategy of solid-phase peptide synthesis by carefully choosing the resin, the scale, and the best conditions for the fundamental steps in peptide synthesis. The final dipeptides were analyzed for their binding to RAD52 in biophysical and biochemical tests.<sup>241, 250</sup> The expected outcome of the screening was to identify dipeptides able to disrupt the interaction between RAD52 monomers, representing a novel approach for RAD52 inhibition and opening to new drug discovery campaigns targeting RAD52.

For clarity, my doctoral research activity focused on the design and synthesis of small molecules and non-natural dipeptides. Biochemical, biophysical and biological profile evaluations were carried out in the context of the research group. Details of the test protocols are given in the appendix.



### 3. Part I: STRUCTURE-BASED DESIGN APPROACH TO THE IDENTIFICATION OF RAD51-BRCA2 PPI DISRUPTORS

To identify potential PPI disruptors in recent years, my research group conducted a successful VS campaign using libraries of compounds from ZINC on the crystallographic structure of the RAD51-BRC4 complex with PDB ID 1N0W. RAD51-BRC4 interaction occurs in two different hydrophobic pockets: zone I (FxxA motif) and zone II (LDfE motif). Both pockets were considered for the design of potential inhibitors.<sup>174-176</sup> Targeting Zone II has so far produced compound **ARN24089** (Figure 18), the most effective PPI inhibitor of RAD51-BRCA2, which was also sufficiently potent to trigger SL in combination with olaparib in BxPC-3 pancreatic cancer cells.<sup>175</sup> Unfortunately, compound **ARN24089** showed low kinetic solubility, which did not allow studies of metabolic and pharmacokinetic (DM/PK) profile, preventing its further study in cancer models *in vivo*.<sup>175</sup>

In this context, the main part of my PhD project focused on the development of RAD51-BRCA2 PPI disruptors that could show promising properties and would avoid possible solubility problems once optimized in their binding and cell viability properties in combination with PARPi.

#### 3.1 Hit identification and optimization targeting Zone II

As a first step, a database was prepared using a library of commercially available compounds from the ASINEX and LifeChemicals databases (1.5M). This database was subsequently optimized through various filtrations including with the PPI-HitProfiler tool to 750K filtered ligands. The VS was conducted by centering the grid on the position of BRCA Phe1546. The 10K compounds with the best scores were docked again with Glide XP and the 1K compounds with the best scores were selected (*Appendix*). Taking advantage of this VS campaign based on high-throughput docking targeting the LFDE binding pocket (Zone II), among 42 compounds were visually inspected, purchased and tested by ELISA assay (*Appendix*) and the dicarboxylic acid compound **1** (**ARN22142**) with a phenyl-furanyl-quinoline core, was selected (Figure 22A) as the second-best candidate in terms of EC<sub>50</sub> and chemical tractability. Indeed, the same VS allowed our group to identify the *hit* compound that led to the development of **ARN24089**, at that time judged less challenging in terms of chemical tractability. The compound **1** has been previously reported by Horak *et al.*, as part of a series of molecules studied for antimicrobial activity against resistant

strains of *S. Aureus* and *Haemolyticus*.<sup>251</sup> After resynthesis, compound **1** confirmed to inhibit RAD51-BRC4 interaction in ELISA assay in the low micromolar range, with a significant  $E_{\max}$  value above 90% (Figure 22A) (*Appendix*). The percentage of  $E_{\max}$  was calculated using CAM833,<sup>210</sup> a known disruptor of RAD51-BRCA2 interaction, as internal reference. In addition, direct binding of **1** to RAD51 was observed using microscale thermophoresis (MST). Despite positioning at a low millimolar range, MST reasonably supported the ELISA results (Figure 22A). Therefore, **1** was evaluated in a BRCA-competent pancreatic cancer cell model, BxPC-3, showing low toxicity based on cell viability analysis and a moderate inhibitory effect (max 23% at 40  $\mu$ M) on homologous recombination (HR) (Figure 22A). Moreover compound **1** proved to increase the sensitivity to olaparib in BxPC-3 cancer cells. Importantly, **1** showed high kinetic solubility in PBS buffer (up to 500  $\mu$ M), which made it an ideal starting point for the development of PPI inhibitors with favorable physicochemical properties. Therefore, **1** was chosen as the starting point for a structure-activity relationship (SAR) campaign.

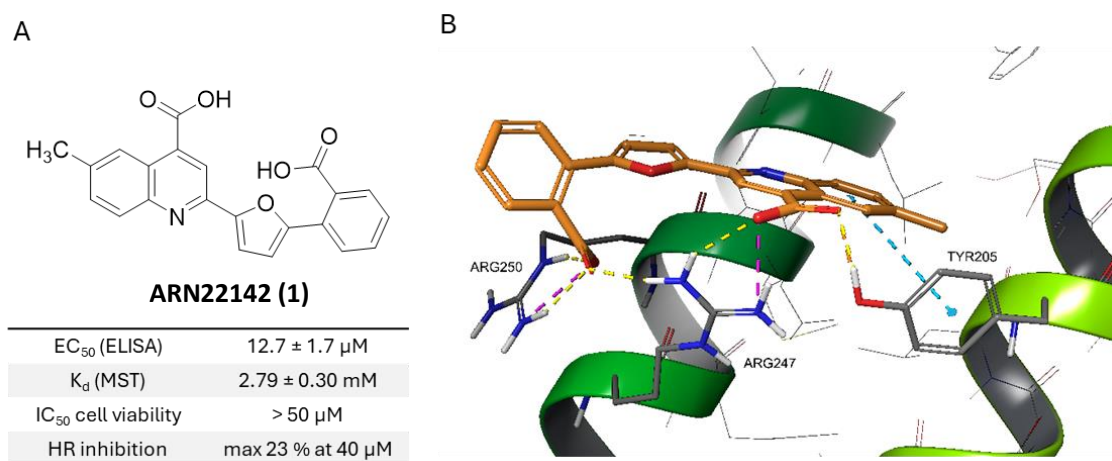


**Figure 22.** **A)** Structure of *hit* compound **1** (ARN22142) and its preliminary evaluation for PPI inhibition and physical-chemical properties; **B)** Proposed docking pose of **1** into the LFDE binding site (Zone II) of RAD51 (PDB ID 1N0W).

To guide the chemical exploration of **1**, its binding to the LFDE pocket (zone II) of RAD51 (Figure 22B) was investigated in depth. The docking hypothesis conducted by the computational unit of the research group suggests that quinoline reaches the inner part of the pocket, where it establishes a network of H-bonds with Arg247 and Tyr205 via the carboxyl group, plus an additional  $\pi/\pi$  interaction with Tyr205. There is also the possibility of establishing H-bonds between suitable

methyl substituents on the quinolinic ring and a Ser208 residue. On the other hand, the second carboxyl group on the quinoline forms H-bonds with Arg250 and others with Arg247. Overall, furan and the unsubstituted portion of the phenyl ring result in the most solvent-exposed area.

To improve RAD51-BRCA2 PPI inhibitory activity of **1** and its ability to synergize with olaparib in BxPC-3 cancer cells, a chemical modifications campaign around the phenyl-furan-quinoline scaffold was conducted (Figure 23, Table 3). In the first set of modifications, I focused on the phenyl A ring to probe the role of carboxylic acid at the ortho position (pink, Figure 23). I first moved the carboxylic group to the meta and para position (**2-3** respectively, Table 3) and then removed it (**4**, Table 3). Next, I explored the ortho position by replacing the carboxylic acid with methyl and small hydrogen bond acceptor/donator (HBA/HBD) groups, e.g., methoxy, hydroxy, and fluorine (**5-8**, Table 3). In addition, I replaced the phenyl ring with pyridine, moving the nitrogen to both para and meta positions (**9-10**, Table 3).

In the second step, I focused on position 6 of quinoline to explore the possibility of establishing H-bonds between HBA/HBD substituents with Ser208 (green, Figure 23). I started by removing the methyl group (**11**, Table 3), also in combination with the removal of the carboxyl group on the A ring (**12**, Table 3). The goal was to clarify the importance of the methyl group and whether it was possible to explore that region for further steric expansion as well. Therefore, I replaced methyl with fluorine, methoxy, trifluoromethyl, ethyl, bromine, hydroxyl and amine groups, differing in hydrophilicity, steric hindrance, with heteroatoms or pure aliphatic groups, in combination with the unsubstituted A ring (**13-19**, Table 3). Finally, I substituted the furan ring with thiophene to test whether the furan core was necessary for activity (blue, Figure 23; **20**, Table 3).

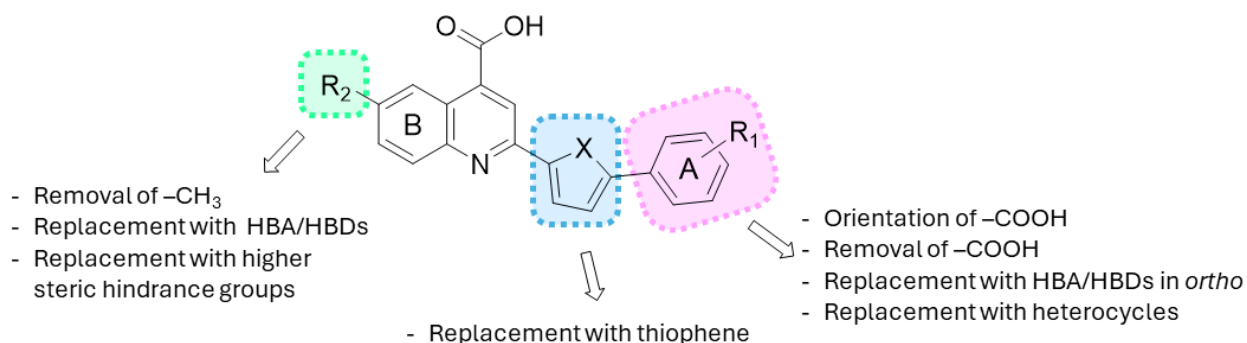
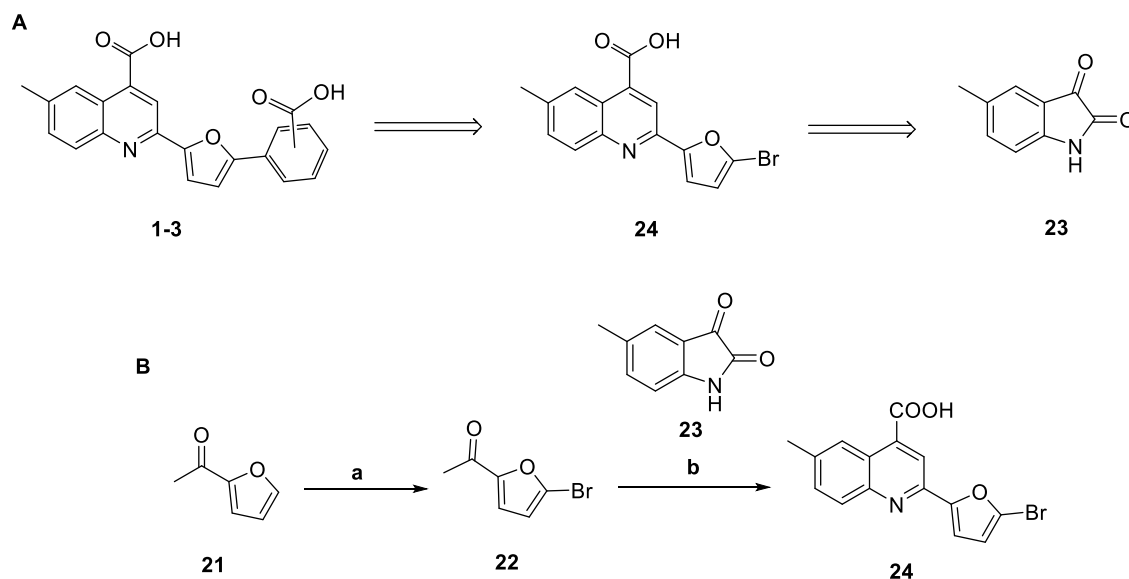


**Figure 23.** Overview of chemical exploration around phenyl-furan-quinoline scaffold.

### 3.2 Chemistry

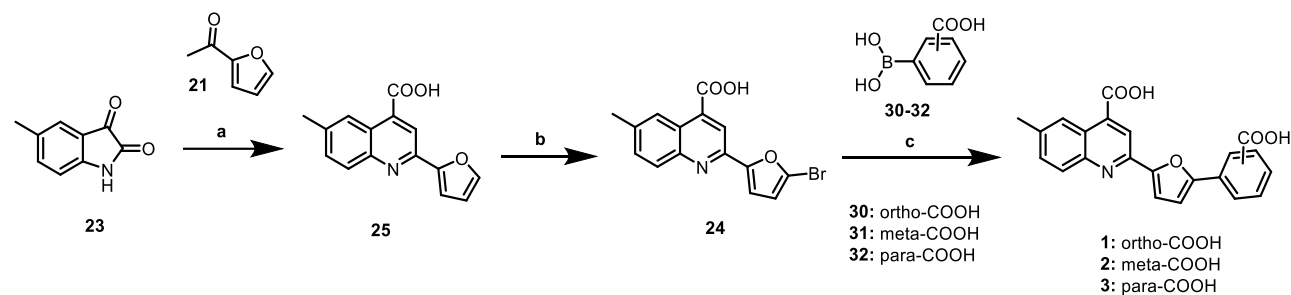
The desired starting *hit* compound **1** was obtained by taking advantage of the synthetic strategy previously reported by Horak *et al.*<sup>251</sup>. Subsequently, to obtain a library of analogues substituted on the phenyl ring by the carboxyl group at different positions, the retrosynthetic scheme was designed as shown in Scheme 1A. The strategy would also apply to obtain analogues with different substituents on the phenyl ring. Compound **21**, commercially available, was subjected to bromination to obtain compound **22**. A Pfitzinger reaction was then conducted in the presence of commercially available isatin **23** to obtain the quinolinic derivative **24**. This would then undergo Suzuki coupling with a series of differently substituted boronic acids to obtain the various analogues of the *hit* compound. Unfortunately, the Pfitzinger reaction with the brominated compound **22**, monitored by UPLC-MS, showed a very low conversion of the reagents, resulting in a too low yield of compound **24** (Scheme 1B).



**Scheme 1.** (A) Retrosynthetic scheme for ortho/meta/para-carboxylic acid phenyl furanyl-quinolinic derivatives **1-3**; (B) Reagents and conditions: (a) N-Bromo succinimide, DMF, rt, overnight, 39% yield; (b) KOH, EtOH:H<sub>2</sub>O 3:1, 80 °C in MW, 3 h, <10% yield.

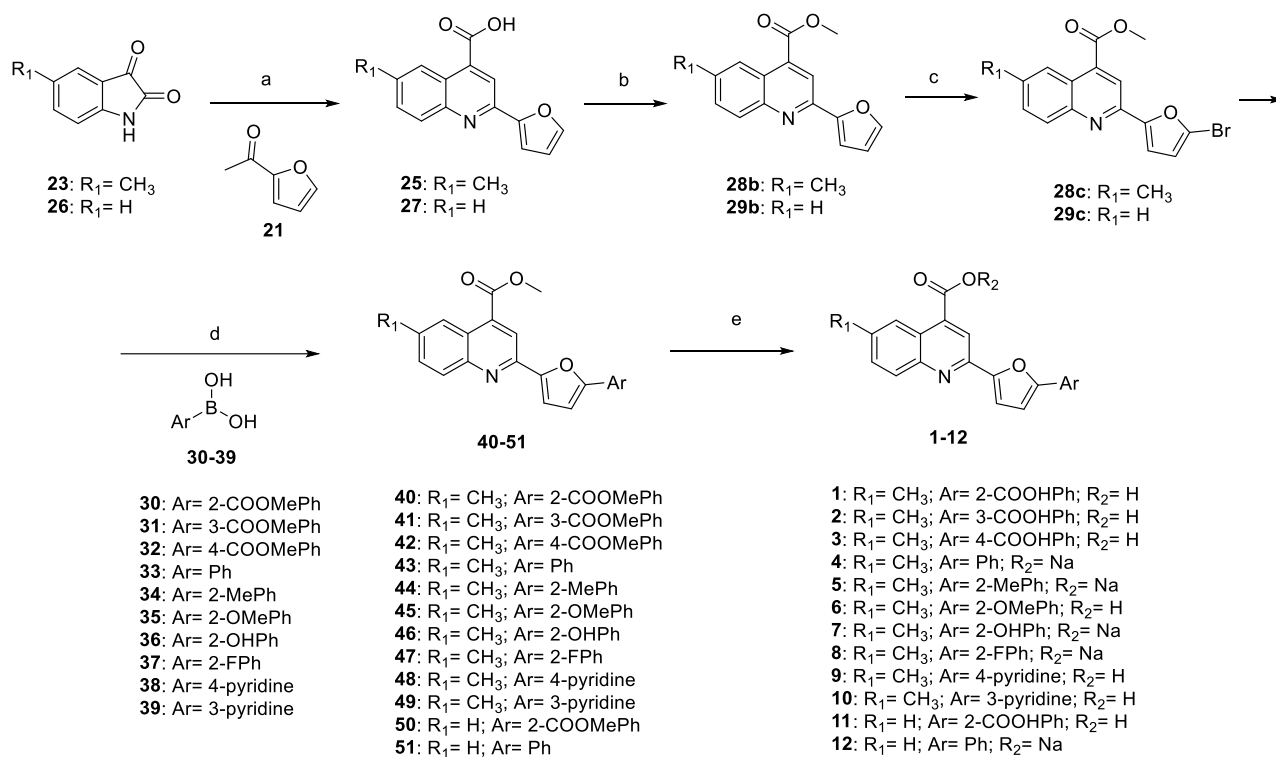
To avoid this issue, Pfitzinger reaction was conducted with non-substituted 2-acetyl furan **21** (Scheme 2). A high yield of compound **25** was obtained and therefore bromination was subsequently conducted on **25** to yield the brominated intermediate **24**. The latter underwent Suzuki coupling with ortho/meta/para-carboxylic phenyl boronic acids **30-32** as shown in Scheme

2. Unfortunately, this strategy showed some issues because boronic acids in Suzuki couplings showed low reactivity (probably due to the intramolecular interactions of the boronic acid with carboxylic group mostly in the ortho position of phenyl ring) and the final compounds **1-3** showed difficulties in their isolation and purification.



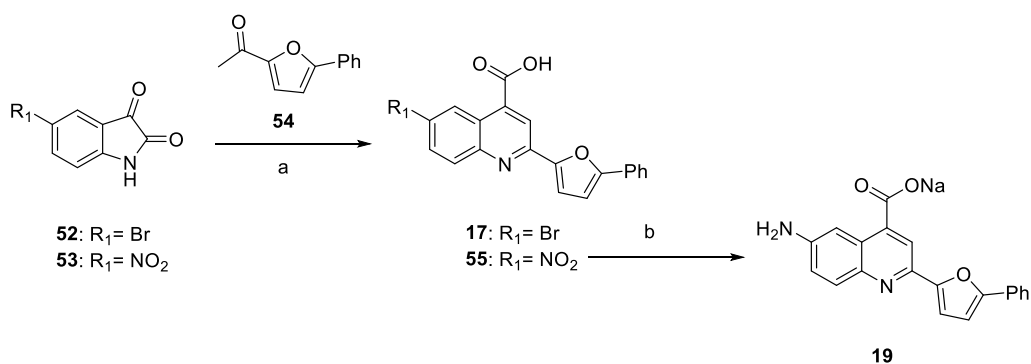
**Scheme 2.** Reagents and conditions: (a) KOH, EtOH:H<sub>2</sub>O 3:1, 3 h, 80 °C in MW, 75% yield; (b) N-Bromo succinimide, DMF, overnight, yield 84%; (c) Pd(PPh<sub>3</sub>)<sub>4</sub>, K<sub>2</sub>CO<sub>3</sub>, dioxane:water (10:1, 0.1 M), 2 h, inert atm, 0-24% yields.

For this reason, the final synthetic strategy to obtain the *hit* molecule **1** and its derivatives was developed as shown in Scheme 3. After Pfitzinger reaction of isatins **23** and **26** with furan **21**, the obtained quinolinic intermediates **25** and **27** were converted to methyl esters **28b-29b** and then brominated to obtain compounds **28c-29c**. These last underwent Suzuki coupling with various boronic acids (**30-39**) substituted mostly with ester groups yielding the aryl derivatives **40-51**. Once **40-51** had been isolated, a basic hydrolysis with NaOH was carried out until complete conversion to the desired **1-12** retained as salts or acidified to form the corresponding undissociated acids.



**Scheme 3.** Reagents and conditions: (a) KOH, EtOH:H<sub>2</sub>O 3:1, 3 h, 80 °C in MW, 54-75% yield; (b) SOCl<sub>2</sub>, MeOH dry, 3 h, 80 °C in MW, 65-80% yield; (c) N-Bromo succinimide, DMF, overnight, 35 °C, 67-77% yield; (d) Pd(PPh<sub>3</sub>)<sub>4</sub>, K<sub>2</sub>CO<sub>3</sub>, dioxane:water (10:1, 0.1 M), 2 h, inert atm, 100 °C, 37-89% yield; (e) NaOH 30%, THF, 24-120 h, rt, quantitative yield.

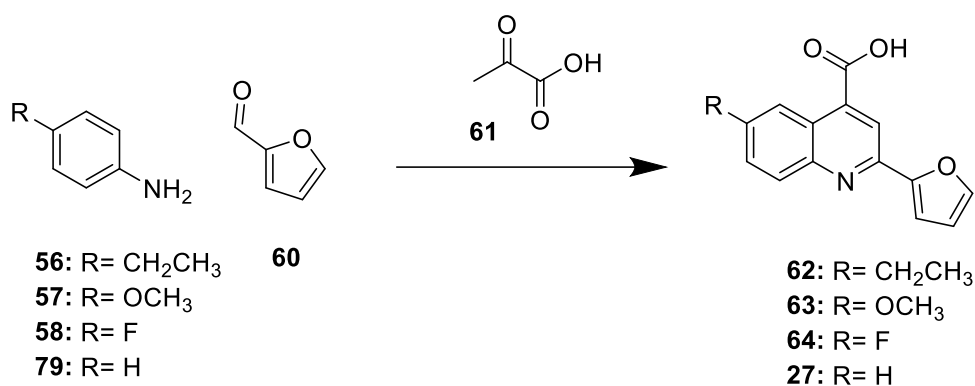
Pfitzinger reaction of isatins **52-53** with the phenyl intermediate **54** previously prepared gave the 6-bromo substituted quinolinic derivative **17** and the 6-nitro intermediate **55** that was subsequently reduced to the desired 6-amine derivative **19** (Scheme 4).<sup>252</sup> Compounds **17** and **19** were retained as salts or acidified to form the corresponding undissociated acid.



**Scheme 4.** Reagents and conditions: (a) KOH, EtOH:H<sub>2</sub>O 3:1, 3 h, 80 °C in MW, 28-37% yield; (b) NaOH, anhydrous MeOH, 1.5 h, 90 °C in MW, 25% yield.

Since some isatins are commercially unavailable and with low yields in their synthesis, the alternative Doebner<sup>253</sup> reaction was evaluated for the development of quinoline scaffold differently substituted in position 6. This is a three-component reaction in which an aldehyde reacts with an aniline to form an imine intermediate that undergoes Michael addition by the enolic form of pyruvic acid. After a cyclization at the benzene ring and two proton shifts, the quinoline-4-carboxylic acid is formed by water elimination.

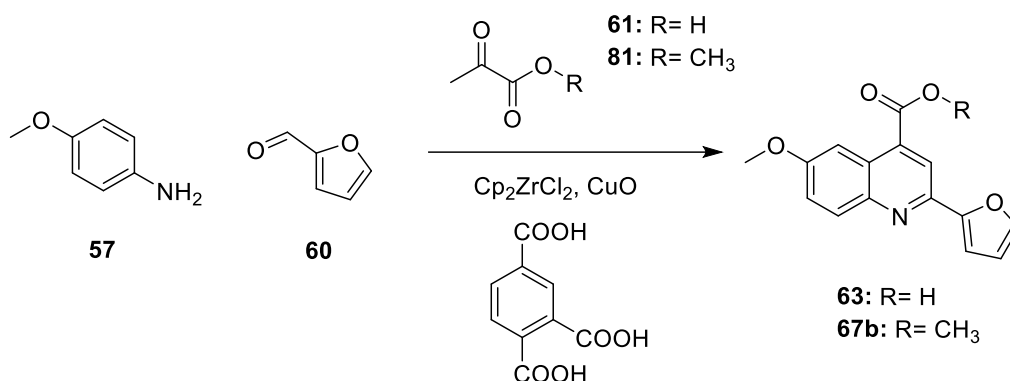
Thus, quinolinic compounds **62** and **27** were easily synthesized by Doebner reaction using aniline **56** and **79**, furfural **60** and pyruvic acid **61** in the presence of strong base such as Et<sub>3</sub>N (Scheme 5).



**Scheme 5.** Reagents and conditions: Et<sub>3</sub>N, EtOH, N<sub>2</sub>, 80 °C for 5h and then rt for 12h, 58-62% yield (products **62** and **27**), 12-16% yield (products **63** and **64**).

On the other hand, anilines with para substituents such as methoxy and fluoro **57-58** did not allow to reach satisfactory yields of the correspondent quinoline derivatives **63-64** (Scheme 5). Different conditions had therefore been studied to optimize the yields of this reaction. Among these, the use of the zirconocene catalyst Cp<sub>2</sub>ZnCl<sub>2</sub> had been reported to increase reaction yields in the presence of a co-catalyst, trimellitic acid.<sup>254</sup> The presence of CuO catalyzed the oxydehydrogenation of the intermediate dihydroquinolines to generate the final quinolines (Table 2). Although the high yields reported in the article, the reaction conducted by us under the same conditions did not lead to the same results, showing yields below 22%. A screening of conditions was therefore conducted to increase the yield of the reported Doebner reaction.<sup>254</sup> The table below shows the different conditions studied, such as the nature of the solvent, temperature, reaction time and catalyst addition (Table 2). None of the conditions tested showed an increase in yield.

**Table 2.** Screening of conditions for three-component Doebner reaction for the synthesis of derivatives **63** and **67b** using para-methoxy aniline **57**, furfural **60** and pyruvic acid **61** or methyl pyruvate **81** in presence of the  $\text{Cp}_2\text{ZrCl}_2$ , trimellitic acid and CuO as catalysts.



entry	cat	R	solvent	T (°C)	t reaz (h)	inert atm	yield (%)
1	yes	Me	iPrOH:H <sub>2</sub> O 3:1	60	2	no	22
2	yes	Me	iPrOH	60	6 (+12 rt)	no	20
3	no	Me	iPrOH	80	6 (+12 rt)	no	0
4	yes	Me	iPrOH:H <sub>2</sub> O 3:1	60	2 (+12 rt)	yes	8
5	no	H	EtOH	80	4.5	yes	16
6	yes	H	iPrOH:H <sub>2</sub> O 3:1	60	18	no	19
7*	yes	Me	iPrOH:H <sub>2</sub> O 3:1	60	3	no	10
8*	yes	Me	iPrOH:H <sub>2</sub> O 3:1	60	2	no	8
9*	yes	Me	iPrOH:H <sub>2</sub> O 3:1	60	2	no	14

\*different adding procedure: (7) furfural added at rt after 1 h, CuO and methyl pyruvate added at 60 °C after 1.5 h; (8-9)  $\text{Cp}_2\text{ZrCl}_2$ , trimellitic acid and CuO were preactivated separately at 60 °C and added to the reaction mixture at rt (8) or at 60 °C (9).

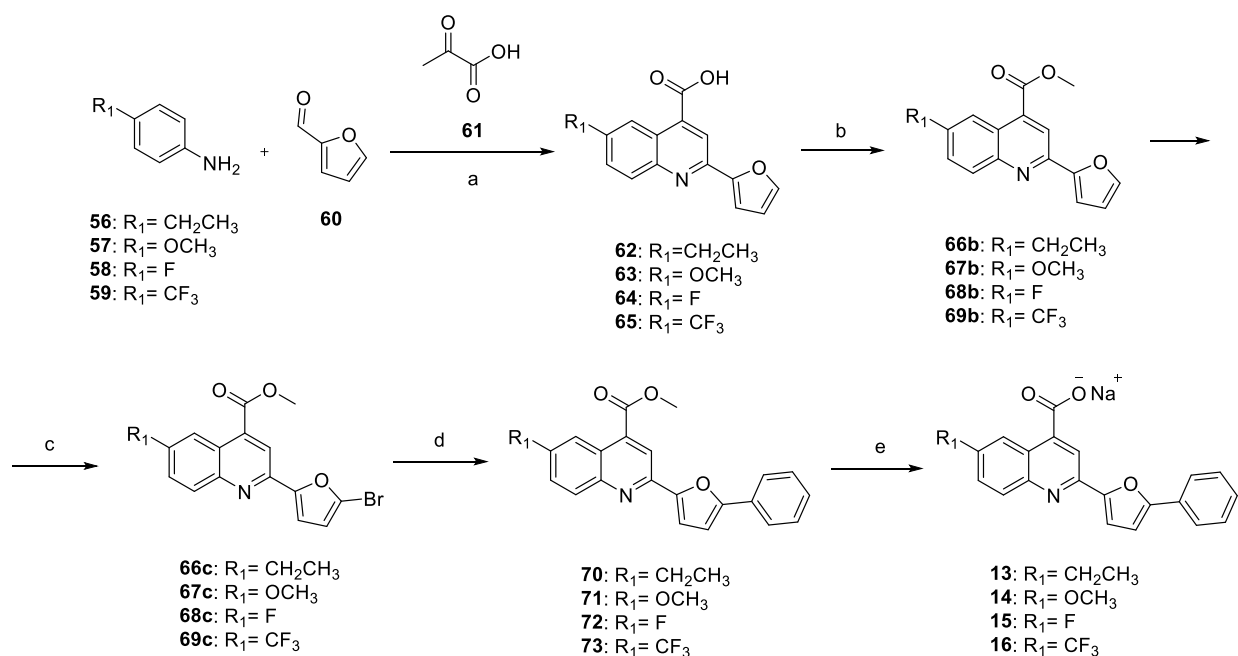
General adding procedure (1-6): solvent (2 M), furfural **60**, 4-methoxyaniline **57** and reagent **61/81** were added in one portion. After 10 min, catalysts were added if specified.

Meanwhile, a patent published by a Japanese group reported the synthesis of quinolines using a Doebner reaction in the presence of Lewis acid  $\text{BF}_3$  as catalyst.<sup>255, 256</sup> Despite the lower yields when using furfural **60** rather than other aromatic aldehydes as benzaldehyde, the reaction tested with para-fluoro aniline **58** shows higher yields than those obtained by the use of  $\text{Et}_3\text{N}$  and is



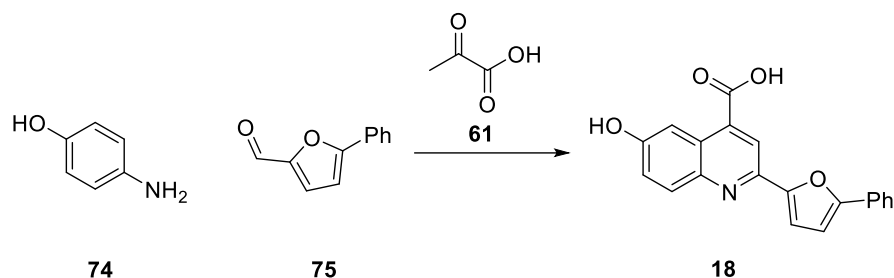
therefore chosen as a model reaction for the synthesis of differently substituted quinolines at position 6 (Scheme 6).

Therefore, substituted anilines **56-59**, furfural **60** and pyruvic acid **61** react with each other in the Mannich-type Doebner reaction optimized using Lewis acid  $\text{BF}_3$  to form furan-quinolines **62-65**. **62-65** were subjected to esterification to obtain the corresponding esters **66b-69b** that had been subsequently brominated to **66c-69c**. Compounds **66c-69c** underwent Suzuki coupling with phenyl boronic acid **33** to give intermediates **70-73**. Finally basic hydrolysis led to final compounds **13-16** retained as salts (Scheme 6).



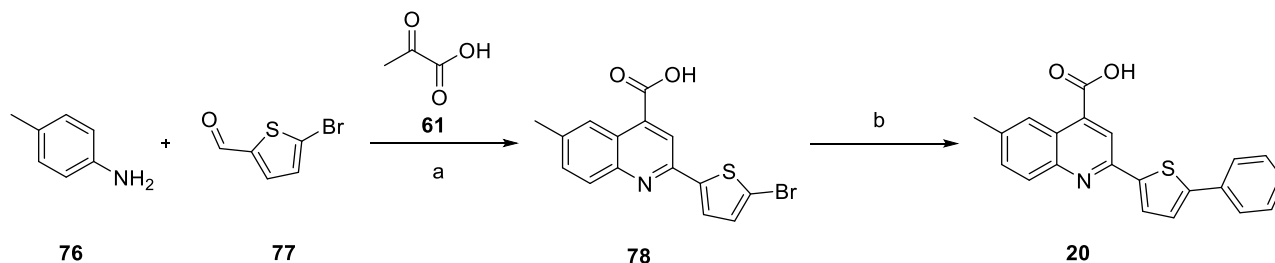
**Scheme 6.** Reagents and conditions: (a)  $\text{BF}_3 \cdot \text{OEt}_2$ , ACN, 24 h, 60 °C, 43-76% yield; (b)  $\text{SOCl}_2$ , MeOH dry, 3 h, 80 °C in MW, 51-75% yield; (c) N-Bromo succinimide, DMF, overnight, 35 °C, yield 35-75%; (d) phenyl boronic acid **33**,  $\text{Pd}(\text{PPh}_3)_4$ ,  $\text{K}_2\text{CO}_3$ , dioxane:water (10:1, 0.1 M), 2 h, inert atm, 60-85% yield; (e) NaOH 30%, THF, 24-120 h, rt, quantitative yield.

Due to yield problems, compound **18** was obtained by Doebner reaction with aminophenol **74** and the previously synthesized phenyl substituted furan **75** in the presence of pyruvic acid **61** and  $\text{BF}_3$  as catalyst (Scheme 7).



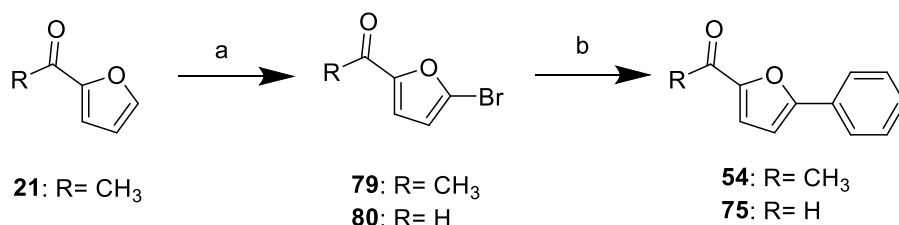
**Scheme 7.** Reagents and conditions:  $\text{BF}_3 \cdot \text{OEt}_2$ , ACN, 24 h, 60 °C, yield 7%.

Derivative **20** was synthesized by Suzuki coupling between bromo-thiophenyl quinoline **78** and phenyl boronic acid **33**. The intermediate **78** was obtained from para-toluidine **75** via Doebner reaction with commercially available **77** (Scheme 8).



**Scheme 8.** Reagents and conditions: (a)  $\text{BF}_3 \cdot \text{OEt}_2$ , ACN, 24 h, 60 °C, 83% yield; (b) phenyl boronic acid **33**,  $\text{Pd}(\text{PPh}_3)_4$ ,  $\text{K}_2\text{CO}_3$ , dioxane:water (10:1, 0.1 M), 2 h, inert atm, 76% yield.

For the reactions shown in the previous Scheme 4 and Scheme 7, the furan reagents **54** and **75** were synthesized by Suzuki coupling reaction with phenyl boronic acid **33** and compounds **79** and **80** respectively as reported in the literature.<sup>257, 258</sup> The compound **79** was obtained by previous bromination of commercially available 2-acetyl furan **21** (Scheme 9).



**Scheme 9.** Reagents and conditions: (a) N-bromosuccinimide, DMF, rt, 4 h, 41% yield; (b) phenyl boronic acid **33**,  $\text{Pd}(\text{PPh}_3)_4$ ,  $\text{K}_2\text{CO}_3$ , dioxane:water (10:1, 0.1 M), 2 h, inert atm, 100 °C, 61-81% yield.

### 3.3 SAR studies and biological evaluation

All derivatives (**1-20**, Table 3) were subjected to a preliminary screening by the biochemical competitive ELISA assay to assess their ability to bind RAD51 and displace BRC4 (*appendix*). The compounds were also evaluated considering  $E_{\max}$  by taking RAD51-BRCA2 PPI disruptor CAM833 as an internal standard. The RAD51-BRCA2 interaction is crucial in recruiting the recombinase RAD51 in cell nuclei, where it uses HR to repair DNA double-strand breaks. Therefore, HR inhibition in BxPC-3 cells was studied. In this way, the molecules showing a specific mechanism of action that inhibits cellular HR through direct inhibition of the RAD51-BRCA2 PPI were selected.

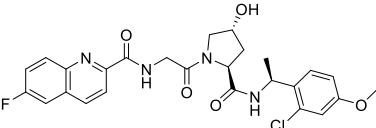
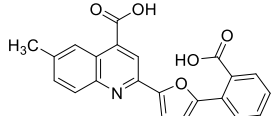
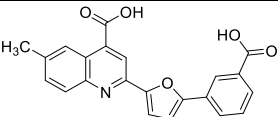
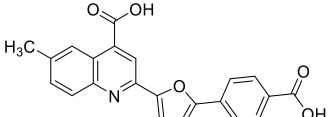
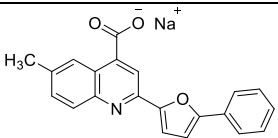
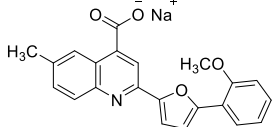
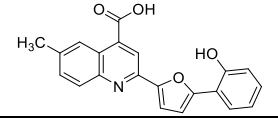
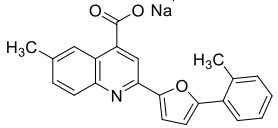
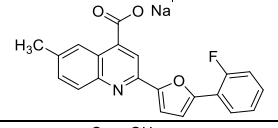
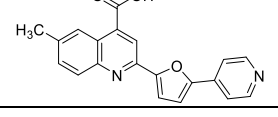
Analyzing the results and comparing them with the  $EC_{50}=12.7 \pm 1.7 \mu\text{M}$  of **1**, the reorientation of the carboxylic acid at the para and meta position produced derivatives **2-3** with reduced inhibitory activity towards the RAD51-BRC4 interaction (**2**,  $EC_{50}=47.4 \pm 6.56 \mu\text{M}$ ; **3**,  $EC_{50}=57.5 \pm 3.7 \mu\text{M}$ , Table 3). Derivative **2** failed the HR assay while derivative **3** showed poor solubility. The intramolecular interactions established by the carboxylic acid probably give the derivatives different degrees of solvation and orientation affecting the physical-chemical properties as solubility. Removal of the carboxylic function resulted in compound **4**, which showed a slight reduction in ELISA activity ( $EC_{50}=57 \pm 6 \mu\text{M}$ ), compared to starting compound **1** ( $EC_{50}=12.7 \pm 1.7 \mu\text{M}$ , Table 3). Despite this, **4** induced a significant inhibition of HR in cell and demonstrated an increasing dose-response pattern (max. 63% at  $80 \mu\text{M}$ ), in contrast to compound **1**, which did not exhibit an increasing dose-response pattern, reaching its maximum HRi of 23% at  $40 \mu\text{M}$ . Substitution of the carboxyl group with EDGs containing oxygen in the ortho position was not well tolerated, resulting in derivatives **5-6** with strongly reduced activity (**5**,  $EC_{50}=97.5 \pm 4.5 \mu\text{M}$ ; **6**,  $EC_{50}=105.8 \pm 3 \mu\text{M}$ , Table 3). On the other hand, substitution with a methyl group gave rise to compound **7** which, despite acceptable activity (**7**,  $EC_{50}=54 \pm 4.3 \mu\text{M}$ ), encountered solubility problems that prevented its progression to in-cell evaluation. Ortho insertion of a small electron-withdrawing halogen, such as fluorine, resulted in derivative **8**, which maintained ELISA activity ( $EC_{50}=24 \pm 6 \mu\text{M}$ ) and showed significant HR inhibition (max 54% at  $60 \mu\text{M}$ , Table 3). Replacing the phenyl ring with a pyridine gave rise to derivatives **9** and **10**, which suffered a drastic loss of solubility in the ELISA experiment (**10**) and in the HR inhibition assay (**9**), despite the significant activity of **9** ( $EC_{50}=22 \pm 4 \mu\text{M}$ , Table 3). After this first series of modifications, compounds **4** and

**8** were identified as the most promising derivatives. Indeed, both significantly inhibited HR in the cell-based assay, showing biological activity consistent with the inhibition of PPI RAD51-BRCA2. Importantly, these results represent the first milestone in exploiting the phenylfuran-carboxyquinoline scaffold to develop RAD51-BRCA2 PPI inhibitors capable of inducing HR deficiency in cells.

Compound **4** showed a slight reduction in ELISA activity but a better HR inhibition, despite the lack of carboxyl function, originally predicted to activate interactions with RAD51 Arg247/Arg250 (Figure 22B). Indeed, the improved biological profile of **4** could suggest the lack of essentiality of the carboxyl group in the ortho or that two negatively charged carboxylates could hinder cell permeability. Furthermore, the exploration of the ortho position did not lead to the maintenance of activity, except for the substitution with fluorine **8**, suggesting limitations related to this ortho position. To enrich the preliminary chemical investigation, I shifted the focus to position 6 on quinoline moiety by first removing the methyl group (**11**, Table 3) and then coupling it with the removal of the carboxylate on phenyl ring (**12**, Table 3). Comparing **11** and **12** with **4**, while no substantial differences were observed in terms of PPI inhibition (**11**,  $EC_{50}=52.1 \pm 2.8 \mu\text{M}$ ; **12**,  $EC_{50}=62.8 \pm 6.8 \mu\text{M}$ ), the analogue **4** was the only one able to inhibit HR in the cellular assay (Table 3). Facing these results, **4** was considered the best compound to develop a series of monocarboxylic acid derivatives exploring the 6-position of quinoline (**13-19**, Table 3). Interestingly, substitution of the 6-position with small EDGs always produced active PPI inhibitors (**13**,  $EC_{50}=51.9 \pm 6.4 \mu\text{M}$ , **14**,  $EC_{50}=29.35 \pm 2.25 \mu\text{M}$  and **19**,  $EC_{50}=35.5 \pm 2.5 \mu\text{M}$ ), whereas EWGs as fluorine and trifluoromethyl did not show good PPI disruption abilities (**15**,  $EC_{50}=101.2 \pm 27.8 \mu\text{M}$  and **16**,  $EC_{50}=81.1 \pm 15.7 \mu\text{M}$ , Table 3). Notably, substitution with bromine and hydroxyl resulted in the lowest micromolar PPI inhibitory activity (**17**,  $EC_{50}=9.4 \pm 2.2 \mu\text{M}$ ; **18**,  $EC_{50}=3.8 \pm 0.1 \mu\text{M}$ , Table 3). Concerning the cellular HR assay, **13**, **14**, **18** and **19** achieved the highest HR inhibition in a dose-response increasing trend except for **18**, whereas the bromine derivative **17** was inactive and had been discarded (Table 3). Notably, **14**, **18** and **19** were more potent than **4** in HR inhibition assay. The same improvement in potency was not observed for analogue **13**, which was no better than **4** and was therefore discarded (Table 3). Compound **18** showed a high improvement of HR inhibition but did not show a dose-response increasing trend, hence the focus was shifted on the compounds **14** and **19** that showed the best results in the preliminary assays. Finally, replacing furan with thiophene resulted in the PPI inhibitor **20** ( $EC_{50}=43.8 \pm 6.8 \mu\text{M}$ , Table

3), which showed a strong HR inhibition (89% at 20  $\mu$ M) despite a poor dose-dependent trend (*Appendix*). However, **20** caused the decrease of cell viability alone and in combination with olaparib at lower concentrations than the ones seen to inhibit HR, an event that strongly suggested potential off-target effects.

**Table 3.** Structures and preliminary screening of *hit* compound **1** (ARN22142) and its derivatives **2–20**.

Cpd	Structure	EC <sub>50</sub> ELISA <sup>a</sup> ( $\mu$ M)	E <sub>max</sub> % ELISA <sup>a</sup>	HR inhibition assay <sup>b</sup>
<b>CAM833</b>		8.5 $\pm$ 2	ref <sup>a</sup>	na <sup>d</sup>
<b>1</b> <b>ARN22142</b>		12.7 $\pm$ 1.7	92	23% (40 $\mu$ M)
<b>2</b>		57.5 $\pm$ 3.7	46	na <sup>d</sup>
<b>3</b>		47.4 $\pm$ 6.56	59.5 $\pm$ 4	ns <sup>c</sup>
<b>4</b>		57 $\pm$ 6	44.5 $\pm$ 2	63% (80 $\mu$ M)
<b>5</b>		97.5 $\pm$ 4.5 (solubility issue at 300 $\mu$ M)	30 $\pm$ 7.9	nt <sup>e</sup>
<b>6</b>		105.8 $\pm$ 3.0	21 $\pm$ 4	nt <sup>e</sup>
<b>7</b>		54 $\pm$ 4.3 (solubility issue at 500 $\mu$ M)	51 $\pm$ 6.8	ns <sup>c</sup>
<b>8</b>		24 $\pm$ 6	88.6 $\pm$ 5	54% (60 $\mu$ M)
<b>9</b>		22 $\pm$ 4	68.4 $\pm$ 7	ns <sup>c</sup>

10		ns <sup>c</sup>	ns <sup>c</sup>	nt <sup>e</sup>
11		52.1 ± 2.8	65	na <sup>d</sup>
12		62.8 ± 6.8	50 ± 8.3	na <sup>d</sup>
13		51.9 ± 6.4	56 ± 8	76% (80 μM)
14 ARN26912		29.35 ± 2.25	76 ± 9	81% (80 μM)
15		101.2 ± 27.8	19 ± 1	nt <sup>e</sup>
16		81.1 ± 15.7	42 ± 5.5	nt <sup>e</sup>
17		9.4 ± 2.2	66 ± 3.5	na <sup>d</sup>
18		3.8 ± 0.1	78 ± 1.9	60% (20 μM) (no dose dependent)
19		35.5 ± 2.5	49 ± 5.7	77% (20 μM)
20		43.8 ± 6.8	56 ± 9	89% (20 μM)

<sup>a</sup> ELISA assay results are expressed as EC<sub>50</sub> value (all points were tested in triplicate with error bars indicating the standard deviation); CAM833, a known RAD51-BRCA2 disruptor developed by Scott *et al.*<sup>210</sup> was used as internal reference compound to calculate E<sub>max</sub>% value (percentage of the maximum activity of the tested compound and compared to the maximum activity of CAM833 at the same concentration).

<sup>b</sup> HR inhibition values are expressed as percentage of max inhibition at each used concentration after 5 h BxPC-3 cells treatment.

<sup>c</sup> Not soluble or solubility issues.

<sup>d</sup> Not active.

<sup>e</sup> Not tested.

The most promising compounds **4**, **14**, **19** and **20** in comparison with **1** were tested in cell viability assays in combination with PARPi olaparib (10  $\mu$ M) to assess their effect on PARPi efficacy in BRCA2-competent p53-mutated pancreatic cancer cells BxPC-3 (Table 4). Their efficacy is assessed by calculating the combination index (CI), a parameter used to calculate an additive or synergistic effect due in this case to the simultaneous impairment of two DNA repair mechanisms, resulting in pharmacologically induced synthetic lethality. Combination index was calculated according to the procedure reported in Fischel *et al.*<sup>259</sup> where:  $CI < 0.8$ , the association is synergistic;  $0.8 < CI < 1.2$ , the association is additive;  $CI > 1.2$ , the association is antagonistic. The compounds showing synergic effects with olaparib were also tested in combination with talazoparib (500 nM). Compound **4** showed an additive effect on the efficacy of olaparib ( $CI=0.83$  at 40  $\mu$ M, Table 4). The *hit* compound **1** was much less active ( $CI=0.94$  at 50  $\mu$ M, Table 4), confirming that **4** can be taken as a reference for the modifications in position 6 on quinoline. Compound **14** showed a synergistic effect in combination with olaparib in BxPC-3 cells ( $CI=0.76$  at 40  $\mu$ M, Table 4, Figure 24) but not with talazoparib ( $CI=0.94$  at 60  $\mu$ M, Table 4, Figure 24). On the other hand, compound **19** showed the strongest effect in combination with talazoparib in BxPC-3 cells ( $CI=0.58$  at 20  $\mu$ M, Table 4, Figure 24) but not with olaparib showing only an additive effect ( $CI=0.84$  at 20  $\mu$ M, Table 4, Figure 24). These conflicting results suggest that the two compounds act slightly differently since the two PARPi olaparib and talazoparib also have different mechanisms of action. Indeed, talazoparib has been shown to be the most potent PARP-trapping inhibitor, whereas olaparib has no defined mechanism.<sup>117</sup> Finally, the cell viability results of compound **20** on BxPC-3 cells ( $CI=0.78$  at 2.5  $\mu$ M, Table 4) were not in line with the results of the in-cell HR assay (9% HRi at 5  $\mu$ M) suggesting its probable inhibitory action on targets that do not participate in HR but synergize with PARPi. The results of **20** are interesting, but not in the context of our research of RAD51-BRCA2 PPI disruptors, and for this reason compound **20** was not further investigated. The most promising compounds **14** and **19** were also evaluated in biophysical tests as microscale thermophoresis (MST) to confirm the ability to bind RAD51 and calculate their  $K_d$  values. The two compounds showed significantly improved  $K_d$  values compared to the value in the millimolar range of the starting compound **1** (Table 4). Showing excellent ability to inhibit RAD51-BRCA2 protein-protein interaction and synergism with PARPi in pancreatic cancer cells, the two compounds **14** and **19** were evaluated in further biological assays to confirm SL relationship with PARPi.

**Table 4.**  $K_d$  values of *hit* compound **1** and derivatives **4**, **14**, **19** and **20** by MST assay and combination index (CI) in cell viability with olaparib/talazoparib in BRCA2-competent pancreatic cancer cells BxPC-3. CI>1.2 antagonist; CI=0.8-1.2 additive effect; CI<0.8 synergistic effect.

Cpd	structure	$K_d$ MST <sup>a</sup> ( $\mu$ M)	CI Cell viability in BxPC-3 +olaparib <sup>b</sup>	CI Cell viability in BxPC-3 +talazoparib <sup>b</sup>
<b>1</b>		2790	0.94 (50 $\mu$ M)	nt <sup>c</sup>
<b>4</b>		nt <sup>c</sup>	0.83 (40 $\mu$ M)	nt <sup>c</sup>
<b>14</b>		75.14 $\pm$ 0.06	0.76 (40 $\mu$ M)	0.94 (60 $\mu$ M)
<b>19</b>		20-40	0.84 (20 $\mu$ M)	0.58 (20 $\mu$ M)
<b>20</b>		nt <sup>c</sup>	0.78 (2.5 $\mu$ M)	nt <sup>c</sup>

<sup>a</sup>MST measurements were simultaneously performed on 16 capillaries containing a constant concentration (50 nM) of labelled RED-tris-NTA 2nd Generation His-hRAD51 protein (NanoTemper Technologies) and 16 different concentrations of the compounds. Measurements were carried out in MST buffer (20 mM HEPES (pH 8.00), 250 mM KCl, 0.1% (v/v) Pluronic® F-127, 0.1% (v/v) PEG 8000, 5% (v/v) glycerol, 5% DMSO).

<sup>b</sup>CI values of the effect of 144 h BxPC-3 treatment with compounds and olaparib (10  $\mu$ M)/talazoparib (500 nM) treatment compared to alone administration reporting the concentration where the maximum effect is seen.

<sup>c</sup>Not tested.



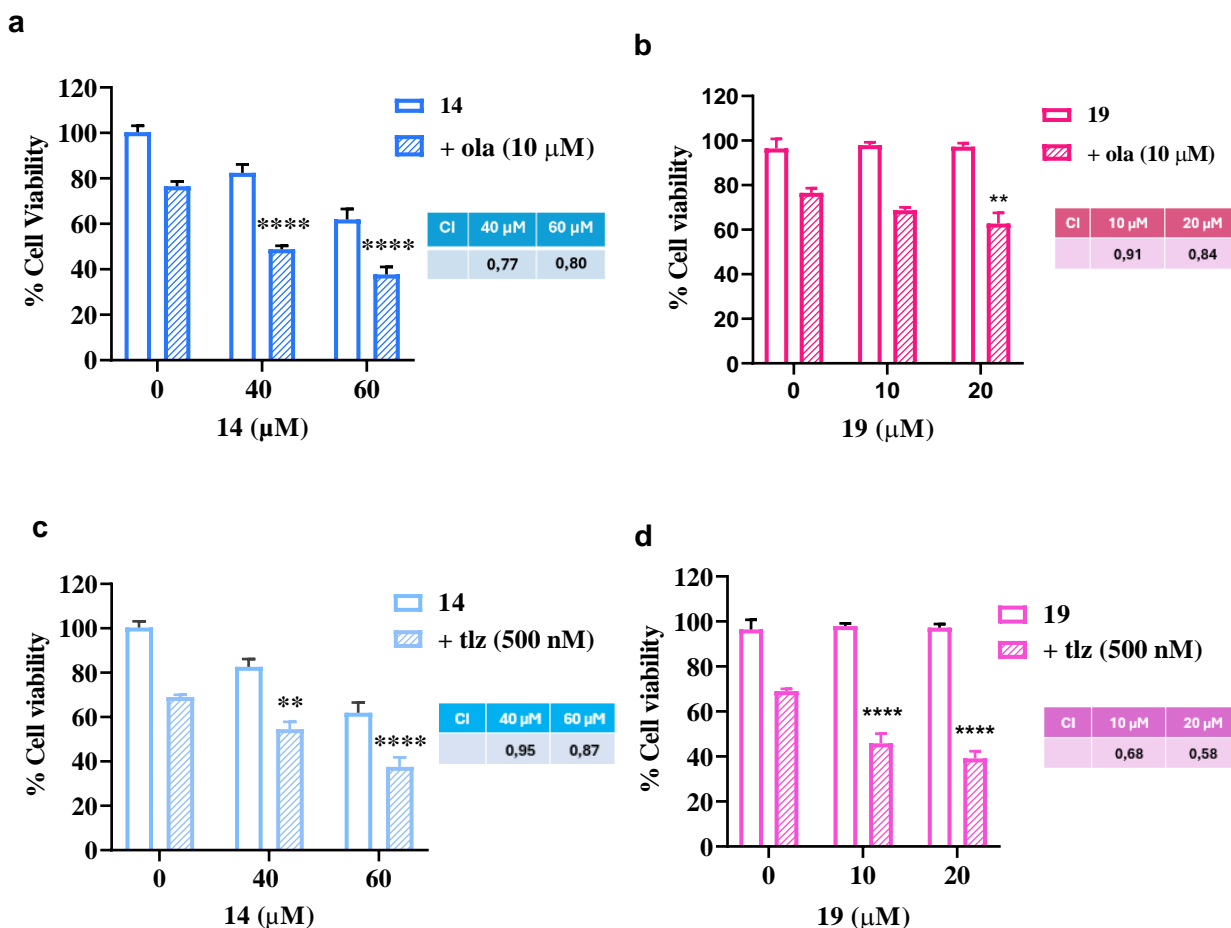


**Figure 24.** The bar graphs show the effect on BxPC-3 cells viability after 144 h of **14** (40-60  $\mu\text{M}$ ) and **19** (10-20  $\mu\text{M}$ ) treatment, administered alone or in combination with olaparib (10  $\mu\text{M}$ ) or talazoparib (500 nM). Data were statistically analyzed using the two-way ANOVA followed by Tukey's multiple comparisons test, to evaluate the differences between the effects caused by the compounds' combination vs those caused by the single PARPi treatment (\*\*  $p < 0.005$ ; \*\*\*\*  $p < 0.0001$ ). The values of combination index (CI) are reported in colored tables.  $\text{CI} > 1.2$  antagonist;  $\text{CI} = 0.8\text{--}1.2$  additive effect;  $\text{CI} < 0.8$  synergistic effect.

In the following we report compound **14** as it has been the best characterized so far. Noteworthy, **14** showed synergistic effects in combination with both olaparib and talazoparib in HPAC cells with wild type p53 which are more sensitive to agents that induce cell death (Figure 25).

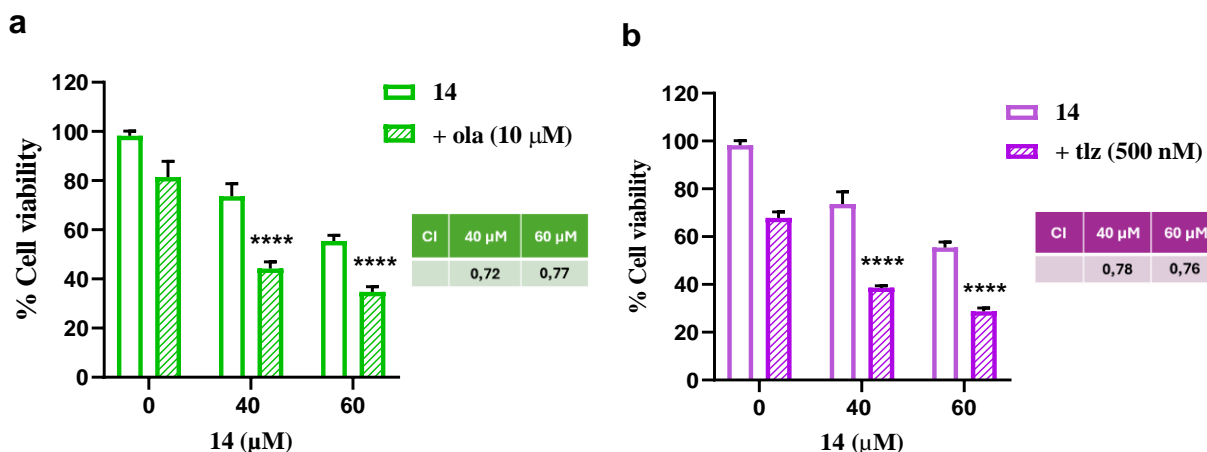


**Figure 25.** The bar graphs show the effect on HPAC cells viability after 144 h of **14** (40-60  $\mu$ M) treatment, administered alone or in combination with olaparib (10  $\mu$ M) (**a**) or talazoparib (500 nM) (**b**). Data were statistically analyzed using the two-way ANOVA followed by Tukey's multiple comparisons test, to evaluate the differences between the effects caused by the compounds' combination vs those caused by the single PARPi treatment (\*\*  $p < 0.005$ ; \*\*\*\*  $p < 0.0001$ ). The values of combination index (CI) are reported in colored tables.  $CI > 1.2$  antagonist;  $CI = 0.8$ -1.2 additive effect;  $CI < 0.8$  synergistic effect.

Further biological tests validated the inhibition of HR and the hypothesis of pharmacologically induced SL. It is well established that, following the induction of DNA damage, a key consequence of the RAD51-BRCA2 interaction is the recruitment of RAD51 in the nucleus to perform DNA repair via the HR pathway.<sup>260</sup> The graph in Figure 26a highlighted the statistically significant decrease in the percentage of RAD51-labelled nuclei detected by immunofluorescence, demonstrating that **14** inhibited the recruitment of RAD51 and lending strength to its putative PPI-inhibiting mechanism of action. To further investigate the pharmacologically induced SL hypothesis, an immunofluorescence assay was performed to assess whether the simultaneous impairment of DSBs and SSBs repair by the **14**/olaparib combination strongly induced an increase of DNA damage in cells. Two key indicators of DNA damage were used: phosphorylation of histone H2AX ( $\gamma$ H2AX) and micronucleus formation. Increased  $\gamma$ H2AX levels suggest that a compound induces DNA damage.<sup>109</sup> Indeed, Figure 26b showed a statistically significant increase in the  $\gamma$ H2AX signal in cells treated with the **14**/olaparib combination compared to cells treated with olaparib alone. To lend strength to these data, the possible increase in micronuclei formation following the combined treatment was evaluated. Micronuclei are formed from chromosome fragments or whole chromosomes that are not properly incorporated into daughter nuclei during

cell division. The increased formation of micronuclei may indicate an impairment of DNA repair pathways.<sup>261</sup> Combined **14**/olaparib treatment resulted in a marked increase in micronuclei formation compared to cells treated with olaparib alone (Figure 26c). These results were both in line with the preliminary hypothesis that the simultaneous impairment of two different DNA damage repair pathways leads to an accumulation of DNA damage over time.

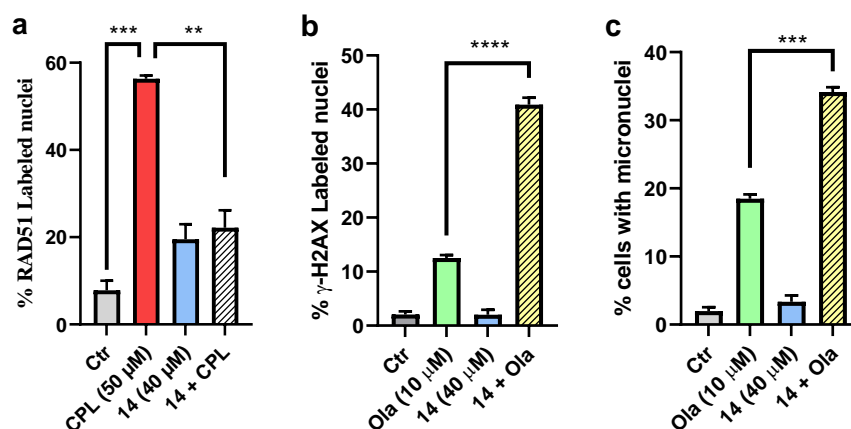


**Figure 26. a. RAD51 nuclear foci assay:** bar graph showing the percentage of labeled nuclei assessed in CPL-exposed, **14** alone-exposed, **14**/CPL combination-exposed BxPC-3 cell cultures for 5 h (\*\*\*  $p = 0.0003$ , \*\* $p = 0.001$ ). **b.  $\gamma$ -H2AX foci assay:** bar graph showing the percentage of  $\gamma$ -H2AX foci labeled assessed in BxPC-3 cells after 72 h of **14**/olaparib treatment, alone or in combination (\*\*\*\*  $p < 0.0001$ , compared to cells treated with olaparib alone). **c. Micronuclei Formation assay:** bar graph showing the percentage of DAPI staining micro-nucleated cells after 72 h of olaparib/**14** treatment compared to olaparib alone ( $p$  \*\*\* = 0.0001). All **A**, **B**, **C** data were statistically evaluated by applying the one-way ANOVA test, followed by Tukey's multiple comparisons test.

Taken together, these results supported the hypothesized involvement of the DNA damage repair mechanisms. Therefore, further experiments were conducted to test whether the **14**/olaparib combination would induce SL.

The SL between **14** and olaparib was demonstrated by studying the involvement of apoptosis. A pan-caspase inhibitor (Z-VAD-FMK) treatment resulted in a significantly increased BxPC-3 and HPAC cell viability following olaparib+**14** co-administration (Figure 27a). In contrast, the administration of Nec-1 (a necroptosis inhibitor) did not affect the antiproliferative effect of the olaparib/talazoparib+**14** combination confirming the involvement of apoptosis (Figure 27b). These results reproduced the desired mechanism of SL triggered by the combination of a RAD51-BRCA2 disruptor and PARP inhibitors.

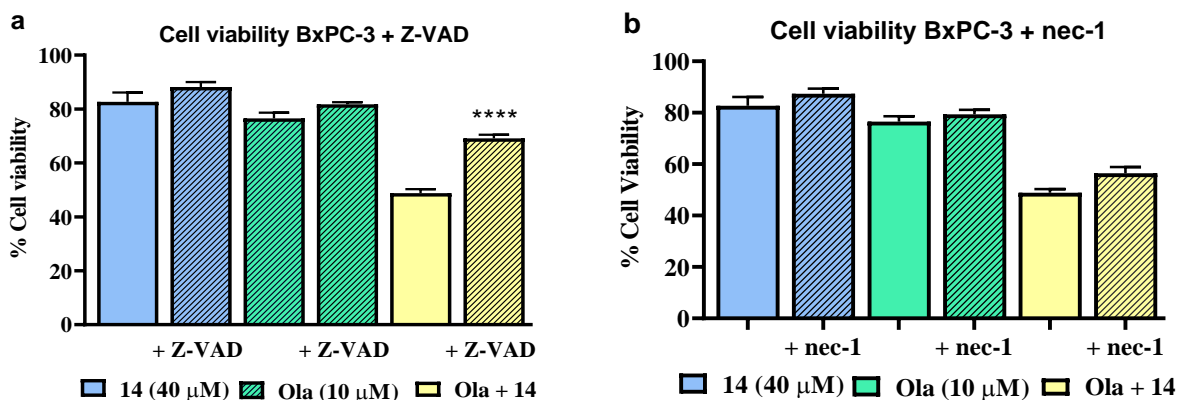


**Figure 27. (a) Apoptosis involvement assay:** BxPC-3 cells were treated for 144 h with 40 μM **14**, given alone or in combination with 10 μM olaparib. 20 μM Z-VAD-FMK was added mid-treatment and then every 24 h. **(b) Necroptosis involvement assay:** BxPC-3 cells were treated for 144 h with 40 μM **14**, given alone or in combination with 10 μM olaparib. 20 μM Necrostatin-1 was added mid-treatment and then every 24 h. Data were statistically analyzed using two-way ANOVA followed by Tukey's multiple comparisons test (\*\*\*\*  $p < 0.0001$ ; \*\*\*  $p = 0.005$ ; \* $p < 0.05$ , compared to the culture treated with **14** in combination with olaparib).

Finally, the cytotoxicity of the compound and its combination with both olaparib and talazoparib was evaluated in Capan-1 BRCA2-mutated pancreatic cancer cells and H6037 BRCA2-wild type normal pancreatic cells (Figure 28a-b). In both cases, the administration of **14** alone or in combination with olaparib did not affect cell viability. Capan-1 cells derive from a human pancreatic adenocarcinoma (very similar to BxPC3 cells) and are defective for BRCA2. Consequently, they do not operate HR dependent on RAD51-BRCA2 interaction and compound **14** should therefore not be significantly active on them, as in normal cells if it is not toxic. This result further supports the idea that synergistic effects in the **14**/olaparib combination arise from and are strictly related to the inhibition of RAD51-BRCA2 PPI and consequently HR.

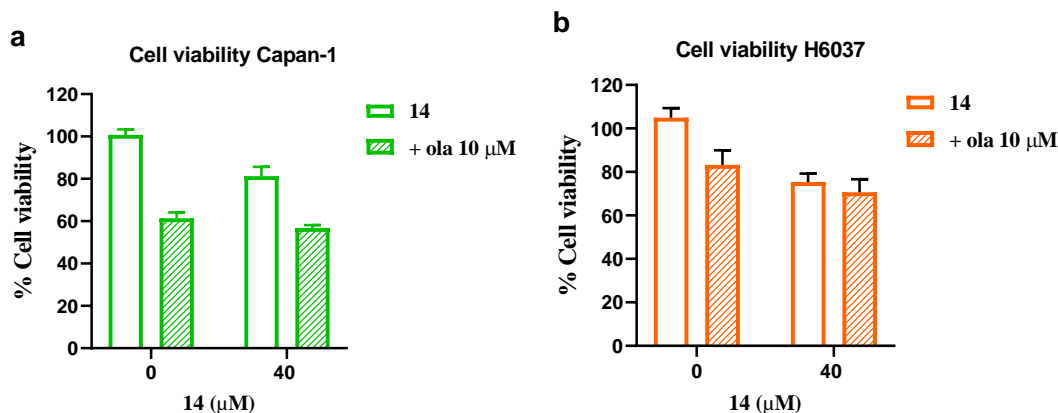


**Figure 28. Cytotoxicity assay:** bar graphs showing the effect on Capan-1 (a) and H6037 (b) cell viability after 144 h of **14** (40 μM)/olaparib (10 μM) treatment, administered alone or in combination. Data were statistically analyzed by two-way ANOVA followed by Tukey's multiple comparisons test. 40 μM **14** caused a ≈25% inhibition of Capan-1 and H6037 cell viability compared to Ctr ( $p = 0.0001$ ). No statistically significant difference was observed when the effect of the **14**/olaparib combination was compared with the effect of single treatments.

Analyses on 3D spheroids of BxPC-3 showed that only 60 μM of **14** maintained its synergism in cell viability ( $CI < 0.8$ ) following co-administration of 10 μM olaparib (Figure 29a) and 2 μM talazoparib (Figure 29b). These results are in line with literature data indicating that, compared to 2D cultures, 3D models are more resistant to cytotoxicity due to increased drug resistance and drug penetration problems.<sup>262, 263</sup> To further evaluate its antitumor effects, spheroid volume during treatment with **14** alone or combined with olaparib or talazoparib was analyzed. Furthermore, assessment of cell death with various dyes showed a significant increase (40%) in spheroid death following treatment with 60 μM of **14** combined with olaparib or talazoparib compared to **14** and PARP inhibitors alone (Figure 29c). In agreement with the results on cell viability, 60 μM of **14** alone had no impact on spheroid volume over the time analyzed, whereas its combination with both PARP inhibitors significantly reduced spheroid volume (20% reduction, Figure 29d). Overall, these results indicate that, despite synergy with olaparib and talazoparib in 2D cultures at a lower concentration, only 60 μM of **14** maintained synergy with both PARP inhibitors in 3D cell cultures.

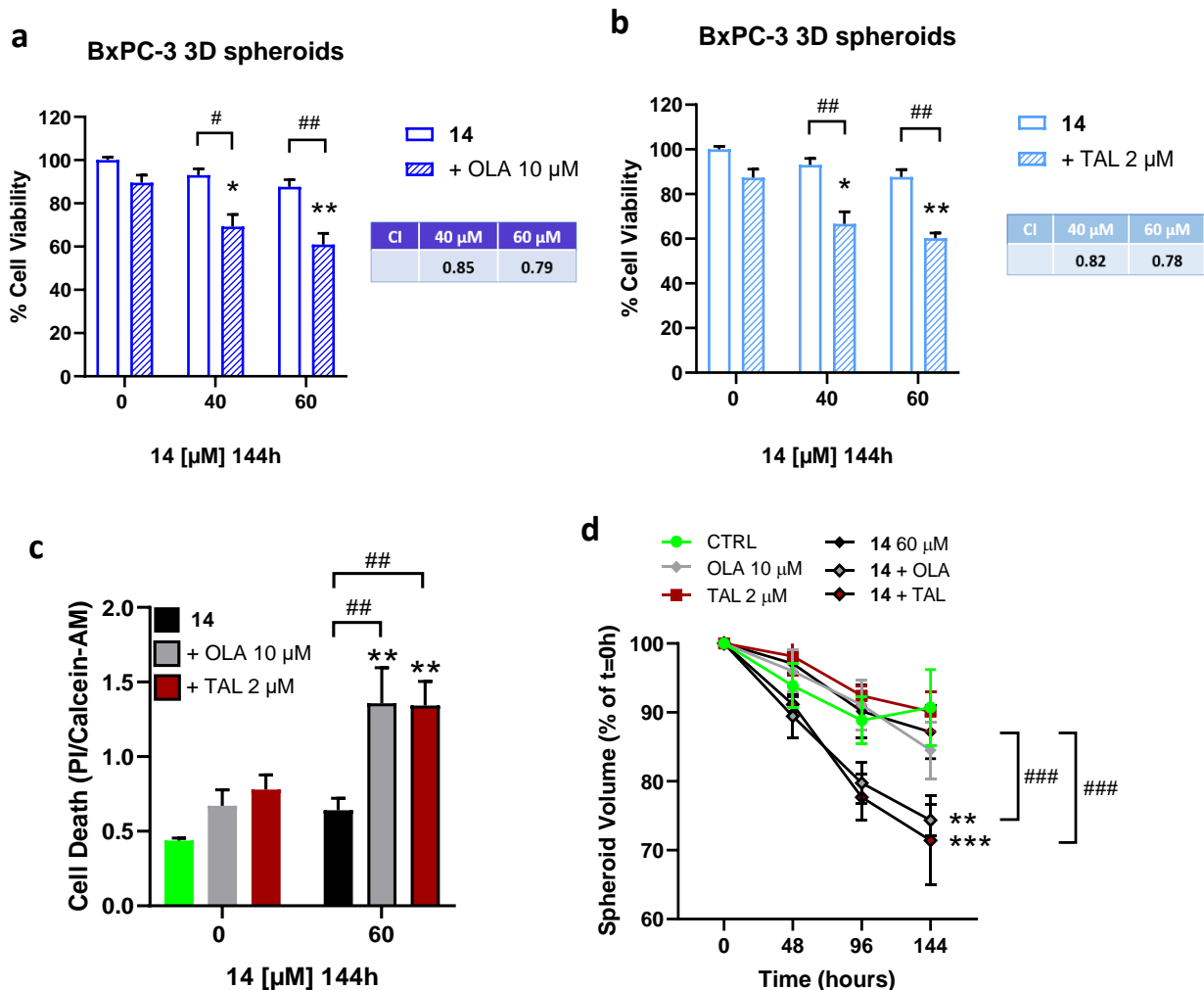


**Figure 29.** The bar graphs show the effect on BxPC-3 cell viability after 144 h of **14** (40-60  $\mu\text{M}$ ) treatment, administered alone or in combination with 10  $\mu\text{M}$  olaparib (**a**)/2  $\mu\text{M}$  talazoparib (**b**). (**c**) After treatment, Calcein-AM and PI were added to each well at the final concentration of 2.5 and 3.75  $\mu\text{M}$  respectively and their Calcein-AM and PI fluorescence signals are measured to determine cell death rate. Results were expressed as PI/Calcein-AM ratio. (**d**) Brightfield imaging of 3D spheroids was performed at 0, 48, 96 and 144 h treatment timings to determine spheroid volume change. Spheroid volume  $V$  was calculated using the general formula:  $V = 0.5 \cdot (\text{Length}) \cdot (\text{Width})^2$ .

Overall, compound **14** showed the best antitumor properties supporting the working hypothesis that the combination of a small molecule disruptor of RAD51-BRCA2 PPI and a PARP inhibitor could reproduce the mechanism of SL in pancreatic cancer cell lines with fully functional BRCA2 gene and HR.

In the future, its metabolic and pharmacokinetic (DM/PK) profile will be analyzed to eventually proceed with further studies in *in vivo* tumor models.

### 3.4 Future perspectives

Studying the docking poses of compounds **4** and **14** in the LFDE pocket on the 1N0W structure of RAD51, it was noted that the removal of the carboxyl on the phenyl moiety led to the docking pose being reversed compared to the docking pose of the *hit* compound **ARN22142** (Figure 30), suggesting new interactions to be explored that will be part of the future SAR studies campaign around compound **14**.

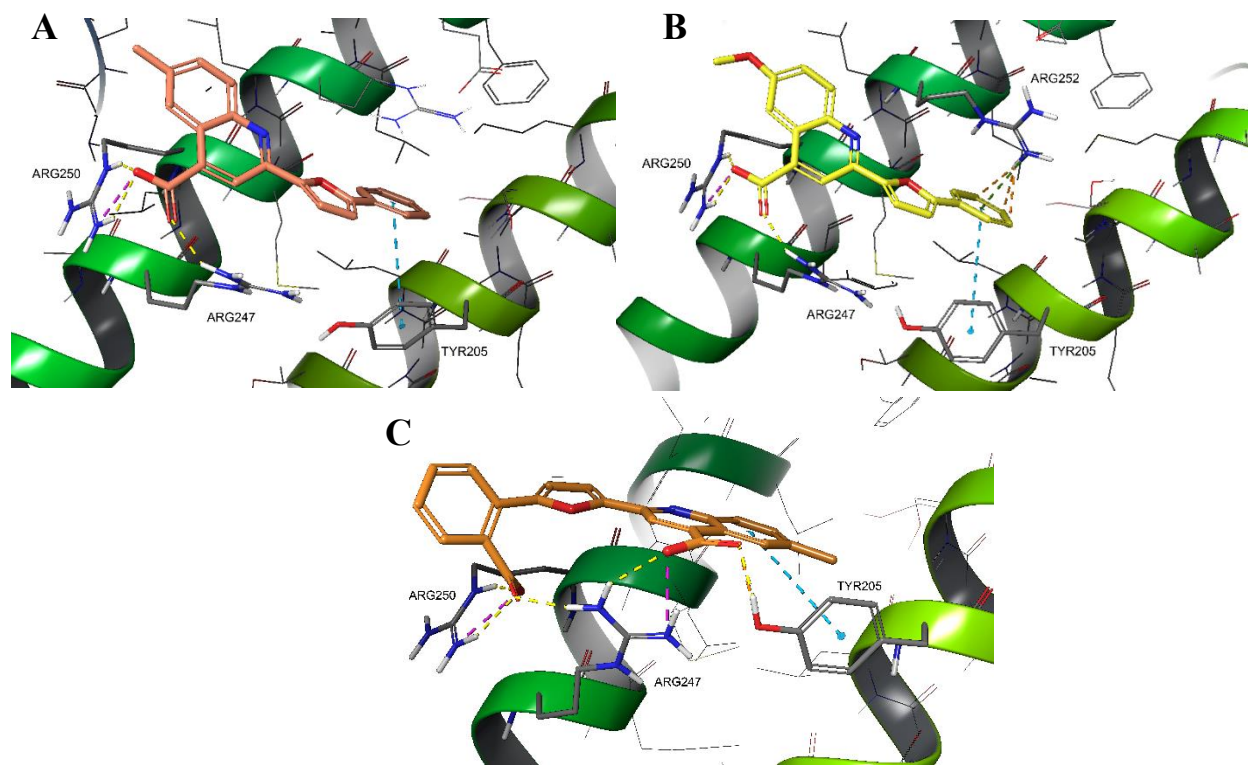


**Figure 30.** Docking pose of **4** (A) and **14** (B) and **ARN22142** (C) into the LFDE binding site (Zone II) of RAD51 (PDB ID 1N0W).

Compared to the interactions of the starting *hit* compound, the carboxylic group on the quinolinic ring of compounds **4** and **14** forms hydrogen bonds with the two Arg247/250 residues. It is very likely that this is the interaction essential to the overturning of the structure within the pocket. The pose overturning brings the quinoline part now being exposed to the solvent, while the phenyl-furan part fits inside the pocket. In particular, the phenyl ring has the possibility of establishing  $\pi/\pi$  interactions with Tyr205, which previously interacted with the quinoline of compound **1**, and a possible cation- $\pi$  interaction between an Arg252 arginine and the phenyl itself was also noted

(Figure 30). Therefore, by analyzing the new docking pose of **14**, structural tuning is currently undergoing to discover more potent and possibly drug-like compounds.

Finally, a new structure of human RAD51 presynaptic complex (PDB ID: 7EJC) has recently been published and shows a larger and defined N-terminal portion of RAD51 compared to 1N0W RAD51-BRC4 complex. The N-terminal domain of RAD51 has been shown to be highly mobile and intrinsically disordered. In this case, being 7EJC a structure with three monomers of RAD51 clustered with ATP and a ligand (J46) that stabilize its dynamics, the N-terminus is more resolved. Docking studies of the most promising compounds **14** and **19** on this new RAD51 structure are underway to assess further interactions to be possibly considered.

### 3.5 Conclusions

In the pursuit of the discovery of potential RAD51-BRCA2 PPI small-molecule disruptors able to trigger SL in pancreatic cancer cells with PARP inhibitors, a series of new phenylfuran-carboxyquinoline derivatives was developed.

To enhance the PPI inhibitory activity of compound **1**, previously identified through a VS on Zone II (LFDE pocket) of RAD51-BRCA2 PPI, a campaign of chemical modifications around the phenyl-furan-quinoline scaffold was conducted. SAR efforts led to compound **14** with the desired biological profile. Indeed, **14** bound RAD51 and inhibited the PPI between RAD51 and BRC4. Noteworthy, **14** was shown to synergize with olaparib and to induce synthetic lethal death in BRCA2-functional pancreatic cancer cells, where it significantly reduced cellular HR, reflecting its mechanism of action. The results were confirmed by 3D biological assays. Noteworthy, in BRCA2-mutated pancreatic cancer cells Capan-1 and BRCA2-wild type normal pancreatic cells H6037, the administration of **14** alone or in combination with olaparib did not affect cell viability. Encouraging results were also obtained with compound **19**, where the amine at position 6 of the quinoline moiety can form important hydrogen bonds with residues in the LFDE pocket of RAD51. Preliminary experiments showed that **19** induced synergistic effect in combination with talazoparib in BRCA2-functional pancreatic cancer cells. Further experiments are ongoing to better characterize the compound.



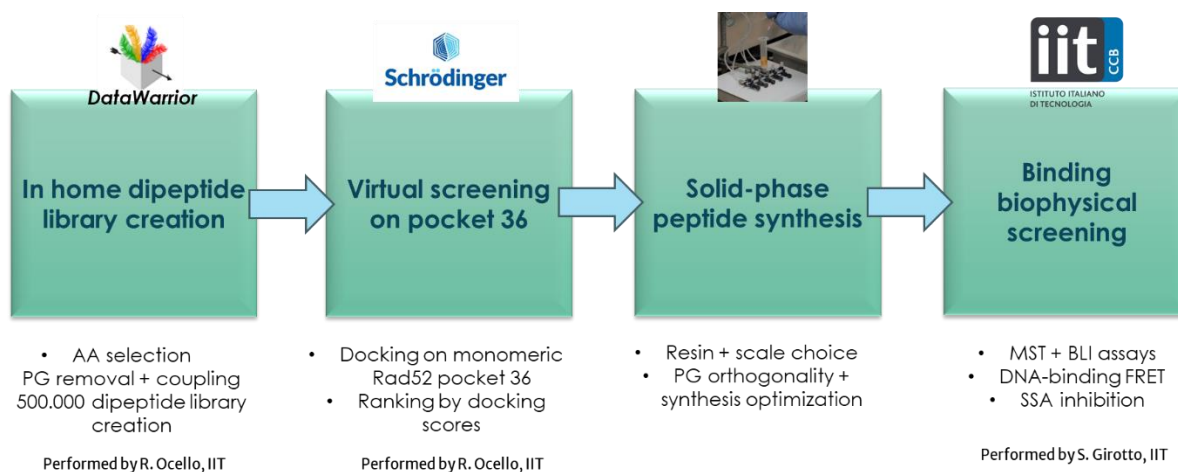
Overall, these results support the working hypothesis that SL can be triggered using only small organic molecules. SL has proven to be a valuable paradigm for the discovery of new anticancer therapies, including the treatment of pancreatic cancer, a major unmet cancer needs. The compounds will be tested in the future in other BRCA2-competent cancer cell lines such as ovarian or breast cancer cells to validate their efficacy in other cancers common in the world population. In particular, the observed SL was triggered by two biochemically different mechanisms: enzyme inhibition (PARP) and protein disruption (RAD51-BRCA2). This highlights how complex and different mechanisms of action can synergistically contribute to the same physiological and, consequently, pharmacological activity.

#### 4. Part II: SYNTHESIS AND EVALUATION OF A COMPUTATIONAL DESIGNED PEPTIDIC LIBRARY TO INHIBIT RAD52

RAD52 is a protein that mediates many DDR pathways that cancer cells rely on when canonical ones are disrupted. Its inhibition induces SL in many cancer cells that are deficient in DNA repair-related proteins including BRCA1/2 and RAD51. Thus, RAD52 becomes crucial in cancer conditions where other DSB repair-related proteins are mutated.<sup>214, 215</sup> This is why RAD52 has become an attractive target for SL-based cancer therapy in recent years to pursue selectivity and targeted cancer therapies.<sup>151</sup>

RAD52 interacts with various partners such as RAD51, RPA, ssDNA, but also with itself, generating high MW superstructures in the presence of DNA. Although there is no FDA-approved RAD52i, the reported inhibitors suggest that the most druggable regions of the protein are the ssDNA binding domain and the oligomerization interface. Indeed, the RAD52 protein is a ring-shaped undecamer that exhibits high thermal stability.<sup>56</sup>

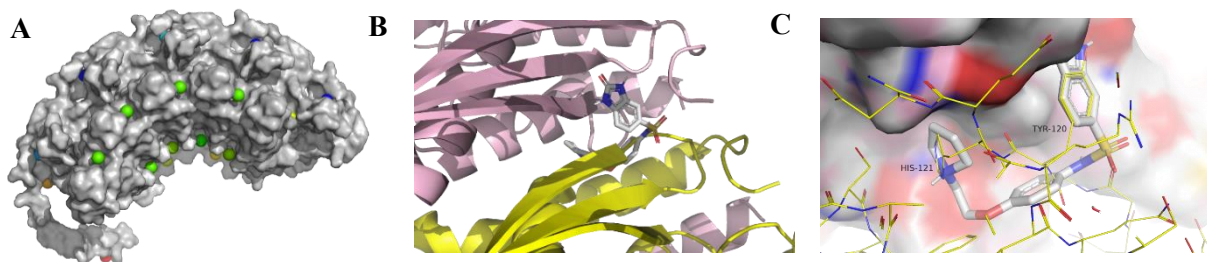
As part of our project, we focused on finding potential disruptors of the monomer-monomer interaction of RAD52 that form the undecamer structure (Figure 31). To go in this direction, it is necessary to find protomer-protomer interaction pockets of RAD52 that can be targeted by small molecules or peptides.



**Figure 31.** Schematic representation of the pipeline for the design of dipeptidic disruptors of RAD52 monomer-monomer interaction.

#### 4.1 Search for RAD52 potential pockets

Initially, the computational unit of the research group conducted a campaign to search a binding pocket of one of the most promising RAD52i, D-I03, whose binding mode on RAD52 is unknown.<sup>237</sup> The search for a potential binding site of compound D-I03 on RAD52 was not satisfactory and forced the computational group to explore the surface of the protein in search of potential pockets. Once the model was simplified by considering only 5 protomers of the crystal structure of the N-terminal domain of RAD52 (PDB 1KN0), it was possible to study the surface contact between adjacent protomers (protein-protein interactions) and to search for potential allosteric sites on the protein surface, as well as potential inhibitors of the interaction with DNA. 38 potential pockets were found, which, once grouped for each repeated pocket, were reduced to 12 potential pockets (Figure 32A). Although the search for a possible binding site for D-I03 resulted in no significant findings, the newly identified RAD52 sites were used for a VS campaign. In each of the 12 identified pockets, a docking was performed for all compounds of an internal Italian Institute of Technology (IIT) library. The most promising molecules were visually inspected, and 65 molecules were selected. The selected molecules were finally grouped according to structural similarity using fingerprint similarity programs. Among the identified molecules, one compound was selected binding a pocket called pocket 36 (Figure 32B). This compound appeared to be a true protein-protein interaction inhibitor, able to inhibit the interaction between protomers, since pocket 36 was located at the protomer-protomer interface and the molecule mapped some key protomer-protomer interactions. The identified pocket is mainly composed of two fundamental aromatic amino acids, Tyr120 and Hys121 (Figure 32C). The first interacts through hydrogen bonds with Ser87 and Gln114 of the other monomer of RAD52, while the second interacts mainly through cation- $\pi$  interactions with Trp84 and Hys86 of the other monomer of RAD52. Thus, the compound was tested with biophysical (MST and DNA binding FRET) and biochemical (SSA inhibition) assays to confirm the druggability of pocket 36 of monomeric RAD52. The compound showed promising results confirming the possibility of targeting pocket 36 and developing inhibitors to bind this protomer-protomer interaction pocket of RAD52.

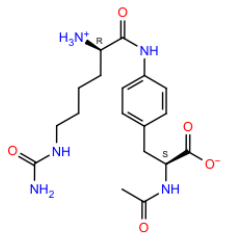
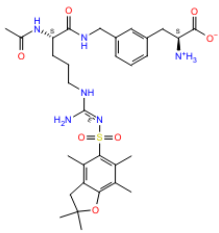
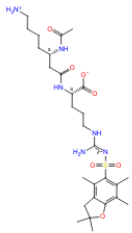
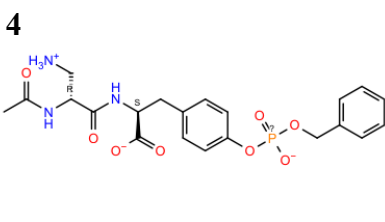
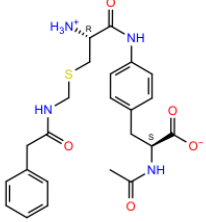
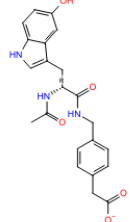
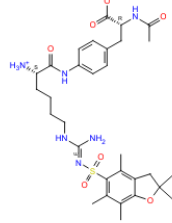
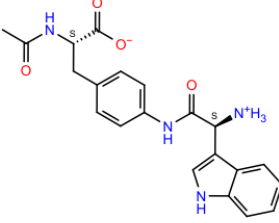
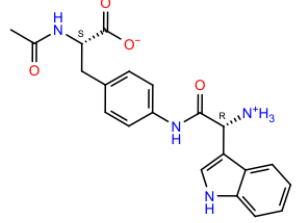
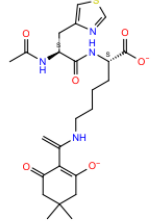
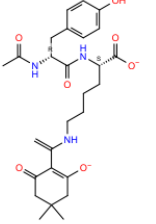


**Figure 32.** **A.** Identified pockets by considering 5 protomers of N-terminal domain of RAD52 (PDB 1KN0). **B.** Protomer-protomer interaction pocket 36 of RAD52 with the molecule docked at the interface. **C.** The identified molecule maps certain key protomer-protomer interactions (Tyr120 and Hys121).

## 4.2 Peptide library creation and Virtual Screening

Once the druggability of pocket 36 of the monomeric RAD52 had been confirmed, my project focused on the synthesis of a small library of dipeptides previously selected by a VS campaign on pocket 36. This project was carried out during my six-month secondment at EPFL in Lausanne in Professor Heinis' Laboratory. The dipeptide library was constructed using the in-house natural and unnatural amino acid of the Laboratory of Therapeutic Proteins and Peptides (LPPT). Initially, the structure of all amino acids (around 600) was analyzed by the Italian computational group. Using an appropriate program (DataWarrior), each amino acid was removed from its protective group (Boc and Fmoc) and made reacting by computational coupling with every in-house amino acid using the DataWarrior program. This procedure generated a library of around 500,000 possible dipeptides that were then acetylated in one free backbone NH residue of each dipeptide. The free carboxylic group, on the other hand, was left neutral, but will inevitably undergo deprotonation at physiological pH. Once the library was created, each compound was docked to pocket 36 of the RAD52 monomer (PDB ID 1KN0) by high-throughput docking with the Schrodinger program and ranked according to its docking scores (Figure 31). The best 11 dipeptides were selected and analyzed for their synthetic feasibility (Table 5). For each dipeptide, its docking pose was studied. Figure 33 shows the docking images of the best three dipeptides selected from this VS on pocket 36 of the RAD52 monomer-monomer interaction.

**Table 5.** Selected dipeptides with related docking scores on pocket 36 of RAD52 monomer.

<p><b>1</b></p>  <p>title Structure2003 + 201485-38-3 [</p> <p>glide gscore -7.278</p> <p>docking score -7.132</p> <p>ionization Penalty Neutral 0.0001</p>	<p><b>2</b></p>  <p>title Structure2003 + 154445-77-9 [</p> <p>glide gscore -7.109</p> <p>docking score -7.098</p> <p>ionization Penalty Neutral 0.0085</p>	<p><b>3</b></p>  <p>title Structure2003 + 203854-47-1 [</p> <p>glide gscore -6.982</p> <p>docking score -6.974</p> <p>ionization Penalty Neutral 0.0078</p>
<p><b>4</b></p>  <p>title Structure2003 + 131570-56-4 [</p> <p>glide gscore -6.947</p> <p>docking score -6.935</p> <p>ionization Penalty Neutral 0.0</p>	<p><b>5</b></p>  <p>title Structure2003 + 159680-21-4 [</p> <p>glide gscore -7.212</p> <p>docking score -6.743</p> <p>ionization Penalty Neutral 0.0</p>	<p><b>6</b></p>  <p>title Structure2003 + 56-69-9 + 176</p> <p>glide gscore -6.733</p> <p>docking score -6.733</p> <p>ionization Penalty Neutral 0.0005</p>
<p><b>7</b></p>  <p>title Structure2003 + 1159680-21-3</p> <p>glide gscore -6.552</p> <p>docking score -6.391</p> <p>ionization Penalty Neutral 0.0081</p>	<p><b>8S</b></p>  <p>title Structure2003 + 58237-94-8 [1,</p> <p>glide gscore -6.887</p> <p>docking score -6.308</p> <p>ionization Penalty Neutral 0.0</p>	<p><b>8R</b></p>  <p>title Structure2003 + 58237-94-8 [1,</p> <p>glide gscore -6.734</p> <p>docking score -6.155</p> <p>ionization Penalty Neutral 0.0</p>
<p><b>9</b></p>  <p>title Structure2003 + 205528-32-1 [</p> <p>glide gscore -6.368</p> <p>docking score -6.151</p> <p>ionization Penalty Neutral 0.0185</p>	<p><b>10</b></p>  <p>title Structure2003 + 112883-29-1 [</p> <p>glide gscore -6.285</p> <p>docking score -6.067</p> <p>ionization Penalty Neutral 0.0192</p>	

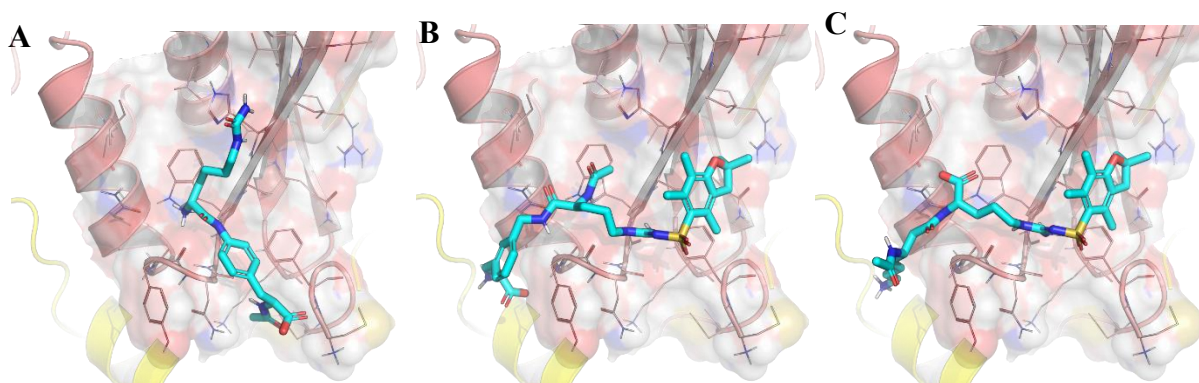


**Figure 33.** Proposed docking poses of dipeptides 1 (A), 2 (B) and 3 (C) on the identified pocket 36 of RAD52 monomer-monomer interaction. Most of the dipeptides interact with previously identified residues on the surface of the other monomer of RAD52, thus mainly Ser87, Gln114, Trp84 and His86. The docking of the dipeptide library had been performed on pocket 36 by R. Ocello, IIT.

### 4.3 Solid-phase peptide synthesis

For each dipeptide selected by the VS on pocket 36 of monomeric RAD52, a parallel solid-phase synthetic strategy was designed to obtain suitable final product quantities. All the dipeptides have a free carboxylic group and one acetylated (capped) amine group. Some of them show sidechain protecting groups (PG) such as pentamethyldihydrobenzofuran-5-sulfonyl (Pbf) for arginine and *N*-1-(4,4-dimethyl-2,6-dioxocyclohex-1-ylidene)ethyl (Dde) for lysine (Table 5). Each dipeptide will undergo RAD52 binding analysis by Microscale Thermophoresis (MST) and Biolayer Interferometry (BLI). For BLI assay each dipeptide must have a biotin tag with PEG3 linker on its amino group. This assay requires one of the binders to be fixed on a streptavidin surface with which the biosensors are coated. The choice to immobilize peptides on the sensor rather than the RAD52 protein is due to the critical stability of the flexible and oligomerization-prone protein. This tendency brings reproducibility problems to the BLI experiment. Biotinylation of RAD52 could also provide additional entropy to the system. Indeed, in the thesis work of B. Balboni<sup>264</sup>, binding experiments of aptamers on RAD52 provided an excellent reference and control BLI experiment by immobilizing the aptamers on the sensor. Thus, to biotinylate each dipeptide, the resin bearing the appropriate dipeptide was split in two different batches and subjected to different reactions. One batch was acylated, the other one was coupled with PEG3-biotin acid. A general scheme for this parallel dipeptide synthesis is shown in Figure 34.

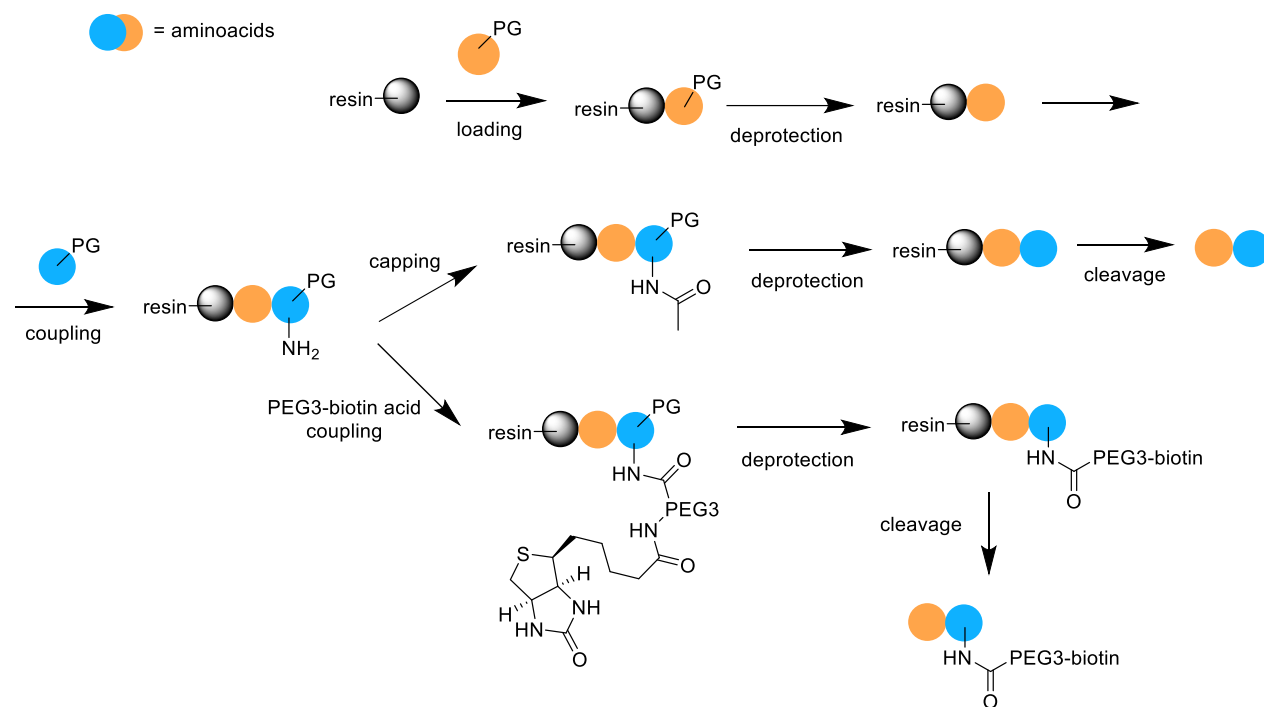


**Figure 34.** Scheme of synthetic strategy of dipeptides and PEG3-biotinylated analogs.

First, the resin choice was essential according to the nature of the PG present on the reacting amino acids. Amino acids used for the synthesis of dipeptides **1**, **2**, **3**, **4**, **5**, **7** and **8** presented both N-fluorenyl methyloxy-carbonyl (Fmoc) and N-tert-butyloxycarbonyl (Boc) groups as PG. For these seven dipeptides, the choice of resin was the polystyrene 4-Hydroxymethylbenzoic acid AM (HMBA AM) resin. This resin is resistant to both the acidic conditions of Boc deprotection and the basic conditions of Fmoc deprotection. Dipeptides **6**, **9** and **10** had no reacting amino acids with Boc as PG. In this case, 2-Chlorotrityl chloride (CTC) resin allowed higher final product yields and was stable under basic conditions of Fmoc deprotection. Figure 35 shows an example of amino acid used for dipeptides **1** and **6** that were synthesized with HMBA resin and CTC resin, respectively. To obtain adequate amounts of final products (approximately 20 mg), a scale of 0.1 mmol of resin was chosen.

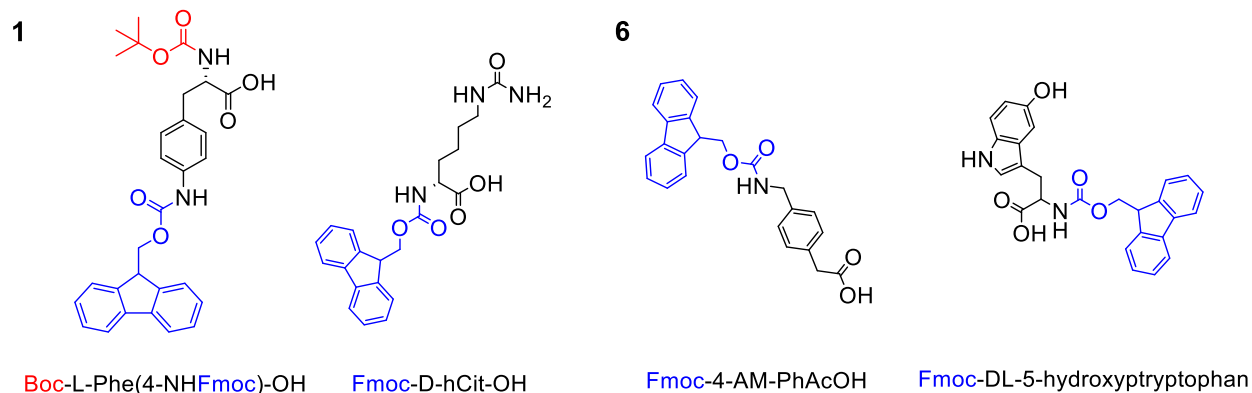


**Figure 35.** Amino acids for synthesis of dipeptide **1** showing the co-presence of Fmoc and Boc PG (HMBA resin is used), whereas amino acids of dipeptide **6** have only Fmoc groups and CTC resin can be used.

Analyzing the structure of amino acids for the synthesis of different dipeptides, issues with the orthogonality of PG deprotection were observed. Specifically, dipeptides **2** and **8** presented two amino groups in which one must be acylated in the ‘capping’ step, while the other must remain free. In Figure 36, the reacting amino acids have two Fmoc groups (dipeptide **2**) and two Boc groups (dipeptide **8**) on the two amino groups blue colored. For the synthesis of these two dipeptides, one of the two amine PG was replaced with N-Allyloxy carbonyl (Alloc), an orthogonal group to Boc and Fmoc deprotections.



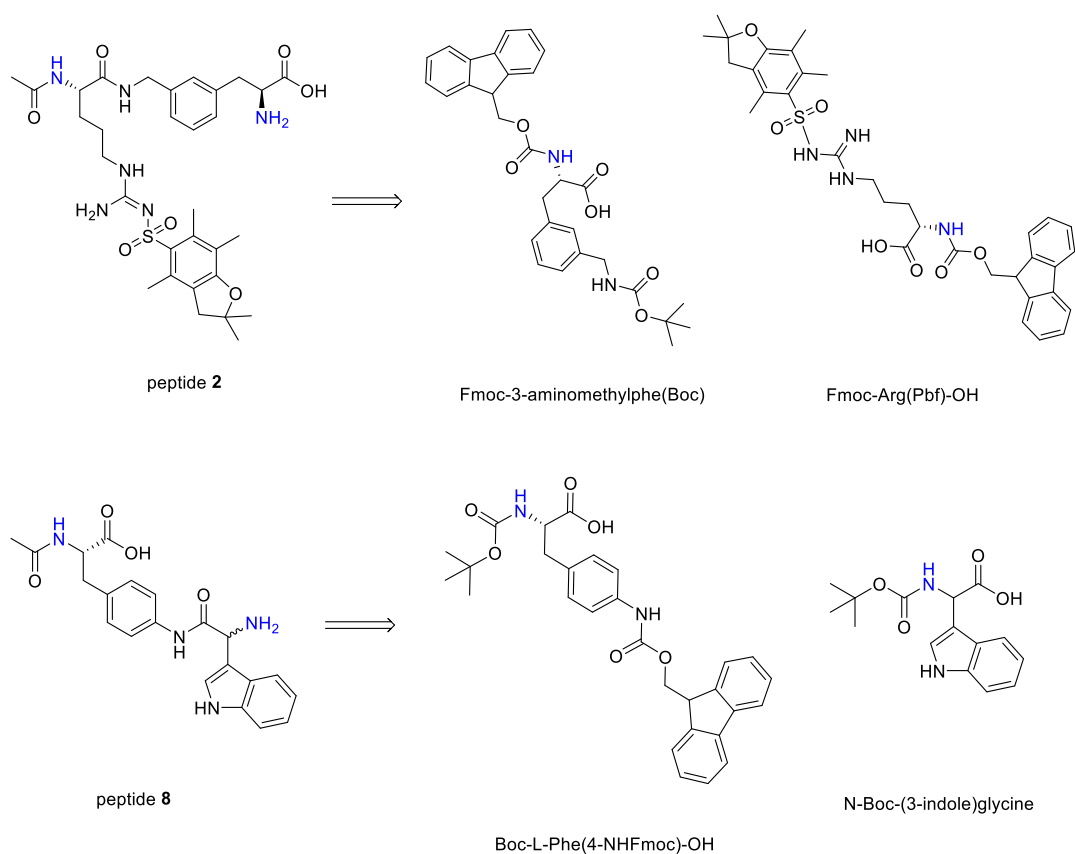


**Figure 36.** Retrosynthetic scheme showing the presence on dipeptides **2** and **8** of two aminic groups where one is free while the other is acylated. On the right part of the scheme, the two different amino acid are presenting the same protecting groups of the  $\text{NH}_2$  of interest: Fmoc for AAs of dipeptide **2** and Boc for AAs of dipeptide **8**. One of the two Fmoc/Boc PG must be replaced with orthogonal Alloc PG.

To verify the loading capacity of the resin and the feasibility of Alloc PG substitution, a test was conducted. The amino acid Boc-L-Phe(4-NHFmoc)-OH was loaded on the HMBA resin by a coupling reaction (Figure 37A). After the capping procedure, Boc-L-Phe(4-NHFmoc)-OH on the resin was deprotected from the Boc PG and the Alloc substitution was conducted. After one night, the substituted amino acid was released from the HMBA resin (Figure 37A). Detailed procedures can be found in Experimental Part 6.2. Finally, analysis of the crude by UPLC-MS revealed the formation of final product (Figure 37B), which, despite the deprotection of the Fmoc group under the basic HMBA resin cleavage conditions, confirmed the possibility of replacing the Boc group with the Alloc group on the resin and confirmed that the resin could be used for the synthesis of the dipeptides of interest.

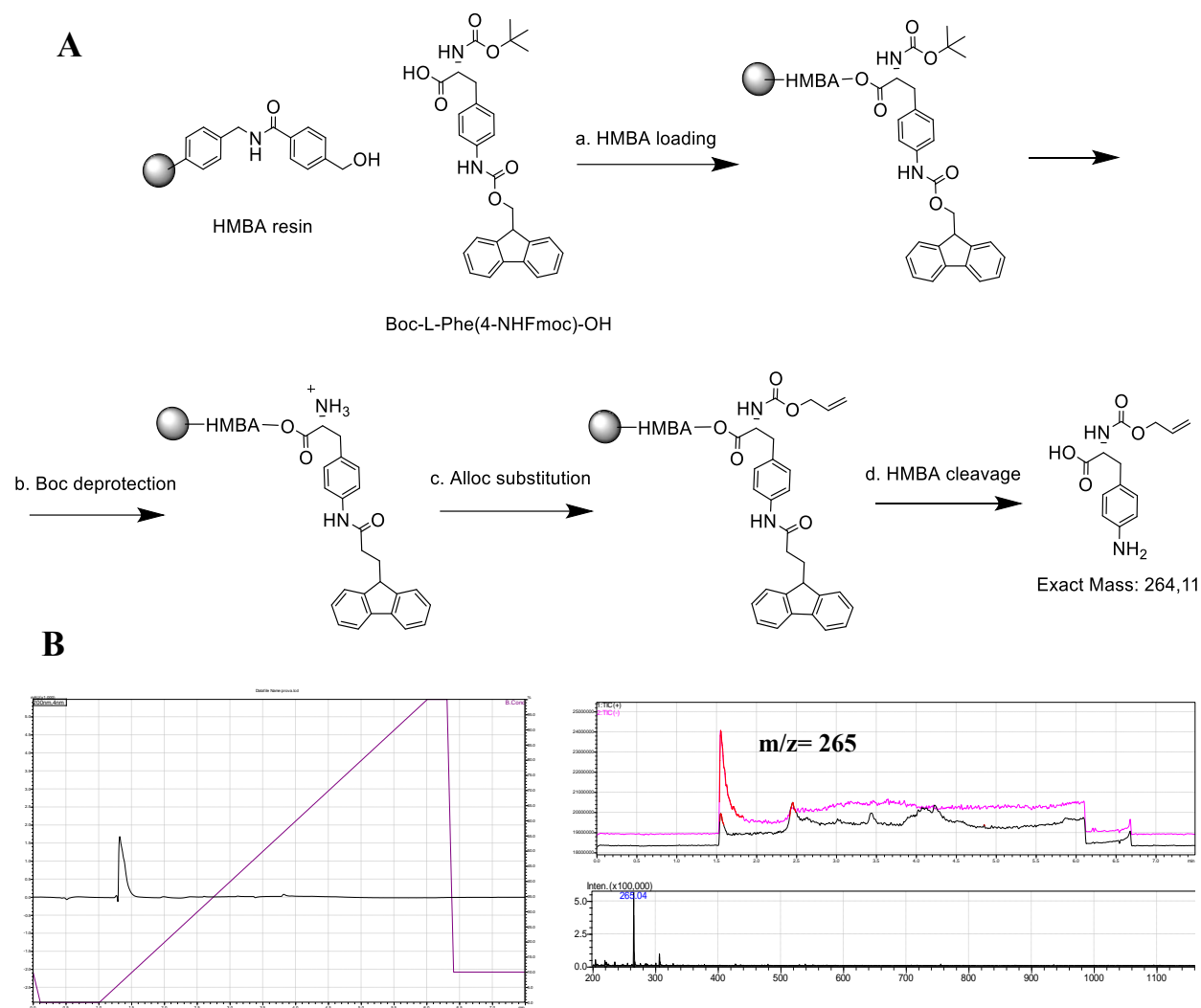


**Figure 37. A) Reagents and conditions:** a. Polystyrene AM HMBA resin, Boc-L-Phe(4-NHFmoc)-OH, HOBT, DMAP, DIC, DMF, 3 h, rt; b. TFA:DCM 1:1, TIPS 2.5%, H<sub>2</sub>O 2.5%, 2x15 min, rt; c. Allyl chloroformate, pyridine, DCM, 12 h, rt; d. NaOH 0.1 M:dioxane 1:3, 4 h, rt. **B) UPLC-MS** of crude of the reaction on the left; TIC+/- of crude compound with mass spectra of the major pick confirming the formation of Alloc-substituted product on the right.

As can be seen in Table 5, some dipeptides present PGs of side chains that are required in the interaction with RAD52 residues. Compounds **2**, **3** and **7** show Pbf PG of the guanidine chain of arginine. This group is usually removed under acidic conditions (90% TFA). Where a Boc group is also present, the Boc deprotection step would cause PG orthogonality issues. This was indeed the case for compounds **3** and **7** (Figure 38). For compound **2**, since Boc PG was removed before coupling with arginine, there were no orthogonality issues.

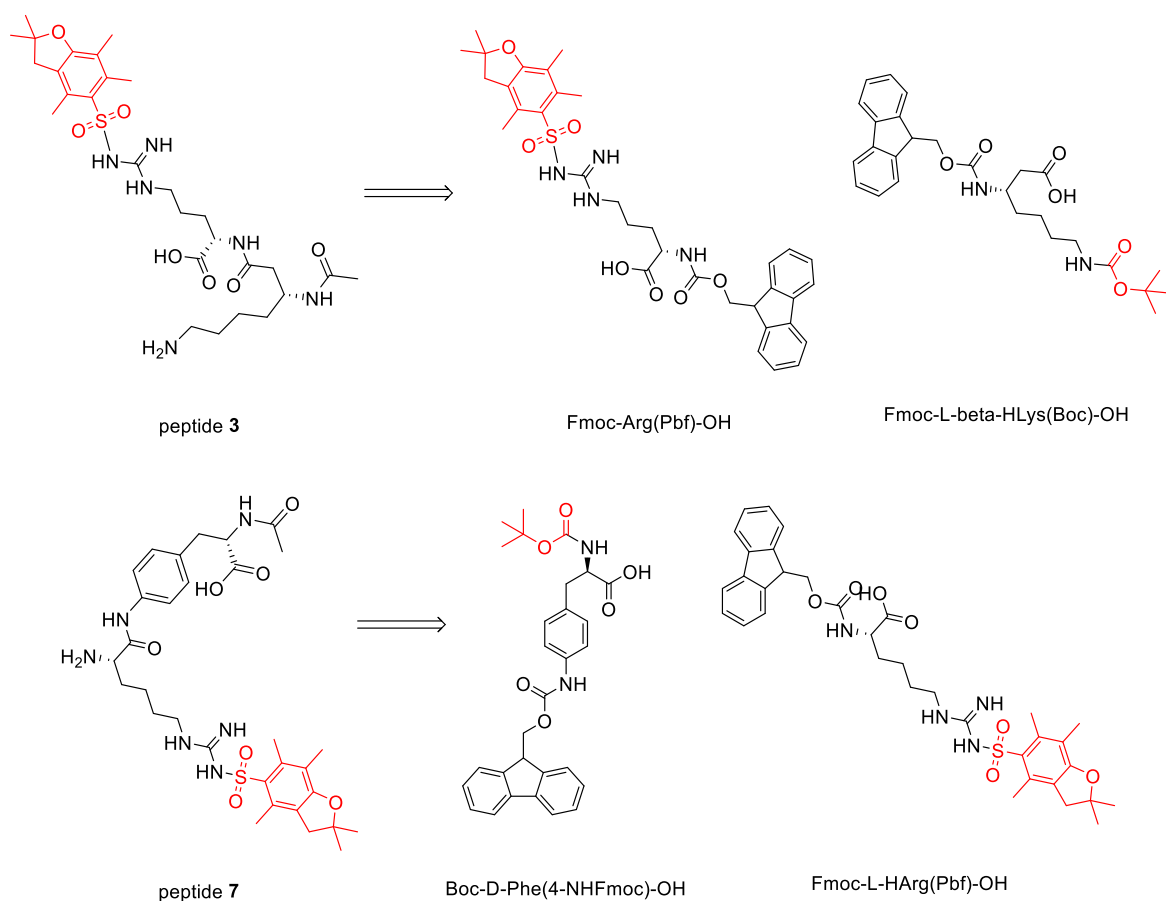


**Figure 38.** Retrosynthetic scheme showing the co-presence of Boc and Pbf on amino acids reacting for the synthesis of dipeptides **3** and **7**.

To evaluate alternative Boc deprotection conditions without affecting Pbf, three trials of different deprotection conditions were conducted by taking an equimolar amount of the amino acids Boc-D-Phe(4-NHFmoc)-OH and Fmoc-Arg(Pbf)-OH within the same Eppendorf tube (Figure 39A). The first trial was conducted with 50% TFA in DCM while the second with 90% TFA in DCM. The third was carried out with 4 M HCl in dioxane. In all trials, TIPS:H<sub>2</sub>O 1:1 were used as scavengers at 10% while the negative control (Trial 4) presented only DCM (Figure 39B). Detailed procedures can be found in Experimental Part 6.2. After 5 minutes at rt, each solution was subjected to UPLC-MS analysis. The first two trials showed both Boc and Pbf-deprotected amino acids, whereas for the third condition the complete formation of Boc-deprotected amino acid was observed without touching Pbf PG on arginine (Figure 39C).

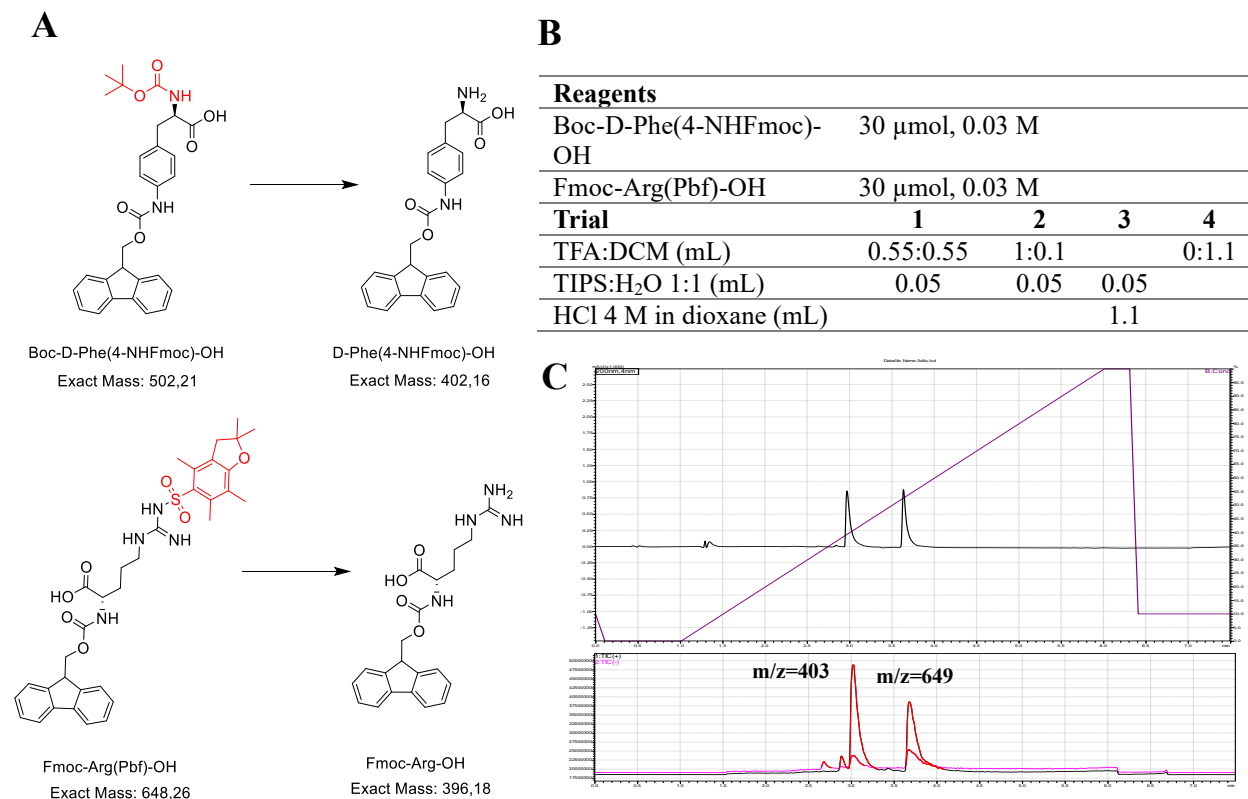
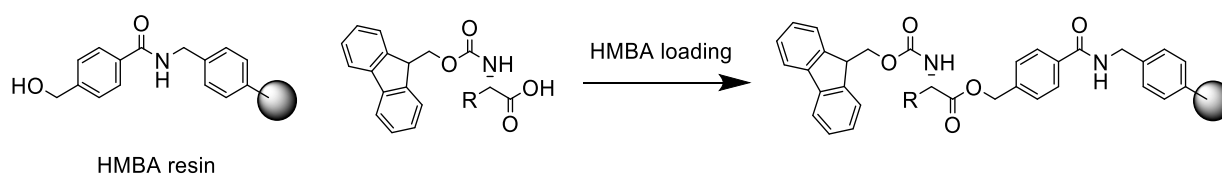


**Figure 39. A)** Boc and Pbf deprotection products of Boc-D-Phe(4-NHFmoc)-OH and Fmoc-Arg(Pbf)-OH. The different conditions are shown in Table **B** with the 4 different trials for 5 min at rt. **C)** UPLC-MS of the crude of Trial 3 showed the formation of the Boc deprotected D-Phe(4-NHFmoc)-OH without touching the Pbf PG on arginine confirming the orthogonality between the two PGs.

After these studies of conditions for PG orthogonal deprotections, I proceeded with the parallel solid-phase synthesis of the dipeptides shown in Table 5.

From the first synthesis showed in Table 6 (Trial 1) and detailed in Experimental section 6.2, various yields were achieved depending on the reactivity of the single amino acids and the nature of the resin. HMBA resin showed lower yields (0-16%) than CTC resin (42-92%). The crucial step was the loading step of the first amino acid on the resin. This step was therefore studied and optimized. A second synthesis of the dipeptides that showed the lower yields was carried out. The coupling reagent HOBt was not added and 2.5 equivalents of DIC reagent were added after 20 min at 0 °C. In addition, coupling was conducted with 5 eq of amino acid (Trial 2, Table 6). By this procedure, dipeptides **1**, **2** and **4** with the corresponding biotinylated analogs showed higher yields (16-67%). Finally, dipeptides **3**, **5** and **8** were also resynthesized. In HMBA resin loading step, the equivalents of DIC were increased from 2.5 to 5 and the time reaction was increased (Trial 3, Table

6). In this case, only dipeptide **5** showed higher yields (37%) while dipeptide **3** always showed yields around 12%. Compound **8** should present a mixture of diastereoisomers **8S** and **8R** but instead presented only one with low yields (4%). Probably the amino acid was not a racemic mixture or a change in stereochemistry occurred during the solid-phase peptide synthesis. Detailed procedures can be found in Experimental Part 6.2.



Resin	
Polystyrene AM HMBA resin	100 $\mu$ mol, 104 mg
<b>Trial 1</b> ( $V_{TOT}$ =0.52 mL), 3 h, rt, DMF	
Amino acid	2.5 eq, 0.5 M
HOBt	2.5 eq, 0.5 M
DIC	1 eq, 0.2 M
DMAP	0.1 eq, 0.02 M
<b>Trial 2</b> ( $V_{TOT}$ =1.02 mL), 2 h, rt, DMF	
Amino acid	5 eq, 0.5 M
DMAP	0.1 eq, 0.01 M
DIC (added after 20 min at 0 °C)	2.5 eq, 0.25 M
<b>Trial 3</b> ( $V_{TOT}$ =1.02 mL), 24 h, rt, DMF	
Amino acid	5 eq, 0.5 M
DMAP	0.1 eq, 0.01 M
DIC (added after 20 min at 0 °C)	5 eq, 0.5 M

**Table 6.** HMBA loading screening of the first amino acid for the parallel peptide synthesis.

Once the synthesis was completed (Experimental part 6.2), each dipeptide was purified by “reversed phase” preparative HPLC with a gradient eluent phase 5-35% ACN in H<sub>2</sub>O. Once the fractions containing the desired product were concentrated by lyophilization, the purity of each pure dipeptide was analyzed by UPLC-MS. Some of them were also analyzed by <sup>1</sup>H and <sup>13</sup>C NMR to confirm the success of the peptide synthesis. The final compounds have been preliminarily analyzed in binding RAD52 by Microscale Thermophoresis (MST) assay, and the corresponding biotinylated analogs will be analyzed by Biolayer Interferometry (BLI) assay. The most promising

dipeptides will be then subjected to further biophysical and biochemical assays such as DNA binding Fluorescence Resonance Energy Transfer (FRET) and Single Strand Annealing (SSA) inhibition.

#### 4.4 Binding affinity evaluation

The library of 10 dipeptides was preliminary evaluated in its ability to bind the His-hRAD52 protein by microscale thermophoresis (MST) screening at 100  $\mu$ M fixed concentration of each dipeptide. This experiment allowed us to assess which dipeptides were the most promising to bind RAD52 and possibly disrupt the interaction between the RAD52 monomers that form its undecameric structure. As the peptides were tested at 100  $\mu$ M, we can consider:

- Binding: a binding that occurs at a concentration below 100  $\mu$ M;
- Weak binding: a binding that occurs at a concentration around 100  $\mu$ M;
- No binding: no binding or binding that might occur at concentrations above 100  $\mu$ M.

Peptide	Binding check	Replicates
1	Binding	8
2	Binding	8
3	No Binding	8
4	No Binding	8
5	Weak Binding	7
6	Weak Binding	7
7	No Binding	7
8R/S	No Binding	7
9	Weak Binding	7
10	No Binding	7

**Table 8.** MST results using polyhistidine-tagged human RAD52 protein diluted to 5 nM in assay buffer and peptides (stock solution in 100% DMSO) tested at 100  $\mu$ M in assay buffer with a final 5% DMSO concentration.

For each dipeptide, between 7 and 8 replicates were performed to confirm the RAD52 binding. The dipeptides **1** and **2** were able to bind RAD52 proteins at a concentration below 100  $\mu$ M and will be studied more deeply as they are the most promising.

In the future, the  $K_d$  values of the 10 dipeptides will be evaluated to further investigate the inhibitory capacity of RAD52 protein. An assay by Biolayer Interferometry (BLI) using the corresponding biotinylated dipeptides could give more accurate measures of protein-dipeptide interaction binding affinity and kinetics by confirming those with the best binding abilities. Subsequently, the best dipeptides capable of binding RAD52 will be evaluated in further biophysical tests for their possible ability to inhibit the binding of RAD52 to DNA by FRET assay and in the biochemical test of inhibition of the SSA mechanism in which RAD52 is most involved.

#### **4.5 Conclusions**

To obtain novel inhibitors of RAD52 that could show SL with inhibition of proteins involved in DDR mechanisms such as PARP1 and BRCA1/2, a campaign was conducted to identify new potential disruptors of the monomer-monomer interaction of RAD52 that forms the undecamer structure.

Initially, the computational research unit searched for possible new monomer-monomer interaction pockets of RAD52 through in-depth computational techniques. Therefore, following the identification of pocket 36 as an interesting protomer-protomer interaction surface, a library of dipeptides using the in-house inventory of Professor Heinis' LPPT laboratory (EPFL) was created using the DataWarrior program by performing the coupling reaction with each possible amino acid. The choice of peptides as PPI inhibitors is because they can mimic a protein surface to effectively compete for binding and their small size is in line with the size of the identified pocket and of small molecules. A VS through high-throughput docking of the approximately 500,000 dipeptides selected the 10 most promising dipeptides capable of binding RAD52 in pocket 36. These dipeptides were evaluated for their synthetic feasibility and subsequently synthesized and purified to obtain a quantity suitable for subsequent binding analyses on the RAD52 protein. In this context, since BLI analyses will be conducted, each dipeptide was synthesized with its PEG3-biotin tagged analog. All dipeptides were obtained in optimized satisfactory yields. Each dipeptide was purified by HPLC and characterized by UPLC-MS. Some of them were also characterized by  $^1\text{H}$  and  $^{13}\text{C}$

NMR. All dipeptides showed purity requirements to be tested by biophysical assays. A preliminary RAD52 binding screening by MST identified dipeptides **1** and **2** as promising RAD52 inhibitors, demonstrating the ability to bind RAD52 at a concentration below 100  $\mu$ M. The BLI biophysical assay will allow us to confirm these promising results, and a precise binding  $K_d$  value will be calculated. Further biophysical and biochemical assays such as RAD52-DNA binding FRET and SSA inhibition may strengthen the inhibitory nature of the most promising dipeptides.

As a final goal cell viability assays in the future could confirm the possibility of triggering a three-pathways SL in combination with PARPi and RAD51-BRCA2 disruptors in BRCA2-functional pancreatic cancer cells. The potential RAD52i could also be tested in BRCA2-mutated cancer cells in combination with PARPi to increase their efficacy and avoid resistance mechanisms especially if established by the activation of alternative DDR mechanisms such as SSA.



## 5. Concluding remarks and future perspectives

The main outcome of my PhD research was to confirm that “fully small molecule-induced SL” can be developed as a new combination strategy in cancer therapy. For this purpose, my work focused on the design and synthesis of small molecules as potential disruptors of the RAD51-BRCA2 PPI and peptides as potential disruptors of the monomer-monomer interaction of RAD52 that can induce SL in combination with PARPi to target pancreatic cancer.

The first part of the thesis reported the development of a library of potential RAD51-BRCA2 PPI disruptors starting from a *hit* identified by VS on Zone II of RAD51. Optimization of a general synthetic strategy gave access to a series of derivatives of the phenyl furanyl-quinolinic structure for SAR investigation, which led to compound **14** with the desired biological profile. Indeed, **14** inhibited RAD51-BRCA2 PPI, reduced cellular HR, and triggered cell death in combination with Olaparib in BRCA2-functional BxPC-3 and HPAC pancreatic cancer cells, fully reproducing the SL paradigm. This paradigm was also confirmed in 3D spheroids of BxPC-3 and HPAC cells at a slightly higher concentration. Encouraging results were also obtained with derivative **19** which induced a synergistic effect in combination with talazoparib in BRCA2-functional pancreatic cancer cells. Further experiments are ongoing to better characterize this promising compound.

In the future, the metabolic and pharmacokinetic (DM/PK) profile of **14** will be analyzed to eventually proceed with further studies in *in vivo* tumor models. These compounds will also be tested in other BRCA2-competent cancer cell lines, such as ovarian or breast cancer cells, to validate their efficacy in other common cancers.

The second part of the thesis concerned the synthesis of dipeptides that can potentially inhibit the monomer-monomer interaction of RAD52. Inhibition of this protein was seen to have SL relationships with PARP and BRCA2 proteins. A VS was performed as a *hit* identification strategy on an identified pocket on the monomer-monomer interaction surface of RAD52. In this context, we considered the possibility of targeting this new monomeric RAD52 interaction pocket through the development of dipeptides in line with the size of the identified pocket. A dipeptidic library was created by taking into consideration the in-house aminoacidic inventory of Professor Heinis' LPPT lab at EPFL in Lausanne where I did my six-month PhD secondment. Following the docking of each dipeptide, the best 10 were selected and synthesized after the optimization of the solid-phase peptide synthetic strategy. This approach allowed the identification of dipeptides capable of

binding RAD52 by biophysical binding assays (MST) and will be confirmed by further BLI tests. The ability to inhibit SSA and DNA binding will be evaluated in further biochemical assays to confirm the possibility of achieving “fully small molecule-induced SL” in the future. Indeed, the final goal of this project is to achieve a three-pathways SL in combination with PARPi and RAD51-BRCA2 disruptors in BRCA2-functional pancreatic cancer cells. This paradigm can be established through cell viability studies in combination with the RAD51-BRCA2 PPI disruptor **14** identified in Part I of the thesis and a PARPi such as Olaparib or Talazoparib. To conclude, these results are in line with our main research goal to confirm that “fully small molecule-induced SL” with PARP inhibitors can be developed as a new combination strategy in cancer therapy.

## 6. Experimental section

### 6.1 Experimental section: Part I

#### 6.1.1 Material and methods

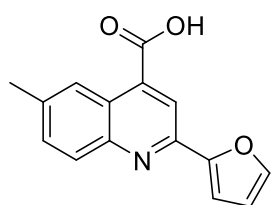
Solvents and reagents were obtained from commercial suppliers and used without further purification. If required, solvents were distilled prior to use. For simplicity, solvents and reagents are indicated as follows: acetonitrile (ACN), dichloromethane (DCM), diethyl ether (Et<sub>2</sub>O), petroleum ether (PE), dimethyl sulfoxide (DMSO), ethanol (EtOH), ethyl acetate (EtOAc), methanol (MeOH), triethylamine (TEA) and 1,2-dichloroethane (EDC). Thin layer chromatography analyses were performed using pre-coated Supelco silica gel on TLC Al foils 0.2 mm and visualized by UV (254 nm/365 nm), and/or KMnO<sub>4</sub> stain. Automated column chromatography purifications were conducted using a Teledyne ISCO apparatus (CombiFlash Rf) with prepacked silica gel columns of different sizes (from 4 to 120 g). Mixtures of increasing polarity of EP and EtOAc or DCM and MeOH were used as eluents. NMR experiments were run on a Bruker Avance III 400 or Bruker 600 system (400.13/600 MHz for <sup>1</sup>H, and 100.62/151 MHz for <sup>13</sup>C), equipped with a BBI probe and Z-gradients. Spectra were acquired at 300 K, using deuterated dimethyl sulfoxide (DMSO-*d*<sup>6</sup>) or deuterated chloroform (Chloroform-*d*) as solvent. Chemical shifts for <sup>1</sup>H and <sup>13</sup>C spectra were recorded in parts per million using the residual non-deuterated solvent as the internal standard (for DMSO-*d*<sup>6</sup>: 2.50 ppm, <sup>1</sup>H; 39.52 ppm, <sup>13</sup>C; for Chloroform-*d*: 7.26 ppm, <sup>1</sup>H; 77.16 ppm, <sup>13</sup>C). Data are reported as follows: chemical shift (ppm), multiplicity (indicated as: bs, broad signal; s, singlet; d, doublet; t, triplet; q, quartet; m, multiplet), coupling constants (*J*) in Hertz (Hz) and integrated intensity. UPLC-MS analyses were run on a Waters ACQUITY UPLC-MS system consisting of an QDa mass spectrometer equipped with an Electrospray Ionization interface and a 2489 UV/Vis Detector. PDA range was 210-400 nm. The analyses were performed on an XBridge BEH C18 column (10 × 2.1 mm i.d., particle size 2.5 μm) with a XBridge BEH C18 VanGuard Cartridge precolumn (5 mm × 2.1 mm i.d., particle size 1.8 μm). The mobile phases were H<sub>2</sub>O (0.1% formic acid) (A) and ACN (0.1% formic acid) (B). Electrospray ionization in positive and negative mode was applied in the mass scan range 50–1200 Da. The following gradient was used: 0–0.78 min, 20% B; 0.78-2.87 min, 20–95% B; 2.87-3.54 min, 95% B; 3.54-3.65 min, 95-20% B; 3.65-5-73, 20% B. Flow rate: 0.8 mL/min. Compounds were named using the naming algorithm developed by CambridgeSoft Corporation and used in

ChemBioDraw Ultra 16.0. All final compounds displayed >96% purity as determined by UPLC-MS and NMR analysis.

#### 6.1.2 General procedure A for the synthesis of 2-(furan-2-yl)quinoline-4-carboxylic acid intermediates **25**, **27**, **17**, **55**.

This procedure has been conducted for the preparation of **25**, **27** (Scheme 3), **17**, **55** (Scheme 4). In a microwave vessel, the appropriate isatin (**23**, **26**, **52**, **53**, 1.00 equiv), acetylfuran (**21**, **54**, 1.20 equiv) and KOH (3 equiv) were stirred in EtOH/H<sub>2</sub>O (3:1 v/v, 0.5 M) at room temperature. The reaction is conducted in the microwave reactor and kept stirring at 80 °C for 3 hours, 80 W. After 3 hours, the solution is transferred to a flask and is quenched with water. The ethanol is evaporated by rotavapor and the aqueous solution is extracted with Et<sub>2</sub>O (3x50 mL) to isolate excess furan. The aqueous phase is then acidified to pH 3 with conc. HCl until the precipitation of the desired product. The latter is filtered, resolubilized with acetone and concentrated in vacuum. The product obtained is characterized by UPLC-MS and <sup>1</sup>H NMR.

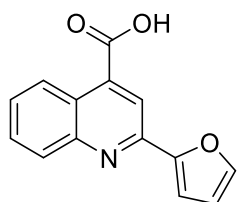
##### 2-(Furan-2-yl)-6-methylquinoline-4-carboxylic acid (**25**)



Compound **25** was synthesized via general procedure A using 5-methylisatin **23** (2 g, 12.41 mmol) with 2-acetylfuran **21** (1.64 g, 14.9 mmol) and KOH (2.1 g, 37.23 mmol). After work-up, 2.88 g (11.3 mmol, 75% yield) of pure product were obtained.

<sup>1</sup>H NMR (401 MHz, Chloroform-d)  $\delta$  8.44 (d,  $J$  = 1.8 Hz, 1H), 8.25 (s, 1H), 7.98 (d,  $J$  = 8.7 Hz, 1H), 7.77 (d,  $J$  = 1.7 Hz, 1H), 7.63 (dd,  $J$  = 8.7, 2.0 Hz, 1H), 7.34 (d,  $J$  = 3.5 Hz, 1H), 6.67 (dd,  $J$  = 3.5, 1.8 Hz, 1H), 2.54 (s, 3H) ppm. UPLC-MS (ESI,  $m/z$ )  $R_t$  = 2.05 min, 254 (M+H)<sup>+</sup>

##### 2-(Furan-2-yl)quinoline-4-carboxylic acid (**27**)

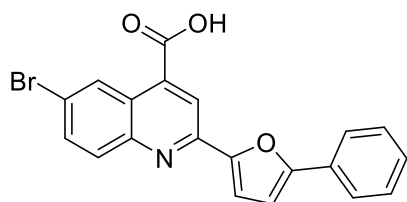


Compound **27** was synthesized via general procedure A using isatin **26** (1 g, 6.8 mmol), 2-acetylfuran **21** (0.898 g, 8.16 mmol) and KOH (1.14 g, 20.39 mmol). After work-up, 0.876 g (3.66 mmol, 54% yield) of pure product were obtained.

<sup>1</sup>H NMR (401 MHz, Chloroform-d)  $\delta$  8.44 (dd,  $J$  = 8.7, 1.8 Hz, 1H), 8.25 (s, 1H), 7.98 (dd,  $J$  = 8.7, 1.8 Hz, 1H), 7.79 (t,  $J$  = 8.7 Hz, 1H), 7.77 (dd,  $J$  = 8.7, 1.7 Hz, 1H), 7.63 (t,  $J$  = 8.7 Hz, 1H),

7.34 (d, J = 3.5 Hz, 1H), 6.67 (dd, J = 3.5, 1.8 Hz, 1H) ppm. UPLC-MS (ESI, m/z) Rt = 2.7 min, 240 (M+H)<sup>+</sup>

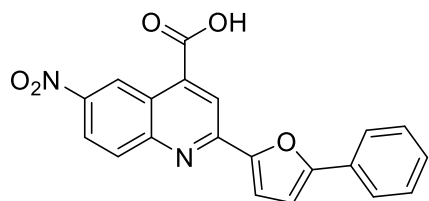
#### 6-Bromo-2-(5-phenylfuran-2-yl)quinoline-4-carboxylic acid (**17**)



Compound **17** was synthesized via general procedure A using 5-bromoindolin 2,3-dione **52** (105 mg, 0.464 mmol), 5-phenyl-2-acetyl furan **54** (103.8 mg, 0.557 mmol) and KOH (78.19 mg, 1.39 mmol). After work-up, 68 mg (0.172 mmol, 37% yield) of pure product were obtained.

<sup>1</sup>H NMR (600 MHz, DMSO-d<sub>6</sub>) δ 8.90 (d, J = 2.2 Hz, 1H), 8.44 (s, 1H), 8.02 (d, J = 9.0 Hz, 1H), 7.94 (dd, J = 9.0, 2.3 Hz, 1H), 7.92 – 7.88 (m, 2H), 7.58 (d, J = 3.6 Hz, 1H), 7.51 (t, J = 7.8 Hz, 2H), 7.42 – 7.36 (m, 1H), 7.25 (d, J = 3.6 Hz, 1H) ppm. <sup>13</sup>C NMR (151 MHz, DMSO-d<sub>6</sub>) δ 167.31, 155.76, 152.10, 148.78, 147.64, 136.37, 133.91, 131.86, 129.98, 129.56, 129.56, 128.93, 128.17, 125.03, 124.56, 124.56, 121.32, 119.76, 114.71, 109.51 ppm. UPLC-MS (ESI, m/z) Rt = 3.63 min, 394-396 (M+H)<sup>+</sup>

#### 6-Nitro-2-(5-phenylfuran-2-yl)quinoline-4-carboxylic acid (**55**)

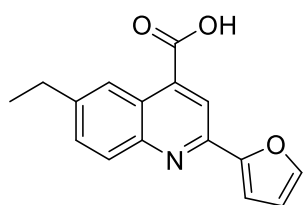


Compound **55** was synthesized via general procedure A using 5-nitroisatin **53** (0.17 mg, 0.885 mmol), 5-phenyl-2-acetyl furan **54** (0.181 g, 0.973 mmol) and KOH (0.149 g, 2.65 mmol). After work-up, 0.087 g (0.241 mmol, 28% yield) of product were obtained. The product contained a 10% impurity corresponding to the reduced amine form **19**. The characterization reported concerns only the desired compound **55**.

<sup>1</sup>H NMR (600 MHz, DMSO-d<sub>6</sub>) δ 10.62 (d, J = 1.9 Hz, 1H), 8.22 (s, 1H), 8.05 (dd, J = 9.1, 2.4 Hz, 1H), 8.02 - 7.94 (d, J = 9.1 Hz, 1H), 7.92 - 7.88 (m, 2H), 7.82 - 7.77 (m, 2H), 7.56 - 7.49 (d, J = 3.6 Hz, 1H), 7.42 (d, J = 3.6 Hz, 1H), 7.09 (d, J = 3.5 Hz, 1H) ppm. UPLC-MS (ESI, m/z) Rt = 3.4 min, 361 (M+H)<sup>+</sup>

6.1.3 Doebner trials with TEA for the synthesis of quinoline-4-carboxylic acid intermediates **62**, **27**, **64** (Scheme 5).

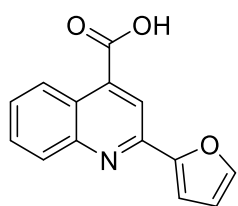
#### 6-Ethyl-2-(furan-2-yl)quinoline-4-carboxylic acid (**62**)



In a 10 ml three necked round bottom flask, para-ethylaniline **56** (0.102 mL, 0.825 mmol) is dissolved in 2 ml of EtOH. To this solution, furaldehyde **60** (0.068 mL, 0.825 mmol), pyruvic acid **61** (0.058 mL, 0.825 mmol) and TEA (0.115 mL, 0.825 mmol) were added at room temperature. The reaction mixture was then refluxed at 80°C for 5 h under N<sub>2</sub>. The reaction is then left overnight at rt with N<sub>2</sub>. An extraction is conducted with basic water (NaOH 10%) and DCM, the basic water is acidified with conc HCl until pH 3 and extracted with DCM. DCM is anhydriified with Na<sub>2</sub>SO<sub>4</sub> and concentrated with rotavapor to afford 130 mg (0.486 mmol, 58% yield) of pure product **62** characterized by <sup>1</sup>H NMR.

<sup>1</sup>H NMR (401 MHz, Chloroform-d) δ 8.52 (d, J = 1.9 Hz, 1H), 8.32 (s, 1H), 8.01 (d, J = 8.7 Hz, 1H), 7.79 (dd, J = 1.8, 0.7 Hz, 1H), 7.68 (dd, J = 8.7, 2.0 Hz, 1H), 7.45 - 7.32 (m, 1H), 6.68 (dd, J = 3.5, 1.8 Hz, 1H), 2.84 (q, J = 7.6 Hz, 2H), 1.32 (t, J = 7.6 Hz, 3H) ppm. UPLC-MS (ESI, m/z) Rt = 2.61 min, 268 (M+H)<sup>+</sup>

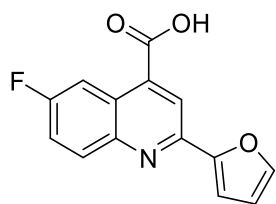
#### 2-(Furan-2-yl)quinoline-4-carboxylic acid (**27**)



In a 10 ml three necked round bottom flask, aniline **79** (0.195 mL, 2.15 mmol) is dissolved in 5 ml of EtOH. To this solution, furaldehyde **60** (0.178 mL, 2.15 mmol), pyruvic acid **61** (0.151 mL, 2.15 mmol) and TEA (0.3 mL, 2.15 mmol) were added at room temperature. The reaction mixture was then refluxed at 80°C for 52 h under N<sub>2</sub>. An extraction is conducted with basic water (NaOH 10%) and DCM, the basic water is acidified with conc HCl until pH 3 and extracted with DCM. DCM is anhydriified with Na<sub>2</sub>SO<sub>4</sub> and concentrated with rotavapor to afford 318 mg (1.33 mmol, 62% yield) of pure product **27** characterized by 1H-NMR.

<sup>1</sup>H NMR (401 MHz, Chloroform-d) δ 8.44 (dd, J = 8.7, 1.8 Hz, 1H), 8.25 (s, 1H), 7.98 (dd, J = 8.7, 1.8 Hz, 1H), 7.79 (t, J = 8.7 Hz, 1H), 7.77 (dd, J = 8.7, 1.7 Hz, 1H), 7.63 (t, J = 8.7 Hz, 1H), 7.34 (d, J = 3.5 Hz, 1H), 6.67 (dd, J = 3.5, 1.8 Hz, 1H) ppm. UPLC-MS (ESI, m/z) Rt = 2.7 min, 240 (M+H)<sup>+</sup>

### 6-Fluoro-2-(furan-2-yl)quinoline-4-carboxylic acid (**64**)



In a 10 ml three necked round bottom flask, para-fluoroaniline **58** (0.172 mL, 1.8 mmol) is dissolved in 5 ml of EtOH. To this solution, furfuraldehyde **60** (0.149 mL, 1.8 mmol), pyruvic acid **61** (0.127 mL, 1.8 mmol) and TEA (0.25 mL, 1.8 mmol) were added at room temperature. The reaction mixture was then refluxed at 80°C for 52 h under N<sub>2</sub>. An extraction is conducted with basic water (NaOH 10%) and DCM, the basic water is acidified with conc HCl until pH 3 and extracted with DCM. DCM is anhydridified with Na<sub>2</sub>SO<sub>4</sub> and concentrated with rotavapor to afford 58 mg (0.23 mmol, 12% yield) of pure product **27** characterized by <sup>1</sup>H-NMR.

<sup>1</sup>H NMR (401 MHz, DMSO-d<sub>6</sub>) δ 8.42 (dd, J = 11.0, 2.9 Hz, 1H), 8.35 (s, 1H), 8.13 (dd, J = 9.3, 5.8 Hz, 1H), 7.94 (dd, J = 1.8, 0.8 Hz, 1H), 7.73 (dd, J = 9.3, 8.1, 2.9 Hz, 1H), 7.42 (dd, J = 3.5, 0.8 Hz, 1H), 6.72 (dd, J = 3.4, 1.8 Hz, 1H) ppm. UPLC-MS (ESI, m/z) Rt = 2.59 min, 258 (M+H)<sup>+</sup>

6.1.4 Doebner trials with Cp<sub>2</sub>ZrCl<sub>2</sub>/brønsted acid/CuO cooperative catalysis system for the synthesis of quinoline-4-carboxylate intermediates **67b**, **63** (Table 2).

**Entry 1.** A three-necked 10 mL flask, equipped with a magnetic stirrer and a septum, was charged with i-PrOH (0.375 mL), H<sub>2</sub>O (0.125 mL), furfural **60** (0.082 mL, 1 mmol), 4-methoxyaniline **57** (135 mg, 1.1 mmol) and methyl pyruvate **81** (0.135 mL, 1.5 mmol) in one portion. After 10 min, Cp<sub>2</sub>ZrCl<sub>2</sub> (15 mg, 0.05 mmol), trimellitic acid (10 mg, 0.05 mmol), and CuO (4 mg, 0.05 mmol) were added and stirred at 60 °C. After 2 h, the reaction mixture was quenched with distilled water (5 mL). The aqueous phase was extracted with DCM (3×5 mL), dried over Na<sub>2</sub>SO<sub>4</sub> and concentrated in vacuo to give desired product. The corresponding solid product was obtained through column chromatography with 100% DCM to afford 64 mg (0.226 mmol, 22% yield) of pure product **67b**.

**Entry 2.** A three-necked 10 mL flask, equipped with a magnetic stirrer and a septum, was charged with i-PrOH (0.5 mL), furfural **60** (0.082 mL, 1 mmol), 4-methoxyaniline **57** (135 mg, 1.1 mmol) and methyl pyruvate **81** (0.135 mL, 1.5 mmol) in one portion. After 10 min, Cp<sub>2</sub>ZrCl<sub>2</sub> (15 mg, 0.05 mmol), trimellitic acid (10 mg, 0.05 mmol), and CuO (4 mg, 0.05 mmol) were added and stirred at 60 °C for 6 h and rt overnight to complete the reaction. The reaction mixture was then quenched

with distilled water (5 mL). The aqueous phase was extracted with DCM (3×5 mL), dried over Na<sub>2</sub>SO<sub>4</sub> and concentrated in vacuo to give desired product. The corresponding solid product was obtained through column chromatography with EP:AcOEt 95:5 to afford 64 mg (0.198 mmol, 20% yield) of pure product **67b**.

**Entry 3.** A three-necked 10 mL flask, equipped with a magnetic stirrer and a septum, was charged with i-PrOH (0.5 mL), furfural **60** (0.082 mL, 1 mmol), 4-methoxyaniline **57** (123 mg, 1 mmol) and methyl pyruvate **81** (0.09 mL, 1 mmol) in one portion. Triethylamine (0.139 mL, 1 mmol) was added, and the reaction was stirred at 60 °C for 6 h and rt overnight to complete the reaction. The formation of **67b** is not seen and the reaction is abandoned.

**Entry 4.** A three-necked 10 mL flask, equipped with a magnetic stirrer and a septum, was charged with i-PrOH (0.75 mL), H<sub>2</sub>O (0.25 mL), furfural **60** (0.166 mL, 2 mmol), 4-methoxyaniline **57** (270 mg, 2.2 mmol) and methyl pyruvate **81** (0.271 mL, 3 mmol) in one portion. After 10 min, Cp<sub>2</sub>ZrCl<sub>2</sub> (30 mg, 0.1 mmol), trimellitic acid (21 mg, 0.1 mmol), and CuO (8 mg, 0.1 mmol) were added and stirred at 60 °C for 6 h and rt overnight under N<sub>2</sub> to complete the reaction. The reaction mixture was then quenched with distilled water (5 mL). The aqueous phase was extracted with DCM (3×5 mL), dried over Na<sub>2</sub>SO<sub>4</sub> and concentrated in vacuo to give desired product. The corresponding solid product was obtained through column chromatography with 100% DCM to afford 50 mg (0.176 mmol, 8% yield) of pure product **67b**.

**Entry 5.** A three-necked 10 mL flask, equipped with a magnetic stirrer and a septum, was charged with EtOH (3 mL), furfural **60** (0.134 mL, 1.62 mmol), 4-methoxyaniline **57** (200 mg, 1.62 mmol) and pyruvic acid **61** (0.114 mL, 1.62 mmol) and triethylamine (0.226 mL, 1.62 mmol) in one portion. The reaction was stirred at 80 °C for 4.5 h under N<sub>2</sub>. The reaction was concentrated in vacuum and extraction with DCM:NaOH 15% (3×15 mL) was conducted. The aqueous phase was then acidified with concentrated HCl and the precipitate was filtered and weighted. The acid water was then extracted with DCM (3×10 mL), dried over Na<sub>2</sub>SO<sub>4</sub> and concentrated in vacuo to give the desired product. The product was characterized by <sup>1</sup>H NMR and UPLC-MS and results as pure. 72 mg (0.267 mmol, 16% yield) of pure product **63** were obtained.

**Entry 6.** A three-necked 10 mL flask, equipped with a magnetic stirrer and a septum, was charged with i-PrOH (0.75 mL), H<sub>2</sub>O (0.25 mL), furfural **60** (0.166 mL, 2 mmol), 4-methoxyaniline **57** (123 mg, 1 mmol) and pyruvic acid **61** (0.211 mL, 3 mmol) in one portion. After 10 min, Cp<sub>2</sub>ZrCl<sub>2</sub>



(15 mg, 0.05 mmol), trimellitic acid (10 mg, 0.05 mmol), and CuO (4 mg, 0.05 mmol) were added and stirred at 60 °C for 18 h to complete the reaction. The reaction was concentrated in vacuum and extraction with DCM:NaOH 15% (3x15 mL) was conducted. The aqueous phase was then acidified with concentrated HCl and the precipitate was filtered and weighted. The acid water was then extracted with DCM (3x10 mL), dried over Na<sub>2</sub>SO<sub>4</sub> and concentrated in vacuo to give the desired product. The solid products were purified through column chromatography with EP:AcOEt 95:5 to afford 52 mg (0.193 mmol, 19% yield) of pure product **63**.

**Entry 7.** A three-necked 10 mL flask, equipped with a magnetic stirrer and a septum, was charged with i-PrOH (0.75 mL), H<sub>2</sub>O (0.25mL), 4-methoxyaniline **57** (270 mg, 2.2 mmol), Cp<sub>2</sub>ZrCl<sub>2</sub> (30 mg, 0.1 mmol) and trimellitic acid (21 mg, 0.1 mmol). After 1 h reaction at rt, furfural **60** (0.166 mL, 2 mmol) was added and the reaction is left at 60 °C for 0.5 h. Finally, methyl pyruvate **81** (0.271 mL, 3 mmol) and CuO (8 mg, 0.1 mmol) were added in one portion. The reaction was then stirred at 60 °C for 3 h. The reaction mixture was quenched with distilled water (5 mL). The aqueous phase was extracted with DCM (3x5 mL), dried over Na<sub>2</sub>SO<sub>4</sub> and concentrated in vacuo to give desired product. The corresponding solid product was obtained through column chromatography with EP:AcOEt 95:5 to afford 52 mg (0.184 mmol, 10% yield) of pure product **67b**.

**Entry 8.** A three-necked 10 mL flask, equipped with a magnetic stirrer and a septum, was charged with i-PrOH (0.375 mL), H<sub>2</sub>O (0.125mL), furfural **60** (0.166 mL, 2 mmol), 4-methoxyaniline **57** (270 mg, 2.2 mmol) and methyl pyruvate **81** (0.271 mL, 3 mmol) in one portion and the reagents were stirred at rt for 30 min. Cp<sub>2</sub>ZrCl<sub>2</sub> (30 mg, 0.1 mmol), trimellitic acid (21 mg, 0.1 mmol), and CuO (8 mg, 0.1 mmol) in i-PrOH:H<sub>2</sub>O (3:1, 0.5 mL) were stirred at 60 °C in a 5 mL flask and added at rt to the reaction mixture after 30 min. The reaction is conducted at 60 °C for 2 h. The reaction mixture was then quenched with distilled water (5 mL). The aqueous phase was extracted with DCM (3x5 mL), dried over Na<sub>2</sub>SO<sub>4</sub> and concentrated in vacuo to give desired product. The corresponding solid product was obtained through column chromatography with EP:AcOEt 95:5 to afford 44 mg (0.155 mmol, 8% yield) of pure product **67b**.

**Entry 9.** A three-necked 10 mL flask, equipped with a magnetic stirrer and a septum, was charged with i-PrOH (0.375 mL), H<sub>2</sub>O (0.125mL), furfural **60** (0.166 mL, 2 mmol), 4-methoxyaniline **57** (270 mg, 2.2 mmol) and methyl pyruvate **81** (0.271 mL, 3 mmol) in one portion and the reagents

were stirred at 60 °C for 30 min. Cp<sub>2</sub>ZrCl<sub>2</sub> (30 mg, 0.1 mmol), trimellitic acid (21 mg, 0.1 mmol), and CuO (8 mg, 0.1 mmol) in i-PrOH:H<sub>2</sub>O (3:1, 0.5 mL) were stirred at 60 °C in a 5 mL flask and added at 60 °C to the reaction mixture after 30 min. The reaction is conducted at 60 °C for 2 h. The reaction mixture was then quenched with distilled water (5 mL). The aqueous phase was extracted with DCM (3×5 mL), dried over Na<sub>2</sub>SO<sub>4</sub> and concentrated in vacuo to give desired product. The corresponding solid product was obtained through column chromatography with EP:AcOEt 95:5 to afford 82 mg (0.289 mmol, 14% yield) of pure product **67b**.

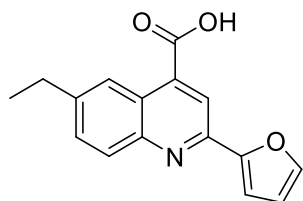
**67b:** <sup>1</sup>H NMR (401 MHz, DMSO-d<sub>6</sub>) δ 8.26 (s, 1H), 8.11 (d, J = 2.9 Hz, 1H), 7.97 (d, J = 9.2 Hz, 1H), 7.90 (d, J = 1.7 Hz, 1H), 7.46 (dd, J = 9.2, 2.9 Hz, 1H), 7.31 (d, J = 3.4 Hz, 1H), 6.69 (dd, J = 3.4, 1.8 Hz, 1H), 3.90 (s, 3H), 3.88 (s, 3H) ppm. UPLC-MS (ESI, m/z) Rt = 3.26 min, 284 (M+H)<sup>+</sup>

**63:** <sup>1</sup>H NMR (401 MHz, DMSO-d<sub>6</sub>) δ 8.26 (s, 1H), 8.11 (d, J = 2.9 Hz, 1H), 7.97 (d, J = 9.2 Hz, 1H), 7.90 (d, J = 1.7 Hz, 1H), 7.46 (dd, J = 9.2, 2.9 Hz, 1H), 7.31 (d, J = 3.4 Hz, 1H), 6.69 (dd, J = 3.4, 1.8 Hz, 1H), 3.88 (s, 3H) ppm. UPLC-MS (ESI, m/z) Rt = 2.3 min, 270 (M+H)<sup>+</sup>

#### 6.1.5 General procedure B for the synthesis of 2-(furan-2-yl)quinoline-4-carboxylic acid intermediates **62-65**, **18**, **78**.

This procedure has been conducted for the preparation of **62-65** (Scheme 6), **18** (Scheme 7) and **78** (Scheme 8). In a one-neck flask, furfural (**60**, **75**, **77**, 2 equiv) and boron-diethyl ether trifluoride (0.5 equiv) were added to a solution of the appropriate substituted aniline (**56-59**, **74**, **76**, 1.8 equiv) in dry acetonitrile (0.2 M). The mixture was stirred at 65 °C for 20 min. Subsequently, a solution of pyruvic acid **61** (1 equiv) in acetonitrile (0.6 M) was added drop by drop. The reaction was conducted at 65 °C under stirring for 24 h. Then the mixture was cooled down to room temperature and water was added. An extraction with DCM (3x40 mL) was performed. The organic phase obtained was then extracted with an aqueous NaOH 5% solution (3x20 mL). The basic water was adjusted to pH 3 with conc HCl until a precipitate was formed. The latter was filtered and dried by vacuum. The precipitate obtained was characterized by UPLC-MS and <sup>1</sup>H NMR.

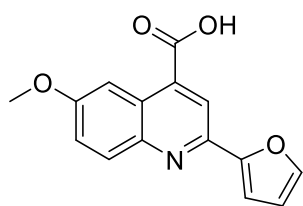
### 6-Ethyl-2-(furan-2-yl)quinoline-4-carboxylic acid (**62**)



Compound **62** was obtained following the described procedure B using 4-ethylaniline **56** (0.45 mL, 3.6 mmol), furfural **60** (0.33 mL, 4 mmol), complexed boron-diethyl ether trifluoride (0.123 mL, 1 mmol) and pyruvic acid **61** (0.141 mL, 2 mmol). 228 mg (0.853 mmol, 43% yield) of pure product were obtained.

$^1\text{H}$  NMR (401 MHz, Chloroform- $d$ )  $\delta$  8.52 (d,  $J$  = 1.9 Hz, 1H), 8.32 (s, 1H), 8.01 (d,  $J$  = 8.7 Hz, 1H), 7.79 (dd,  $J$  = 1.8, 0.7 Hz, 1H), 7.68 (dd,  $J$  = 8.7, 2.0 Hz, 1H), 7.45 - 7.32 (m, 1H), 6.68 (dd,  $J$  = 3.5, 1.8 Hz, 1H), 2.84 (q,  $J$  = 7.6 Hz, 2H), 1.32 (t,  $J$  = 7.6 Hz, 3H) ppm. UPLC-MS (ESI,  $m/z$ )  $R_t$  = 2.61 min, 268 ( $M+H$ ) $^+$

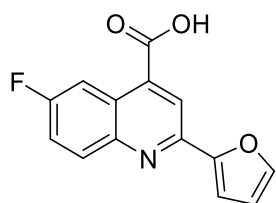
### 2-(Furan-2-yl)-6-methoxyquinoline-4-carboxylic acid (**63**)



Compound **63** was obtained following the described procedure B using 4-methoxyaniline **57** (0.222 g, 1.8 mmol), furfural **60** (0.166 mL, 2 mmol), complexed boron-diethyl ether trifluoride (0.062 mL, 0.5 mmol) and pyruvic acid **61** (0.07 mL, 1 mmol). 170 mg (0.631 mmol, 63% yield) of pure product were obtained.

$^1\text{H}$  NMR (401 MHz, DMSO- $d_6$ )  $\delta$  8.26 (s, 1H), 8.11 (d,  $J$  = 2.9 Hz, 1H), 7.97 (d,  $J$  = 9.2 Hz, 1H), 7.90 (d,  $J$  = 1.7 Hz, 1H), 7.46 (dd,  $J$  = 9.2, 2.9 Hz, 1H), 7.31 (d,  $J$  = 3.4 Hz, 1H), 6.69 (dd,  $J$  = 3.4, 1.8 Hz, 1H), 3.88 (s, 3H) ppm. UPLC-MS (ESI,  $m/z$ )  $R_t$  = 2.3 min, 270 ( $M+H$ ) $^+$

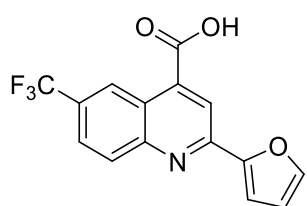
### 6-Fluoro-2-(furan-2-yl)quinoline-4-carboxylic acid (**64**)



Compound **64** was obtained following the described procedure B using 4-fluoroaniline **58** (0.5 mL, 5.4 mmol), furfural **60** (0.49 mL, 6 mmol), complexed boron-diethylether trifluoride (0.185 mL, 1.5 mmol) and pyruvic acid **61** (0.21 mL, 3 mmol). 173 mg (0.673 mmol, 67% yield) of pure product were obtained.

$^1\text{H}$  NMR (401 MHz, DMSO- $d_6$ )  $\delta$  8.42 (dd,  $J$  = 11.0, 2.9 Hz, 1H), 8.35 (s, 1H), 8.13 (dd,  $J$  = 9.3, 5.8 Hz, 1H), 7.94 (dd,  $J$  = 1.8, 0.8 Hz, 1H), 7.73 (dd,  $J$  = 9.3, 8.1, 2.9 Hz, 1H), 7.42 (dd,  $J$  = 3.5, 0.8 Hz, 1H), 6.72 (dd,  $J$  = 3.4, 1.8 Hz, 1H) ppm. UPLC-MS (ESI,  $m/z$ )  $R_t$  = 2.59 min, 258 ( $M+H$ ) $^+$

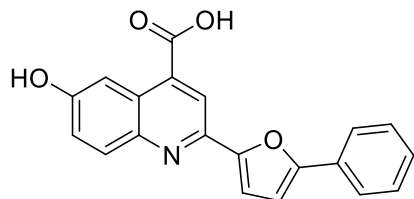
### 2-(Furan-2-yl)-6-(trifluoromethyl)quinoline-4-carboxylic acid (**65**)



Compound **65** was obtained following the described procedure B using 4-trifluoromethylaniline **59** (0.223 mL, 1.8 mmol), furfural **60** (0.166 mL, 2 mmol), complexed boron-diethyl ether trifluoride (0.062 mL, 0.5 mmol) and pyruvic acid **61** (0.07 mL, 1 mmol). 235 mg (0.765 mmol, 76% yield) of pure product were obtained.

$^1\text{H}$  NMR (401 MHz, Chloroform- $d$ )  $\delta$  9.19 (s, 1H), 8.49 (s, 1H), 8.23 (d,  $J$  = 8.9 Hz, 1H), 7.96 (dd,  $J$  = 8.9, 2.1 Hz, 1H), 7.82 (dd,  $J$  = 1.8, 0.8 Hz, 1H), 7.45 (dd,  $J$  = 3.5, 0.8 Hz, 1H), 6.70 (dd,  $J$  = 3.5, 1.8 Hz, 1H) ppm.  $R_t$  = 3.07 min, 308 ( $M+H$ ) $^+$

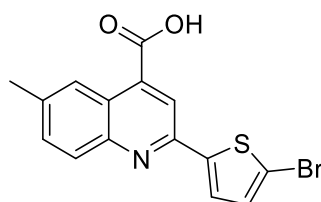
### 6-Hydroxy-2-(5-phenylfuran-2-yl)quinoline-4-carboxylic acid (**18**)



Compound **18** was obtained following the described procedure B using of 4-amminophenol **74** (150 mg, 1.37 mmol), 5-phenylfurfural **75** (260.34 mg, 1.51 mmol, 1.1 equiv), complexed boron-diethyl ether trifluoride (0.062 mL, 0.687 mmol) and 0.1 mL (0.1% mol) of acetic acid are added and heated to 65 °C for 3 h under stirring. After 3 h, pyruvic acid **61** (0.07 mL, 0.995 mmol) is added. 22 mg (0.066 mmol, 7% yield) of pure product were obtained.

$^1\text{H}$  NMR (600 MHz, DMSO- $d_6$ )  $\delta$  8.33 (s, 1H), 8.02 (d,  $J$  = 2.7 Hz, 1H), 7.97 (d,  $J$  = 9.1 Hz, 1H), 7.92 – 7.86 (m, 2H), 7.50 (t,  $J$  = 7.8 Hz, 2H), 7.44 – 7.34 (m, 3H), 7.20 (d,  $J$  = 3.5 Hz, 1H) ppm.  $^{13}\text{C}$  NMR (151 MHz, DMSO- $d_6$ )  $\delta$  168.12, 157.32, 154.66, 152.82, 145.14, 144.38, 131.47, 130.25, 129.53, 128.57, 125.59, 124.31, 124.31, 123.34, 118.65, 112.39, 109.20, 107.30 ppm. UPLC-MS (ESI,  $m/z$ )  $R_t$  = 2.85 min, 332 ( $M+H$ ) $^+$

### 2-(5-Bromothiophen-2-yl)-6-methylquinoline-4-carboxylic acid (**78**)



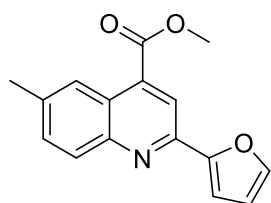
Compound **78** was obtained following the described procedure B using para-toluidine **76** (144 mg, 1.35 mmol), 5-bromothiophene-2-carbaldehyde **77** (286 mg, 1.5 mmol), complexed boron-diethyl ether trifluoride (0.046 mL, 0.375 mmol) and pyruvic acid **61** (0.053 mL, 0.75 mmol). 113 mg (0.324 mmol, 83% yield) of product were obtained.

$^1\text{H}$  NMR (401 MHz, DMSO- $d_6$ )  $\delta$  8.36 (s, 1H), 8.32 (s, 1H), 7.96 – 7.89 (m, 2H), 7.66 (dd,  $J$  = 8.6, 1.9 Hz, 1H), 7.35 (d,  $J$  = 4.0 Hz, 1H), 2.52 (s, 3H) ppm. UPLC-MS (ESI,  $m/z$ )  $R_t$  = 3.6 min, 348/350 ( $M+H$ ) $^+$

#### 6.1.6 General procedure C for the synthesis of methyl 2-(furan-2-yl)quinoline-4-carboxylate intermediates **28b**, **29b**, **66b-69b**.

This procedure has been conducted for the preparation of **28b-29b** (Scheme 3), **66b-69b** (Scheme 6). In a microwave tube, to a solution of the quinoline (**25**, **27**, **62-65**, 1 equiv) in dry MeOH (0.4 M),  $\text{SOCl}_2$  (3 equiv) was added drop by drop at 0  $^\circ\text{C}$  under stirring. The tube was placed in the microwave reactor and the reaction was kept stirring for 3 hours at 80  $^\circ\text{C}$ , 80 W. The reaction was cooled to room temperature and 10 mL of MeOH were added and evaporated by rotavapor with basic trap. Then, DCM/ $\text{K}_2\text{CO}_3$  20% (3x40 mL) and DCM/brine (1x40 mL) extractions were performed. The organic phase was dried over  $\text{Na}_2\text{SO}_4$ , filtered and concentrated under reduced pressure. The cleaned product was characterized by UPLC-MS and  $^1\text{H}$  NMR.

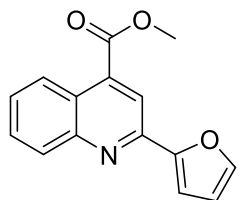
##### Methyl 2-(furan-2-yl)-6-methylquinoline-4-carboxylate (**28b**)



The compound **28b** was obtained following the described procedure C using quinoline **25** (1 g, 3.95 mmol) and  $\text{SOCl}_2$  (0.864 mL, 11.85 mmol). 683 mg (2.56 mmol, 65% yield) of pure product were obtained.

$^1\text{H}$  NMR (401 MHz, Chloroform- $d$ )  $\delta$  8.44 (d,  $J$  = 1.8 Hz, 1H), 8.25 (s, 1H), 7.98 (d,  $J$  = 8.7 Hz, 1H), 7.77 (d,  $J$  = 1.7 Hz, 1H), 7.63 (dd,  $J$  = 8.7, 2.0 Hz, 1H), 7.34 (d,  $J$  = 3.5 Hz, 1H), 6.67 (dd,  $J$  = 3.5, 1.8 Hz, 1H), 3.90 (s, 3H), 2.54 (s, 3H) ppm. UPLC-MS (ESI,  $m/z$ )  $R_t$  = 3.35 min, 268 ( $M+H$ ) $^+$

##### Methyl 2-(furan-2-yl)quinoline-4-carboxylate (**29b**)

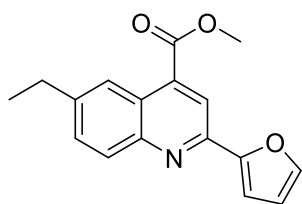


The compound **29b** was obtained following the described procedure C using quinoline **27** (0.876 g, 3.66 mmol) and  $\text{SOCl}_2$  (0.801 mL, 10.99 mmol). 745 mg (2.94 mmol, 80% yield) of pure product were obtained.

$^1\text{H}$  NMR (401 MHz, Chloroform- $d$ )  $\delta$  8.44 (dd,  $J$  = 8.7, 1.8 Hz, 1H), 8.25 (s, 1H), 7.98 (dd,  $J$  = 8.7, 1.8 Hz, 1H), 7.79 (t,  $J$  = 8.7 Hz, 1H), 7.77 (dd,  $J$  = 8.7, 1.7 Hz, 1H), 7.63

(t, J = 8.7 Hz, 1H), 7.34 (d, J = 3.5 Hz, 1H), 6.67 (dd, J = 3.5, 1.8 Hz, 1H), 3.90 (s, 3H) ppm. UPLC-MS (ESI, m/z) Rt = 3.23 min, 254 (M+H)<sup>+</sup>

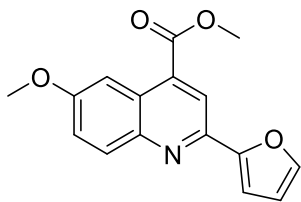
#### Methyl 6-ethyl-2-(furan-2-yl)quinoline-4-carboxylate (66b)



The compound **66b** was obtained following the described procedure C using quinoline **62** (0.377 g, 1.41 mmol) and SOCl<sub>2</sub> (0.309 mL, 4.23 mmol). 274 mg (0.96 mmol, 70% yield) of pure product were obtained.

<sup>1</sup>H NMR (401 MHz, Chloroform-d) δ 8.52 (d, J = 1.9 Hz, 1H), 8.32 (s, 1H), 8.01 (d, J = 8.7 Hz, 1H), 7.79 (dd, J = 1.8, 0.7 Hz, 1H), 7.68 (dd, J = 8.7, 2.0 Hz, 1H), 7.45 - 7.32 (m, 1H), 6.68 (dd, J = 3.5, 1.8 Hz, 1H), 3.90 (s, 3H), 2.84 (q, J = 7.6 Hz, 2H), 1.32 (t, J = 7.6 Hz, 3H) ppm. UPLC-MS (ESI, m/z) Rt = 3.52 min, 282 (M+H)<sup>+</sup>

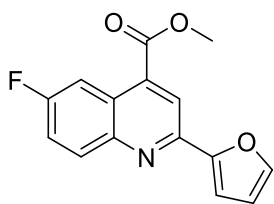
#### Methyl 2-(furan-2-yl)-6-methoxyquinoline-4-carboxylate (67b)



The compound **67b** was obtained following the described procedure C using quinoline **63** (0.17 g, 0.631 mmol) and SOCl<sub>2</sub> (0.138 mL, 1.89 mmol). 100 mg (0.35 mmol, 56% yield) of pure product were obtained.

<sup>1</sup>H NMR (401 MHz, DMSO-d<sub>6</sub>) δ 8.26 (s, 1H), 8.11 (d, J = 2.9 Hz, 1H), 7.97 (d, J = 9.2 Hz, 1H), 7.90 (d, J = 1.7 Hz, 1H), 7.46 (dd, J = 9.2, 2.9 Hz, 1H), 7.31 (d, J = 3.4 Hz, 1H), 6.69 (dd, J = 3.4, 1.8 Hz, 1H), 3.90 (s, 3H), 3.88 (s, 3H) ppm. UPLC-MS (ESI, m/z) Rt = 3.26 min, 284 (M+H)<sup>+</sup>

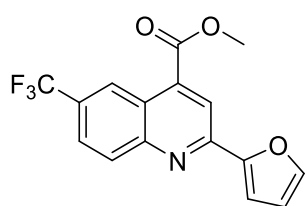
#### Methyl 6-fluoro-2-(furan-2-yl)quinoline-4-carboxylate (68b)



The compound **68b** was obtained following the described procedure C using quinoline **64** (0.31 g, 1.21 mmol) and SOCl<sub>2</sub> (0.265 mL, 3.63 mmol). 246 mg (0.9 mmol, 75% yield) of pure product were obtained.

<sup>1</sup>H NMR (401 MHz, DMSO-d<sub>6</sub>) δ 8.42 (dd, J = 11.0, 2.9 Hz, 1H), 8.35 (s, 1H), 8.13 (dd, J = 9.3, 5.8 Hz, 1H), 7.94 (dd, J = 1.8, 0.8 Hz, 1H), 7.73 (dd, J = 9.3, 8.1, 2.9 Hz, 1H), 7.42 (dd, J = 3.5, 0.8 Hz, 1H), 6.72 (dd, J = 3.4, 1.8 Hz, 1H), 3.90 (s, 3H) ppm. UPLC-MS (ESI, m/z). Rt = 3.36 min, 272 (M+H)<sup>+</sup>

### Methyl 2-(furan-2-yl)-6-(trifluoromethyl)quinoline-4-carboxylate (**69b**)



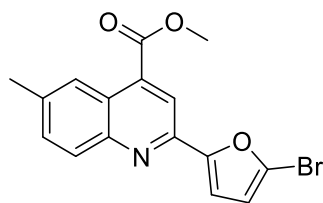
The compound **69b** was obtained following the described procedure C using quinoline **65** (0.245 g, 0.798 mmol) and SOCl<sub>2</sub> (0.175 mL, 2.39 mmol). 130 mg (0.405 mmol, 51% yield) of pure product were obtained.

<sup>1</sup>H NMR (401 MHz, Chloroform-d)  $\delta$  9.19 (s, 1H), 8.49 (s, 1H), 8.23 (d,  $J$  = 8.9 Hz, 1H), 7.96 (dd,  $J$  = 8.9, 2.1 Hz, 1H), 7.82 (dd,  $J$  = 1.8, 0.8 Hz, 1H), 7.45 (dd,  $J$  = 3.5, 0.8 Hz, 1H), 6.70 (dd,  $J$  = 3.5, 1.8 Hz, 1H), 3.90 (s, 3H) ppm. Rt = 3.59 min, 322 (M+H)<sup>+</sup>

#### 6.1.7 General procedure D for the synthesis of methyl 2-(5-bromofuran-2-yl)quinoline-4-carboxylate intermediates **28c**, **29c**, **66c-69c**.

This procedure has been conducted for the preparation of **28c-29c** (Scheme 3), **66c-69c** (Scheme 6). In a microwave tube, a solution of the appropriate ester intermediate (**28b-29b**, **66b-69b**, 1 equiv) was stirred in DMF (0.4 M) prior to the addition of N-bromosuccinimide (1.5 equiv) at room temperature. The tube was then placed in the microwave reactor and kept under stirring at 35 °C for 40 minutes, 80 W. Then, the mixture was added drop by drop to 20 mL of cold distilled water at 0°C under stirring. The formation of a precipitate was observed and filtered. The desired compound was obtained after purification over silica gel unless otherwise noted.

### Methyl 2-(5-bromofuran-2-yl)-6-methylquinoline-4-carboxylate (**28c**)

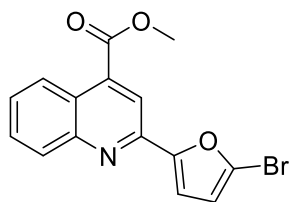


The compound **28c** was obtained following the described procedure D using intermediate ester **28b** (570 mg, 2.13 mmol) and N-bromosuccinimide (569 mg, 3.2 mmol). The crude was purified by direct phase flash column chromatography (EP:EtOAc 95:5) to afford

the desired **28c** (567 mg, 1.64 mmol, 77% yield) characterized by UPLC-MS and <sup>1</sup>H NMR.

<sup>1</sup>H NMR (401 MHz, Chloroform-d)  $\delta$  8.44 (d,  $J$  = 1.8 Hz, 1H), 8.25 (s, 1H), 7.98 (d,  $J$  = 8.7 Hz, 1H), 7.63 (dd,  $J$  = 8.7, 2.0 Hz, 1H), 7.34 (d,  $J$  = 3.5 Hz, 1H), 6.67 (d,  $J$  = 3.5, 1H), 2.54 (s, 3H) ppm. UPLC-MS (ESI, m/z) Rt = 3.7 min, 346-348 (M+H)<sup>+</sup>

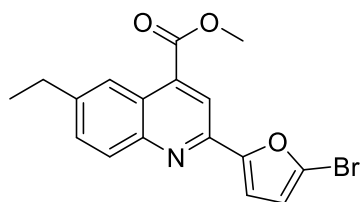
### Methyl 2-(5-bromofuran-2-yl)quinoline-4-carboxylate (**29c**)



The compound **29c** was obtained following the described procedure D using intermediate ester **29b** (750 mg, 2.94 mmol) and N-bromosuccinimide (785.36 mg, 4.41 mmol). The crude was purified by direct phase flash column chromatography (EP:EtOAc 95:5) to afford the desired **29c** (652 mg, 1.96 mmol, yield 67%).) characterized by UPLC-MS and <sup>1</sup>H NMR.

<sup>1</sup>H NMR (401 MHz, Chloroform-d) δ 8.66 - 8.54 (m, 1H), 8.15 (s, 1H), 8.03 (dd, J = 8.6, 1.3 Hz, 1H), 7.65 (ddd, J = 8.3, 6.8, 1.4 Hz, 1H), 7.50 (ddd, J = 8.3, 6.8, 1.3 Hz, 1H), 7.17 (d, J = 3.5 Hz, 1H), 6.46 (d, J = 3.5 Hz, 1H), 3.98 (s, 3H) ppm. UPLC-MS (ESI, m/z) Rt = 3.6 min, 332-334 (M+H)<sup>+</sup>

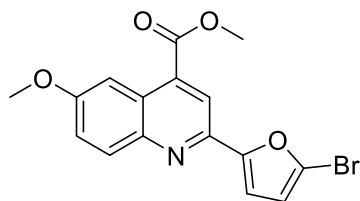
### Methyl 2-(5-bromofuran-2-yl)-6-ethylquinoline-4-carboxylate (**66c**)



The compound **66c** was obtained following the described procedure D using intermediate ester **66b** (274 mg, 0.98 mmol) and N-bromosuccinimide (261.65 mg, 1.47 mmol). The crude was purified by direct phase flash column chromatography (EP:EtOAc 95:5) to afford the desired **66c** (241 mg, 0.67 mmol, 75% yield) characterized by UPLC-MS and <sup>1</sup>H NMR.

<sup>1</sup>H NMR (401 MHz, DMSO-d<sub>6</sub>) δ 8.31 (s, 1H), 8.20 (s, 1H), 8.01 (d, J = 8.7 Hz, 1H), 7.72 (dd, J = 8.6, 2.0 Hz, 1H), 7.45 (d, J = 3.5 Hz, 1H), 6.85 (d, J = 3.5 Hz, 1H), 3.99 (s, 3H), 2.80 (q, J = 7.6 Hz, 2H), 1.25 (t, J = 7.6 Hz, 3H) ppm. UPLC-MS (ESI, m/z) Rt = 3.64 min, 362-364 (M+H)<sup>+</sup>

### Methyl 2-(5-bromofuran-2-yl)-6-methoxyquinoline-4-carboxylate (**67c**)

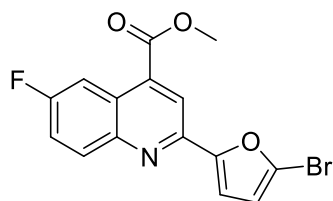


The compound **67c** was obtained following the described procedure D using intermediate ester **67b** (250 mg, 0.883 mmol) and N-bromosuccinimide (235.61 mg, 1.32 mmol). The crude precipitate obtained is purified by flash chromatography column with EP:EtOAc 95:5 eluent. The crude was purified by direct phase flash column chromatography (EP:EtOAc 95:5) to afford the desired **67c** (234 mg, 0.65 mmol, 73% yield) characterized by UPLC-MS and <sup>1</sup>H NMR.



$^1\text{H}$  NMR (401 MHz, DMSO- $d_6$ )  $\delta$  8.25 (s, 1H), 8.06 - 8.02 (m, 2H), 7.53 (dd,  $J$  = 9.3, 2.8 Hz, 1H), 7.41 (d,  $J$  = 3.6 Hz, 1H), 6.86 (d,  $J$  = 3.5 Hz, 1H), 4.02 (s, 3H), 3.92 (s, 3H) ppm. UPLC-MS (ESI,  $m/z$ )  $R_t$  = 3.85 min, 360-362 ( $M+H$ ) $^+$

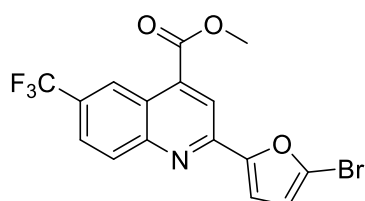
#### Methyl 2-(5-bromofuran-2-yl)-6-fluoroquinoline-4-carboxylate (**68c**)



The compound **68c** was obtained following the described procedure D using intermediate ester **68b** (560 mg, 2.07 mmol) and N-bromosuccinimide (554 mg, 3.11 mmol). The crude was purified by direct phase flash column chromatography (EP:EtOAc 95:5) to afford the desired **68c** (502 mg, 1.45 mmol, 70% yield) characterized by UPLC-MS and  $^1\text{H}$  NMR.

$^1\text{H}$  NMR (401 MHz, DMSO- $d_6$ )  $\delta$  8.42 (dd,  $J$  = 11.0, 2.9 Hz, 1H), 8.35 (s, 1H), 8.13 (dd,  $J$  = 9.3, 5.8 Hz, 1H), 7.73 (ddd,  $J$  = 9.3, 8.1, 2.9 Hz, 1H), 7.42 (d,  $J$  = 3.5 Hz, 1H), 6.72 (d,  $J$  = 3.4 Hz, 1H) ppm. UPLC-MS (ESI,  $m/z$ )  $R_t$  = 3.66 min, 350-352 ( $M+H$ ) $^+$

#### Methyl 2-(5-bromofuran-2-yl)-6-(trifluoromethyl)quinoline-4-carboxylate (**69c**)



The compound **69c** was obtained following the described procedure D using intermediate ester **69b** (300 mg, 0.94 mmol) and N-bromosuccinimide (249.31 mg, 1.40 mmol). The crude was purified by direct phase flash column chromatography (EP:EtOAc 95:5) to afford the desired **69c** (130 mg, 0.33 mmol, 35% yield) characterized by UPLC-MS and  $^1\text{H}$ -NMR.

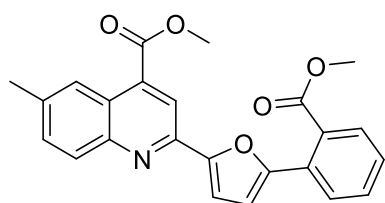
$^1\text{H}$  NMR (401 MHz, Chloroform- $d$ )  $\delta$  9.09 (dt,  $J$  = 2.0, 0.9 Hz, 1H), 8.37 (d,  $J$  = 1.1 Hz, 1H), 8.20 (dq,  $J$  = 8.9, 0.8 Hz, 1H), 7.88 (dd,  $J$  = 8.9, 2.0 Hz, 1H), 7.31 (d,  $J$  = 3.5 Hz, 1H), 6.55 (d,  $J$  = 3.5 Hz, 1H), 4.08 (s, 3H) ppm. UPLC-MS (ESI,  $m/z$ )  $R_t$  = 3.84 min, 400-402 ( $M+H$ ) $^+$

#### 6.1.8 General procedure E for the synthesis of methyl 2-(5-arylfuran-2-yl)quinoline-4-carboxylate intermediates **40-51**, **70-73**, **20**.

This procedure has been conducted for the preparation of **40-51** (Scheme 3), **70-73** (Scheme 6), **20** (Scheme 8). In a three-neck flask, the brominated intermediate (**28-29c**, **66-69c**, **78**, 1 equiv) was solubilized in dioxane:H<sub>2</sub>O (10:1, 0.1 M). Boronic acid **30-39** (1.5 equiv) and K<sub>2</sub>CO<sub>3</sub> (3 equiv) were added to the solution and the mixture was degassed with N<sub>2</sub>. Palladium tetrakis (0.05 equiv)

was then added and the reaction was conducted at 100 °C in inert atmosphere stirring for 2 hours. Then, the reaction was cooled to room temperature, 5 mL of water were added and the dioxane was evaporated by rotavapor. A precipitate was formed and filtered. The water was then extracted with AcOEt (3x10 mL). The organic phase was dried over Na<sub>2</sub>SO<sub>4</sub>, filtered and concentrated by vacuum. The crude joints solids were purified over silica gel unless otherwise noted.

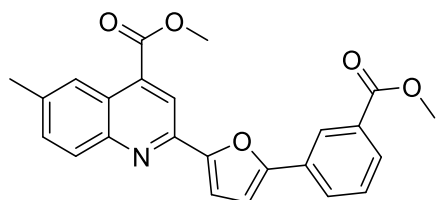
**Methyl 2-(5-(2-(methoxycarbonyl)phenyl)furan-2-yl)-6-methylquinoline-4-carboxylate (40)**



The compound **40** was obtained following the described procedure E using the brominated intermediate **28c** (230 mg, 0.664 mmol), boronic acid **30** (179 mg, 0.996 mmol), K<sub>2</sub>CO<sub>3</sub> (276 mg, 2 mmol) and Pd tetrakis (38 mg, 0.033 mmol). The crude solid obtained was purified by flash chromatography column (EP:EtOAc 95:5) to afford the desired **40** (124 mg, 0.279 mmol, 42% yield) characterized by UPLC-MS and <sup>1</sup>H NMR below. In this case, the extraction basic water contained the by-product dicarboxylate, which was formed by complete hydrolysis under basic conditions of Suzuki reaction. The water was then acidified with HCl conc and a red precipitate was filtered to afford 128 mg (≈45% conversion) of hydrolyzed product **1**.

<sup>1</sup>H NMR (401 MHz, DMSO-d<sub>6</sub>) δ 8.35 (dt, J = 1.9, 0.9 Hz, 1H), 8.23 (s, 1H), 8.00 (d, J = 8.6 Hz, 1H), 7.89 (dd, J = 8.2, 1.2 Hz, 1H), 7.73 – 7.63 (m, 3H), 7.54 – 7.48 (m, 2H), 7.13 (d, J = 3.6 Hz, 1H), 4.03 (s, 3H), 3.90 (s, 3H), 2.54 (s, 3H) ppm. UPLC-MS (ESI, m/z) Rt = 3.71 min, 402 (M+H)<sup>+</sup>

**Methyl 2-(5-(3-(methoxycarbonyl)phenyl)furan-2-yl)-6-methylquinoline-4-carboxylate (41)**

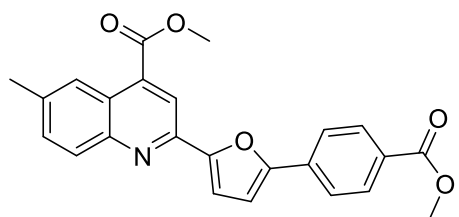


The compound **41** was obtained following the described procedure E using brominated intermediate **28c** (230 mg, 0.664 mmol), boronic acid **31** (179 mg, 0.997 mmol), K<sub>2</sub>CO<sub>3</sub> (276 mg, 2 mmol) and Pd tetrakis (28 mg, 0.033 mmol). The crude solid obtained was purified by flash chromatography column (EP:EtOAc 95:5) to afford the desired **41** (186 mg, 0.46 mmol, 47% yield) characterized by UPLC-MS and <sup>1</sup>H NMR.

<sup>1</sup>H NMR (401 MHz, DMSO-d<sub>6</sub>) δ 8.36 (td, J = 1.7, 0.5 Hz, 1H), 8.31 (s, 1H), 8.25 (p, J = 0.8 Hz, 1H), 8.14 (ddd, J = 7.8, 1.9, 1.2 Hz, 1H), 8.00 (d, J = 8.6 Hz, 1H), 7.91 (ddd, J = 7.8, 1.7, 1.1 Hz,

1H), 7.69 - 7.61 (m, 2H), 7.51 (d, J = 3.6 Hz, 1H), 7.34 (d, J = 3.6 Hz, 1H), 4.02 (s, 3H), 3.90 (s, 3H), 2.52 - 2.49 (s, 3H) ppm. UPLC-MS (ESI, m/z) Rt = 3.87 min, 402 (M+H)<sup>+</sup>

#### Methyl 2-(5-(4-(methoxycarbonyl)phenyl)furan-2-yl)-6-methylquinoline-4-carboxylate (**42**)

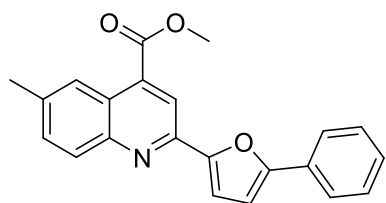


The compound **42** was obtained following the described procedure E using the brominated intermediate **28c** (200 mg, 0.578 mmol), boronic acid **32** (156 mg, 0.867 mmol), K<sub>2</sub>CO<sub>3</sub> (240 mg, 1.73 mmol) and Pd tetrakis (29 mg, 0.033 mmol).

The crude solid obtained was purified by flash chromatography column (EP:AcOEt 9:1) to afford the desired **42** (207 mg, 0.52 mmol, 89% yield) characterized by UPLC-MS and <sup>1</sup>H NMR.

<sup>1</sup>H NMR (401 MHz, Chloroform-d) δ 8.47 (t, J = 1.5 Hz, 1H), 8.39 (s, 1H), 8.12 (dd, J = 8.5, 1.9 Hz, 3H), 7.93 - 7.85 (m, 2H), 7.61 (dd, J = 8.7, 1.9 Hz, 1H), 7.48 (s, 1H), 7.00 (d, J = 3.5 Hz, 1H), 4.11 (s, 3H), 3.95 (s, 3H), 2.58 (s, 3H) ppm. UPLC-MS (ESI, m/z) Rt = 3.85 min, 402 (M+H)<sup>+</sup>

#### Methyl 6-methyl-2-(5-phenylfuran-2-yl)quinoline-4-carboxylate (**43**)

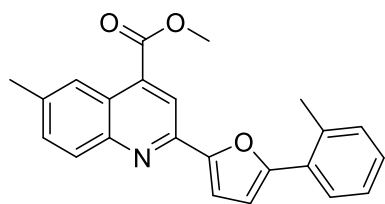


The compound **43** was obtained following the described procedure E using brominated intermediate **28c** (210 mg, 0.606 mmol), boronic acid **33** (111 mg, 0.909 mmol), K<sub>2</sub>CO<sub>3</sub> (251 mg, 1.82 mmol) and Pd tetrakis (35 mg, 0.03 mmol). The crude solid

obtained was purified by flash chromatography column (EP:AcOEt 95:5) to afford the desired **43** (178 mg, 0.518 mmol, 86% yield) characterized by UPLC-MS and <sup>1</sup>H NMR.

<sup>1</sup>H NMR (401 MHz, DMSO-d<sub>6</sub>) δ 8.30 (s, 1H), 8.24 (s, 1H), 7.97 (d, J = 8.6 Hz, 1H), 7.91 - 7.82 (m, 2H), 7.65 (dd, J = 8.7, 1.9 Hz, 1H), 7.52 - 7.44 (m, 3H), 7.40 - 7.33 (m, 1H), 7.20 (d, J = 3.6 Hz, 1H), 4.02 (s, 3H), 2.50 (s, 3H) ppm. UPLC-MS (ESI, m/z) Rt = 3.88 min, 344 (M+H)<sup>+</sup>

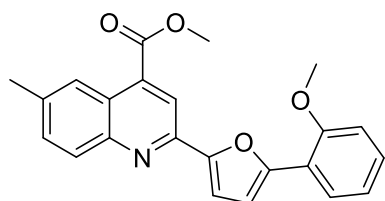
#### Methyl 6-methyl-2-(5-(o-tolyl)furan-2-yl)quinoline-4-carboxylate (**44**)



The compound **44** was obtained following the described procedure E using the brominated intermediate **28c** (200 mg, 0.577 mmol), boronic acid **34** (118 mg, 0.867 mmol),  $K_2CO_3$  (239 mg, 1.73 mmol, 2 M in water) and Palladium tetrakis (33 mg, 0.029 mmol). The crude solid obtained was purified by flash chromatography column (DCM 100%) to afford the desired **44** (175 mg, 0.49 mmol, 85% yield) characterized by UPLC-MS and  $^1H$  NMR.

$^1H$  NMR (401 MHz,  $DMSO-d_6$ )  $\delta$  8.32 (s, 1H), 8.29 (s, 1H), 8.01 (d,  $J$  = 8.6 Hz, 1H), 7.87 (dd,  $J$  = 7.2, 2.2 Hz, 1H), 7.69 (dd,  $J$  = 8.7, 2.0 Hz, 1H), 7.53 (d,  $J$  = 3.6 Hz, 1H), 7.41 – 7.28 (m, 3H), 7.02 (d,  $J$  = 3.6 Hz, 1H), 4.03 (s, 3H), 2.57 (s, 3H), 2.54 (s, 3H). UPLC-MS (ESI,  $m/z$ )  $R_t$  = 4.05 min, 358 ( $M+H$ ) $^+$

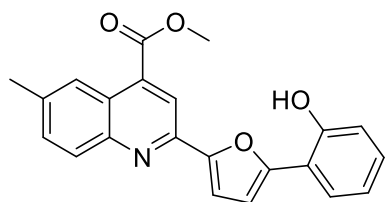
#### Methyl 2-(5-(2-methoxyphenyl)furan-2-yl)-6-methylquinoline-4-carboxylate (**45**)



The compound **45** was obtained following the described procedure E using the brominated intermediate **28c** (200 mg, 0.577 mmol), boronic acid **35** (132 mg, 0.867 mmol),  $K_2CO_3$  (239 mg, 1.73 mmol, 2 M in water) and Palladium tetrakis (33 mg, 0.029 mmol). The crude solid obtained was purified by flash chromatography column (DCM 100%) to afford the desired **45** (186 mg, 0.498 mmol, 86% yield) characterized by UPLC-MS and  $^1H$  NMR.

$^1H$  NMR (401 MHz,  $DMSO-d_6$ )  $\delta$  8.36 (s, 1H), 8.27 (s, 1H), 8.05 – 7.98 (m, 2H), 7.74 – 7.67 (m, 1H), 7.51 (d,  $J$  = 3.6 Hz, 1H), 7.43 – 7.34 (m, 1H), 7.22 – 7.10 (m, 3H), 4.04 (s, 3H), 3.97 (s, 3H), 2.55 (s, 3H). UPLC-MS (ESI,  $m/z$ )  $R_t$  = 3.91 min, 374 ( $M+H$ ) $^+$

#### Methyl 2-(5-(2-hydroxyphenyl)furan-2-yl)-6-methylquinoline-4-carboxylate (**46**)

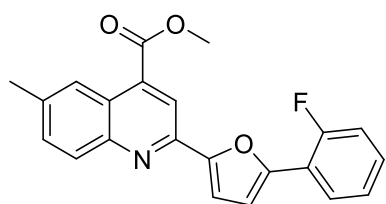


The compound **46** was obtained following the described procedure E using the brominated intermediate **28c** (200 mg, 0.577 mmol), boronic acid **36** (120 mg, 0.867 mmol),  $K_2CO_3$  (239 mg, 1.73 mmol, 2 M in water) and Palladium tetrakis (33 mg,

0.029 mmol). The crude solid obtained was purified by flash chromatography column (10-20% AcOEt/EP) to afford the desired **46** (181 mg, 0.504 mmol, 87% yield) characterized by  $^1\text{H}$  NMR.

$^1\text{H}$  NMR (401 MHz, DMSO- $d_6$ )  $\delta$  10.35 (s, 1H), 8.34 (s, 1H), 8.27 (s, 1H), 8.01 (d,  $J$  = 8.6 Hz, 1H), 7.93 (dd,  $J$  = 7.8, 1.7 Hz, 1H), 7.69 (dd,  $J$  = 8.7, 1.9 Hz, 1H), 7.49 (d,  $J$  = 3.5 Hz, 1H), 7.25 – 7.16 (m, 2H), 7.04 – 6.94 (m, 2H), 4.04 (s, 3H), 2.54 (s, 3H). UPLC-MS (ESI,  $m/z$ )  $R_t$  = 3.68 min, 360 ( $M+H$ ) $^+$

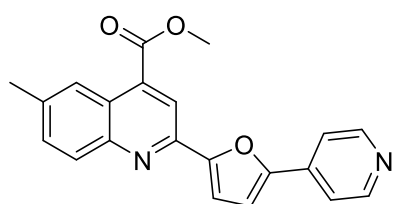
#### Methyl 2-(5-(2-fluorophenyl)furan-2-yl)-6-methylquinoline-4-carboxylate (**47**)



The compound **47** was obtained following the described procedure E using the brominated intermediate **28c** (135 mg, 0.389 mmol) boronic acid **37** (82 mg, 0.584 mmol), KF (67.97 mg, 1.17 mmol, 1.2 M in water) and Palladium tetrakis (23 mg, 0.0195 mmol). The solution is left stirring at reflux for 4 h. The crude solid obtained was purified by flash chromatography column (EP:AcOEt 95:5 and DCM:EP 1:1) to afford the desired **47** (52 mg, 0.39 mmol, 37% yield) characterized by UPLC-MS and  $^1\text{H}$  NMR.

$^1\text{H}$  NMR (600 MHz, DMSO- $d_6$ )  $\delta$  8.37 (s, 1H), 8.30 - 8.26 (m, 1H), 8.06 (td,  $J$  = 8.0, 2.0 Hz, 1H), 8.02 (d,  $J$  = 8.5 Hz, 1H), 7.70 (dd,  $J$  = 8.6, 1.9 Hz, 1H), 7.55 (d,  $J$  = 3.6 Hz, 1H), 7.48 - 7.43 (m, 1H), 7.42 - 7.36 (m, 2H), 7.10 (t,  $J$  = 3.5 Hz, 1H), 4.04 (s, 3H), 2.54 (s, 3H) ppm. UPLC-MS (ESI,  $m/z$ )  $R_t$  = 4.39 min, 362 ( $M+H$ ) $^+$

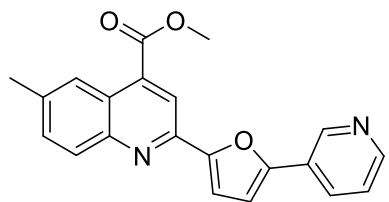
#### Methyl 6-methyl-2-(5-(pyridin-4-yl)furan-2-yl)quinoline-4-carboxylate (**48**)



The compound **48** was obtained by following the described procedure E using the brominated intermediate **28c** (181 mg, 0.523 mmol), boronic acid **38** (110 mg, 0.784 mmol),  $\text{K}_2\text{CO}_3$  (217 mg, 1.57 mmol) and Palladium tetrakis (30 mg, 0.026 mmol). A CombiFlash chromatographic column to the crude solid is conducted ( $\text{SiO}_2$  gold 12 g; DCM:MeOH 9:1) to afford the desired **48** (130 mg, 0.377 mmol, 72% yield) characterized by UPLC-MS and  $^1\text{H}$  NMR.

$^1\text{H}$  NMR (401 MHz, DMSO- $d_6$ )  $\delta$  8.71 - 8.65 (m, 2H), 8.40 (d,  $J$  = 3.1 Hz, 2H), 8.03 (d,  $J$  = 8.6 Hz, 1H), 7.90 - 7.84 (m, 2H), 7.70 (dd,  $J$  = 8.7, 2.0 Hz, 1H), 7.61 - 7.53 (m, 2H), 4.02 (s, 3H), 2.55 (s, 3H) ppm. UPLC-MS (ESI,  $m/z$ )  $R_t$  = 1.49 min, 331 ( $M+H$ ) $^+$

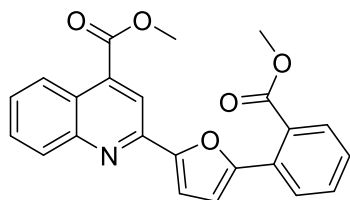
**Methyl 6-methyl-2-(5-(pyridin-3-yl)furan-2-yl)quinoline-4-carboxylate (49)**



The compound **49** was obtained by following the described procedure E using the brominated intermediate **28c** (150 mg, 0.433 mmol), boronic acid **39** (80 mg, 0.649 mmol),  $\text{K}_2\text{CO}_3$  (179 mg, 1.30 mmol) and Palladium tetrakis (25 mg, 0.022 mmol). The crude solid obtained was purified by flash chromatography column (DCM:MeOH 9:1) to afford the desired **49** (88 mg, 0.255 mmol, 59% yield).

$^1\text{H}$  NMR (401 MHz, DMSO- $d_6$ )  $\delta$  9.23 (d,  $J$  = 2.3 Hz, 1H), 8.63 (dd,  $J$  = 5.0, 1.6 Hz, 1H), 8.42 (d,  $J$  = 4.6 Hz, 3H), 8.02 (d,  $J$  = 8.6 Hz, 1H), 7.68 (m, 2H), 7.57 (d,  $J$  = 3.6 Hz, 1H), 7.46 (d,  $J$  = 3.6 Hz, 1H), 4.02 (s, 3H), 2.54 (s, 3H) ppm. UPLC-MS (ESI,  $m/z$ )  $R_t$  = 3.36 min, 345 ( $M+H$ ) $^+$

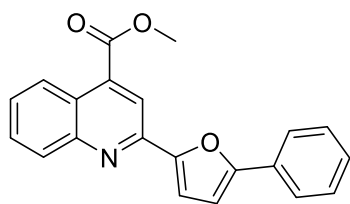
**Methyl 2-(5-(2-(methoxycarbonyl)phenyl)furan-2-yl)quinoline-4-carboxylate (50)**



The compound **50** was obtained following the described procedure E using brominated intermediate **29c** (200 mg, 0.602 mmol), boronic acid **30** (216 mg, 1.20 mmol),  $\text{K}_2\text{CO}_3$  (250 mg, 1.81 mmol) and Pd tetrakis (49 mg, 0.04 mmol). The crude solid obtained was purified by flash chromatography column (EP:AcOEt 95:5) to afford the desired **50** (130 mg, 0.336 mmol, 56% yield) characterized by UPLC-MS and  $^1\text{H}$  NMR.

$^1\text{H}$  NMR (401 MHz, Chloroform- $d$ )  $\delta$  8.69 (ddd,  $J$  = 8.5, 1.5, 0.7 Hz, 1H), 8.33 (s, 1H), 8.16 (d,  $J$  = 8.5 Hz, 1H), 7.77 - 7.68 (m, 3H), 7.62 - 7.52 (m, 2H), 7.48 - 7.38 (m, 2H), 6.80 (d,  $J$  = 3.6 Hz, 1H), 4.06 (s, 3H), 3.85 (s, 3H) ppm. UPLC-MS (ESI,  $m/z$ )  $R_t$  = 3.88 min, 344 ( $M+H$ ) $^+$

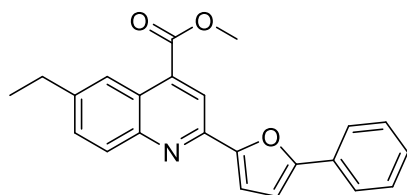
### Methyl 2-(5-phenylfuran-2-yl)quinoline-4-carboxylate (**51**)



The compound **51** was obtained following the described procedure E using brominated intermediate **29c** (100 mg, 0.3 mmol), boronic acid **33** (55 mg, 0.451 mmol), K<sub>2</sub>CO<sub>3</sub> (125 mg, 0.9 mmol) and Pd tetrakis (17 mg, 0.015 mmol). The crude solid obtained was purified by flash chromatography column (EP:AcOEt 95:5) to afford the desired **51** (70 mg, 0.212 mmol, 71% yield) characterized by UPLC-MS and <sup>1</sup>H NMR.

<sup>1</sup>H NMR (401 MHz, DMSO-d<sub>6</sub>) δ 8.67 (dd, J = 8.4, 1.5 Hz, 1H), 8.00 (s, 1H), 7.97 - 7.93 (m, 1H), 7.89 (dd, J = 8.3, 1.2 Hz, 2H), 7.67 (ddd, J = 8.4, 6.8, 1.5 Hz, 1H), 7.55 - 7.43 (m, 3H), 7.40 (d, J = 3.5 Hz, 1H), 7.39 - 7.31 (m, 1H), 7.20 (d, J = 3.6 Hz, 1H), 4.01 (s, 3H) ppm. UPLC-MS (ESI, m/z) Rt = 3.97 min, 330 (M+H)<sup>+</sup>

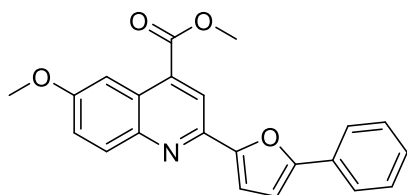
### Methyl 6-ethyl-2-(5-phenylfuran-2-yl)quinoline-4-carboxylate (**70**)



The compound **70** was obtained following the described procedure E using brominated intermediate **66c** (193 mg, 0.54 mmol), boronic acid **33** (98.76 mg, 0.81 mmol), K<sub>2</sub>CO<sub>3</sub> (220.64 mg, 1.62 mmol) and Pd tetrakis (31.20 mg, 0.027 mmol). The crude solid obtained was purified by flash chromatography column (EP:AcOEt 95:5) to afford the desired **70** (117 mg, 0.33 mmol, 61% yield) characterized by UPLC-MS and <sup>1</sup>H NMR.

<sup>1</sup>H NMR (401 MHz, Chloroform-d) δ 8.47 (s, 1H), 8.41 (s, 2H), 7.85 (dt, J = 8.1, 1.2 Hz, 2H), 7.67 (d, J = 8.9 Hz, 1H), 7.45 (t, J = 7.6 Hz, 3H), 7.35 (t, J = 7.4 Hz, 1H), 6.90 (d, J = 3.7 Hz, 1H), 4.11 (s, J = 1.2 Hz, 3H), 2.90 - 2.84 (q, J = 7.6 Hz, 2H), 1.37 - 1.33 (t, J = 7.6 Hz, 3H) ppm. UPLC-MS (ESI, m/z) Rt = 4.03 min, 398 (M+H)<sup>+</sup>

### Methyl 6-methoxy-2-(5-phenylfuran-2-yl)quinoline-4-carboxylate (**71**)

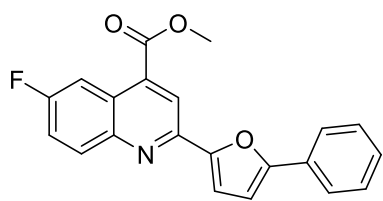


The compound **71** was obtained following the described procedure E using brominated intermediate **67c** (113 mg, 0.31 mmol), boronic acid **33** (57.06 mg, 0.47 mmol), K<sub>2</sub>CO<sub>3</sub> (129.36 mg, 0.94 mmol) and Pd tetrakis (18.03 mg, 0.015 mmol). The

crude solid obtained was purified by flash chromatography column (EP:AcOEt 95:5) to afford the desired **71** (67 mg, 0.186 mmol, 60% yield) characterized by UPLC-MS and  $^1\text{H}$  NMR.

$^1\text{H}$  NMR (401 MHz, Chloroform- $d$ )  $\delta$  8.49 (s, 1H), 8.17 (d,  $J$  = 2.8 Hz, 1H), 7.84 (d,  $J$  = 7.8 Hz, 2H), 7.45 (t,  $J$  = 7.5 Hz, 5H), 7.34 (t,  $J$  = 7.6 Hz, 1H), 6.90 (d,  $J$  = 3.8 Hz, 1H), 4.11 (d,  $J$  = 0.9 Hz, 3H), 3.99 – 3.97 (m, 3H). UPLC-MS (ESI,  $m/z$ )  $R_t$  = 3.79 min, 360 ( $M+H$ ) $^+$

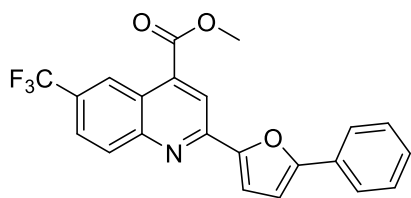
#### Methyl 6-fluoro-2-(5-phenylfuran-2-yl)quinoline-4-carboxylate (**72**)



The compound **72** was obtained following the described procedure E using brominated intermediate **68c** (100 mg, 0.29 mmol), boronic acid **33** (53.65 mg, 0.44 mmol),  $\text{K}_2\text{CO}_3$  (118.5 mg, 0.87 mmol) and Pd tetrakis (7.33 mg, 0.015 mmol). The crude solid obtained was purified by flash chromatography column (DCM:PE 85:15). To afford the desired **72** (85 mg, 0.245 mmol, 85% yield) characterized by UPLC-MS and  $^1\text{H}$  NMR.

$^1\text{H}$  NMR (401 MHz, Chloroform- $d$ )  $\delta$  8.54 - 8.42 (m, 2H), 8.22 (s, 1H), 7.91 - 7.79 (m, 2H), 7.58 - 7.41 (m, 4H), 7.34 (t,  $J$  = 7.4 Hz, 1H), 6.88 (d,  $J$  = 3.4 Hz, 1H), 4.09 (s, 3H) ppm. UPLC-MS (ESI,  $m/z$ )  $R_t$  = 3.86 min, 348 ( $M+H$ ) $^+$

#### Methyl 2-(5-phenylfuran-2-yl)-6-(trifluoromethyl)quinoline-4-carboxylate (**73**)

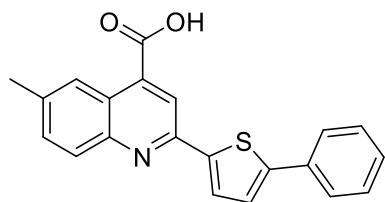


The compound **73** was obtained following the described procedure E using brominated intermediate **69c** (115 mg, 0.29 mmol), boronic acid **33** (54 mg, 0.44 mmol),  $\text{K}_2\text{CO}_3$  (118 mg, 0.87 mmol) and Pd tetrakis (17.33 mg, 0.015 mmol). The crude solid obtained was purified by flash chromatography column (EP:AcOEt 95:5) to afford the desired **73** (70 mg, 0.18 mmol, 62% yield) characterized by UPLC-MS and  $^1\text{H}$  NMR.

$^1\text{H}$  NMR (401 MHz, Chloroform- $d$ )  $\delta$  9.08 (d,  $J$  = 1.9 Hz, 1H), 8.53 (s, 1H), 8.49 (d,  $J$  = 8.9 Hz, 1H), 7.94 (dd,  $J$  = 9.1, 2.1 Hz, 1H), 7.89 - 7.79 (m, 3H), 7.51 - 7.44 (m, 2H), 7.42 - 7.35 (m, 1H), 6.93 (d,  $J$  = 3.7 Hz, 1H), 4.13 (s, 3H) ppm. UPLC-MS (ESI,  $m/z$ )  $R_t$  = 4.03 min, 398 ( $M+H$ ) $^+$



### 6-Methyl-2-(5-phenylthiophen-2-yl)quinoline-4-carboxylic acid (**20**)



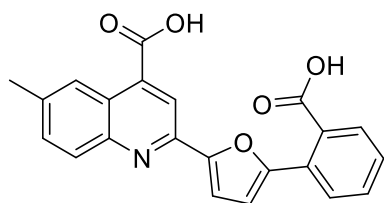
The compound **20** was obtained following the described procedure E using the intermediate **78** (105 mg, 0.301 mmol), boronic acid **33** (55 mg, 0.452 mmol), K<sub>2</sub>CO<sub>3</sub> (125 mg, 0.904 mmol) and Palladium tetrakis (17 mg, 15.08 mmol). After removing the dioxane by vacuum, the product remained in the basic water, which was then acidified to form a precipitate at pH 3 that was filtered and purified by flash chromatography column (0-10% AcOEt/EP) to afford the desired **20** (79 mg, 0.229 mmol, 76% yield) characterized by UPLC-MS, <sup>1</sup>H NMR and <sup>13</sup>C NMR.

<sup>1</sup>H NMR (401 MHz, DMSO-d<sup>6</sup>) δ 8.40 – 8.35 (m, 1H), 7.94 (s, 1H), 7.90 (d, J = 3.9 Hz, 1H), 7.83 – 7.74 (m, 3H), 7.58 (d, J = 3.9 Hz, 1H), 7.53 – 7.47 (dd, J = 7.9, 1.9 Hz, 1H), 7.53 – 7.47 (t, J = 7.9 Hz, 2H), 7.39 – 7.30 (m, 1H), 2.49 – 2.44 (m, 3H) ppm. <sup>13</sup>C NMR (151 MHz, DMSO-d<sup>6</sup>) δ 169.76, 150.92, 150.21, 146.99, 145.76, 145.21, 134.87, 134.17, 131.73, 129.66, 129.66, 128.45, 128.45, 127.53, 127.09, 125.89, 125.89, 125.35, 125.22, 114.90, 21.89 ppm. UPLC-MS (ESI, m/z) Rt = 3.47 min, 346 (M+H)<sup>+</sup>

#### 6.1.9 General procedure F for the synthesis of 2-(5-arylfuran-2-yl)quinoline-4-carboxylic acid derivatives **1-16**.

This procedure has been conducted for the preparation of **1-12** (Scheme 3), **13-16** (Scheme 6). The intermediate **40-51**, **70-73** (1 equiv) was solubilized in THF (0.2 M) in a flask. NaOH 30% (20 equiv) was added to the solution and the reaction was left stirring at room temperature until complete conversion was reached. The product was then concentrated by rotavapor and 5 mL of distilled water were added. In some cases, the product solubilized in water while in others a precipitate was obtained. In the former case, HCl conc was added until pH 3 was reached and a red precipitate in the form of undissociated acid was filtered. In the second case, the precipitate was filtered and the dissociated acid form was obtained. In both cases, the product obtained after filtration was dried using a high vacuum pump.

### 2-(5-(2-Carboxyphenyl)furan-2-yl)-6-methylquinoline-4-carboxylic acid (1)

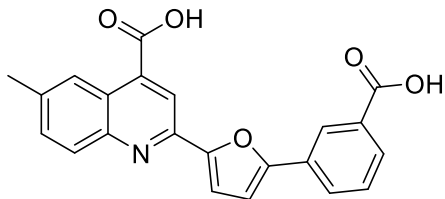


The compound **1** was obtained following the described procedure F using intermediate **40** (128 mg, 0.319 mmol) and NaOH 30% (0.85 ml, 6.38 mmol). After acid precipitation, desired **1** (118 mg, 0.469 mmol, quantitative yield) was obtained and characterized by UPLC-MS,  $^1\text{H}$  NMR and  $^{13}\text{C}$  NMR.

$^1\text{H}$  NMR (401 MHz, DMSO- $d_6$ )  $\delta$  8.35 (s, 1H), 8.21 (s, 1H), 7.96 (d,  $J$  = 8.6 Hz, 1H), 7.79 (d,  $J$  = 7.7 Hz, 1H), 7.68 – 7.56 (m, 3H), 7.50 – 7.41 (m, 2H), 6.98 (d,  $J$  = 3.6 Hz, 1H), 2.51 (s, 3H).  $^{13}\text{C}$  NMR (101 MHz,  $\text{CD}_3\text{OD}$ )  $\delta$  180.47, 178.97, 175.03, 155.54, 153.47, 149.38, 149.26, 148.10, 140.99, 137.48, 133.24, 128.81, 128.73, 128.51, 127.64, 127.11, 126.76, 125.30, 116.07, 113.52, 111.77, 24.24. UPLC-MS (ESI,  $m/z$ )  $R_t$  = 2.73 min, 374 ( $\text{M}+\text{H}$ ) $^+$

In agreement with Horak, Y. *et al.*, Ukrainica Bioorganica Acta, **2008**, 6(1), 49-54.<sup>251</sup>

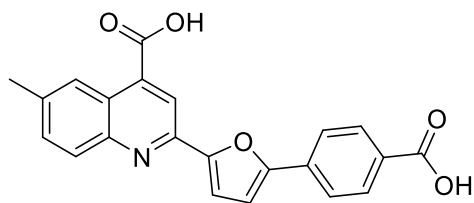
### 2-(5-(3-Carboxyphenyl)furan-2-yl)-6-methylquinoline-4-carboxylic acid (2)



The compound **2** was obtained following the described procedure F using intermediate **41** (186 mg, 0.46 mmol) and NaOH 30% (1.24 ml, 9.2 mmol). After acid precipitation, the desired **2** (170 mg, 0.46 mmol, quantitative yield) was obtained and characterized by UPLC-MS,  $^1\text{H}$  NMR and  $^{13}\text{C}$  NMR.

$^1\text{H}$  NMR (401 MHz, DMSO- $d_6$ )  $\delta$  8.39 - 8.34 (m, 2H), 8.32 (s, 1H), 8.16 - 8.08 (m, 1H), 8.00 (d,  $J$  = 8.6 Hz, 1H), 7.90 (dt,  $J$  = 7.7, 1.4 Hz, 1H), 7.69 - 7.57 (m, 2H), 7.52 (d,  $J$  = 3.6 Hz, 1H), 7.33 (d,  $J$  = 3.6 Hz, 1H), 2.51 (d,  $J$  = 1.0 Hz, 3H);  $^{13}\text{C}$  NMR (101 MHz, DMSO- $d_6$ )  $\delta$  167.84, 167.40, 154.24, 152.84, 147.39, 147.26, 137.90, 137.28, 133.04, 132.11, 130.44, 129.95, 129.51, 129.30, 128.66, 124.74, 123.79, 118.41, 113.82, 110.20, 22.05. UPLC-MS (ESI,  $m/z$ )  $R_t$  = 2.87 min, 374 ( $\text{M}+\text{H}$ ) $^+$

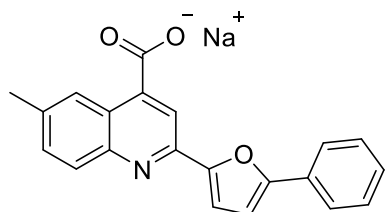
### 2-(5-(4-Carboxyphenyl)furan-2-yl)-6-methylquinoline-4-carboxylic acid (**3**)



The compound **3** was obtained following the general procedure F using intermediate **42** (150 mg, 0.373 mmol) and NaOH 30% (1 ml, 7.47 mmol). After acid precipitation, the desired **3** (139 mg, 0.372 mmol, quantitative yield) was obtained and characterized by UPLC-MS, <sup>1</sup>H-NMR and <sup>13</sup>C-NMR.

<sup>1</sup>H NMR (401 MHz, DMSO-d<sup>6</sup>) δ 8.36 (s, 1H), 7.91 (d, J = 8.1 Hz, 2H), 7.87 (s, 1H), 7.80 (d, J = 8.6 Hz, 1H), 7.73 (d, J = 8.1 Hz, 2H), 7.46 (dd, J = 8.6, 2.0 Hz, 1H), 7.30 (d, J = 3.5 Hz, 1H), 7.11 (d, J = 3.5 Hz, 1H), 2.44 (s, 3H) ppm; <sup>13</sup>C NMR (101 MHz, DMSO-d<sup>6</sup>) δ 167.84, 167.40, 154.73, 153.67, 147.62, 147.21, 137.90, 134.74, 133.04, 131.62, 130.09, 129.95, 129.51, 129.30, 127.08, 125.06, 123.02, 118.41, 112.06, 108.90, 22.05. UPLC-MS (ESI, m/z) Rt = 3.79 min, 360 (M+H)<sup>+</sup>

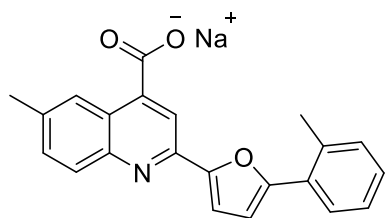
### Sodium 6-methyl-2-(5-phenylfuran-2-yl)quinoline-4-carboxylate (**4**)



The compound **4** was obtained following the described procedure F using intermediate **43** (158 mg, 0.46 mmol) and NaOH 30% (1.23 ml, 9.20 mmol). After filtration, the desired **4** (151 mg, 0.46 mmol, quantitative yield) was obtained and characterized by UPLC-MS, <sup>1</sup>H NMR and <sup>13</sup>C NMR.

<sup>1</sup>H NMR (401 MHz, DMSO-d<sup>6</sup>) δ 8.39 (dt, J = 1.9, 0.8 Hz, 1H), 7.91 (s, 1H), 7.86 - 7.83 (m, 2H), 7.81 (d, J = 8.6 Hz, 1H), 7.50 - 7.42 (m, 3H), 7.35 - 7.29 (m, 2H), 7.15 (d, J = 3.6 Hz, 1H), 2.44 (d, J = 1.0 Hz, 3H) ppm. <sup>13</sup>C NMR (101 MHz, DMSO-d<sup>6</sup>) δ 166.64, 166.36, 154.08, 152.89, 147.40, 147.21, 138.21, 136.08, 133.21, 130.97, 130.59, 130.11, 129.63, 129.10, 129.03, 124.56, 124.43, 123.44, 118.46, 113.87, 110.39, 22.02 ppm. UPLC-MS (ESI, m/z) Rt = 3.27 min, 330 (M+H)<sup>+</sup>

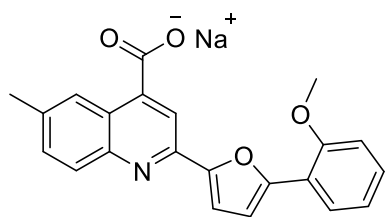
### Sodium 6-methyl-2-(5-(*o*-tolyl)furan-2-yl)quinoline-4-carboxylate (5)



The compound **5** was obtained following the described procedure F using intermediate **44** (115 mg, 0.322 mmol) and NaOH 30% (0.858 ml, 6.44 mmol). After filtration, the desired **5** (117 mg, 0.32 mmol, quantitative yield) was obtained and characterized by UPLC-MS,  $^1\text{H}$  NMR and  $^{13}\text{C}$  NMR.

$^1\text{H}$  NMR (401 MHz,  $\text{CD}_3\text{OD}$ )  $\delta$  8.15 (s, 1H), 8.03 (s, 1H), 8.00 – 7.90 (m, 2H), 7.59 (dd,  $J$  = 8.7, 2.0 Hz, 1H), 7.43 (d,  $J$  = 3.6 Hz, 1H), 7.36 – 7.22 (m, 3H), 6.87 (d,  $J$  = 3.6 Hz, 1H), 2.60 (s, 3H), 2.54 (s, 3H).  $^{13}\text{C}$  NMR (101 MHz,  $\text{CD}_3\text{OD}$ )  $\delta$  173.53, 155.12, 152.13, 147.99, 147.83, 146.66, 136.16, 134.68, 131.87, 130.90, 129.44, 127.78, 127.32, 126.96, 125.82, 125.31, 114.38, 111.75, 110.97, 20.77, 17.67. UPLC-MS (ESI,  $m/z$ )  $R_t$  = 3.49 min, 344 ( $\text{M}+\text{H}$ ) $^+$

### Sodium 2-(5-(2-methoxyphenyl)furan-2-yl)-6-methylquinoline-4-carboxylate (6)

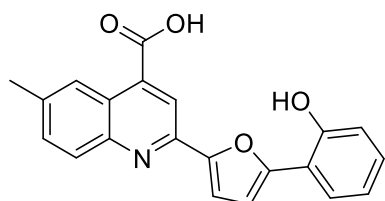


The compound **6** was obtained following the described procedure F using intermediate **45** (132 mg, 0.353 mmol) and NaOH 30% (0.942 ml, 7.07 mmol). After filtration, the desired **6** (134 mg, 0.352 mmol, quantitative yield) was obtained and characterized

by UPLC-MS,  $^1\text{H}$  NMR and  $^{13}\text{C}$  NMR.

$^1\text{H}$  NMR (401 MHz,  $\text{CD}_3\text{OD}$ )  $\delta$  8.17 (dd,  $J$  = 7.9, 1.8 Hz, 2H), 8.04 (s, 1H), 7.98 (d,  $J$  = 8.7 Hz, 1H), 7.59 (dd,  $J$  = 8.7, 2.0 Hz, 1H), 7.39 (dd,  $J$  = 3.6, 0.5 Hz, 1H), 7.33 (ddd,  $J$  = 8.6, 7.2, 1.7 Hz, 1H), 7.15 (d,  $J$  = 3.6 Hz, 1H), 7.13 – 7.07 (m, 2H), 4.00 (s, 3H), 2.54 (s, 3H).  $^{13}\text{C}$  NMR (101 MHz,  $\text{CD}_3\text{OD}$ )  $\delta$  174.97, 157.47, 153.55, 152.62, 149.34, 149.30, 148.08, 137.52, 133.28, 130.09, 128.66, 127.34, 126.77, 125.27, 121.89, 120.40, 116.00, 113.79, 113.73, 112.32, 55.92, 21.78. UPLC-MS (ESI,  $m/z$ )  $R_t$  = 3.32 min, 360 ( $\text{M}+\text{H}$ ) $^+$

### 2-(5-(2-hydroxyphenyl)furan-2-yl)-6-methylquinoline-4-carboxylic acid (7)

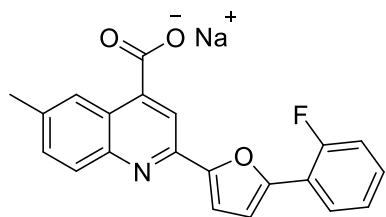


The compound **7** was obtained following the described procedure F using intermediate **46** (158 mg, 0.44 mmol) and NaOH 30% (1.17 ml, 8.79 mmol). After acid precipitation and  $\text{Et}_2\text{O}$  washing,

the desired **7** (151 mg, 0.437 mmol, quantitative yield) was obtained and characterized by UPLC-MS,  $^1\text{H}$  NMR and  $^{13}\text{C}$  NMR.

$^1\text{H}$  NMR (401 MHz, DMSO- $d_6$ )  $\delta$  10.51 (s, 1H), 8.38 (s, 1H), 8.30 (s, 1H), 7.98 (d,  $J$  = 8.6 Hz, 1H), 7.90 (dd,  $J$  = 7.9, 1.7 Hz, 1H), 7.66 (dd,  $J$  = 8.6, 1.9 Hz, 1H), 7.47 (d,  $J$  = 3.5 Hz, 1H), 7.23 – 7.14 (m, 2H), 7.08 (d,  $J$  = 8.1 Hz, 1H), 6.97 (t,  $J$  = 7.5 Hz, 1H), 2.52 (s, 3H).  $^{13}\text{C}$  NMR (101 MHz, DMSO- $d_6$ )  $\delta$  167.69, 154.21, 152.16, 150.71, 147.19, 147.08, 136.90, 132.40, 128.98, 128.95, 125.42, 124.46, 123.31, 119.34, 117.54, 116.72, 116.30, 112.98, 112.20, 21.59. UPLC-MS (ESI,  $m/z$ )  $R_t$  = 2.74 min, 346 (M+H) $^+$

### Sodium 2-(5-(2-fluorophenyl)furan-2-yl)-6-methylquinoline-4-carboxylate (**8**)



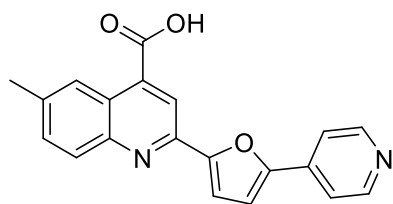
The compound **8** was obtained following the described procedure F using intermediate **47** (80 mg, 0.221 mmol) and NaOH 30% (0.59 mL, 4.43 mmol). After filtration, the desired **8** (81 mg, 0.22 mmol, quantitative yield) was obtained and characterized by

UPLC-MS,  $^1\text{H}$  NMR and  $^{13}\text{C}$  NMR.

$^1\text{H}$  NMR (600 MHz, DMSO- $d_6$ )  $\delta$  8.45 - 8.38 (s, 1H), 8.03 (td,  $J$  = 8.0, 2.0 Hz, 1H), 7.98 (s, 1H), 7.86 (d,  $J$  = 8.5 Hz, 1H), 7.52 (dd,  $J$  = 8.6, 2.1 Hz, 1H), 7.46 - 7.34 (m, 4H), 7.07 (t,  $J$  = 3.5 Hz, 1H), 2.48 (s, 3H) ppm.  $^{13}\text{C}$  NMR (151 MHz, DMSO- $d_6$ )  $\delta$  169.38, 158.93, 157.27, 153.47, 149.68, 147.99, 146.93, 134.68, 131.35, 129.61, 128.33, 126.64, 126.10, 125.22, 124.73, 117.87, 116.40, 114.71, 112.81, 111.60, 21.46 ppm. UPLC-MS (ESI,  $m/z$ )  $R_t$  = 3.47 min, 348 (M+H) $^+$

In agreement with Horak, Y. *et al.*, Ukrainica Bioorganica Acta, **2008**, 6(1), 49-54.<sup>251</sup>

### 6-Methyl-2-(5-(pyridin-4-yl)furan-2-yl)quinoline-4-carboxylic acid (**9**)



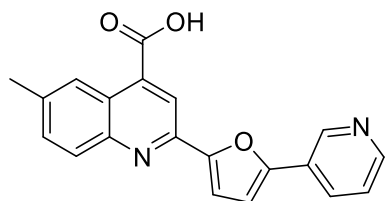
The compound **9** was obtained following the described procedure F using intermediate **48** (130 mg, 0.377 mmol) and NaOH 30% (1 mL, 7.55 mmol). After acid precipitation, the desired **9** (124 mg, 0.377 mmol, quantitative yield) was obtained and

characterized by UPLC-MS,  $^1\text{H}$  NMR and  $^{13}\text{C}$  NMR.

$^1\text{H}$  NMR (401 MHz, DMSO- $d_6$ )  $\delta$  8.71 – 8.65 (m, 2H), 8.40 (d,  $J$  = 3.1 Hz, 2H), 8.03 (d,  $J$  = 8.6 Hz, 1H), 7.90 – 7.84 (m, 2H), 7.70 (dd,  $J$  = 8.7, 2.0 Hz, 1H), 7.61 – 7.53 (m, 2H), 2.55 (s, 3H)

ppm.  $^{13}\text{C}$  NMR (101 MHz,  $\text{DMSO-d}_6$ )  $\delta$  167.89, 154.09, 152.44, 150.73, 147.46, 147.46, 147.10, 138.19, 137.58, 136.68, 133.13, 129.63, 124.73, 123.95, 123.95, 118.33, 113.52, 113.11, 22.08 ppm. UPLC-MS (ESI,  $m/z$ )  $R_t$  = 1.49 min, 331 ( $\text{M}+\text{H}$ ) $^+$

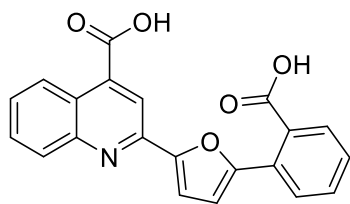
**6-Methyl-2-(5-(pyridin-3-yl)furan-2-yl)quinoline-4-carboxylic acid (10)**



The compound **10** was obtained following the described procedure F using intermediate **49** (88 mg, 0.255 mmol) and NaOH 30% (0.681 mL, 5.11 mmol). After acid precipitation, the desired **10** (84 mg, 0.255 mmol, quantitative yield) was obtained and characterized by UPLC-MS,  $^1\text{H}$  NMR and  $^{13}\text{C}$  NMR.

$^1\text{H}$  NMR (401 MHz,  $\text{DMSO-d}_6$ )  $\delta$  9.23 (d,  $J$  = 2.3 Hz, 1H), 8.63 (dd,  $J$  = 5.0, 1.6 Hz, 1H), 8.42 (d,  $J$  = 4.6 Hz, 3H), 8.02 (d,  $J$  = 8.6 Hz, 1H), 7.68 (m, 2H), 7.57 (d,  $J$  = 3.6 Hz, 1H), 7.46 (d,  $J$  = 3.6 Hz, 1H), 2.55 (s, 3H).  $^{13}\text{C}$  NMR (101 MHz,  $\text{DMSO-d}_6$ )  $\delta$  167.89, 154.09, 152.44, 150.73, 148.95, 147.46, 147.10, 138.19, 137.58, 136.68, 134.11, 133.41, 133.13, 129.63, 124.73, 123.95, 118.33, 113.52, 113.11, 22.08. UPLC-MS (ESI,  $m/z$ )  $R_t$  = 2.28 min, 331( $\text{M}+\text{H}$ ) $^+$

**2-(5-(2-carboxyphenyl)furan-2-yl)quinoline-4-carboxylic acid (11)**

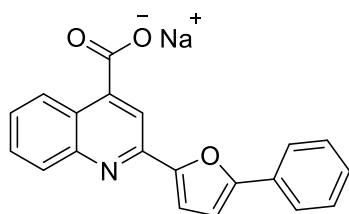


The compound **11** was obtained following the described procedure F using intermediate **50** (90 mg, 0.232 mmol) and NaOH 30% (0.619 mL, 4.65 mmol). After acid precipitation, the desired **11** (83 mg, 0.231 mmol, quantitative yield) was obtained and characterized by UPLC-MS,  $^1\text{H}$  NMR and  $^{13}\text{C}$  NMR.

$^1\text{H}$  NMR (401 MHz,  $\text{DMSO-d}_6$ )  $\delta$  8.57 (dd,  $J$  = 8.6, 1.5 Hz, 1H), 8.26 (s, 1H), 8.11 - 8.02 (m, 1H), 7.81 (ddd,  $J$  = 8.3, 6.9, 1.4 Hz, 2H), 7.68 - 7.64 (m, 2H), 7.63 - 7.57 (m, 1H), 7.54 - 7.45 (m, 2H), 6.99 (d,  $J$  = 3.6 Hz, 1H) ppm.  $^{13}\text{C}$  NMR (101 MHz,  $\text{DMSO-d}_6$ )  $\delta$  170.24, 167.77, 154.41, 152.84, 148.68, 148.26, 138.23, 132.22, 131.35, 131.17, 130.98, 129.60, 129.15, 129.07, 128.56, 128.23, 128.08, 125.98, 123.74, 118.03, 113.55, 111.54 ppm. UPLC-MS (ESI,  $m/z$ )  $R_t$  = 2.58 min, 360 ( $\text{M}+\text{H}$ ) $^+$

In agreement with Horak, Y. *et al.*, *Ukrainica Bioorganica Acta*, **2008**, 6(1), 49-54.<sup>251</sup>

### Sodium 2-(5-phenylfuran-2-yl)quinoline-4-carboxylate (**12**)

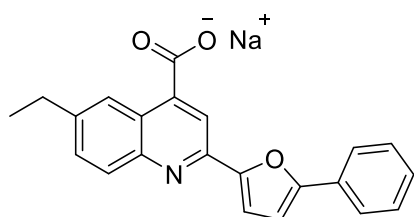


The compound **12** was obtained following the described procedure F using intermediate **51** (70 mg, 0.212 mmol) and NaOH 30% (0.57 ml, 4.25 mmol). After filtration, the desired **12** (71 mg, 0.211 mmol, quantitative yield) was obtained and characterized by UPLC-MS, <sup>1</sup>H

NMR and <sup>13</sup>C NMR.

<sup>1</sup>H NMR (401 MHz, DMSO-d<sub>6</sub>) δ 8.67 (dd, J = 8.4, 1.5 Hz, 1H), 8.00 (s, 1H), 7.97 - 7.93 (m, 1H), 7.89 (dd, J = 8.3, 1.2 Hz, 2H), 7.67 (ddd, J = 8.4, 6.8, 1.5 Hz, 1H), 7.55 - 7.43 (m, 3H), 7.40 (d, J = 3.5 Hz, 1H), 7.39 - 7.31 (m, 1H), 7.20 (d, J = 3.6 Hz, 1H) ppm. <sup>13</sup>C NMR (151 MHz, DMSO-d<sub>6</sub>) δ 154.08, 153.20, 148.23, 147.94, 129.90, 129.15, 129.07, 128.45, 128.03, 127.86, 125.22, 124.79, 123.80, 114.68, 112.05, 108.65. UPLC-MS (ESI, m/z) Rt = 3.5 min, 316 (M+H)<sup>+</sup>

### Sodium 6-ethyl-2-(5-phenylfuran-2-yl)quinoline-4-carboxylate (**13**)

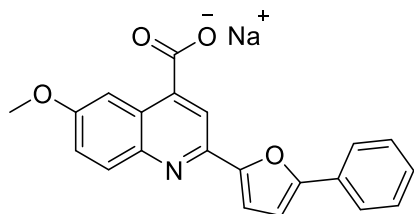


The compound **13** was obtained following the described procedure F using intermediate **70** (117 mg, 0.327 mmol) and NaOH 30% (0.873 ml, 6.55 mmol). After filtration, the desired **13** (119 mg, 0.324 mmol, quantitative yield) was obtained and

characterized by UPLC-MS, <sup>1</sup>H NMR and <sup>13</sup>C NMR.

<sup>1</sup>H NMR (401 MHz, Chloroform-d) δ 8.18 - 8.15 (m, 1H), 8.02 (s, 1H), 7.99 (d, J = 8.7 Hz, 1H), 7.93 - 7.88 (m, 2H), 7.62 (dd, J = 8.7, 2.0 Hz, 1H), 7.44 (dd, J = 8.4, 7.1 Hz, 2H), 7.38 (d, J = 3.6 Hz, 1H), 7.35 - 7.28 (m, 1H), 6.99 (d, J = 3.6 Hz, 1H), 2.83 (q, J = 7.6 Hz, 2H), 1.33 (t, J = 7.6 Hz, 3H). <sup>13</sup>C NMR (101 MHz, Chloroform-d) δ 173.51, 155.52, 152.35, 148.06, 147.74, 146.82, 142.44, 130.85, 130.20, 128.47, 127.71, 127.40, 124.10, 123.89, 123.82, 114.41, 112.28, 107.44, 67.41, 48.18, 47.97, 47.76, 47.55, 47.34, 47.12, 46.91, 28.62, 25.04, 17.77, 14.43. UPLC-MS (ESI, m/z) Rt = 3.46 min, 344 (M+H)<sup>+</sup>

### Sodium 6-methoxy-2-(5-phenylfuran-2-yl)quinoline-4-carboxylate (**14**)

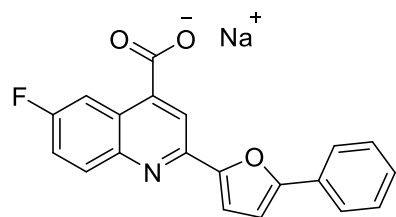


The compound **14** was obtained following the described procedure F using intermediate **71** (115 mg, 0.32 mmol) and NaOH 30% (0.853 ml, 6.40 mmol). After filtration, the desired

**14** (117 mg, 0.32 mmol, quantitative yield) was obtained and characterized by UPLC-MS,  $^1\text{H}$  NMR and  $^{13}\text{C}$  NMR.

$^1\text{H}$  NMR (401 MHz, Chloroform- $d$ )  $\delta$  8.07 (s, 1H), 7.96 (d,  $J$  = 9.2 Hz, 1H), 7.92 - 7.87 (m, 2H), 7.83 (d,  $J$  = 2.9 Hz, 1H), 7.43 (t,  $J$  = 7.7 Hz, 2H), 7.37 (dd,  $J$  = 9.3, 2.8 Hz, 1H), 7.34 - 7.27 (m, 2H), 6.97 (d,  $J$  = 3.6 Hz, 1H), 3.93 (s, 3H).  $^{13}\text{C}$  NMR (101 MHz, Chloroform- $d$ )  $\delta$  173.41, 157.88, 155.23, 152.44, 146.71, 146.24, 144.16, 130.28, 128.92, 128.45, 127.60, 125.16, 123.75, 122.40, 115.29, 111.60, 107.37, 104.30, 56.88, 54.59, 18.44, 18.41, 18.29, 16.92. UPLC-MS (ESI,  $m/z$ )  $R_t$  = 3.52 min, 346 ( $M+H$ ) $^+$

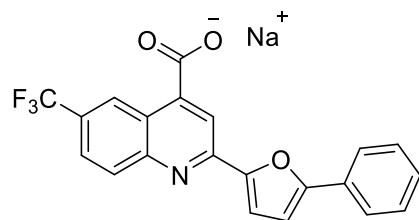
#### Sodium 6-fluoro-2-(5-phenylfuran-2-yl)quinoline-4-carboxylate (**15**)



The compound **15** was obtained following the described procedure F using intermediate **72** (105 mg, 0.30 mmol) and NaOH 30% (0.8 ml, 6 mmol). After filtration, the desired **15** (107mg, 0.30 mmol, quantitative yield) was obtained and characterized by UPLC-MS,  $^1\text{H}$  NMR and  $^{13}\text{C}$  NMR.

$^1\text{H}$  NMR (401 MHz, DMSO- $d_6$ )  $\delta$  8.62 (dd,  $J$  = 11.4, 3.0 Hz, 1H), 8.11 (s, 1H), 7.97 (dd,  $J$  = 9.3, 5.8 Hz, 1H), 7.89 - 7.81 (m, 2H), 7.54 (ddd,  $J$  = 9.2, 8.1, 3.1 Hz, 1H), 7.47 (t,  $J$  = 7.7 Hz, 2H), 7.39 - 7.31 (m, 2H), 7.17 (d,  $J$  = 3.5 Hz, 1H).  $^{13}\text{C}$  NMR (101 MHz, DMSO- $d_6$ )  $\delta$  168.26, 160.78, 158.38, 154.56, 153.36, 149.30, 149.24, 148.00, 147.98, 146.00, 131.50, 131.41, 130.27, 129.48, 128.47, 126.36, 126.25, 124.23, 119.60, 119.34, 116.79, 112.51, 111.72, 111.49, 109.07, 40.41, 31.11, 17.49. UPLC-MS (ESI,  $m/z$ )  $R_t$  = 3.37 min, 334 ( $M+H$ ) $^+$

#### Sodium 2-(5-phenylfuran-2-yl)-6-(trifluoromethyl)quinoline-4-carboxylate (**16**)



The compound **16** was obtained following the described procedure F using intermediate **73** (60 mg, 0.151 mmol) and NaOH 30% (0.4 ml, 3 mmol). After filtration, the desired **16** (61 mg, 0.151 mmol, quantitative yield) was obtained and

characterized by UPLC-MS,  $^1\text{H}$  NMR and  $^{13}\text{C}$  NMR.

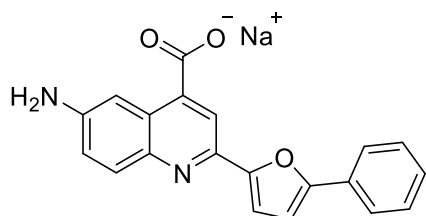
$^1\text{H}$  NMR (401 MHz, Chloroform- $d$ )  $\delta$  8.90 - 8.84 (m, 1H), 8.20 (d,  $J$  = 12.9 Hz, 2H), 7.91 (td,  $J$  = 8.9, 1.8 Hz, 3H), 7.50 (d,  $J$  = 3.7 Hz, 1H), 7.45 (dd,  $J$  = 8.4, 7.0 Hz, 2H), 7.38 - 7.31 (m, 1H), 7.03



(d, J = 3.6 Hz, 1H).  $^{13}\text{C}$  NMR (101 MHz, Chloroform-d)  $\delta$  172.01, 156.36, 151.93, 150.55, 149.36, 148.56, 129.97, 129.11, 128.53, 128.02, 127.74, 127.35, 127.02, 125.94, 125.64, 125.00, 124.96, 124.79, 124.74, 123.99, 123.21, 122.95, 116.18, 113.96, 107.73, 17.84, 17.80. UPLC-MS (ESI, m/z) Rt = 3.87 min, 384 (M+H) $^{+}$

6.1.10 Procedure G for the synthesis of 6-amino-2-(5-phenylfuran-2-yl)quinoline-4-carboxylic acid **19** (Scheme 4).

#### Sodium 6-amino-2-(5-phenylfuran-2-yl)quinoline-4-carboxylate (**19**)



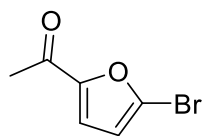
In a microwave tube, the intermediate **55** (80 mg, 0.22 mmol, 1 eq) was solubilized in anhydrous methanol (0.2 M) and NaOH (106 mg, 2.66 mmol, 12 eq) was added. The reaction was conducted in microwave reactor at 90 °C for 1.5 hours.

Next, 1 mL of water was added and the methanol was removed by rotavapor. The basic water left was acidified by HCl conc drop by drop. At neutral pH, the formation of a precipitate is observed, which is filtered and dried by vacuum to afford 18 mg (0.054 mmol, 25% yield) of pure compound **19** characterized by UPLC-MS,  $^1\text{H}$  NMR and  $^{13}\text{C}$  NMR (Scheme 4). The presence of counterion sodium had been confirmed by elemental analysis of the pure product **19** by Inductively Coupled Plasma Optical Emission spectroscopy (ICP-OES).

$^1\text{H}$  NMR (600 MHz, DMSO- $d_6$ )  $\delta$  8.14 (s, 1H), 7.87 - 7.83 (dd, J = 9.0, 2.5 Hz, 2H), 7.76 (d, J = 9.0 Hz, 1H), 7.65 (d, J = 2.5 Hz, 1H), 7.51 - 7.44 (t, J = 9.0 Hz, 2H), 7.37 - 7.31 (m, 1H), 7.26 (d, J = 3.5 Hz, 1H), 7.22 (dd, J = 9.0, 2.5 Hz, 1H), 7.16 (d, J = 3.5 Hz, 1H) ppm.  $^{13}\text{C}$  NMR (151 MHz, DMSO- $d_6$ )  $\delta$  169.02, 153.92, 153.50, 148.66, 143.31, 142.83, 130.62, 130.43, 129.50, 128.29, 126.59, 124.11, 122.68, 117.88, 110.90, 109.06, 103.77 ppm. UPLC-MS (ESI, m/z) Rt = 2.63 min, 331 (M+H) $^{+}$

6.1.11 Procedure H for the synthesis of 1-(5-bromofuran-2-yl)ethan-1-one **79** (Scheme 9).

#### 1-(5-Bromofuran-2-yl)ethan-1-one (**79**)

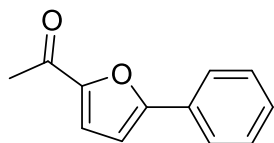


In agreement with Ismail, M. A. *et al.*<sup>257</sup>, in a flask, 2-acetyl furan **21** (1 g, 9.08 mmol, 1 eq) was solubilized in 10 mL of DMF and N-bromosuccinimide (1.94 g, 10.90 mmol, 1.2 eq) was added slowly at 0 °C. The reaction was left reacting at room temperature for 4 h. Then, the mixture was added drop by drop to 50 mL of cold distilled water at 0°C under stirring. The formation of a sticky precipitate was observed. The aqueous solution is extracted with DCM (3x40 mL) and the organic solvent is dried over Na<sub>2</sub>SO<sub>4</sub> and concentrated by vacuum. The desired compound was obtained after purification by column chromatography (EP:AcOEt 98:2) over silica gel to afford the desired **79** (710 mg, 3.76 mmol, 41% yield) characterized by <sup>1</sup>H NMR.

<sup>1</sup>H NMR (600 MHz, DMSO-d<sub>6</sub>) δ 7.50 (d, J = 3.6 Hz, 1H), 6.87 (d, J = 3.6 Hz, 1H), 2.39 (s, 3H).

6.1.12 Procedure I for the synthesis of 1-(5-phenylfuran-2-yl)ethan-1-one **54** (Scheme 9).

#### 1-(5-Phenylfuran-2-yl)ethan-1-one (**54**)

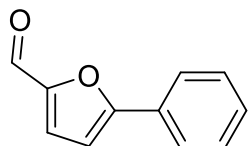


In a three-necked flask, the compound **79** (2 g, 10.58 mmol, 1 eq) was solubilized in dioxane:H<sub>2</sub>O (10:1, 0.1 M). Phenyl boronic acid **33** (1.55 g, 12.7 mmol, 1.2 eq) and K<sub>2</sub>CO<sub>3</sub> (2.92 g, 21.16 mmol, 2 eq) were added to the solution and the mixture was degassed with N<sub>2</sub>. Palladium tetrakis (611 mg, 0.53 mmol, 0.05 eq) was then added and the reaction was conducted at 100 °C in inert atmosphere stirring for 2 hours. Then, the reaction was cooled to room temperature, 50 mL of water is added and the dioxane was evaporated by rotavapor. An extraction with DCM (3x50 mL) was performed. The organic phase was dried over Na<sub>2</sub>SO<sub>4</sub>, filtered and concentrated by vacuum. An automated Combi-flash chromatography column is conducted (SiO<sub>2</sub> gold 80 g; DCM:MeOH 8:2) to afford the desired **54** (1.2 g, 6.44 mmol, 61% yield) as dark orange oil characterized by UPLC-MS and <sup>1</sup>H NMR.

<sup>1</sup>H NMR (600 MHz, DMSO-d<sub>6</sub>) δ 7.88 – 7.83 (m, 2H), 7.56 (d, J = 3.7 Hz, 1H), 7.53 – 7.47 (m, 1H), 7.45 – 7.39 (m, 2H), 7.21 (d, J = 3.7 Hz, 1H), 2.46 (s, 3H). UPLC-MS (ESI, m/z) Rt = 2.73 min, 173 (M+H)<sup>+</sup>

6.1.13 Procedure L for synthesis of 5-phenylfuran-2-carbaldehyde **75** (Scheme 9).

### 5-Phenylfuran-2-carbaldehyde (**75**)



In agreement with M. S. McClure *et al.*<sup>258</sup>, a three-neck flask, 200 mg (1.14 mmol, 1 eq) of 5-bromo 2-acetyl furan **80** were solubilized in dioxane:H<sub>2</sub>O (10:1, 0.1 M). Phenyl boronic acid **33** (209 mg, 1.71 mmol, 1.5 eq) and K<sub>2</sub>CO<sub>3</sub> (473 mg, 3.43 mmol, 3 eq) were added to the solution and the mixture was degassed with N<sub>2</sub>. Palladium tetrakis (132 mg, 0.114 mmol, 0.1 eq) was then added and the reaction was conducted at 100 °C in inert atmosphere stirring for 3 hrs. Then, the reaction was cooled to room temperature, 10 mL of water were added and the dioxane was evaporated by rotavapor. The left water was then extracted with DCM (3x10 mL). The organic solvent is brought to dryness by Na<sub>2</sub>SO<sub>4</sub> and vacuum obtaining the desired **75** (160 mg, 0.929 mmol, 81% yield) as dark yellow oil characterized by UPLC-MS and <sup>1</sup>H NMR.

<sup>1</sup>H NMR (400 MHz, Chloroform-d): δ 9.67 (s, 1H), 7.86-7.83 (m, 2H), 7.49-7.44 (m, 3H), 7.34 (d, 1H, J = 3 Hz), 6.86 (d, 1H, J = 3 Hz). UPLC-MS (ESI, m/z) Rt = 2.85 min, 187 (M+H)<sup>+</sup>

## 6.2 Experimental section: Part II

### 6.2.1 Material and methods

Solvents and reagents were obtained from commercial suppliers and used without further purification. For simplicity, solvents and reagents are indicated as follows: acetonitrile (ACN), dichloromethane (DCM), dimethyl sulfoxide (DMSO), dimethylformamide (DMF), Ac<sub>2</sub>O (Acetic anhydride), DMAP (4-Dimethylaminopyridine), DIC (N,N-Diisopropylcarbodiimide), TFA (Trifluoroacetic acid), TIPS (Triisopropylsilane), DIPEA (N,N-Diisopropylethylamine), HATU (Hexafluorophosphate Azabenzotriazole Tetramethyl Uronium), NMM (N-Methylmorpholine), PEG3 (3x polyethylene glycol), HFIP (Hexafluoro-2-propanol), Phe (Phenylalanine), Arg (Arginine), hCit (Homocitrulline), HLys (Homolysine), HArg (Homoarginine), Lys (Lysine), Tyr (Tyrosine), Bzl (Benzyl), Dap (Diaminopropionic Acid), Cys (Cysteine), Phacm (Phenylacetamide), AM-PhAcOH (Amino-Methylphenylacetic Acid), Ala (Alanine), Thz (Thiazole). Dipeptides were analyzed by LC-MS analysis with a UHPLC and single quadrupole MS system (Shimadzu LCMS-2020) using a C18 reversed phase column (Phenomenex Kinetex 2.1 mm × 50 mm C18 column, 100 Å pore, 2.6 µm particle) and a linear gradient of solvent B (acetonitrile, 0.05% formic acid) over solvent A (H<sub>2</sub>O, 0.05% formic acid) at a flow rate of 1 mL/min. Mass analysis was performed in positive ion mode. Data was collected and analyzed using the software of the LC-MS the Shimadzu 2020 instrument. Automated HPLC column chromatography purifications were conducted using a using a Waters HPLC system (2489 UV detector, 2535 pump, Fraction Collector III), a 19 mm × 250 mm Waters XTerra MS C18 OBD Prep Column C18 column (125 Å pore, 10 µm particle), solvent systems A (H<sub>2</sub>O, 0.1% v/v TFA) and B (ACN, 0.1% v/v TFA), and a gradient of 5–35% solvent B over 34 min. NMR experiments were run on a Bruker 600 system (600 MHz for <sup>1</sup>H, and 151 MHz for <sup>13</sup>C), equipped with a BBI probe and Z-gradients. Spectra were acquired at 300 K, using deuterated dimethyl sulfoxide (DMSO-*d*<sup>6</sup>) as solvent. Chemical shifts for <sup>1</sup>H and <sup>13</sup>C spectra were recorded in parts per million using the residual non-deuterated solvent as the internal standard (for DMSO-*d*<sup>6</sup>: 2.50 ppm, <sup>1</sup>H; 39.52 ppm, <sup>13</sup>C). Data are reported as follows: chemical shift (ppm), multiplicity (indicated as: bs, broad signal; s, singlet; d, doublet; t, triplet; q, quartet; m, multiplet), coupling constants (*J*) in Hertz (Hz) and integrated intensity.

## 6.2.2 HMBA resin loading and N-Allyloxy carbonyl (Alloc) substitution trial (Figure 37)

### HMBA resin loading

78 mg of Polystyrene AM HMBA resin (50  $\mu$ mol scale, 0.64 mmol/g loading) were swollen with 2 mL of mixture DCM:DMF 9:1 for 30 min in a 5 mL syringe. Solvent was filtered and Boc-L-Phe(4-NHFmoc)-OH (62.7 mg, 0.125 mmol) was dissolved in DMF (0.5 M) and added in the syringe. Next, HOBt (16.9 mg, 0.125 mmol) was added. In parallel, DIC (7.8  $\mu$ L, 0.05 mmol) and DMAP (0.6  $\mu$ L, 0.005 mmol) were dissolved in DMF (0.5 M) and added to the reaction. The resin was shaken for 3 h at rt. Then the resin was filtered and Ac<sub>2</sub>O (9.4  $\mu$ L, 0.1 mmol) and pyridine (8  $\mu$ L, 0.1 mmol) in DMF (0.1 M) were added to the resin to cap the unreacted amino acids and left reacting for 0.5 h at rt. The resin was then filtered and washed with MeOH, DCM and DMF (3x2 mL each).

### TFA Boc deprotection

In the 5 mL syringe, 1.5 mL TFA, 1.5 mL DCM, 75  $\mu$ L TIPS, 75  $\mu$ L H<sub>2</sub>O were added to resin and left shaking at rt for 15 min. The reaction was repeated once again. The resin was filtered and washed with DCM (3x2 mL) and with DMF (3x2 mL).

### Alloc substitution

In the 5 mL syringe, pyridine (17  $\mu$ L, 0.21 mmol) in DCM (0.03 M) was added to the resin and then allyl chloroformate (10  $\mu$ L, 0.1 mmol) in DCM (0.12 M) was added. The reaction was left shaking at rt overnight (16 h). The resin was filtered and washed with DCM (3x2 mL) and DMF (3x2 mL).

### HMBA resin cleavage

The aminoacidic product was cleaved from the resin with 1.56 mL of a dioxane:NaOH 0.1 M (3:1) solution for 4 h. The solution was then analyzed by UPLC-MS and showed the presence of the pure product. UPLC-MS (ESI, m/z) Rt = 1.56 min, 265 (M+H)<sup>+</sup>

### 6.2.3 N-Tert-butyloxycarbonyl (Boc) deprotection screening (Figure 39)

**Trial 1.** A solution containing Boc-D-Phe(4-NHFmoc)-OH (15 mg, 0.03 mmol) and Fmoc-Arg(Pbf)-OH (19 mg, 0.03 mmol) were placed inside a 2 mL eppendorf tube to which 0.55 mL of TFA, 0.55 mL of DCM, 0.025 mL of TIPS and 0.25 mL of water are added (0.03 M).

**Trial 2.** A solution containing Boc-D-Phe(4-NHFmoc)-OH (15 mg, 0.03 mmol) and Fmoc-Arg(Pbf)-OH (19 mg, 0.03 mmol) were placed inside a 2 mL eppendorf tube to which 1 mL TFA, 0.1 mL DCM, 0.0275 mL TIPS and 0.0275 mL of H<sub>2</sub>O are added (0.03 M).

**Trial 3.** A solution containing Boc-D-Phe(4-NHFmoc)-OH (15 mg, 0.03 mmol) and Fmoc-Arg(Pbf)-OH (19 mg, 0.03 mmol) were placed inside a 2 mL eppendorf tube to which 1 mL HCl 4 M in dioxane, 0.025 mL TIPS and 0.025 mL H<sub>2</sub>O are added (0.03 M total concentration of concerned amino acid).

**Trial 4.** A solution containing Boc-D-Phe(4-NHFmoc)-OH (15 mg, 0.03 mmol) and Fmoc-Arg(Pbf)-OH (19 mg, 0.03 mmol) were placed inside a 2 mL eppendorf tube to which 1 mL DCM are added as a negative standard (0.03 M).

After 5 minutes, UPLC-MS was performed for each solution. The trial 3 solution (HCl 4 M) showed the disappearance of the Boc group on D-Phe(4-NH-Fmoc)-OH product and the protective Pbf group still on the arginine unlike the other two trials after 5 minutes which showed a higher concentration of arginine deprotected by the Pbf group.

### 6.2.4 HMBA resin loading trials (Table 6)

**Trial 1.** In a 5 mL plastic syringe with septum, 104 mg of HMBA polystyrene resin (0.1 mmol, 0.96 mmol/g loading) were washed with 2 mL of DMF:DCM 1:9 solution. Once the resin was swollen for 30 minutes, the solution was filtered and 0.25 mmol (2.5 eq, 0.5 M in DMF) of each amino acid of interest were added. Next, 34 mg (0.25 mmol, 2.5 eq) of HOBT were added to the solution. Next, 20  $\mu$ L of a DMF solution containing DIC (15.7  $\mu$ L, 0.1 mmol, 1 eq) and DMAP (1.22 mg, 0.01 mmol, 0.1 eq) were added and the solution was left to react with the resin for 3 h at rt under agitation. After 3 h the solution is filtered and capped stirring for 30 minutes at rt by adding a 0.5 M DMF solution of Ac<sub>2</sub>O (19  $\mu$ L, 0.2 mmol, 2 eq) and pyridine (16  $\mu$ L, 0.2 mmol, 2

eq). Once the solution was filtered, the resin was washed with MeOH, DCM and DMF (3x2 mL each).

**Trial 2.** In a 5 mL plastic syringe with septum, 104 mg of HMBA resin (0.1 mmol, 0.96 mmol/g loading) were swollen with 3 mL DMF for 10 min. After the solvent was discarded, a 0.5 M DMF solution of amino acid (0.5 mmol, 5 eq) was added. Next, DMAP (1.22 mg, 0.01 mmol, 0.1 eq) was added. The solution was cooled to 0 °C with an ice bath and DIC (39 µL, 0.25 mmol, 2.5 eq) was added dropwise. After stirring for 20 minutes at 0°C, the mixture was shaken at rt for 2 h. Then, the reaction mixture was discarded, and the resin was washed with DMF (3x2 mL) and DCM (3x2 mL) and finally dried.

**Trial 3.** In a 5 mL plastic syringe with septum, 104 mg of HMBA resin (0.1 mmol, 0.96 mmol/g loading) were swollen with 3 mL DMF for 10 min. After the solvent was discarded, a 0.5 M DMF solution of amino acid (0.5 mmol, 5 eq) was added. Next, DMAP (1.22 mg, 0.01 mmol, 0.1 eq) was added. The solution was cooled to 0 °C with an ice bath and DIC (39 µL, 0.25 mmol, 2.5 eq) was added dropwise. After stirring for 20 minutes at 0°C, the mixture was shaken at rt for 2 h. Then, other 39 µL (0.25 mmol, 2.5 eq) of DIC were added to the mixture dropwise and the mixture was stirred at rt overnight. The day after, the reaction mixture was discarded, and the resin was washed with DMF (3x2 mL) and DCM (3x2 mL) and finally dried.

#### 6.2.5 General procedure for CTC resin loading

In a 5 mL plastic syringe with septum, 77 mg of 2-Chlorotriptyl chloride (CTC) resin (0.1 mmol, 1.3 mmol/g loading) were added and swollen with 2 mL of DCM. The resin was left shaking for 30 minutes, after which the solvent was filtered and 0.3 mmol (3 eq, 0.3 M in DMF) of the corresponding amino acid were added with 105 µL of DIPEA (0.6 mmol, 6 eq, 2 M in DMF). The resin was left to react with the respective amino acids stirring for 2 h at rt. The resin was washed with DCM (3x2 mL) and DMF (3x2 mL) and finally dried.

## 6.2.6 General procedures of solid-phase peptide synthesis

### General procedure for Fmoc deprotection

The amino acids on the resin were deprotected from the Fmoc group by 0.9 ml of piperidine 20% in DMF for 5 min twice at rt under agitation. The solution was then filtered, and the resin washed with DMF (3x2 mL) and DCM (3x2 mL).

### General procedure for Coupling reaction

The coupling reaction was carried out by adding a solution of the concerned amino acid (5 eq, 0.5 M in DMF) to the resins with the first amino acid on. Next, HATU (0.5 mmol, 5 eq, 0.5 M in DMF) and NMM (1 mmol, 10 eq, 4 M in DMF) were added. The coupling reaction was left to stir at rt for 2 h, after which the solution was filtered and the resin was washed with DMF (5x2 mL).

### General procedure for Alloc deprotection

The affected dipeptides on the resin were deprotected from the Alloc group by suspending the resin in 2 ml of dry DCM and transferring it in a 15 mL falcon tube. Next,  $\text{PhSiH}_3$  (0.296 mL, 2.4 mmol, 24 eq) and  $\text{Pd(PPh}_3)_4$  (28 mg, 0.025 mmol, 0.25 eq) were added. The reaction was conducted stirring in inert atm by  $\text{N}_2$  flux constantly degassing the solution. After 1 h, syringe filtration was performed and the resin is washed with a solution of sodium diethyldithiocarbamate  $\text{C}_5\text{H}_{10}\text{NS}_2\text{Na}$  0.012 M in DMF and DIPEA in DMF (0.01% v/v DMF) and finally with DMF (3x2 mL) and DCM (3x2 mL).

### General procedure for Resin splitting

Once the dry resin has been left overnight in the fridge, 2 mL of DMF were added and the resin was split in two into another 5 mL syringe by quickly transporting 1 ml of the suspended resin in solution with a pipette. The DMF was then filtered and the resin was dried.

### General procedure for Capping

The resin ( $\approx 0.05$  mmol) was treated with 1 mL of 5%  $\text{Ac}_2\text{O}$  and 6% lutidine solution in DMF for 0.5 h while stirring at rt. The reaction was repeated one more time. The resin was then filtered and washed with DMF (6x2 mL).



#### General procedure for PEG3-biotin acid coupling

The resin ( $\approx 0.05$  mmol) was treated in a 5 mL syringe with a solution containing PEG3-biotin acid (45 mg, 0.1 mmol, 2 eq, 0.5 M in DMF). Next, HATU (38 mg, 0.1 mmol, 2 eq, 0.5 M in DMF) and NMM (0.219  $\mu$ L, 0.2 mmol, 4 eq, 4 M in DMF) were added to attach the biotin-acid containing PEG3 as linker to the N-terminus of the dipeptide. The resin was then filtered and washed with DMF (6x2 mL).

#### General procedure for HMBA resin cleavage

HMBA resins were treated with 3 mL of a 3:1 dioxane:NaOH 0.1 M solution for 4 h at 50 °C while stirring. The solution was then filtered into a 50 mL falcon tube and subjected to analysis by UPLC-MS. Many solutions confirmed the formation of the desired dipeptides. Nevertheless, it was likely that much of the dipeptide was still attached to the HMBA resin, which was why the reaction was repeated overnight and the solution was filtered into the same 50 mL falcon tube.

#### General procedure for CTC resin cleavage

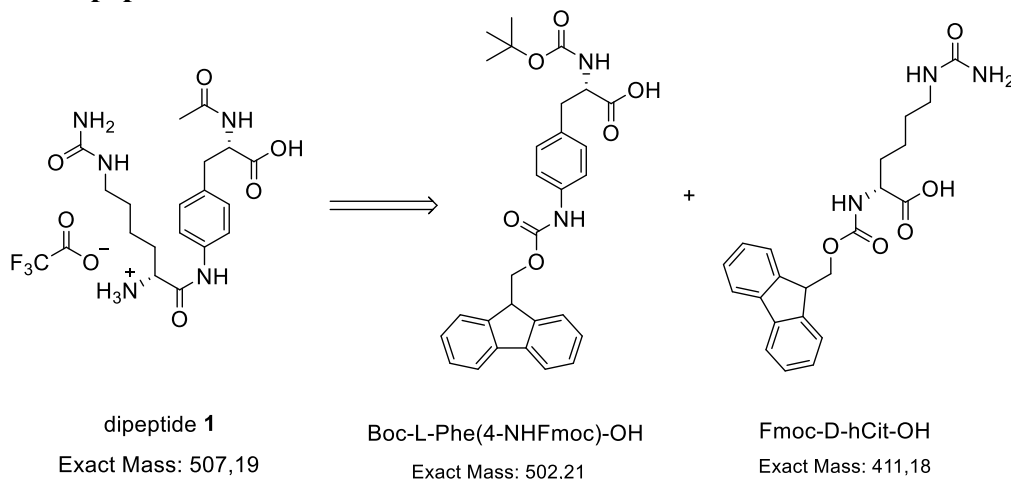
CTC resins were treated with 3.2 mL of a 20% solution of HFIP in DCM for 1 h at rt under stirring. After filtering the solutions in a 50 mL falcon tube, the reaction was repeated one more time and refiltered in the same falcon tube. The filtered solutions were subjected to UPLC-MS analysis, which confirmed the formation of the desired products.

#### 6.2.7 General procedure for HPLC purification

All the solutions of CTC/HMBA resin cleavage were lyophilized and 1 mL of DMSO was added to the solid in the 50 mL falcon tube. Then 9 mL of a 1:9 ACN:H<sub>2</sub>O (0.1% v/v TFA) were added and the crude was inserted by a 10 mL syringe into the HPLC system. HPLC was conducted with solvent A (H<sub>2</sub>O, 0.1% v/v TFA) and solvent B (ACN, 0.1% v/v TFA), and a gradient of 5–35% solvent B over 34 min. The fractions containing the desired dipeptide were lyophilized and the resulting pure product was weighted and analyzed by UPLC-MS.

## 6.2.8 Synthesis of Dipeptides **1-10** and **1B-10B**

### Synthesis of Dipeptide **1**



HMBA resin Boc-L-Phe(4-NHFmoc)-OH loading (**Trial 1**) - Fmoc deprotection – Fmoc-D-hCit-OH coupling - TFA Boc deprotection – Resin splitting - Capping - Fmoc deprotection - HMBA resin cleavage

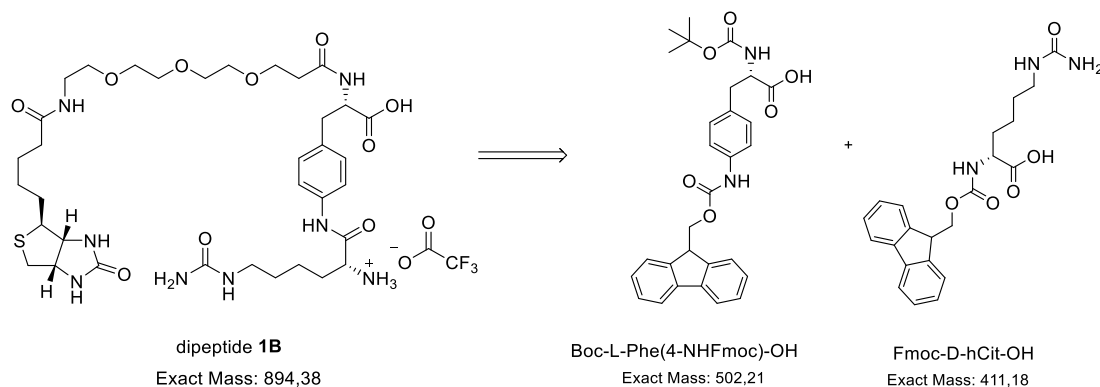
With the first trial using the procedure reported in Trial 1 of HMBA resin loading, the desired dipeptide **1** was not obtained. Trial 2 of HMBA resin loading of the amino acid Boc-L-Phe(4-NHFmoc)-OH has then been conducted carrying on with the same solid-phase peptide synthesis steps:

HMBA resin Boc-L-Phe(4-NHFmoc)-OH loading (**Trial 2**) - Fmoc deprotection – Fmoc-D-hCit-OH coupling - TFA Boc deprotection – Resin splitting - Capping - Fmoc deprotection - HMBA resin cleavage

By this procedure, the formation of the desired dipeptide was seen by UPLC-MS, which, once purified by HPLC, was lyophilized and weighed showing a yield of 67% (19 mg, 0.033 mmol). Dipeptide **1** was characterized by UPLC-MS and successful synthesis was confirmed by  $^1\text{H}$  NMR.

$^1\text{H}$  NMR (600 MHz, DMSO- $d_6$ )  $\delta$  12.68 (s, 2H), 10.40 (s, 1H), 8.22 (d,  $J$  = 5.4 Hz, 2H), 8.18 (d,  $J$  = 8.2 Hz, 1H), 7.52 – 7.46 (m, 2H), 7.23 – 7.18 (m, 2H), 5.94 (s, 1H), 5.38 (s, 2H), 4.37 (ddd,  $J$  = 9.6, 8.2, 5.0 Hz, 1H), 3.88 (d,  $J$  = 5.9 Hz, 1H), 3.00 (dd,  $J$  = 13.9, 4.9 Hz, 1H), 2.93 (t,  $J$  = 6.9 Hz, 2H), 2.79 (dd,  $J$  = 13.9, 9.6 Hz, 1H), 2.52 – 2.51 (m, 2H), 1.78 (s, 3H), 1.38 (q,  $J$  = 6.6 Hz, 2H), 1.35 – 1.29 (m, 2H). UPLC-MS (ESI,  $m/z$ )  $R_t$  = 1.32 min, 394 ( $M+H$ ) $^+$ , 392 ( $M-H$ ) $^-$

## Synthesis of Dipeptide 1B



HMBA resin Boc-L-Phe(4-NHFmoc)-OH loading (**Trial 1**) - Fmoc deprotection – Fmoc-D-hCit-OH coupling - TFA Boc deprotection – Resin splitting - PEG3-biotin coupling - Fmoc deprotection - HMBA resin cleavage

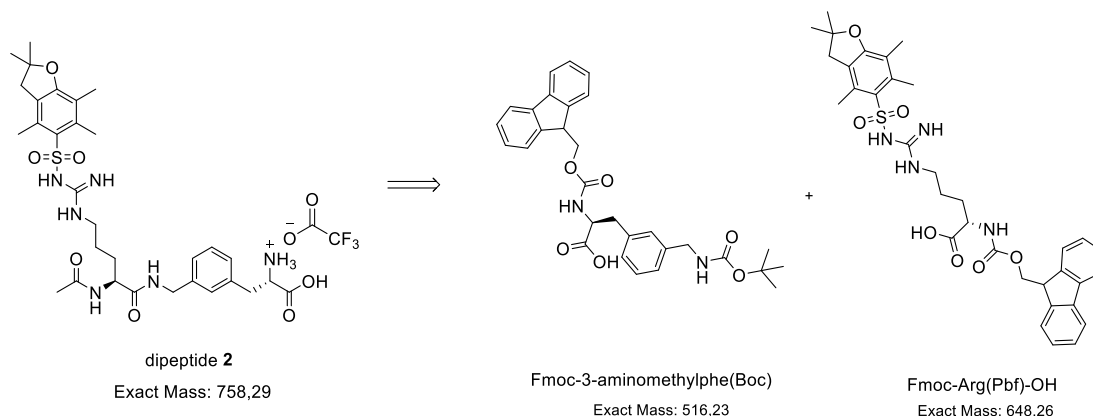
By Trial 1 of HMBA resin loading, the yield of biotinylated dipeptide 1B after HPLC results 12% (5.3 mg, 0.006 mmol). Since the yield is low, dipeptide 1B was synthesized with Trial 2:

HMBA resin Boc-L-Phe(4-NHFmoc)-OH loading (**Trial 2**) - Fmoc deprotection – Fmoc-D-hCit-OH coupling - TFA Boc deprotection – Resin splitting - PEG3-biotin coupling - Fmoc deprotection - HMBA resin cleavage

Dipeptide 1B showed an improved yield after HPLC of 47% (21 mg, 0.024 mmol) and was characterized by UPLC-MS and successful synthesis was confirmed by  $^1\text{H}$  NMR.

$^1\text{H}$  NMR (600 MHz, DMSO- $d_6$ )  $\delta$  12.68 (s, 2H), 10.40 (s, 1H), 8.22 (d,  $J = 5.4$  Hz, 3H), 8.16 (d,  $J = 8.1$  Hz, 1H), 7.83 (t,  $J = 5.7$  Hz, 1H), 7.53 – 7.47 (m, 2H), 7.23 – 7.17 (m, 2H), 6.39 (d,  $J = 33.4$  Hz, 2H), 5.95 (s, 1H), 5.32 (s, 2H), 4.43 – 4.39 (m, 1H), 4.32 – 4.29 (m, 1H), 4.12 (dd,  $J = 7.7$ , 4.4 Hz, 1H), 3.88 (q,  $J = 5.9$  Hz, 1H), 3.52 (tt,  $J = 6.6$ , 3.2 Hz, 2H), 3.48 (s, 4H), 3.47 – 3.42 (m, 4H), 3.38 (t,  $J = 6.0$  Hz, 2H), 3.17 (q,  $J = 5.9$  Hz, 2H), 3.09 (ddd,  $J = 8.6$ , 6.2, 4.4 Hz, 1H), 3.00 (dd,  $J = 13.9$ , 5.1 Hz, 1H), 2.93 (t,  $J = 6.9$  Hz, 2H), 2.85 – 2.81 (m, 1H), 2.81 (s, 1H), 2.57 (d,  $J = 12.4$  Hz, 1H), 2.32 (td,  $J = 6.6$ , 1.5 Hz, 2H), 2.06 (t,  $J = 7.4$  Hz, 2H), 1.79 (dq,  $J = 8.3$ , 6.1 Hz, 2H), 1.60 (ddt,  $J = 13.5$ , 9.9, 6.1 Hz, 1H), 1.52 – 1.42 (m, 3H), 1.38 (q,  $J = 6.6$  Hz, 2H), 1.31 (dddd,  $J = 15.0$ , 11.9, 6.2, 2.8 Hz, 4H). UPLC-MS (ESI,  $m/z$ )  $R_t = 2.41$  min, 781 ( $M+H$ ) $^+$ , 391 ( $M+2H$ ) $^{2+}$ , 779 ( $M-H$ ) $^-$ .

## Synthesis of Dipeptide 2



HMBA resin Fmoc-3-aminomethylphe(Boc) loading (**Trial 1**) - Fmoc deprotection - Alloc substitution – TFA Boc deprotection – Fmoc-Arg(Pbf)-OH coupling - Fmoc deprotection – Resin splitting - Capping - Alloc deprotection – HMBA resin cleavage

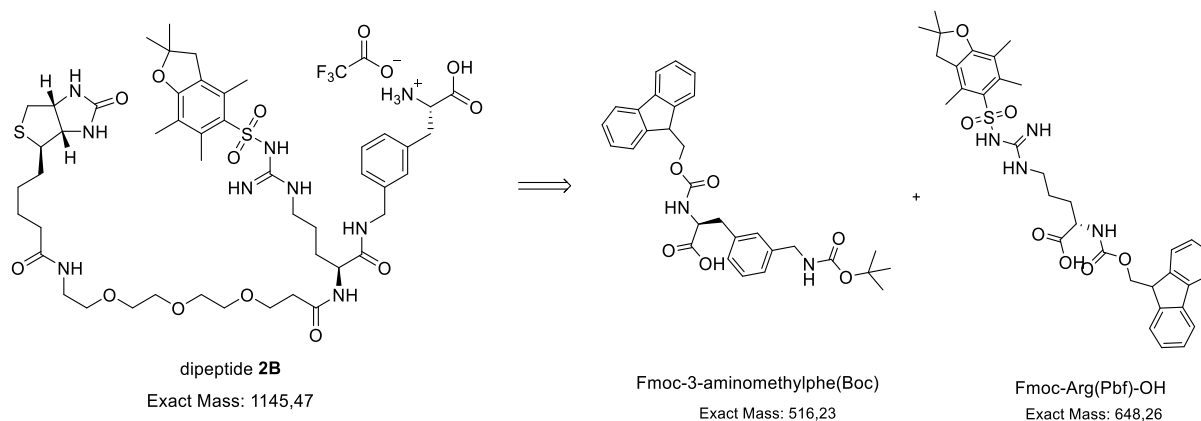
By Trial 1 of HMBA resin loading, the desired product was not obtained. Therefore, dipeptide 2 was resynthesized by HMBA resin loading trial 2 following the same solid-phase peptide synthesis procedures.

HMBA resin Fmoc-3-aminomethylphe(Boc) loading (**Trial 2**) - Fmoc deprotection - Alloc substitution – TFA Boc deprotection – Fmoc-Arg(Pbf)-OH coupling - Fmoc deprotection – Resin splitting - Capping - Alloc deprotection – HMBA resin cleavage

Once the compound is purified by HPLC, dipeptide 2 is weighed and characterized by UPLC-MS. The yield of this procedure results in 50% (19 mg, 0.025 mmol).

UPLC-MS (ESI, m/z)  $R_t = 2.77$  min, 645 (M+H)<sup>+</sup>, 643 (M-H)<sup>-</sup>.

## Synthesis of Dipeptide 2B



HMBA resin Fmoc-3-aminomethylphe(Boc) loading (**Trial 1**) - Fmoc deprotection - Alloc substitution – TFA Boc deprotection – Fmoc-Arg(Pbf)-OH coupling - Fmoc deprotection – Resin splitting - PEG3-biotin coupling - Alloc deprotection - HMBA resin cleavage

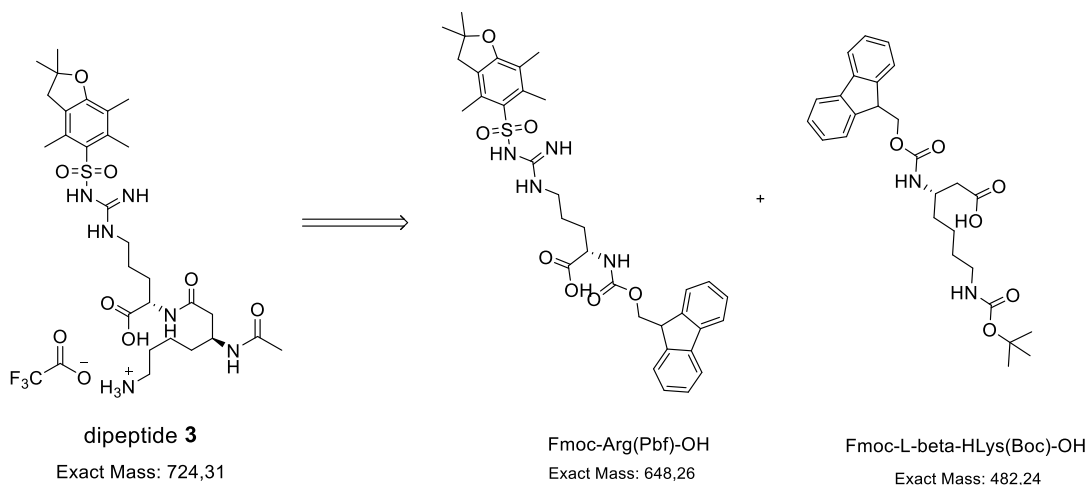
By Trial 1 of HMBA resin loading, the desired product was not obtained. Therefore, dipeptide 2B was resynthesized by HMBA resin loading trial 2 following the same solid-phase peptide synthesis procedures.

HMBA resin Fmoc-3-aminomethylphe(Boc) loading (**Trial 2**) - Fmoc deprotection - Alloc substitution – TFA Boc deprotection – Fmoc-Arg(Pbf)-OH coupling - Fmoc deprotection – Resin splitting - PEG3-biotin coupling - Alloc deprotection - HMBA cleavage

Once the compound is purified by HPLC, dipeptide 2B is weighed and characterized by UPLC-MS. The yield of this procedure results in 30% (17 mg, 0.015 mmol).

UPLC-MS (ESI, m/z)  $R_t = 2.82$  min, 1032 (M+H)<sup>+</sup>, 517 (M+2H)<sup>2+</sup>, 1030 (M-H)<sup>-</sup>.

## Synthesis of Dipeptide 3



HMBA resin Fmoc-Arg(Pbf)-OH loading (**Trial 1**) - Fmoc deprotection – Fmoc-L-beta-HLys(Boc)-OH coupling - Fmoc deprotection – Resin splitting - Capping - HCl 4 M Boc deprotection - HMBA resin cleavage

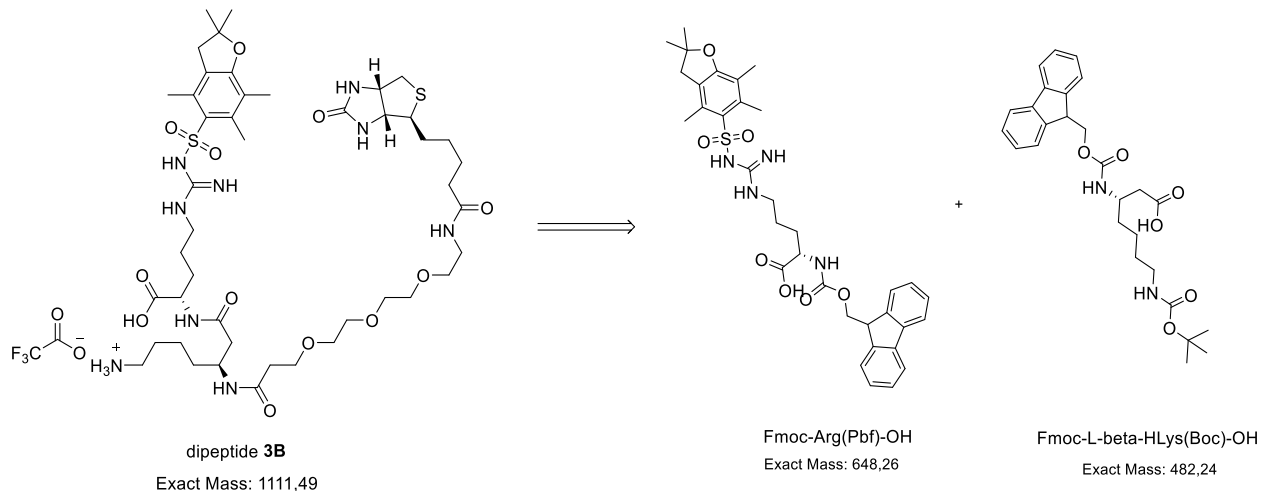
Using Trial 1 of HMBA resin loading, the yield of dipeptide 3 after HPLC results in 10% (3.6 mg, 0.005 mmol). Since the yield results were low, dipeptide 3 was synthesized with Trial 3.

HMBA resin Fmoc-Arg(Pbf)-OH loading (**Trial 3**) - Fmoc deprotection – Fmoc-L-beta-HLys(Boc)-OH coupling - Fmoc deprotection - Capping - HCl 4 M Boc deprotection - HMBA resin cleavage

Dipeptide 3 showed a similar yield following HPLC of 12% (4.3 mg, 0.006 mmol) and it was characterized by UPLC-MS.

UPLC-MS (ESI, m/z) Rt = 2.69 min, 611 (M+H)<sup>+</sup>, 609 (M-H)<sup>-</sup>.

## Synthesis of Dipeptide 3B

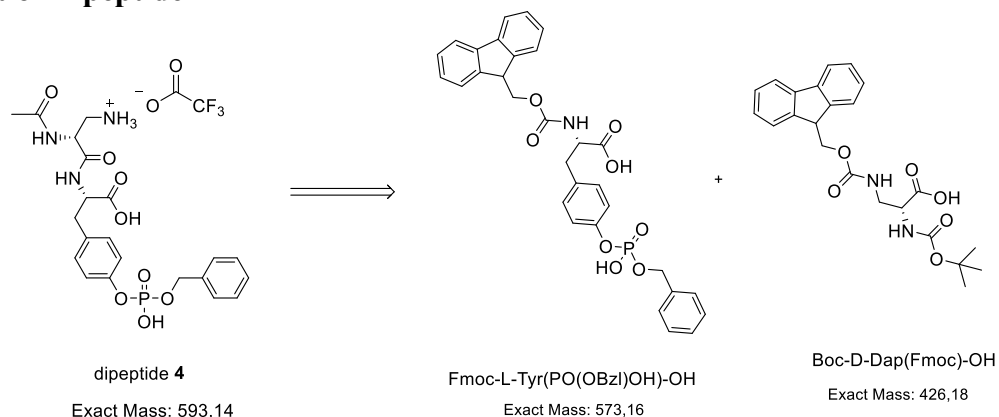


HMBA resin Fmoc-Arg(Pbf)-OH loading (**Trial 1**) - Fmoc deprotection – Fmoc-L-beta-HLys(Boc)-OH coupling - Fmoc deprotection – Resin splitting - PEG3-biotin acid coupling - HCl 4 M Boc deprotection - HMBA resin cleavage

Once synthesized and purified by HPLC, dipeptide 3B was lyophilized and weighed showing a yield of 10% (5.6 mg, 0.005 mmol). Dipeptide 3B was characterized by UPLC-MS.

UPLC-MS (ESI, m/z) Rt = 2.77 min, 998 (M+H)<sup>+</sup>, 500 (M+2H)<sup>2+</sup>, 996 (M-H)<sup>-</sup>.

## Synthesis of Dipeptide 4



HMBA resin Fmoc-L-Tyr(PO(OBzl)OH)-OH loading (**Trial 1**) - Fmoc deprotection – Boc-D-Dap(Fmoc)-OH coupling – HCl 4 M Boc deprotection – Resin splitting - Capping - Fmoc deprotection - HMBA resin cleavage

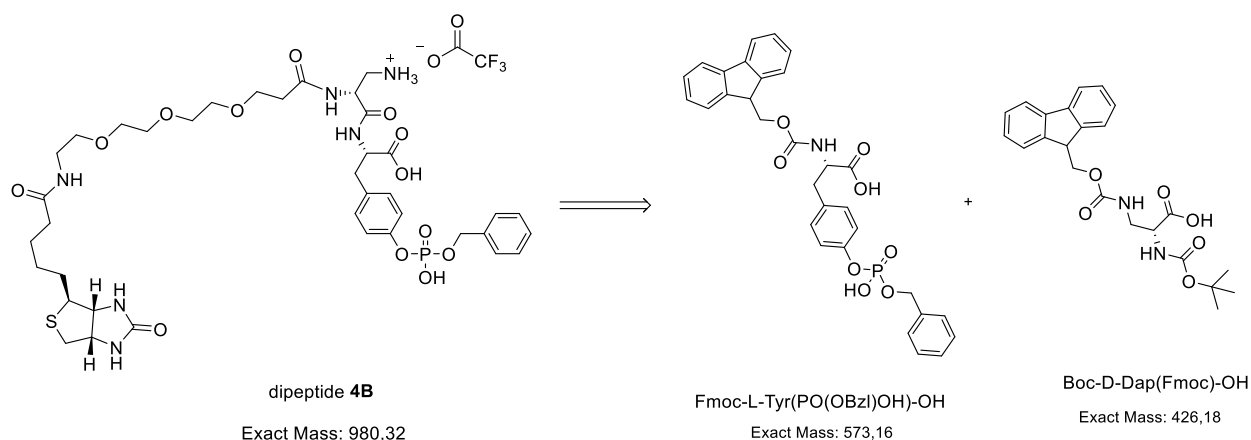
By Trial 1 of HMBA resin loading, the desired product was not obtained. Therefore, dipeptide 4 was resynthesized by HMBA resin loading Trial 2 following the same solid-phase peptide synthesis procedures.

HMBA resin Fmoc-L-Tyr(PO(OBzl)OH)-OH loading (**Trial 2**) - Fmoc deprotection – Boc-D-Dap(Fmoc)-OH coupling – HCl 4 M Boc deprotection – Resin splitting - Capping - Fmoc deprotection - HMBA resin cleavage

Once the compound is purified by HPLC, dipeptide 4 is weighed and characterized by UPLC-MS. The yield of this procedure is 43% (12.75 mg, 0.022 mmol).

UPLC-MS (ESI, m/z)  $R_t = 2.45$  min, 480 (M+H)<sup>+</sup>, 959 (2M+H)<sup>+</sup>, 478 (M-H)<sup>-</sup>, 957 (2M-H)<sup>-</sup>.

### Synthesis of Dipeptide 4B



HMBA resin Fmoc-L-Tyr(PO(OBzl)OH)-OH loading (**Trial 1**) - Fmoc deprotection – Boc-D-Dap(Fmoc)-OH coupling – HCl 4 M Boc deprotection – Resin splitting - PEG3-biotin acid coupling - Fmoc deprotection - HMBA resin cleavage

By Trial 1 of HMBA resin loading, the desired product was not obtained. Therefore, dipeptide 4B was resynthesized by HMBA resin loading trial 2 following the same solid-phase peptide synthesis procedures.

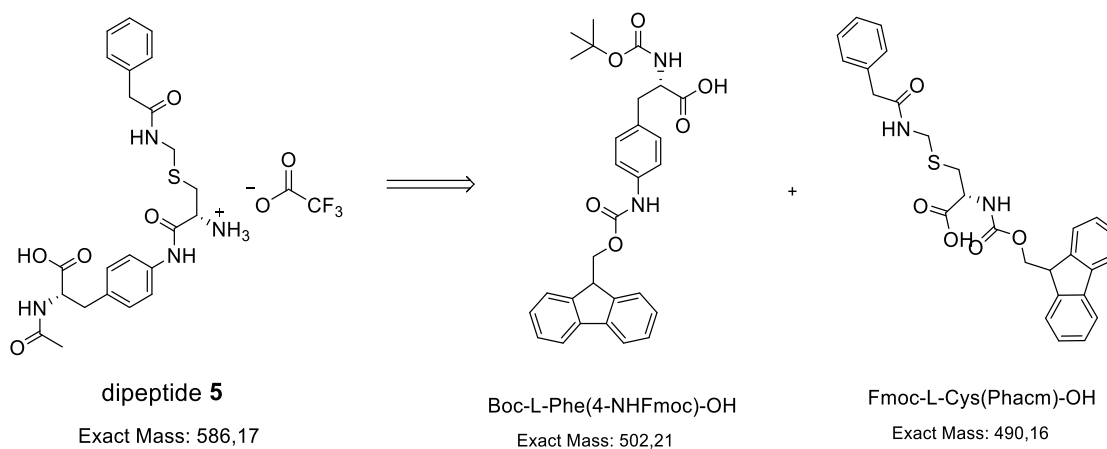
HMBA resin Fmoc-L-Tyr(PO(OBzl)OH)-OH loading (**Trial 2**) - Fmoc deprotection – Boc-D-Dap(Fmoc)-OH coupling – HCl 4 M Boc deprotection – Resin splitting - PEG3-biotin acid coupling - Fmoc deprotection - HMBA resin cleavage



Once the compound is purified by HPLC, dipeptide 4 is weighed and characterized by UPLC-MS. The yield of this procedure is 16% (7.84 mg, 0.008 mmol).

UPLC-MS (ESI, m/z)  $R_t = 2.56$  min, 867 (M+H)<sup>+</sup>, 434 (M+2H)<sup>2+</sup>, 865 (M-H)<sup>-</sup>.

### Synthesis of Dipeptide 5



HMBA resin Boc-L-Phe(4-NHFmoc)-OH loading (**Trial 1**) - Fmoc deprotection – Fmoc-L-Cys(Phacm)-OH coupling - TFA Boc deprotection – Resin splitting - Capping - Fmoc deprotection – HMBA resin cleavage

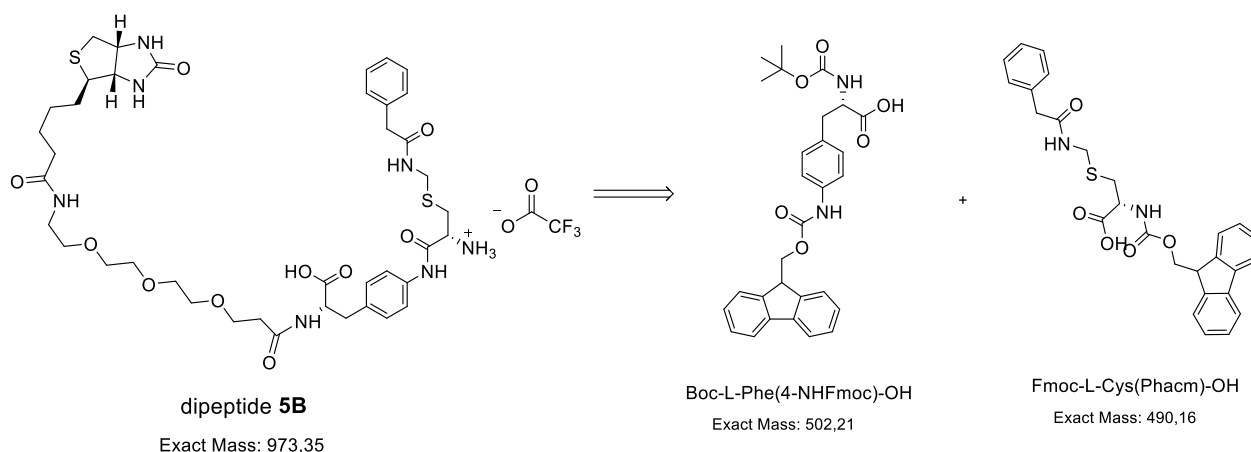
Using HMBA resin loading Trial 1, the yield of dipeptide 5 after HPLC results in 3% (0.88 mg, 0.0015 mmol). Since the yield is found to be low, dipeptide 5 was then resynthesized by HMBA resin loading Trial 3 following the same solid-phase peptide synthesis procedures.

HMBA resin Boc-L-Phe(4-NHFmoc)-OH loading (**Trial 3**) - Fmoc deprotection – Fmoc-L-Cys(Phacm)-OH coupling - TFA Boc deprotection - Capping - Fmoc deprotection – HMBA resin cleavage

Once the compound is purified by HPLC, dipeptide 5 is weighed and characterized by UPLC-MS. The yield of this procedure is 37% (10.8 mg, 0.019 mmol).

UPLC-MS (ESI, m/z)  $R_t = 2.47$  min, 473 (M+H)<sup>+</sup>, 471 (M-H)<sup>-</sup>.

## Synthesis of Dipeptide 5B

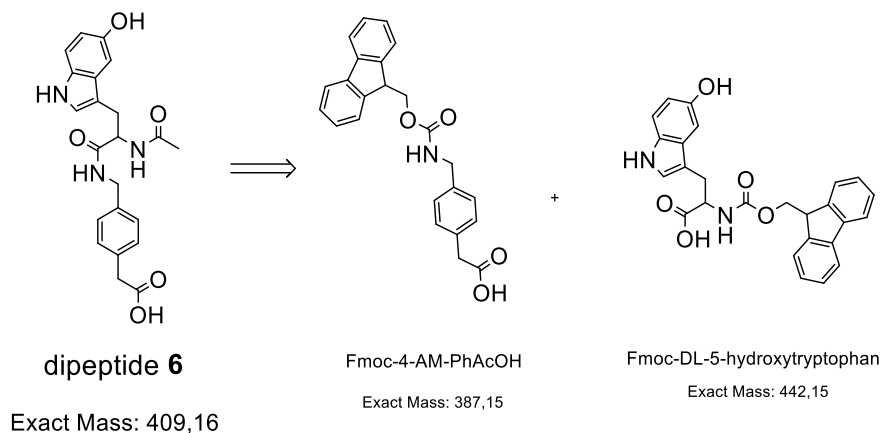


HMBA resin Boc-L-Phe(4-NHFmoc)-OH loading (**Trial 1**) - Fmoc deprotection – Fmoc-L-Cys(Phacm)-OH coupling - TFA Boc deprotection – Resin splitting - PEG3-biotin acid coupling - Fmoc deprotection – HMBA resin cleavage

Once synthesized and purified by HPLC, dipeptide 3B was lyophilized and weighed showing a yield of 8% (3.9 mg, 0.004 mmol). Peptide 5B was characterized by UPLC-MS.

UPLC-MS (ESI, m/z)  $R_t = 2.55$  min, 860 (M+H)<sup>+</sup>, 431 (M+2H)<sup>2+</sup>, 858 (M-H)<sup>-</sup>.

## Synthesis of Dipeptide 6

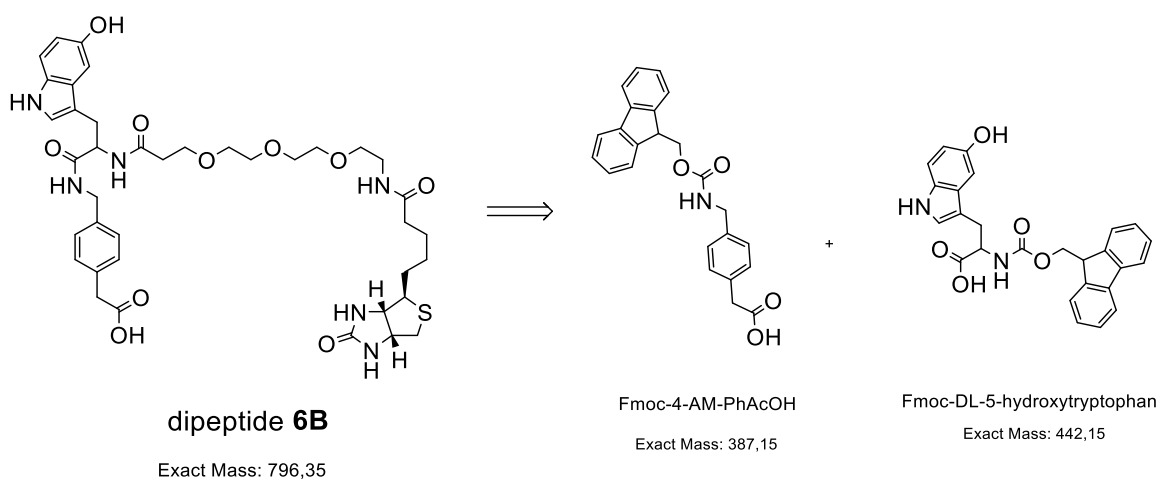


CTC resin Fmoc-4-AM-PhAcOH loading - Fmoc deprotection – Fmoc-DL-5-hydroxytryptophan coupling - Fmoc deprotection – Resin splitting - Capping - CTC resin cleavage

Dipeptide 6 was synthesized with CTC resin and purified by HPLC. The dipeptide was subsequently weighed showing a yield of 70% (14.3 mg, 0.035 mmol) and characterized by UPLC-MS. The successful synthesis is also confirmed by  $^1\text{H}$  NMR.

$^1\text{H}$  NMR (600 MHz, DMSO- $d_6$ )  $\delta$  12.27 (s, 2H), 10.46 (d,  $J$  = 2.4 Hz, 1H), 8.41 (t,  $J$  = 6.0 Hz, 1H), 8.03 (d,  $J$  = 8.1 Hz, 1H), 7.16 – 7.13 (m, 2H), 7.11 (d,  $J$  = 8.6 Hz, 1H), 7.08 – 7.04 (m, 2H), 7.00 (d,  $J$  = 2.4 Hz, 1H), 6.90 (d,  $J$  = 2.3 Hz, 1H), 6.58 (dd,  $J$  = 8.6, 2.3 Hz, 1H), 4.52 (d,  $J$  = 5.7 Hz, 1H), 4.22 (dd,  $J$  = 6.0, 2.8 Hz, 2H), 3.52 (s, 2H), 3.07 – 2.98 (m, 1H), 2.82 (dd,  $J$  = 14.5, 8.6 Hz, 1H), 1.80 (s, 3H). UPLC-MS (ESI,  $m/z$ )  $R_t$  = 2.50 min, 410 ( $M+H$ ) $^+$ , 819 ( $2M+H$ ) $^+$ , 408 ( $M-H$ ) $^-$ , 817 ( $2M-H$ ) $^-$ .

### Synthesis of Dipeptide 6B



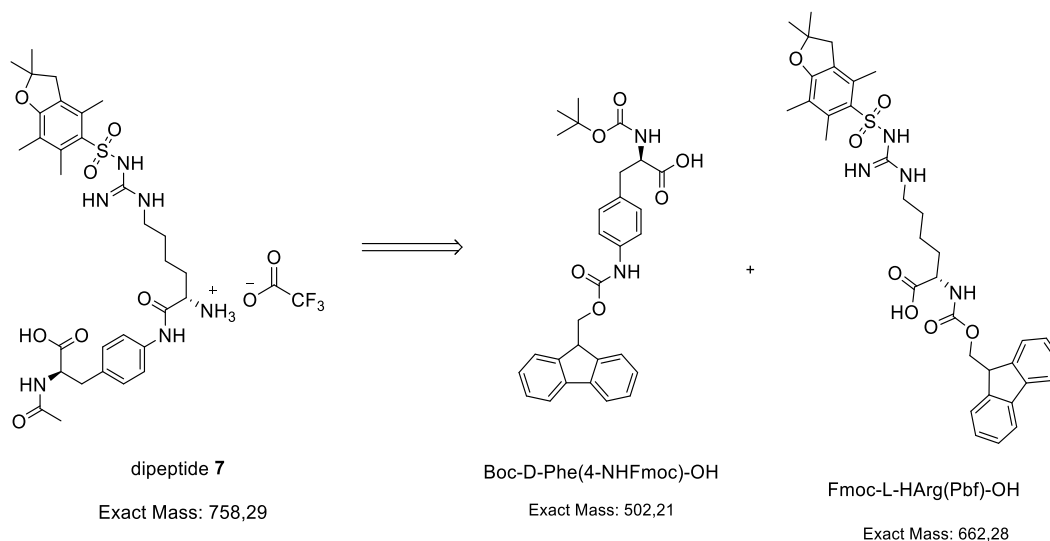
CTC resin Fmoc-4-AM-PhAcOH loading - Fmoc deprotection – Fmoc-DL-5-hydroxytryptophan coupling - Fmoc deprotection – Resin splitting - PEG3-biotin acid coupling - CTC resin cleavage

Dipeptide 6B was synthesized with CTC resin and purified by HPLC. The dipeptide was subsequently weighed showing a yield of 42% (16.7 mg, 0.021 mmol) and characterized by UPLC-MS. The successful synthesis is also confirmed by  $^1\text{H}$  NMR.

$^1\text{H}$  NMR (600 MHz, DMSO- $d_6$ )  $\delta$  12.27 (s, 2H), 10.46 (d,  $J$  = 2.4 Hz, 1H), 8.34 (t,  $J$  = 6.0 Hz, 1H), 8.05 (d,  $J$  = 8.1 Hz, 1H), 7.82 (t,  $J$  = 5.7 Hz, 1H), 7.17 – 7.12 (m, 2H), 7.11 (d,  $J$  = 8.6 Hz, 1H), 7.07 – 7.03 (m, 2H), 7.00 (d,  $J$  = 2.4 Hz, 1H), 6.89 (d,  $J$  = 2.3 Hz, 1H), 6.58 (dd,  $J$  = 8.6, 2.3 Hz, 1H), 6.41 (s, 1H), 6.35 (s, 1H), 4.53 (td,  $J$  = 8.2, 5.9 Hz, 1H), 4.29 (ddd,  $J$  = 7.7, 5.2, 1.0 Hz,

1H), 4.22 (qd,  $J = 15.3, 5.9$  Hz, 2H), 4.11 (dd,  $J = 7.7, 4.4$  Hz, 1H), 3.55 – 3.52 (m, 2H), 3.51 (s, 2H), 3.47 (s, 5H), 3.37 (t,  $J = 5.9$  Hz, 5H), 3.17 (q,  $J = 5.9$  Hz, 2H), 3.11 – 3.00 (m, 2H), 2.88 – 2.78 (m, 2H), 2.57 (d,  $J = 12.4$  Hz, 1H), 2.35 (td,  $J = 6.7, 2.2$  Hz, 2H), 2.08 – 2.02 (m, 2H), 1.64 – 1.56 (m, 1H), 1.47 (dddd,  $J = 29.1, 17.1, 8.7, 5.0$  Hz, 3H), 1.35 – 1.23 (m, 2H). UPLC-MS (ESI,  $m/z$ )  $R_t = 2.60$  min, 797 ( $M+H$ )<sup>+</sup>, 795 ( $M-H$ )<sup>-</sup>.

## Synthesis of Dipeptide 7

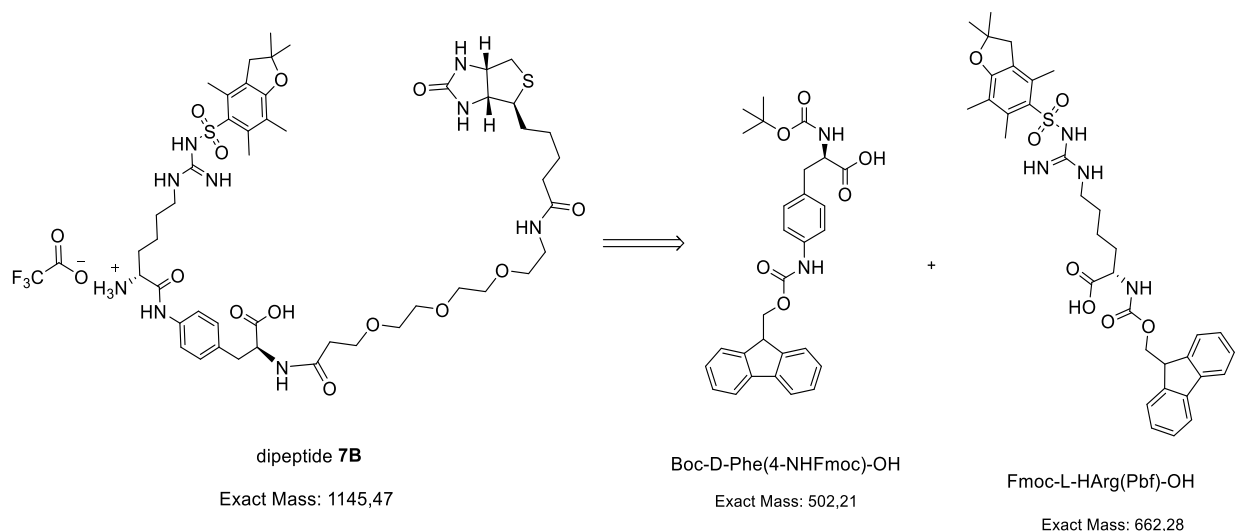


HMBA resin Boc-D-Phe(4-NHFmoc-OH) loading (**Trial 1**) - Fmoc deprotection – Fmoc-L-HArg(Pbf)-OH coupling - HCl 4 M Boc deprotection – Resin splitting - Capping - Fmoc deprotection - HMBA resin cleavage

Dipeptide 7 was synthesized by the experimental procedure described above and, after being purified by HPLC, showed a yield of 13% (4.92 mg, 0.0065 mmol). The compound was characterized by UPLC-MS.

UPLC-MS (ESI,  $m/z$ )  $R_t = 2.77$  min, 645 ( $M+H$ )<sup>+</sup>, 643 ( $M-H$ )<sup>-</sup>.

## Synthesis of Dipeptide 7B

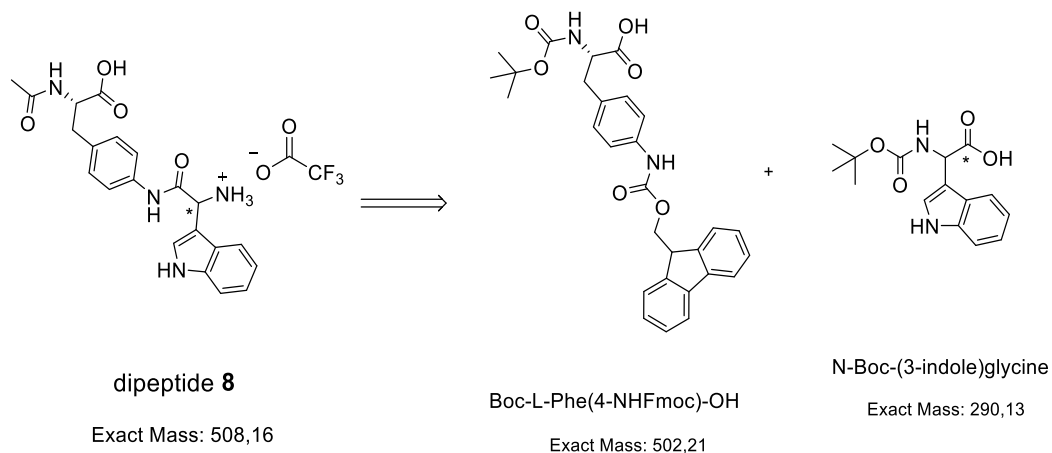


HMBA resin Boc-D-Phe(4-NHFmoc-OH) loading (**Trial 1**) - Fmoc deprotection – Fmoc-L-HArg(Pbf)-OH coupling - HCl 4 M Boc deprotection – Resin splitting – PEG3-biotin acid coupling - Fmoc deprotection - HMBA resin cleavage

Dipeptide 7B was synthesized by the experimental procedure described above and, after being purified by HPLC, showed a yield of 16% (9.16 mg, 0.008 mmol). The compound was characterized by UPLC-MS.

UPLC-MS (ESI, m/z)  $R_t = 2.81$  min, 1032 (M+H)<sup>+</sup>, 517 (M+2H)<sup>2+</sup>, 1030 (M-H)<sup>-</sup>.

## Synthesis of Dipeptide 8



HMBA resin Boc-L-Phe(4-NHFmoc)-OH loading (**Trial 1**) – TFA Boc deprotection - Alloc substitution - Fmoc deprotection – N-Boc-(3-indole)glycine coupling - Alloc deprotection - Resin splitting - Capping – TFA Boc deprotection – HMBA resin cleavage

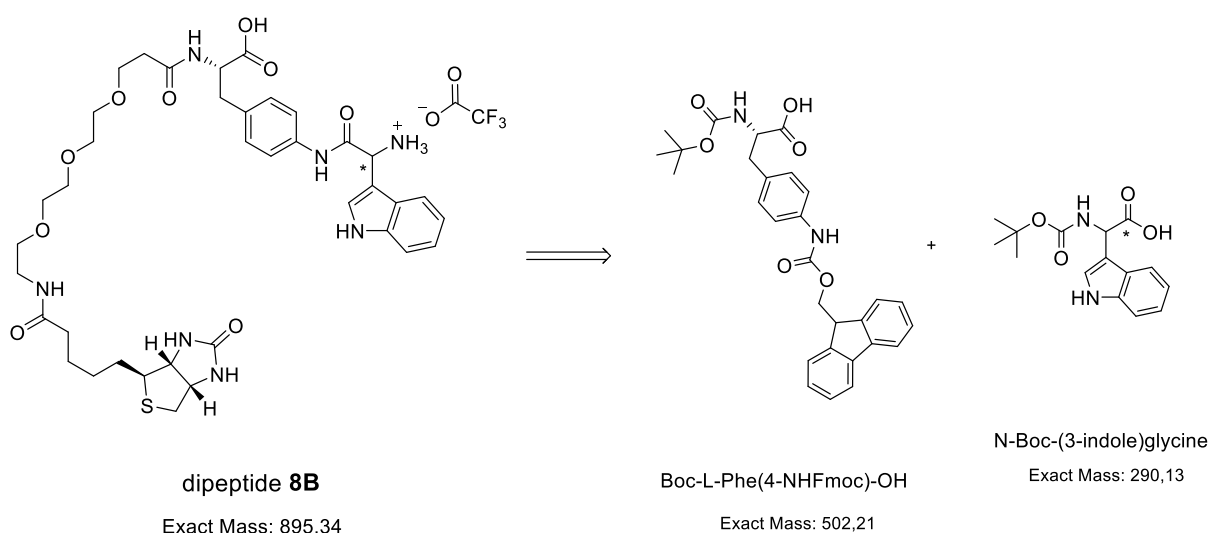
Dipeptide 8 was synthesized through the experimental procedure described above. Using a racemic mixture of the amino acid N-Boc-(3-indole)glycine, the diastereoisomers 8S and 8R should be formed, but UPLC-MS of the crude shows only one peak instead of a diastereoisomeric mixture. Probably the amino acid is not a racemic mixture or a change in stereochemistry occurs during peptide synthesis. Dipeptide 8, after being purified by HPLC, showed a yield of 3% (0.76 mg, 0.0015 mmol). As the yield was low, dipeptide 8 was resynthesized by Trial 3 of HMBA resin loading but showed the same yield (1.02 mg, 0.002 mmol, 4% yield) and again the presence of only one diastereoisomer.

HMBA resin Boc-L-Phe(4-NHFmoc)-OH loading (**Trial 3**) – TFA Boc deprotection - Alloc substitution - Fmoc deprotection – N-Boc-(3-indole)glycine coupling - Alloc deprotection - Capping – TFA Boc deprotection – HMBA resin cleavage

The compound was characterized by UPLC-MS, which showed inconsistencies in the mass of positive ions generated during the analysis.

UPLC-MS (ESI, m/z) Rt = 2.43 min, 378 (unknown), 789 (2M+H)<sup>+</sup>, 392 (M-H)<sup>-</sup>, 787 (2M-H)<sup>-</sup>.

### Synthesis of Dipeptide 8B

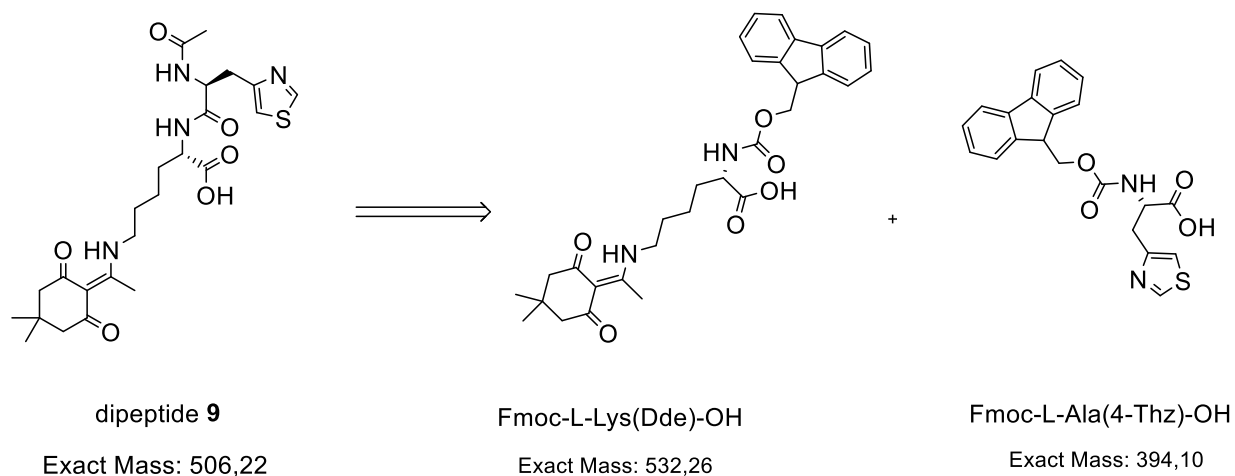


HMBA resin Boc-L-Phe(4-NHFmoc)-OH loading (**Trial 1**) – TFA Boc deprotection - Alloc substitution - Fmoc deprotection – N-Boc-(3-indole)glycine coupling - Alloc deprotection - Resin splitting – PEG3-biotin acid coupling – TFA Boc deprotection – HMBA resin cleavage

Dipeptide 8B was synthesized through the experimental procedure described above. Again, UPLC-MS of the crude showed the formation of a single diastereoisomer. After being purified by HPLC, dipeptide 8B showed a yield of 3% (1.34 mg, 0.0015 mmol). The compound was characterized by UPLC-MS.

UPLC-MS (ESI, m/z)  $R_t = 2.51$  min, 782 (M+H)<sup>+</sup>, 780 (M-H)<sup>-</sup>.

### Synthesis of Dipeptide 9

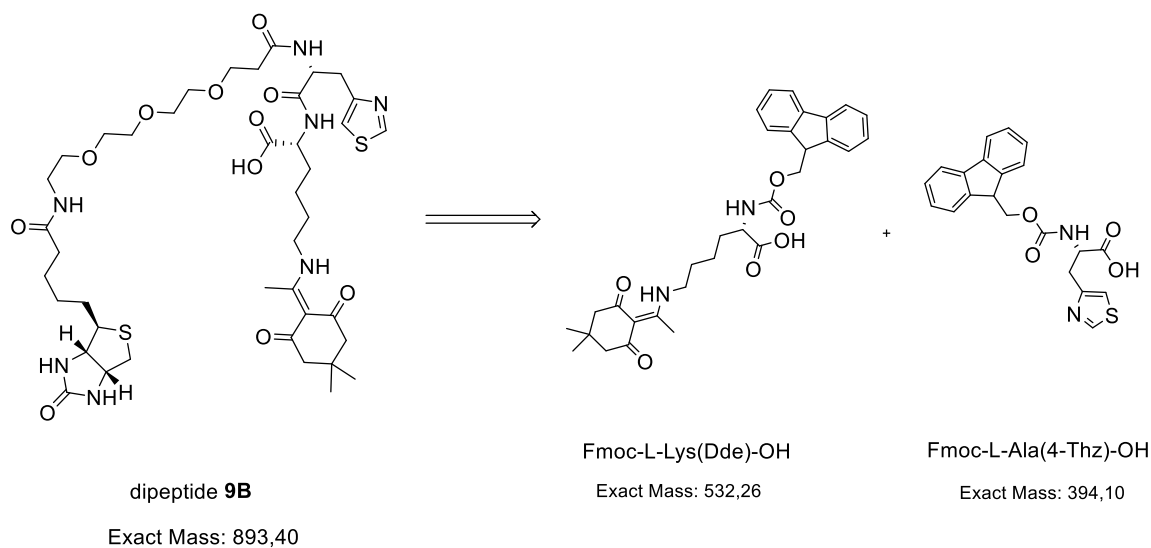


CTC resin Fmoc-L-Lys(Dde)-OH loading - Fmoc deprotection – Fmoc-L-Ala(4-Thz)-OH coupling - Fmoc deprotection – Resin splitting - Capping – CTC resin cleavage

Dipeptide 9 was synthesized with CTC resin and purified by HPLC. The dipeptide was subsequently weighed showing a yield of 92% (23.28 mg, 0.046 mmol) and characterized by UPLC-MS.

UPLC-MS (ESI, m/z)  $R_t = 2.66$  min, 507 (M+H)<sup>+</sup>, 505 (M-H)<sup>-</sup>, 1011 (2M-H)<sup>-</sup>.

## Synthesis of Dipeptide 9B

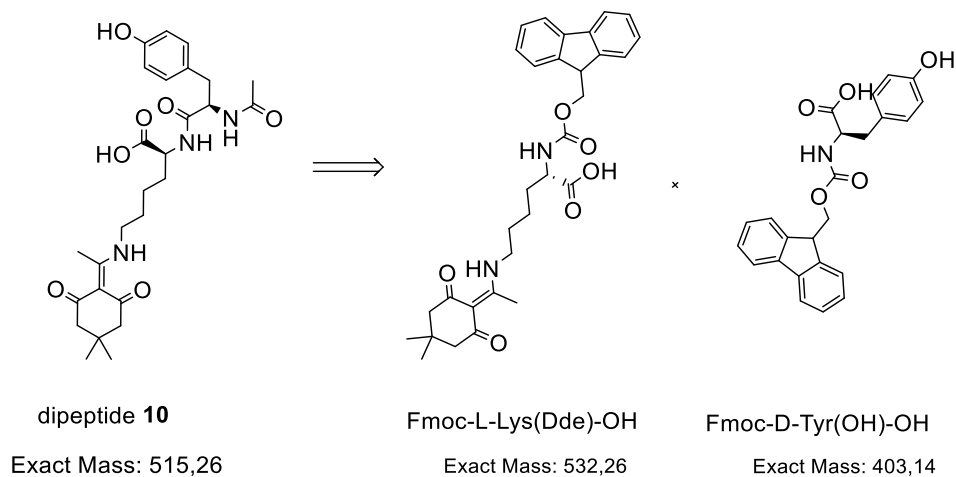


CTC resin Fmoc-L-Lys(Dde)-OH loading - Fmoc deprotection – Fmoc-L-Ala(4-Thz)-OH coupling - Fmoc deprotection – Resin splitting – PEG3-biotin acid coupling – CTC resin cleavage

Dipeptide 9B was synthesized with CTC resin and purified by HPLC. The dipeptide was subsequently weighed showing a yield of 77% (34.38 mg, 0.039 mmol) and characterized by UPLC-MS.

UPLC-MS (ESI, m/z) Rt = 2.72 min, 894 (M+H)<sup>+</sup>, 448 (M+2H)<sup>2+</sup>, 892 (M-H)<sup>-</sup>.

## Synthesis of Dipeptide 10



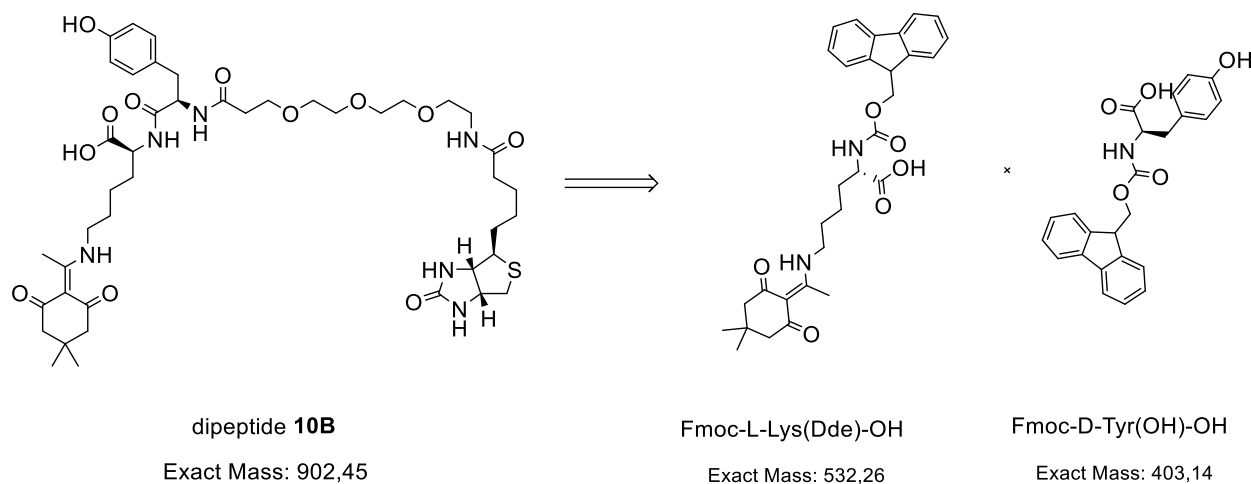


CTC resin Fmoc-L-Lys(Dde)-OH loading - Fmoc deprotection – Fmoc-D-Tyr(OH)-OH coupling  
- Fmoc deprotection – Resin splitting - Capping - CTC cleavage

Dipeptide 10 was synthesized with CTC resin and purified by HPLC. The dipeptide was subsequently weighed showing a yield of 89% (22.9 mg, 0.045 mmol) and characterized by UPLC-MS. The successful synthesis is also confirmed by  $^1\text{H}$  and  $^{13}\text{C}$  NMR.

$^1\text{H}$  NMR (600 MHz,  $\text{DMSO-d}^6$ )  $\delta$  13.25 (t,  $J = 5.4$  Hz, 1H), 9.13 (s, 2H), 8.26 (d,  $J = 8.1$  Hz, 1H), 8.00 (d,  $J = 8.7$  Hz, 1H), 7.03 – 6.97 (m, 2H), 6.65 – 6.59 (m, 2H), 4.52 (td,  $J = 9.0, 5.7$  Hz, 1H), 4.16 (ddd,  $J = 9.4, 8.1, 4.6$  Hz, 1H), 3.39 – 3.32 (m, 2H), 2.76 (dd,  $J = 13.6, 5.7$  Hz, 1H), 2.59 (dd,  $J = 13.4, 9.0$  Hz, 1H), 2.47 (s, 3H), 2.19 (s, 4H), 1.75 (s, 3H), 1.70 – 1.63 (m, 1H), 1.57 – 1.45 (m, 3H), 1.20 (p,  $J = 7.9$  Hz, 2H), 0.90 (s, 6H).  $^{13}\text{C}$  NMR (151 MHz,  $\text{DMSO-d}^6$ )  $\delta$  196.38, 173.41, 172.76, 171.35, 168.79, 155.70, 130.13, 127.91, 114.71, 106.87, 53.98, 52.22, 51.33, 42.42, 40.06, 39.94, 39.92, 39.80, 39.66, 39.52, 39.38, 39.24, 39.10, 37.65, 30.73, 29.66, 28.04, 27.84, 22.57, 22.46, 17.30. UPLC-MS (ESI,  $m/z$ )  $R_t = 2.68$  min, 516 ( $\text{M}+\text{H}$ ) $^+$ , 514 ( $\text{M}-\text{H}$ ) $^-$ , 1029 ( $2\text{M}-\text{H}$ ) $^-$ .

### Synthesis of Dipeptide 10B



CTC resin Fmoc-L-Lys(Dde)-OH loading - Fmoc deprotection – Fmoc-D-Tyr(OH)-OH coupling  
- Fmoc deprotection – Resin splitting – PEG3-biotin acid coupling - CTC cleavage

Dipeptide 10B was synthesized with CTC resin and purified by HPLC. The dipeptide was subsequently weighed showing a yield of 48% (21.66 mg, 0.024 mmol) and characterized by UPLC-MS. The successful synthesis is also confirmed by  $^1\text{H}$  NMR.

$^1\text{H}$  NMR (600 MHz, DMSO- $\text{d}^6$ )  $\delta$  13.25 (t,  $J = 5.3$  Hz, 1H), 9.13 (s, 2H), 8.24 (d,  $J = 8.1$  Hz, 1H), 7.99 (d,  $J = 8.5$  Hz, 1H), 7.82 (t,  $J = 5.7$  Hz, 1H), 7.03 – 6.96 (m, 2H), 6.64 – 6.59 (m, 2H), 6.41 (s, 2H), 4.54 (td,  $J = 8.8, 5.8$  Hz, 1H), 4.30 (ddd,  $J = 7.8, 5.1, 1.0$  Hz, 1H), 4.17 (ddd,  $J = 9.3, 8.1, 4.6$  Hz, 1H), 4.12 (dd,  $J = 7.7, 4.4$  Hz, 1H), 3.51 – 3.47 (m, 6H), 3.46 (dd,  $J = 5.7, 4.6$  Hz, 2H), 3.43 – 3.40 (m, 2H), 3.37 (q,  $J = 6.7$  Hz, 4H), 3.17 (q,  $J = 5.9$  Hz, 2H), 3.09 (ddd,  $J = 8.6, 6.1, 4.4$  Hz, 1H), 2.79 (ddd,  $J = 23.7, 13.1, 5.4$  Hz, 2H), 2.64 – 2.55 (m, 2H), 2.47 (s, 3H), 2.30 (t,  $J = 6.7$  Hz, 2H), 2.20 (s, 4H), 2.06 (t,  $J = 7.6$  Hz, 2H), 1.71 – 1.41 (m, 9H), 1.33 – 1.25 (m, 2H), 1.21 (p,  $J = 8.1$  Hz, 2H), 0.91 (s, 6H). UPLC-MS (ESI,  $m/z$ )  $R_t = 2.74$  min, 903 ( $\text{M}+\text{H}$ ) $^+$ , 452 ( $\text{M}+2\text{H}$ ) $^{2+}$ , 901 ( $\text{M}-\text{H}$ ) $^-$ .

## Appendix

### *Computational methods*

#### *Protein Preparation*

The crystal structure of a RAD51-BRCA2 BRC repeat complex was downloaded from the Protein Data Bank (PDB code 1N0W). The structure was then treated with the Schrödinger Suite 2014-4 Protein Preparation Wizard tool. All the selenomethionines were mutated to methionine, water molecules and ions were removed, and an exhaustive sampling of the orientations of groups, whose hydrogen bonding network needs to be optimized, was performed. Finally, the protein structure was refined to relieve steric clashes with a restrained minimization with the OPLS2005 force field until a final RMSD of 0.30 Å with respect to the input protein coordinates.

#### *Database Preparation*

A commercially available library of compounds composed of ASINEX and LifeChemicals databases collected from ZINC was prepared with the LigPrep tool of the Schrödinger Suite. The 2D (smi file) structures were converted to 3D structures and for each entry all stereoisomers were generated. The resulting molecules were submitted to Epik and all the tautomers and ionization states at  $\text{pH } 7.0 \pm 2.0$  were calculated. Finally, duplicates, compounds with more than 2 chiral centers, Pan-Assay Interference Compounds (PAINS), compounds with Michael acceptor groups, and frequent hitters were deleted. To enrich the database with potential Protein Protein Interaction Inhibitors, the database was filtered with the PPI-HitProfiler tool using the “soft” methods.

#### *High Throughput Docking (Virtual Screening)*

All filtered ligands (about 750K) were docked with Glide SP by centering the grid on the position of BRCA Phe1546. The 10K top-scoring compounds were re-docked with Glide XP and the 1K top-scoring compounds were selected. Both grid generation and docking calculations were performed with the default settings. The selected compounds were visually inspected to identify compounds able to match the interactions between RAD51 and BRCA and 42 compounds were selected and purchased.

#### *Induced-Fit Docking*

IFD (Induced-Fit Docking) calculations were performed with the previously prepared protein structure using both enantiomers of each ligand. All the ligands were prepared using Ligprep utility

in Schrödinger 2019-2. The IFD protocol involves the use of the Glide docking program to generate a number of initial possible ligand poses followed by a protein side chain optimization using the Prime protein structure modeling program. After several iterations, the process produces a list of final poses, ordered by a proprietary scoring function (that is a combination of the Prime Energy and Glide scoring function). The Schrödinger Extended Sampling protocol was selected along with the OPLS3e force field. The grid box was centered on the centroid of residues Tyr205, Arg247, and Phe259. Residues within 5.0 Å of ligand poses were refined during the process. The other parameters were set to their default values. Resulting poses were evaluated by visual inspection. Computational protocols were optimized and performed by Federico Falchi, Associate Professor from Department of Pharmacy and Biotechnology, University of Bologna and Riccardo Ocello PhD from Computational and Chemical Biology (CCB), Italian Institute of Technology IIT.

#### *Biochemical ELISA assay procedure*

Competitive ELISA screening assay using biotinylated BRC4 peptide to disrupt the BRC4–RAD51 interaction was performed by modifying the method described by Rajendra *et al.*<sup>207</sup>. BRC4-biotinylated peptide (N-term biotin-KEPTLLGFHTASGKKVKIAKESLDKVKNLFDEKEQ from Life Technologies) was used to coat 384-well plates (Nunc). After washing with PBS containing 0.05% Tween-20 (PBST) and blocking with the solution BSA 1% /PBST, overnight hybridization with in-house TES Pharma produced human RAD51 protein was performed. Recombinant Human RAD51 protein, fused to GST-tag, was expressed in BL21 DE3 Gold E. coli and purified by GSTrap FF column (AKTA Instrument GE-Healthcare, US. GST-tag was removed using the Thrombin (GE Healthcare) before the elution. Eluted protein was quantified (BCA, ThermoFisher) and checked by SDS gel stained with Coomassie brilliant blue. Test compounds were added in dose response from 0.01 to 100 µM in triplicate with constant DMSO 1%. Antibody raised against RAD51 (Millipore) and HRP-secondary antibody staining to develop the 3,3',5,5'- tetramethylbenzidine signal (Sigma) quenched with 1 M HCl was used as the assay readout. Colorimetric measure was read on a Victor5 (PerkinElmer) plate reader. Unbiotinylated-BRC4 and RAD51 were included in the assay as positive control. Results were

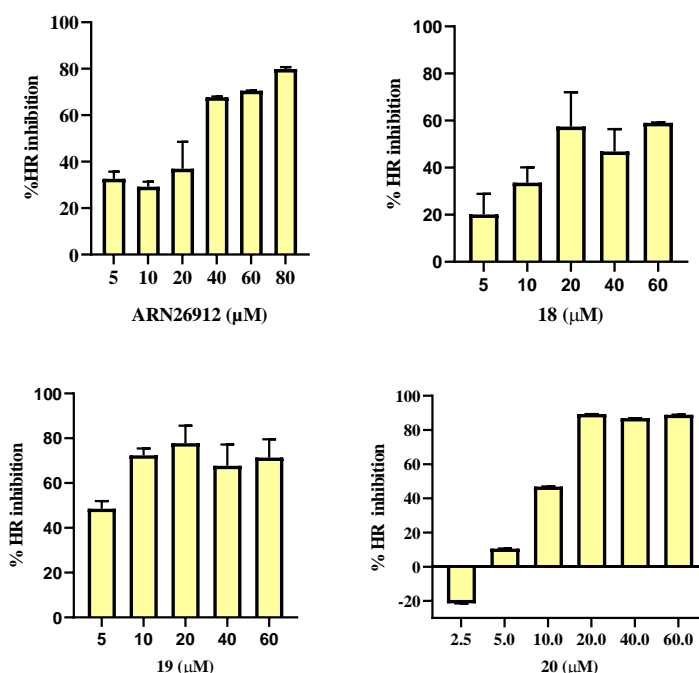
analyzed by using GraphPad software. The experiments were performed by Francesca De Franco PhD, TES Pharma s.r.l.

#### *Protocol for the Expression and Purification of His-hRAD51*

hRAD51 was expressed in *E. coli* Rosetta2(DE3)pLysS cells. A saturated overnight culture of Rosetta2(DE3)pLysS/pET15b-His-hRAD51 was diluted (1:1000) into a fresh TB-5052 autoinduction medium containing ampicillin (100 µg/mL). The flasks were shaken at 200 rpm at 20 °C for 72 h. The pellet was subsequently resuspended in an appropriate volume of buffer A (20 mM Tris-HCl (pH 8.00), 500 mM NaCl, 10 mM imidazole, 2 mM DTT, 10% (v/v) glycerol) supplemented with protease inhibitor cocktail (SIGMA-FAST protease inhibitor cocktail tablets, EDTA-50 free). The cell suspension was lysed on ice through sonication (24 rounds of 30 in.; amplitude 85%; Tip KE76; Bandelin Sonoplus HD2070 sonicator). The disrupted cell suspension was centrifuged for 30 min at 20,000 g. The supernatant fraction was filtered with a 0.45 µm (MiniSart syringe filter 0.45 µm) membrane to remove residual particulates before chromatography. The supernatant was applied onto a HisTrap HP chromatography column (Cytiva), equilibrated with buffer A. A wash step was performed using 10% of buffer B (20 mM Tris-HCl (pH 8.00), 500 mM NaCl, 500 mM imidazole, 2 mM DTT, 10% (v/v) glycerol). The protein was then eluted with a linear gradient from 10% to 100% of buffer B over 10 column volumes. Fractions (0.5 mL) were collected and analysed by SDS-PAGE. Collected fractions corresponding to the recombinant protein were dialyzed overnight at 4 °C against buffer C (50 mM Tris-HCl (pH 8.00), 200 mM KCl, 0.25 mM EDTA, 2 mM DTT, 10% (v/v) glycerol). Dialyzed protein was loaded onto RESOURCE Q anion exchange chromatography column (Cytiva) equilibrated in buffer C. The elution was performed with a linear gradient of buffer D (50 mM Tris-HCl (pH 8.00), 1 M KCl, 0.25 mM EDTA, 2 mM DTT, 10% (v/v) glycerol). Fractions (0.5 mL) were collected and analysed by SDS-PAGE. Fractions containing His-hRAD51 were pooled and dialyzed against the storage buffer (20 mM HEPES (pH 8.00), 250 mM KCl, 0.1 mM EDTA, 2 mM DTT, 10% (v/v) glycerol). The protein yield was determined from the optical absorption at 280 nm (extinction coefficient 14 900 M<sup>-1</sup> cm<sup>-1</sup>) of the final sample. This protocol was optimized and performed by Stefania Giroto PhD from Computational and Chemical Biology (CCB), Italian Institute of Technology IIT.

### *Homologous Recombination Assay*

Homologous recombination (HR) was assessed using a commercially available kit (Norgen, 35600). This assay is based on cell transfection with two plasmids able to recombine upon cell entry. The efficiency of HR was assessed by Real-Time PCR, using primer mixtures included in the assay kit. Different primer mixtures allow differentiation between the original plasmid backbones and their recombination product. BxPC3 cells ( $2 \times 10^5$  per well) were seeded in a 24-well plate and allowed to adhere overnight. Co-transfection with the two plasmids (1  $\mu$ g each) was performed in Lipofectamine2000 (Invitrogen, 11668019), according to the manufacturer's instructions. During the 5 h of transfection, cells were exposed to different doses of compounds, dissolved in DMSO. After washing with PBS, cells were harvested, and DNA was isolated using QIAamp DNA Mini kit (Qiagen, 51304). Sample concentration was measured using an ONDA Nano Genius photometer. The efficiency of HR was assessed by Real-Time PCR, using 25 ng of template and primer mixtures included in the assay kit, following the protocol indicated by the manufacturer. Data analysis was based on the  $2^{-\Delta\Delta C_t}$  method: (Recombination Product/Backbone Plasmids) treated versus (Recombination Product/Backbone Plasmids) control. This protocol was optimized and performed by Laura Poppi PhD from Department of Experimental, Diagnostic and Specialty Medicine, University of Bologna. Following graphs: Evaluation of HR inhibition caused by increasing doses of **14** (ARN26912), **18**, **19** and **20**.



### *hRAD51 Microscale Thermophoresis*

The labelling of hRAD51 recombinant protein was performed with the Monolith His-Tag labelling kit RED-tris-NTA 2nd Generation kit (NanoTemper Technologies). To determine a concentration-dependent MST binding curve, MST measurements were simultaneously performed on 16 capillaries containing a constant concentration (50 nM) of labelled RED-tris-NTA 2nd Generation His-hRAD51 protein and 16 different concentrations of the compounds. The highest concentration tested was 300  $\mu$ M. Measurements were carried out in MST buffer (20 mM HEPES (pH 8.00), 250 mM KCl, 0.1% (v/v) Pluronic® F-127, 0.1% (v/v) PEG 8000, 5% (v/v) glycerol, 5% DMSO). This protocol was optimized and performed by Stefania Girotto PhD from Computational and Chemical Biology (CCB), Italian Institute of Technology IIT.

### *Cells immunofluorescence assay*

Immunofluorescence was used for studying RAD51 nuclear translocation and for evidencing an increase in  $\gamma$ -H2AX inside the nucleus following the treatment with compounds of interest.

To visualize RAD51 in cell nuclei, BxPC-3 cells were seeded on glass coverslips placed in a 6-well culture plate ( $2 \times 10^5$  cells/well) and allowed to adhere overnight. Cultures were then preincubated with a specific dose of the target compound for 1 h and subsequently exposed to 50  $\mu$ M cisplatin for an additional 1.5 h. Medium was removed, and cells were maintained in the presence of the compound for 5 h. To visualize  $\gamma$ -H2AX, BxPC-3 cells were seeded on glass coverslips placed in a 6-well culture plate ( $13 \times 10^4$  cells/well) and allowed to adhere overnight. The next day, cells were treated with the desired compound for 72 h. At the end of cell treatment, cultures growing on coverslips were fixed in PBS containing 4% formalin for 13 min, permeabilized in 70% ethanol, air-dried, and washed twice with PBS. Samples were incubated in 5% bovine serum albumin (BSA) in PBS for 30 min and subsequently exposed to anti-RAD51 rabbit monoclonal antibody (1:1000 in 5% BSA/PBS, BioAcademia, 70-001) or anti- $\gamma$ -H2AX [phospho-139] rabbit polyclonal (1:2000 in BSA/PBS, Abcam, 11174) overnight at 4 °C. After washing, coverslips were incubated with a secondary anti-rabbit rhodamine-labelled (1:1000 in 5% BSA/PBS, Novus Biologicals, NB120-6792), for 30 min, washed, air dried, and mounted with a solution 2  $\mu$ g/mL DAPI in DABCO. Images were acquired using a Nikon fluorescent microscope equipped with filters for FITC, TRITC and DAPI. The percentage of cells bearing RAD51 or  $\gamma$ -

H2AX nuclear foci was estimated by two independent observers analyzing approximately 200 cells for each treatment sample and compared to the corresponding DAPI. This protocol was optimized and performed by Laura Poppi PhD from Department of Experimental, Diagnostic and Specialty Medicine, University of Bologna.

#### *Cell viability assay*

Cell viability was assessed with the CellTiter-Glo luminescent cell viability assay from Promega (G7571). For this experiment,  $1 \times 10^3$ ,  $5 \times 10^3$  or  $2 \times 10^4$  cells, depending on the cell line, were seeded in 200  $\mu$ L of culture medium into each well of a 96-multiwell white body plate and allowed to adhere overnight. After 144 h incubation in the presence of PARPi and the RAD51-BRCA2 disruptor alone or in combination, the plate was allowed to equilibrate at room temperature for 30 min and the CellTiter-Glo reactive was directly added to each well. The plate was kept on a shaker for 10 min to induce cell lysis, and its luminescence was measured with a Fluoroskan Ascent FL reader (Labsystems). This protocol was optimized and performed by Laura Poppi PhD from Department of Experimental, Diagnostic and Specialty Medicine, University of Bologna.

#### *Combination Index*

The combination index between PARPi and RAD51-BRCA2 inhibitor was assessed by applying the following formula, as reported in ref. 46 and 47: (Surviving cells treated with the combination) / [(Surviving cells treated with PARPi)  $\times$  (Surviving cells treated with RAD51-BRCA2 inhibitor)]  $\times$  100. According to ref. 46 and 47, a result ranging from 0.8 to 1.2 denotes an additive effect. Synergism is indicated by a result  $< 0.8$ . A result  $> 1.2$  indicates an antagonistic effect.

#### *Cell Cultures and Treatments*

BxPC-3, HPAC and CAPAN-1 cells were grown in RPMI 1640 (Merck, R0883) supplemented with 10% FBS, 100 U/mL penicillin/streptomycin, and 2 mM glutamine. HEK293 cell line was grown in DMEM High Glucose (Merck, D6546) supplemented with 10 % FBS, 100 U/mL penicillin/streptomycin, and 2 mM glutamine. The human primary pancreatic epithelial cell line (Cell Biologics, H6037) was grown in its specific medium (Cell Biologics, H6621) supplemented with epithelial cell growth supplement (Cell Biologics, H6621-Kit). All the cell line cultures were



routinely tested for Mycoplasma contamination. This protocol was optimized and performed by Laura Poppi PhD from Department of Experimental, Diagnostic and Specialty Medicine, University of Bologna.

### *3D Spheroids Cell Viability*

Cell viability for 3D cell cultures was assessed via MTT [3-(4, 5-dimethylthiazol-2-yl)-2,5-diphenyltetrazolium bromide] assay as described in Masi *et al.* (2020)<sup>265</sup> and adapting the protocol reported in Bresciani G *et al.* (2019)<sup>266</sup>. BxPC-3 cells ( $3 \cdot 10^5$  cells/well) were seeded in sterile 1% agarose in 1X PBS-coated 96-multiwell plates, grown for 96 h to allow spheroids formation and treated for 144 h as previously indicated. After treatment, a sterile solution of 1 mg/mL MTT in 1X PBS was added to each well at the final concentration of 0.1 mg/mL. Plates were incubated at 37 °C for 4 h and formazan crystals were solubilized overnight by adding a 1:1 volume of SDS 10%/0.01M HCl solution to each well. Absorbance was measured at 570 nm and 690 nm wavelengths. This protocol was optimized and performed by Mirco Masi PhD from Computational and Chemical Biology (CCB), Italian Institute of Technology IIT.

### *hRAD52 Microscale Thermophoresis*

The hRAD52 protein was labeled with the Monolith Labeling Kit RED-NHS 2nd Generation which reacts with primary amine groups of lysine residues of the recombinant protein, according to manufacturer indications (NanoTemper Technologies). MST measurements were performed using Monolith NT.115 Pico instrument (NanoTemper Technologies, Munich, Germany). Assays were conducted at 20% LED excitation power and MST medium power on premium capillaries from NanoTemper Technologies. Measurements were carried out at 22 °C in the following assay buffer: 25 mM Hepes pH 7.5, 5% glycerol, 250 mM NaCl, 0.1% Pluronic, 0.1% PEG, 1 mM DTT. Before MST experiments, to remove aggregates, the labelled protein stocks were centrifuged at 20000g for 10 minutes. For binding check experiments, protein was diluted to 5 nM in assay buffer and peptides (stock solution in 100% DMSO) were tested at 100  $\mu$ M in assay buffer with a final 5% DMSO concentration. Eight independent experiments were performed to obtain binding parameters. This protocol was optimized and performed by Stefania Giroto PhD from Computational and Chemical Biology (CCB), Italian Institute of Technology IIT.

## **Financial support**

This work was supported by the Associazione Italiana per la Ricerca sul Cancro AIRC (Progetto IG 2018, id 21386), the Italian Institute of Technology (IIT), and the University of Bologna.

## **Acknowledgements**

I would like to thank all the collaborators on the project, specifically Laura Poppi, Greta Bagnolini, Mirco Masi, Francesco Rinaldi, Viola Previtali, Jose Antonio Ortega, Samuel Harry Myers, Andrea Ciamarone, Francesca De Franco, Federico Falchi, Riccardo Ocello, and Stefania Girotto. I would also like to express my gratitude to Professor Cavalli and Professor Roberti for giving me the opportunity to contribute to this project with them and to all these collaborators who were always kind and supportive. I would also like to thank Professor Heinis for giving me the opportunity to spend six months in his laboratory together with researchers from all over the world. I thank AIRC for funding the project, the University of Bologna and IIT for collaborating and preparing young researchers for the world of research.

## **Abbreviations and acronyms**

53BP1: Tumor Suppressor p53 Binding Protein 1

ADME: Absorption, Distribution, Metabolism, and Excretion

AML: Acute Myeloid Leukemia.

ATRA: All-Trans Retinoic Acid

BCL2: B-cell lymphoma 2

BIR: Break Induced Replication

$\beta$ -NAD<sup>+</sup>: Nicotinamide Adenine Dinucleotide

BRAF: v-raf murine sarcoma viral oncogene homolog B1

BRC4myr: myristoylated BRC4

CHK2: Checkpoint Kinase 2

CKS1B: Cyclin-Dependent Kinases Regulatory Subunit 1B

CML: Chronic Myeloid Leukemia

CRISPR-Cas9: Clustered Regularly Interspaced Short Palindromic Repeats-associated protein 9

dHJ: Double Holliday Junction

DM/PK: Drug Metabolism and Pharmacokinetics

EGFR: Epidermal Growth Factor Receptor

ELISA: Enzyme-Linked Immunosorbent Assay

ERK: Extracellular Signal-Regulated Kinase

EXO1: Exonuclease 1

FDA: Food and Drug Administration

FLT3-ITD: FMS-like Tyrosine Kinase-3 Internal Tandem Duplication

FluorIA: Fluorescence-based protein-protein Interaction Assay

FP: Fluorescence Polarization

hDNA: Heteroduplex DNA

HER2: Human Epidermal growth factor Receptor 2

HRD: Homologous Recombination Deficiency

HTS: High-Throughput Screening

IR: Ionizing Radiation

MDR1: Multidrug Resistance Protein 1

MEK: Mitogen-Activated Protein Kinase Kinase

MIT: Massachusetts Institute of Technology

MRE11: Meiotic recombination 11

mTOR: Mechanistic Target of Rapamycin

MUS81: Structure-Specific Endonuclease Subunit.

NBS1: Nibrin protein

NSCLC: Non-Small Cell Lung Cancer.

PBS: Phosphate-Buffered Saline

PFS: Progression-Free Survival

PI3K: Phosphoinositide 3-kinase

PLK1: Polo-Like Kinase 1

MW: Molecular Weight

PML-RAR: Promyelocytic Leukemia/Retinoic Acid Receptor

RAF: Rapidly Accelerated Fibrosarcoma

RAS: Rat Sarcoma

RIF1 - Replication Timing Regulatory Factor 1

ROS: Reactive Oxygen Species

RPA: Replication Protein A

SAXS: Small-Angle X-ray Scattering

SDSA: Synthesis-Dependent Strand Annealing

ssDNA: single stranded Deoxyribonucleic Acid

STAG2: Cohesin subunit SA-2

TP53BP1: Tumor Protein p53-Binding Protein 1

VEGFR: Vascular Endothelial Growth Factor Receptor

## References

- (1) <https://www.wcrf.org/cancer-trends/worldwide-cancer-data/#:~:text=Find%20information%20about%20world%20cancer.and%208.8%20million%20in%20women>. (accessed).
- (2) Wilkinson, A. N. Mitigating COVID-19's impact on missed and delayed cancer diagnoses. *Can Fam Physician* **2022**, 68 (5), 323-324. DOI: 10.46747/cfp.6805323 From NLM Medline.
- (3) <https://gco.iarc.fr/today/en/dataviz/maps-heatmap?mode=population>. (accessed).
- (4) Rulten, S. L.; Grose, R. P.; Gatz, S. A.; Jones, J. L.; Cameron, A. J. M. The Future of Precision Oncology. *Int J Mol Sci* **2023**, 24 (16). DOI: 10.3390/ijms241612613 From NLM Medline.
- (5) Shin, S. H.; Bode, A. M.; Dong, Z. Addressing the challenges of applying precision oncology. *NPJ Precis Oncol* **2017**, 1 (1), 28. DOI: 10.1038/s41698-017-0032-z From NLM PubMed-not-MEDLINE.
- (6) <https://www.theguardian.com/society/2022/apr/22/like-fingerprints-at-a-scene-study-finds-new-clues-about-causes-of-cancer>. (accessed).
- (7) D'Adamo, G. L.; Widdop, J. T.; Giles, E. M. The future is now? Clinical and translational aspects of "Omics" technologies. *Immunol Cell Biol* **2021**, 99 (2), 168-176. DOI: 10.1111/imcb.12404 From NLM Medline.
- (8) Smedley, D.; Smith, K. R.; Martin, A.; Thomas, E. A.; McDonagh, E. M.; Cipriani, V.; Ellingford, J. M.; Arno, G.; Tucci, A.; Vandrovcova, J.; et al. 100,000 Genomes Pilot on Rare-Disease Diagnosis in Health Care - Preliminary Report. *N Engl J Med* **2021**, 385 (20), 1868-1880. DOI: 10.1056/NEJMoa2035790 From NLM Medline.
- (9) Singh, S.; Sarma, D. K.; Verma, V.; Nagpal, R.; Kumar, M. Unveiling the future of metabolic medicine: omics technologies driving personalized solutions for precision treatment of metabolic disorders. *Biochem Biophys Res Commun* **2023**, 682, 1-20. DOI: 10.1016/j.bbrc.2023.09.064 From NLM Medline.
- (10) Degasperis, A.; Zou, X.; Amarante, T. D.; Martinez-Martinez, A.; Koh, G. C. C.; Dias, J. M. L.; Heskin, L.; Chmelova, L.; Rinaldi, G.; Wang, V. Y. W.; et al. Substitution mutational signatures in whole-genome-sequenced cancers in the UK population. *Science* **2022**, 376 (6591). DOI: 10.1126/science.abl9283 From NLM Medline.
- (11) Oprea, T. I.; Bologa, C. G.; Brunak, S.; Campbell, A.; Gan, G. N.; Gaulton, A.; Gomez, S. M.; Guha, R.; Hersey, A.; Holmes, J.; et al. Unexplored therapeutic opportunities in the human genome. *Nat Rev Drug Discov* **2018**, 17 (5), 377. DOI: 10.1038/nrd.2018.52 From NLM PubMed-not-MEDLINE.
- (12) Smith, J. C.; Sheltzer, J. M. Genome-wide identification and analysis of prognostic features in human cancers. *Cell Rep* **2022**, 38 (13), 110569. DOI: 10.1016/j.celrep.2022.110569 From NLM Medline.
- (13) Coleman, N.; Rodon, J. Taking Aim at the Undruggable. *Am Soc Clin Oncol Educ Book* **2021**, 41, 1-8. DOI: 10.1200/EDBK\_325885 From NLM Medline.
- (14) Corti, C.; Cobanaj, M.; Dee, E. C.; Criscitiello, C.; Tolaney, S. M.; Celi, L. A.; Curigliano, G. Artificial intelligence in cancer research and precision medicine: Applications, limitations and priorities to drive transformation in the delivery of equitable and unbiased care. *Cancer Treat Rev* **2023**, 112, 102498. DOI: 10.1016/j.ctrv.2022.102498 From NLM Medline.
- (15) Mikhael, P. G.; Wohlwend, J.; Yala, A.; Karstens, L.; Xiang, J.; Takigami, A. K.; Bourgouin, P. P.; Chan, P.; Mrah, S.; Amayri, W.; et al. Sybil: A Validated Deep Learning Model to Predict Future Lung Cancer Risk From a Single Low-Dose Chest Computed Tomography. *J Clin Oncol* **2023**, 41 (12), 2191-2200. DOI: 10.1200/JCO.22.01345 From NLM Medline.
- (16) Melenhorst, J. J.; Chen, G. M.; Wang, M.; Porter, D. L.; Chen, C.; Collins, M. A.; Gao, P.; Bandyopadhyay, S.; Sun, H.; Zhao, Z.; et al. Decade-long leukaemia remissions with persistence of CD4(+) CAR T cells. *Nature* **2022**, 602 (7897), 503-509. DOI: 10.1038/s41586-021-04390-6 From NLM Medline.
- (17) Wojtukiewicz, M. Z.; Rek, M. M.; Karpowicz, K.; Gorska, M.; Politynska, B.; Wojtukiewicz, A. M.; Moniuszko, M.; Radziwon, P.; Tucker, S. C.; Honn, K. V. Inhibitors of immune checkpoints-PD-1, PD-L1, CTLA-4-new opportunities for cancer patients and a new challenge for internists and general practitioners. *Cancer Metastasis Rev* **2021**, 40 (3), 949-982. DOI: 10.1007/s10555-021-09976-0 From NLM Medline.

- (18) Hochhaus, A.; Larson, R. A.; Guilhot, F.; Radich, J. P.; Branford, S.; Hughes, T. P.; Baccarani, M.; Deininger, M. W.; Cervantes, F.; Fujihara, S.; et al. Long-Term Outcomes of Imatinib Treatment for Chronic Myeloid Leukemia. *N Engl J Med* **2017**, *376* (10), 917-927. DOI: 10.1056/NEJMoa1609324 From NLM Medline.
- (19) Chapman, P. B.; Hauschild, A.; Robert, C.; Haanen, J. B.; Ascierto, P.; Larkin, J.; Dummer, R.; Garbe, C.; Testori, A.; Maio, M.; et al. Improved survival with vemurafenib in melanoma with BRAF V600E mutation. *N Engl J Med* **2011**, *364* (26), 2507-2516. DOI: 10.1056/NEJMoa1103782 From NLM Medline.
- (20) Pagliarini, R.; Shao, W.; Sellers, W. R. Oncogene addiction: pathways of therapeutic response, resistance, and road maps toward a cure. *EMBO Rep* **2015**, *16* (3), 280-296. DOI: 10.15252/embr.201439949 From NLM Medline.
- (21) Setton, J.; Zinda, M.; Riaz, N.; Durocher, D.; Zimmermann, M.; Koehler, M.; Reis-Filho, J. S.; Powell, S. N. Synthetic Lethality in Cancer Therapeutics: The Next Generation. *Cancer Discov* **2021**, *11* (7), 1626-1635. DOI: 10.1158/2159-8290.CD-20-1503 From NLM Medline.
- (22) Huang, A.; Garraway, L. A.; Ashworth, A.; Weber, B. Synthetic lethality as an engine for cancer drug target discovery. *Nat Rev Drug Discov* **2020**, *19* (1), 23-38. DOI: 10.1038/s41573-019-0046-z From NLM Medline.
- (23) Lucchesi, J. C. Synthetic lethality and semi-lethality among functionally related mutants of *Drosophila melanogaster*. *Genetics* **1968**, *59* (1), 37-44. DOI: 10.1093/genetics/59.1.37 From NLM Medline.
- (24) Bender, A.; Pringle, J. R. Use of a screen for synthetic lethal and multicopy suppressor mutants to identify two new genes involved in morphogenesis in *Saccharomyces cerevisiae*. *Mol Cell Biol* **1991**, *11* (3), 1295-1305. DOI: 10.1128/mcb.11.3.1295-1305.1991 From NLM Medline.
- (25) Kaelin, W. G., Jr. The concept of synthetic lethality in the context of anticancer therapy. *Nat Rev Cancer* **2005**, *5* (9), 689-698. DOI: 10.1038/nrc1691 From NLM Medline.
- (26) Heinzl, A.; Marhold, M.; Mayer, P.; Schwarz, M.; Tomasich, E.; Lukas, A.; Krainer, M.; Perco, P. Synthetic lethality guiding selection of drug combinations in ovarian cancer. *PLoS One* **2019**, *14* (1), e0210859. DOI: 10.1371/journal.pone.0210859 From NLM Medline.
- (27) Zhang, B.; Tang, C.; Yao, Y.; Chen, X.; Zhou, C.; Wei, Z.; Xing, F.; Chen, L.; Cai, X.; Zhang, Z.; et al. The tumor therapy landscape of synthetic lethality. *Nat Commun* **2021**, *12* (1), 1275. DOI: 10.1038/s41467-021-21544-2 From NLM Medline.
- (28) Myers, S. H.; Ortega, J. A.; Cavalli, A. Synthetic Lethality through the Lens of Medicinal Chemistry. *J Med Chem* **2020**, *63* (23), 14151-14183. DOI: 10.1021/acs.jmedchem.0c00766 From NLM Medline.
- (29) Kohn, E. C.; Lee, J. M.; Ivy, S. P. The HRD Decision-Which PARP Inhibitor to Use for Whom and When. *Clin Cancer Res* **2017**, *23* (23), 7155-7157. DOI: 10.1158/1078-0432.CCR-17-2186 From NLM Medline.
- (30) Liu, L.; Chen, X.; Hu, C.; Zhang, D.; Shao, Z.; Jin, Q.; Yang, J.; Xie, H.; Liu, B.; Hu, M.; et al. Synthetic Lethality-based Identification of Targets for Anticancer Drugs in the Human Signaling Network. *Sci Rep* **2018**, *8* (1), 8440. DOI: 10.1038/s41598-018-26783-w From NLM Medline.
- (31) Topatana, W.; Juengpanich, S.; Li, S.; Cao, J.; Hu, J.; Lee, J.; Suliyanto, K.; Ma, D.; Zhang, B.; Chen, M.; et al. Advances in synthetic lethality for cancer therapy: cellular mechanism and clinical translation. *J Hematol Oncol* **2020**, *13* (1), 118. DOI: 10.1186/s13045-020-00956-5 From NLM Medline.
- (32) O'Neil, N. J.; Bailey, M. L.; Hieter, P. Synthetic lethality and cancer. *Nat Rev Genet* **2017**, *18* (10), 613-623. DOI: 10.1038/nrg.2017.47 From NLM Medline.
- (33) <https://depmap.org/portal/>. (accessed).
- (34) Goncalves, E.; Segura-Cabrera, A.; Pacini, C.; Picco, G.; Behan, F. M.; Jaaks, P.; Coker, E. A.; van der Meer, D.; Barthorpe, A.; Lightfoot, H.; et al. Drug mechanism-of-action discovery through the integration of pharmacological and CRISPR screens. *Mol Syst Biol* **2020**, *16* (7), e9405. DOI: 10.15252/msb.20199405 From NLM Medline.
- (35) Ma, L.; Boucher, J. I.; Paulsen, J.; Matuszewski, S.; Eide, C. A.; Ou, J.; Eickelberg, G.; Press, R. D.; Zhu, L. J.; Druker, B. J.; et al. CRISPR-Cas9-mediated saturated mutagenesis screen predicts clinical drug resistance with improved accuracy. *Proc Natl Acad Sci U S A* **2017**, *114* (44), 11751-11756. DOI: 10.1073/pnas.1708268114 From NLM Medline.

- (36) Zack, T. I.; Schumacher, S. E.; Carter, S. L.; Cherniack, A. D.; Saksena, G.; Tabak, B.; Lawrence, M. S.; Zhsng, C. Z.; Wala, J.; Mermel, C. H.; et al. Pan-cancer patterns of somatic copy number alteration. *Nat Genet* **2013**, *45* (10), 1134-1140. DOI: 10.1038/ng.2760 From NLM Medline.
- (37) Reid, R. J.; Du, X.; Sunjevaric, I.; Rayannavar, V.; Dittmar, J.; Bryant, E.; Maurer, M.; Rothstein, R. A Synthetic Dosage Lethal Genetic Interaction Between CKS1B and PLK1 Is Conserved in Yeast and Human Cancer Cells. *Genetics* **2016**, *204* (2), 807-819. DOI: 10.1534/genetics.116.190231 From NLM Medline.
- (38) Tong, A. H.; Lesage, G.; Bader, G. D.; Ding, H.; Xu, H.; Xin, X.; Young, J.; Berriz, G. F.; Brost, R. L.; Chang, M.; et al. Global mapping of the yeast genetic interaction network. *Science* **2004**, *303* (5659), 808-813. DOI: 10.1126/science.1091317 From NLM Medline.
- (39) Hurley, R. M.; Wahner Hendrickson, A. E.; Visscher, D. W.; Ansell, P.; Harrell, M. I.; Wagner, J. M.; Negron, V.; Goergen, K. M.; Maurer, M. J.; Oberg, A. L.; et al. 53BP1 as a potential predictor of response in PARP inhibitor-treated homologous recombination-deficient ovarian cancer. *Gynecol Oncol* **2019**, *153* (1), 127-134. DOI: 10.1016/j.ygyno.2019.01.015 From NLM Medline.
- (40) Chan, N.; Pires, I. M.; Bencokova, Z.; Coackley, C.; Luoto, K. R.; Bhogal, N.; Lakshman, M.; Gottipati, P.; Oliver, F. J.; Helleday, T.; et al. Contextual synthetic lethality of cancer cell kill based on the tumor microenvironment. *Cancer Res* **2010**, *70* (20), 8045-8054. DOI: 10.1158/0008-5472.CAN-10-2352 From NLM Medline.
- (41) Kaplan, A. R.; Glazer, P. M. Impact of hypoxia on DNA repair and genome integrity. *Mutagenesis* **2020**, *35* (1), 61-68. DOI: 10.1093/mutage/gez019 From NLM Medline.
- (42) Yap, T. A.; Plummer, R.; Azad, N. S.; Helleday, T. The DNA Damaging Revolution: PARP Inhibitors and Beyond. *Am Soc Clin Oncol Educ Book* **2019**, *39*, 185-195. DOI: 10.1200/EDBK\_238473 From NLM Medline.
- (43) Bailey, M. L.; O'Neil, N. J.; van Pel, D. M.; Solomon, D. A.; Waldman, T.; Hieter, P. Glioblastoma cells containing mutations in the cohesin component STAG2 are sensitive to PARP inhibition. *Mol Cancer Ther* **2014**, *13* (3), 724-732. DOI: 10.1158/1535-7163.MCT-13-0749 From NLM Medline.
- (44) Xu, X., Nowsheen, S. & Deng, M. . Exploring the DNA damage response pathway for synthetic lethality. *GENOME INSTAB. DIS.* *4*, 98–120. <https://doi.org/10.1007/s42764-022-00087-w>. **2023**.
- (45) Li, H.; Zimmerman, S. E.; Weyemi, U. Genomic instability and metabolism in cancer. *Int Rev Cell Mol Biol* **2021**, *364*, 241-265. DOI: 10.1016/bs.ircmb.2021.05.004 From NLM Medline.
- (46) Li, L. Y.; Guan, Y. D.; Chen, X. S.; Yang, J. M.; Cheng, Y. DNA Repair Pathways in Cancer Therapy and Resistance. *Front Pharmacol* **2020**, *11*, 629266. DOI: 10.3389/fphar.2020.629266 From NLM PubMed-not-MEDLINE.
- (47) Nakamura, H.; Takada, K. Reactive oxygen species in cancer: Current findings and future directions. *Cancer Sci* **2021**, *112* (10), 3945-3952. DOI: 10.1111/cas.15068 From NLM Medline.
- (48) Choi, W.; Lee, E. S. Therapeutic Targeting of DNA Damage Response in Cancer. *Int J Mol Sci* **2022**, *23* (3). DOI: 10.3390/ijms23031701 From NLM Medline.
- (49) Gillet, L. C.; Scharer, O. D. Molecular mechanisms of mammalian global genome nucleotide excision repair. *Chem Rev* **2006**, *106* (2), 253-276. DOI: 10.1021/cr040483f From NLM Medline.
- (50) Moon, J.; Kitty, I.; Renata, K.; Qin, S.; Zhao, F.; Kim, W. DNA Damage and Its Role in Cancer Therapeutics. *Int J Mol Sci* **2023**, *24* (5). DOI: 10.3390/ijms24054741 From NLM Medline.
- (51) Zhao, H.; Li, J.; You, Z.; Lindsay, H. D.; Yan, S. Distinct regulation of ATM signaling by DNA single-strand breaks and APE1. *Nat Commun* **2024**, *15* (1), 6517. DOI: 10.1038/s41467-024-50836-6 From NLM Medline.
- (52) Caldecott, K. W. Mammalian DNA base excision repair: Dancing in the moonlight. *DNA Repair (Amst)* **2020**, *93*, 102921. DOI: 10.1016/j.dnarep.2020.102921 From NLM Medline.
- (53) Grundy, G. J.; Parsons, J. L. Base excision repair and its implications to cancer therapy. *Essays Biochem* **2020**, *64* (5), 831-843. DOI: 10.1042/EBC20200013 From NLM Medline.
- (54) Kostyrko, K.; Bosshard, S.; Urban, Z.; Mermod, N. A role for homologous recombination proteins in cell cycle regulation. *Cell Cycle* **2015**, *14* (17), 2853-2861. DOI: 10.1080/15384101.2015.1049784 From NLM Medline.



- (55) Blasiak, J. Single-Strand Annealing in Cancer. *Int J Mol Sci* **2021**, *22* (4). DOI: 10.3390/ijms22042167 From NLM Medline.
- (56) Balboni, B.; Rinaldi, F.; Previtali, V.; Ciamarone, A.; Girotto, S.; Cavalli, A. Novel Insights into RAD52's Structure, Function, and Druggability for Synthetic Lethality and Innovative Anticancer Therapies. *Cancers (Basel)* **2023**, *15* (6). DOI: 10.3390/cancers15061817 From NLM PubMed-not-MEDLINE.
- (57) Chen, L.; Nievera, C. J.; Lee, A. Y.; Wu, X. Cell cycle-dependent complex formation of BRCA1.CtIP.MRN is important for DNA double-strand break repair. *J Biol Chem* **2008**, *283* (12), 7713-7720. DOI: 10.1074/jbc.M710245200 From NLM Medline.
- (58) Al-Minawi, A. Z.; Saleh-Gohari, N.; Helleday, T. The ERCC1/XPF endonuclease is required for efficient single-strand annealing and gene conversion in mammalian cells. *Nucleic Acids Res* **2008**, *36* (1), 1-9. DOI: 10.1093/nar/gkm888 From NLM Medline.
- (59) Bhargava, R.; Onyango, D. O.; Stark, J. M. Regulation of Single-Strand Annealing and its Role in Genome Maintenance. *Trends Genet* **2016**, *32* (9), 566-575. DOI: 10.1016/j.tig.2016.06.007 From NLM Medline.
- (60) So, A.; Le Guen, T.; Lopez, B. S.; Guirouilh-Barbat, J. Genomic rearrangements induced by unscheduled DNA double strand breaks in somatic mammalian cells. *FEBS J* **2017**, *284* (15), 2324-2344. DOI: 10.1111/febs.14053 From NLM Medline.
- (61) Galanos, P.; Vougas, K.; Walter, D.; Polyzos, A.; Maya-Mendoza, A.; Haagensen, E. J.; Kokkalis, A.; Roumelioti, F. M.; Gagos, S.; Tzetis, M.; et al. Chronic p53-independent p21 expression causes genomic instability by deregulating replication licensing. *Nat Cell Biol* **2016**, *18* (7), 777-789. DOI: 10.1038/ncb3378 From NLM Medline.
- (62) Galanos, P.; Pappas, G.; Polyzos, A.; Kotsinas, A.; Svolaki, I.; Giakoumakis, N. N.; Glytsou, C.; Pateras, I. S.; Swain, U.; Souliotis, V. L.; et al. Mutational signatures reveal the role of RAD52 in p53-independent p21-driven genomic instability. *Genome Biol* **2018**, *19* (1), 37. DOI: 10.1186/s13059-018-1401-9 From NLM Medline.
- (63) Shi, T. Y.; Yang, G.; Tu, X. Y.; Yang, J. M.; Qian, J.; Wu, X. H.; Zhou, X. Y.; Cheng, X.; Wei, Q. RAD52 variants predict platinum resistance and prognosis of cervical cancer. *PLoS One* **2012**, *7* (11), e50461. DOI: 10.1371/journal.pone.0050461 From NLM Medline.
- (64) Ho, V.; Chung, L.; Singh, A.; Lea, V.; Abubakar, A.; Lim, S. H.; Chua, W.; Ng, W.; Lee, M.; Roberts, T. L.; et al. Aberrant Expression of RAD52, Its Prognostic Impact in Rectal Cancer and Association with Poor Survival of Patients. *Int J Mol Sci* **2020**, *21* (5). DOI: 10.3390/ijms21051768 From NLM Medline.
- (65) Kohzaki, M.; Ootsuyama, A.; Sun, L.; Moritake, T.; Okazaki, R. Human RECQL4 represses the RAD52-mediated single-strand annealing pathway after ionizing radiation or cisplatin treatment. *Int J Cancer* **2020**, *146* (11), 3098-3113. DOI: 10.1002/ijc.32670 From NLM Medline.
- (66) Noordermeer, S. M.; Adam, S.; Setiawati, D.; Barazas, M.; Pettitt, S. J.; Ling, A. K.; Olivieri, M.; Alvarez-Quilon, A.; Moatti, N.; Zimmermann, M.; et al. The shieldin complex mediates 53BP1-dependent DNA repair. *Nature* **2018**, *560* (7716), 117-121. DOI: 10.1038/s41586-018-0340-7 From NLM Medline.
- (67) Sun, Y.; McCorvie, T. J.; Yates, L. A.; Zhang, X. Structural basis of homologous recombination. *Cell Mol Life Sci* **2020**, *77* (1), 3-18. DOI: 10.1007/s00018-019-03365-1 From NLM Medline.
- (68) Smith, J.; Tho, L. M.; Xu, N.; Gillespie, D. A. The ATM-Chk2 and ATR-Chk1 pathways in DNA damage signaling and cancer. *Adv Cancer Res* **2010**, *108*, 73-112. DOI: 10.1016/B978-0-12-380888-2.00003-0 From NLM Medline.
- (69) Kastan, M. B.; Bartek, J. Cell-cycle checkpoints and cancer. *Nature* **2004**, *432* (7015), 316-323. DOI: 10.1038/nature03097 From NLM Medline.
- (70) Sakaguchi, K.; Ishibashi, T.; Uchiyama, Y.; Iwabata, K. The multi-replication protein A (RPA) system-a new perspective. *FEBS J* **2009**, *276* (4), 943-963. DOI: 10.1111/j.1742-4658.2008.06841.x From NLM Medline.
- (71) Zhao, J.; Tian, S.; Guo, Q.; Bao, K.; Yu, G.; Wang, X.; Shen, X.; Zhang, J.; Chen, J.; Yang, Y.; et al. A PARylation-phosphorylation cascade promotes TOPBP1 loading and RPA-RAD51 exchange in

homologous recombination. *Mol Cell* **2022**, 82 (14), 2571-2587 e2579. DOI: 10.1016/j.molcel.2022.04.031 From NLM Medline.

(72) Stauffer, M. E.; Chazin, W. J. Physical interaction between replication protein A and Rad51 promotes exchange on single-stranded DNA. *J Biol Chem* **2004**, 279 (24), 25638-25645. DOI: 10.1074/jbc.M400029200 From NLM Medline.

(73) Ma, C. J.; Gibb, B.; Kwon, Y.; Sung, P.; Greene, E. C. Protein dynamics of human RPA and RAD51 on ssDNA during assembly and disassembly of the RAD51 filament. *Nucleic Acids Res* **2017**, 45 (2), 749-761. DOI: 10.1093/nar/gkw1125 From NLM Medline.

(74) Jensen, R. B.; Carreira, A.; Kowalczykowski, S. C. Purified human BRCA2 stimulates RAD51-mediated recombination. *Nature* **2010**, 467 (7316), 678-683. DOI: 10.1038/nature09399 From NLM Medline.

(75) Hilario, J.; Amitani, I.; Baskin, R. J.; Kowalczykowski, S. C. Direct imaging of human Rad51 nucleoprotein dynamics on individual DNA molecules. *Proc Natl Acad Sci U S A* **2009**, 106 (2), 361-368. DOI: 10.1073/pnas.0811965106 From NLM Medline.

(76) Luo, S. C.; Yeh, M. C.; Lien, Y. H.; Yeh, H. Y.; Siao, H. L.; Tu, I. P.; Chi, P.; Ho, M. C. A RAD51-ADP double filament structure unveils the mechanism of filament dynamics in homologous recombination. *Nat Commun* **2023**, 14 (1), 4993. DOI: 10.1038/s41467-023-40672-5 From NLM Medline.

(77) Nogueira, A.; Fernandes, M.; Catarino, R.; Medeiros, R. RAD52 Functions in Homologous Recombination and Its Importance on Genomic Integrity Maintenance and Cancer Therapy. *Cancers (Basel)* **2019**, 11 (11). DOI: 10.3390/cancers11111622 From NLM PubMed-not-MEDLINE.

(78) Choi, J.; Kong, M.; Gallagher, D. N.; Li, K.; Bronk, G.; Cao, Y.; Greene, E. C.; Haber, J. E. Repair of mismatched templates during Rad51-dependent Break-Induced Replication. *PLoS Genet* **2022**, 18 (9), e1010056. DOI: 10.1371/journal.pgen.1010056 From NLM Medline.

(79) Heeke, A. L.; Pishvaian, M. J.; Lynce, F.; Xiu, J.; Brody, J. R.; Chen, W. J.; Baker, T. M.; Marshall, J. L.; Isaacs, C. Prevalence of Homologous Recombination-Related Gene Mutations Across Multiple Cancer Types. *JCO Precis Oncol* **2018**, 2018. DOI: 10.1200/PO.17.00286 From NLM PubMed-not-MEDLINE.

(80) Scully, R.; Panday, A.; Elango, R.; Willis, N. A. DNA double-strand break repair-pathway choice in somatic mammalian cells. *Nat Rev Mol Cell Biol* **2019**, 20 (11), 698-714. DOI: 10.1038/s41580-019-0152-0 From NLM Medline.

(81) Bryant, H. E.; Schultz, N.; Thomas, H. D.; Parker, K. M.; Flower, D.; Lopez, E.; Kyle, S.; Meuth, M.; Curtin, N. J.; Helleday, T. Specific killing of BRCA2-deficient tumours with inhibitors of poly(ADP-ribose) polymerase. *Nature* **2005**, 434 (7035), 913-917. DOI: 10.1038/nature03443 From NLM Medline.

(82) Kutuzov, M. M.; Belousova, E. A.; Kurgina, T. A.; Ukraintsev, A. A.; Vasil'eva, I. A.; Khodyreva, S. N.; Lavrik, O. I. The contribution of PARP1, PARP2 and poly(ADP-ribosylation) to base excision repair in the nucleosomal context. *Sci Rep* **2021**, 11 (1), 4849. DOI: 10.1038/s41598-021-84351-1 From NLM Medline.

(83) Sinha, S.; Molla, S.; Kundu, C. N. PARP1-modulated chromatin remodeling is a new target for cancer treatment. *Med Oncol* **2021**, 38 (10), 118. DOI: 10.1007/s12032-021-01570-2 From NLM Medline.

(84) Langelier, M. F.; Planck, J. L.; Roy, S.; Pascal, J. M. Structural basis for DNA damage-dependent poly(ADP-ribosylation) by human PARP-1. *Science* **2012**, 336 (6082), 728-732. DOI: 10.1126/science.1216338 From NLM Medline.

(85) Langelier, M. F.; Eisemann, T.; Riccio, A. A.; Pascal, J. M. PARP family enzymes: regulation and catalysis of the poly(ADP-ribose) posttranslational modification. *Curr Opin Struct Biol* **2018**, 53, 187-198. DOI: 10.1016/j.sbi.2018.11.002 From NLM Medline.

(86) Steffen, J. D.; Brody, J. R.; Armen, R. S.; Pascal, J. M. Structural Implications for Selective Targeting of PARPs. *Front Oncol* **2013**, 3, 301. DOI: 10.3389/fonc.2013.00301 From NLM PubMed-not-MEDLINE.

(87) Galia, A.; Calogero, A. E.; Condorelli, R.; Fraggetta, F.; La Corte, A.; Ridolfo, F.; Bosco, P.; Castiglione, R.; Salemi, M. PARP-1 protein expression in glioblastoma multiforme. *Eur J Histochem* **2012**, 56 (1), e9. DOI: 10.4081/ejh.2012.e9 From NLM Medline.

(88) Ossovskaya, V.; Koo, I. C.; Kaldjian, E. P.; Alvares, C.; Sherman, B. M. Upregulation of Poly (ADP-Ribose) Polymerase-1 (PARP1) in Triple-Negative Breast Cancer and Other Primary Human Tumor Types.

*Genes Cancer* **2010**, *1* (8), 812-821. DOI: 10.1177/1947601910383418 From NLM PubMed-not-MEDLINE.

(89) Choi, E. B.; Yang, A. Y.; Kim, S. C.; Lee, J.; Choi, J. K.; Choi, C.; Kim, M. Y. PARP1 enhances lung adenocarcinoma metastasis by novel mechanisms independent of DNA repair. *Oncogene* **2016**, *35* (35), 4569-4579. DOI: 10.1038/onc.2016.3 From NLM Medline.

(90) Rojo, F.; Garcia-Parra, J.; Zazo, S.; Tusquets, I.; Ferrer-Lozano, J.; Menendez, S.; Eroles, P.; Chamizo, C.; Servitja, S.; Ramirez-Merino, N.; et al. Nuclear PARP-1 protein overexpression is associated with poor overall survival in early breast cancer. *Ann Oncol* **2012**, *23* (5), 1156-1164. DOI: 10.1093/annonc/mdr361 From NLM Medline.

(91) Domagala, P.; Huzarski, T.; Lubinski, J.; Gugala, K.; Domagala, W. PARP-1 expression in breast cancer including BRCA1-associated, triple negative and basal-like tumors: possible implications for PARP-1 inhibitor therapy. *Breast Cancer Res Treat* **2011**, *127* (3), 861-869. DOI: 10.1007/s10549-011-1441-2 From NLM Medline.

(92) Michels, J.; Vitale, I.; Galluzzi, L.; Adam, J.; Olaussen, K. A.; Kepp, O.; Senovilla, L.; Talhaoui, I.; Guegan, J.; Enot, D. P.; et al. Cisplatin resistance associated with PARP hyperactivation. *Cancer Res* **2013**, *73* (7), 2271-2280. DOI: 10.1158/0008-5472.CAN-12-3000 From NLM Medline.

(93) Lord, C. J.; Ashworth, A. BRCAness revisited. *Nat Rev Cancer* **2016**, *16* (2), 110-120. DOI: 10.1038/nrc.2015.21 From NLM Medline.

(94) Helleday, T. The underlying mechanism for the PARP and BRCA synthetic lethality: clearing up the misunderstandings. *Mol Oncol* **2011**, *5* (4), 387-393. DOI: 10.1016/j.molonc.2011.07.001 From NLM Medline.

(95) Farmer, H.; McCabe, N.; Lord, C. J.; Tutt, A. N.; Johnson, D. A.; Richardson, T. B.; Santarosa, M.; Dillon, K. J.; Hickson, I.; Knights, C.; et al. Targeting the DNA repair defect in BRCA mutant cells as a therapeutic strategy. *Nature* **2005**, *434* (7035), 917-921. DOI: 10.1038/nature03445 From NLM Medline.

(96) Golan, T.; Kanji, Z. S.; Epelbaum, R.; Devaud, N.; Dagan, E.; Holter, S.; Aderka, D.; Paluch-Shimon, S.; Kaufman, B.; Gershoni-Baruch, R.; et al. Overall survival and clinical characteristics of pancreatic cancer in BRCA mutation carriers. *Br J Cancer* **2014**, *111* (6), 1132-1138. DOI: 10.1038/bjc.2014.418 From NLM Medline.

(97) Lee, J. M.; Ledermann, J. A.; Kohn, E. C. PARP Inhibitors for BRCA1/2 mutation-associated and BRCA-like malignancies. *Ann Oncol* **2014**, *25* (1), 32-40. DOI: 10.1093/annonc/mdt384 From NLM Medline.

(98) Principe, D. R. Precision Medicine for BRCA/PALB2-Mutated Pancreatic Cancer and Emerging Strategies to Improve Therapeutic Responses to PARP Inhibition. *Cancers (Basel)* **2022**, *14* (4). DOI: 10.3390/cancers14040897 From NLM PubMed-not-MEDLINE.

(99) Jette, N. R.; Kumar, M.; Radhamani, S.; Arthur, G.; Goutam, S.; Yip, S.; Kolinsky, M.; Williams, G. J.; Bose, P.; Lees-Miller, S. P. ATM-Deficient Cancers Provide New Opportunities for Precision Oncology. *Cancers (Basel)* **2020**, *12* (3). DOI: 10.3390/cancers12030687 From NLM PubMed-not-MEDLINE.

(100) O'Malley, D. M.; Krivak, T. C.; Kabil, N.; Munley, J.; Moore, K. N. PARP Inhibitors in Ovarian Cancer: A Review. *Target Oncol* **2023**, *18* (4), 471-503. DOI: 10.1007/s11523-023-00970-w From NLM Medline.

(101) Patel, R.; Fein, D.; Ramirez, C. B.; Do, K.; Saif, M. W. PARP Inhibitors in Pancreatic Cancer: From Phase I to Plenary Session. *Pancreas (Fairfax)* **2019**, *3* (1), e5-e8. DOI: 10.17140/POJ-3-e011 From NLM PubMed-not-MEDLINE.

(102) Sonnenblick, A.; de Azambuja, E.; Azim, H. A., Jr.; Piccart, M. An update on PARP inhibitors--moving to the adjuvant setting. *Nat Rev Clin Oncol* **2015**, *12* (1), 27-41. DOI: 10.1038/nrclinonc.2014.163 From NLM Medline.

(103) Malyuchenko, N. V.; Kotova, E. Y.; Kulaeva, O. I.; Kirpichnikov, M. P.; Studitskiy, V. M. PARP1 Inhibitors: antitumor drug design. *Acta Naturae* **2015**, *7* (3), 27-37. From NLM PubMed-not-MEDLINE.

(104) <https://www.icr.ac.uk/news-archive/kudos-pharmaceuticals-first-patient-treated-with-new-anti-cancer-agent>. (accessed).

- (105) <https://www.fda.gov/drugs/drug-approvals-and-databases/fda-approves-olaparib-plus-bevacizumab-maintenance-treatment-ovarian-fallopian-tube-or-primary>. (accessed).
- (106) Kim, G.; Ison, G.; McKee, A. E.; Zhang, H.; Tang, S.; Gwise, T.; Sridhara, R.; Lee, E.; Tzou, A.; Philip, R.; et al. FDA Approval Summary: Olaparib Monotherapy in Patients with Deleterious Germline BRCA-Mutated Advanced Ovarian Cancer Treated with Three or More Lines of Chemotherapy. *Clin Cancer Res* **2015**, *21* (19), 4257-4261. DOI: 10.1158/1078-0432.CCR-15-0887 From NLM Medline.
- (107) Ledermann, J. A.; Pujade-Lauraine, E. Olaparib as maintenance treatment for patients with platinum-sensitive relapsed ovarian cancer. *Ther Adv Med Oncol* **2019**, *11*, 1758835919849753. DOI: 10.1177/1758835919849753 From NLM PubMed-not-MEDLINE.
- (108) Robson, M.; Im, S. A.; Senkus, E.; Xu, B.; Domchek, S. M.; Masuda, N.; Delaloge, S.; Li, W.; Tung, N.; Armstrong, A.; et al. Olaparib for Metastatic Breast Cancer in Patients with a Germline BRCA Mutation. *N Engl J Med* **2017**, *377* (6), 523-533. DOI: 10.1056/NEJMoa1706450 From NLM Medline.
- (109) Golan, T.; Hammel, P.; Reni, M.; Van Cutsem, E.; Macarulla, T.; Hall, M. J.; Park, J. O.; Hochhauser, D.; Arnold, D.; Oh, D. Y.; et al. Maintenance Olaparib for Germline BRCA-Mutated Metastatic Pancreatic Cancer. *N Engl J Med* **2019**, *381* (4), 317-327. DOI: 10.1056/NEJMoa1903387 From NLM Medline.
- (110) <https://www.fda.gov/drugs/fda-grants-accelerated-approval-rucaparib-brca-mutated-metastatic-castration-resistant-prostate>. (accessed).
- (111) <https://www.fda.gov/drugs/drug-approvals-and-databases/fda-approves-niraparib-first-line-maintenance-advanced-ovarian-cancer>. (accessed).
- (112) <https://www.fda.gov/drugs/drug-approvals-and-databases/fda-approves-talazoparib-gbrcam-her2-negative-locally-advanced-or-metastatic-breast-cancer#:~:text=On%20October%2016%2C%202018%2C%20the,advanced%20or%20metastatic%20breast%20cancer>. (accessed).
- (113) Hengel, S. R.; Spies, M. A.; Spies, M. Small-Molecule Inhibitors Targeting DNA Repair and DNA Repair Deficiency in Research and Cancer Therapy. *Cell Chem Biol* **2017**, *24* (9), 1101-1119. DOI: 10.1016/j.chembiol.2017.08.027 From NLM Medline.
- (114) Mirza, M. R.; Monk, B. J.; Herrstedt, J.; Oza, A. M.; Mahner, S.; Redondo, A.; Fabbro, M.; Ledermann, J. A.; Lorusso, D.; Vergote, I.; et al. Niraparib Maintenance Therapy in Platinum-Sensitive, Recurrent Ovarian Cancer. *N Engl J Med* **2016**, *375* (22), 2154-2164. DOI: 10.1056/NEJMoa1611310 From NLM Medline.
- (115) Anscher, M. S.; Chang, E.; Gao, X.; Gong, Y.; Weinstock, C.; Bloomquist, E.; Adeniyi, O.; Charlab, R.; Zimmerman, S.; Serlemitsos-Day, M.; et al. FDA Approval Summary: Rucaparib for the Treatment of Patients with Deleterious BRCA-Mutated Metastatic Castrate-Resistant Prostate Cancer. *Oncologist* **2021**, *26* (2), 139-146. DOI: 10.1002/onco.13585 From NLM Medline.
- (116) Litton, J. K.; Rugo, H. S.; Ettl, J.; Hurvitz, S. A.; Goncalves, A.; Lee, K. H.; Fehrenbacher, L.; Yerushalmi, R.; Mina, L. A.; Martin, M.; et al. Talazoparib in Patients with Advanced Breast Cancer and a Germline BRCA Mutation. *N Engl J Med* **2018**, *379* (8), 753-763. DOI: 10.1056/NEJMoa1802905 From NLM Medline.
- (117) Pommier, Y.; O'Connor, M. J.; de Bono, J. Laying a trap to kill cancer cells: PARP inhibitors and their mechanisms of action. *Sci Transl Med* **2016**, *8* (362), 362ps317. DOI: 10.1126/scitranslmed.aaf9246 From NLM Medline.
- (118) Boussios, S.; Karihtala, P.; Moschetta, M.; Abson, C.; Karathanasi, A.; Zakyntinakis-Kyriakou, N.; Ryan, J. E.; Sheriff, M.; Rassy, E.; Pavlidis, N. Veliparib in ovarian cancer: a new synthetically lethal therapeutic approach. *Invest New Drugs* **2020**, *38* (1), 181-193. DOI: 10.1007/s10637-019-00867-4 From NLM Medline.
- (119) Coleman, R. L.; Fleming, G. F.; Brady, M. F.; Swisher, E. M.; Steffensen, K. D.; Friedlander, M.; Okamoto, A.; Moore, K. N.; Efrat Ben-Baruch, N.; Werner, T. L.; et al. Veliparib with First-Line Chemotherapy and as Maintenance Therapy in Ovarian Cancer. *N Engl J Med* **2019**, *381* (25), 2403-2415. DOI: 10.1056/NEJMoa1909707 From NLM Medline.
- (120) Kim, D.; Nam, H. J. PARP Inhibitors: Clinical Limitations and Recent Attempts to Overcome Them. *Int J Mol Sci* **2022**, *23* (15). DOI: 10.3390/ijms23158412 From NLM Medline.

- (121) Hopkins, T. A.; Shi, Y.; Rodriguez, L. E.; Solomon, L. R.; Donawho, C. K.; DiGiammarino, E. L.; Panchal, S. C.; Wilsbacher, J. L.; Gao, W.; Olson, A. M.; et al. Mechanistic Dissection of PARP1 Trapping and the Impact on In Vivo Tolerability and Efficacy of PARP Inhibitors. *Mol Cancer Res* **2015**, *13* (11), 1465-1477. DOI: 10.1158/1541-7786.MCR-15-0191-T From NLM Medline.
- (122) Murai, J.; Huang, S. Y.; Das, B. B.; Renaud, A.; Zhang, Y.; Doroshow, J. H.; Ji, J.; Takeda, S.; Pommier, Y. Trapping of PARP1 and PARP2 by Clinical PARP Inhibitors. *Cancer Res* **2012**, *72* (21), 5588-5599. DOI: 10.1158/0008-5472.CAN-12-2753 From NLM Medline.
- (123) Saleh-Gohari, N.; Bryant, H. E.; Schultz, N.; Parker, K. M.; Cassel, T. N.; Helleday, T. Spontaneous homologous recombination is induced by collapsed replication forks that are caused by endogenous DNA single-strand breaks. *Mol Cell Biol* **2005**, *25* (16), 7158-7169. DOI: 10.1128/MCB.25.16.7158-7169.2005 From NLM Medline.
- (124) Mateo, J.; Lord, C. J.; Serra, V.; Tutt, A.; Balmana, J.; Castroviejo-Bermejo, M.; Cruz, C.; Oaknin, A.; Kaye, S. B.; de Bono, J. S. A decade of clinical development of PARP inhibitors in perspective. *Ann Oncol* **2019**, *30* (9), 1437-1447. DOI: 10.1093/annonc/mdz192 From NLM Medline.
- (125) Fu, X.; Li, P.; Zhou, Q.; He, R.; Wang, G.; Zhu, S.; Bagheri, A.; Kupfer, G.; Pei, H.; Li, J. Mechanism of PARP inhibitor resistance and potential overcoming strategies. *Genes Dis* **2024**, *11* (1), 306-320. DOI: 10.1016/j.gendis.2023.02.014 From NLM PubMed-not-MEDLINE.
- (126) Bhamidipati, D.; Haro-Silerio, J. I.; Yap, T. A.; Ngoi, N. PARP inhibitors: enhancing efficacy through rational combinations. *Br J Cancer* **2023**, *129* (6), 904-916. DOI: 10.1038/s41416-023-02326-7 From NLM Medline.
- (127) Sakai, W.; Swisher, E. M.; Karlan, B. Y.; Agarwal, M. K.; Higgins, J.; Friedman, C.; Villegas, E.; Jacquemont, C.; Farrugia, D. J.; Couch, F. J.; et al. Secondary mutations as a mechanism of cisplatin resistance in BRCA2-mutated cancers. *Nature* **2008**, *451* (7182), 1116-1120. DOI: 10.1038/nature06633 From NLM Medline.
- (128) Loehr, A.; Hussain, A.; Patnaik, A.; Bryce, A. H.; Castellano, D.; Font, A.; Shapiro, J.; Zhang, J.; Sautois, B.; Vogelzang, N. J.; et al. Emergence of BRCA Reversion Mutations in Patients with Metastatic Castration-resistant Prostate Cancer After Treatment with Rucaparib. *Eur Urol* **2023**, *83* (3), 200-209. DOI: 10.1016/j.eururo.2022.09.010 From NLM Medline.
- (129) Kondrashova, O.; Topp, M.; Nesic, K.; Lieschke, E.; Ho, G. Y.; Harrell, M. I.; Zapparoli, G. V.; Hadley, A.; Holian, R.; Boehm, E.; et al. Methylation of all BRCA1 copies predicts response to the PARP inhibitor rucaparib in ovarian carcinoma. *Nat Commun* **2018**, *9* (1), 3970. DOI: 10.1038/s41467-018-05564-z From NLM Medline.
- (130) Cruz, C.; Castroviejo-Bermejo, M.; Gutierrez-Enriquez, S.; Llop-Guevara, A.; Ibrahim, Y. H.; Gris-Oliver, A.; Bonache, S.; Moranco, B.; Bruna, A.; Rueda, O. M.; et al. RAD51 foci as a functional biomarker of homologous recombination repair and PARP inhibitor resistance in germline BRCA-mutated breast cancer. *Ann Oncol* **2018**, *29* (5), 1203-1210. DOI: 10.1093/annonc/mdy099 From NLM Medline.
- (131) Zatreanu, D.; Robinson, H. M. R.; Alkhatib, O.; Boursier, M.; Finch, H.; Geo, L.; Grande, D.; Grinkevich, V.; Heald, R. A.; Langdon, S.; et al. Poltheta inhibitors elicit BRCA-gene synthetic lethality and target PARP inhibitor resistance. *Nat Commun* **2021**, *12* (1), 3636. DOI: 10.1038/s41467-021-23463-8 From NLM Medline.
- (132) Schlacher, K.; Christ, N.; Siaud, N.; Egashira, A.; Wu, H.; Jasin, M. Double-strand break repair-independent role for BRCA2 in blocking stalled replication fork degradation by MRE11. *Cell* **2011**, *145* (4), 529-542. DOI: 10.1016/j.cell.2011.03.041 From NLM Medline.
- (133) Ray Chaudhuri, A.; Callen, E.; Ding, X.; Gogola, E.; Duarte, A. A.; Lee, J. E.; Wong, N.; Lafarga, V.; Calvo, J. A.; Panzarino, N. J.; et al. Replication fork stability confers chemoresistance in BRCA-deficient cells. *Nature* **2016**, *535* (7612), 382-387. DOI: 10.1038/nature18325 From NLM Medline.
- (134) Liao, H.; Ji, F.; Helleday, T.; Ying, S. Mechanisms for stalled replication fork stabilization: new targets for synthetic lethality strategies in cancer treatments. *EMBO Rep* **2018**, *19* (9). DOI: 10.15252/embr.201846263 From NLM Medline.
- (135) Pettitt, S. J.; Krastev, D. B.; Brandsma, I.; Drean, A.; Song, F.; Aleksandrov, R.; Harrell, M. I.; Menon, M.; Brough, R.; Campbell, J.; et al. Genome-wide and high-density CRISPR-Cas9 screens identify point



mutations in PARP1 causing PARP inhibitor resistance. *Nat Commun* **2018**, 9 (1), 1849. DOI: 10.1038/s41467-018-03917-2 From NLM Medline.

(136) Christie, E. L.; Pattnaik, S.; Beach, J.; Copeland, A.; Rashoo, N.; Fereday, S.; Hendley, J.; Alsop, K.; Brady, S. L.; Lamb, G.; et al. Multiple ABCB1 transcriptional fusions in drug resistant high-grade serous ovarian and breast cancer. *Nat Commun* **2019**, 10 (1), 1295. DOI: 10.1038/s41467-019-09312-9 From NLM Medline.

(137) Xie, T.; Dickson, K. A.; Yee, C.; Ma, Y.; Ford, C. E.; Bowden, N. A.; Marsh, D. J. Targeting Homologous Recombination Deficiency in Ovarian Cancer with PARP Inhibitors: Synthetic Lethal Strategies That Impact Overall Survival. *Cancers (Basel)* **2022**, 14 (19). DOI: 10.3390/cancers14194621 From NLM PubMed-not-MEDLINE.

(138) Abbotts, R.; Dellomo, A. J.; Rassool, F. V. Pharmacologic Induction of BRCAness in BRCA-Proficient Cancers: Expanding PARP Inhibitor Use. *Cancers (Basel)* **2022**, 14 (11). DOI: 10.3390/cancers14112640 From NLM PubMed-not-MEDLINE.

(139) Gorodetska, I.; Kozeretska, I.; Dubrovskaya, A. BRCA Genes: The Role in Genome Stability, Cancer Stemness and Therapy Resistance. *J Cancer* **2019**, 10 (9), 2109-2127. DOI: 10.7150/jca.30410 From NLM PubMed-not-MEDLINE.

(140) Roy, R.; Chun, J.; Powell, S. N. BRCA1 and BRCA2: different roles in a common pathway of genome protection. *Nat Rev Cancer* **2011**, 12 (1), 68-78. DOI: 10.1038/nrc3181 From NLM Medline.

(141) Foo, T. K.; Xia, B. BRCA1-Dependent and Independent Recruitment of PALB2-BRCA2-RAD51 in the DNA Damage Response and Cancer. *Cancer Res* **2022**, 82 (18), 3191-3197. DOI: 10.1158/0008-5472.CAN-22-1535 From NLM Medline.

(142) Petrucelli, N.; Daly, M. B.; Pal, T. BRCA1- and BRCA2-Associated Hereditary Breast and Ovarian Cancer. In *GeneReviews*((R)), Adam, M. P., Feldman, J., Mirzaa, G. M., Pagon, R. A., Wallace, S. E., Bean, L. J. H., Gripp, K. W., Amemiya, A. Eds.; 1998 [updated 2023 September 21].

(143) Rosen, M. N.; Goodwin, R. A.; Vickers, M. M. BRCA mutated pancreatic cancer: A change is coming. *World J Gastroenterol* **2021**, 27 (17), 1943-1958. DOI: 10.3748/wjg.v27.i17.1943 From NLM Medline.

(144) <https://www.cancer.gov/about-cancer/causes-prevention/genetics/brca-fact-sheet#r28>. (accessed).

(145) Pellegrini, L.; Yu, D. S.; Lo, T.; Anand, S.; Lee, M.; Blundell, T. L.; Venkitaraman, A. R. Insights into DNA recombination from the structure of a RAD51-BRCA2 complex. *Nature* **2002**, 420 (6913), 287-293. DOI: 10.1038/nature01230 From NLM Medline.

(146) Oliver, A. W.; Swift, S.; Lord, C. J.; Ashworth, A.; Pearl, L. H. Structural basis for recruitment of BRCA2 by PALB2. *EMBO Rep* **2009**, 10 (9), 990-996. DOI: 10.1038/embor.2009.126 From NLM Medline.

(147) Carreira, A.; Hilario, J.; Amitani, I.; Baskin, R. J.; Shivji, M. K.; Venkitaraman, A. R.; Kowalczykowski, S. C. The BRC repeats of BRCA2 modulate the DNA-binding selectivity of RAD51. *Cell* **2009**, 136 (6), 1032-1043. DOI: 10.1016/j.cell.2009.02.019 From NLM Medline.

(148) Yang, H.; Jeffrey, P. D.; Miller, J.; Kinnucan, E.; Sun, Y.; Thoma, N. H.; Zheng, N.; Chen, P. L.; Lee, W. H.; Pavletich, N. P. BRCA2 function in DNA binding and recombination from a BRCA2-DSS1-ssDNA structure. *Science* **2002**, 297 (5588), 1837-1848. DOI: 10.1126/science.297.5588.1837 From NLM Medline.

(149) Holloman, W. K. Unraveling the mechanism of BRCA2 in homologous recombination. *Nat Struct Mol Biol* **2011**, 18 (7), 748-754. DOI: 10.1038/nsmb.2096 From NLM Medline.

(150) Byrum, A. K.; Vindigni, A.; Mosammamaparast, N. Defining and Modulating 'BRCAness'. *Trends Cell Biol* **2019**, 29 (9), 740-751. DOI: 10.1016/j.tcb.2019.06.005 From NLM Medline.

(151) Previtali, V.; Bagnolini, G.; Ciamarone, A.; Ferrandi, G.; Rinaldi, F.; Myers, S. H.; Roberti, M.; Cavalli, A. New Horizons of Synthetic Lethality in Cancer: Current Development and Future Perspectives. *J Med Chem* **2024**, 67 (14), 11488-11521. DOI: 10.1021/acs.jmedchem.4c00113 From NLM Medline.

(152) Chu, Y. Y.; Yam, C.; Chen, M. K.; Chan, L. C.; Xiao, M.; Wei, Y. K.; Yamaguchi, H.; Lee, P. C.; Han, Y.; Nie, L.; et al. Blocking c-Met and EGFR reverses acquired resistance of PARP inhibitors in triple-negative breast cancer. *Am J Cancer Res* **2020**, 10 (2), 648-661. From NLM PubMed-not-MEDLINE.

- (153) Liu, J. F.; Brady, M. F.; Matulonis, U. A.; Miller, A.; Kohn, E. C.; Swisher, E. M.; Cella, D.; Tew, W. P.; Cloven, N. G.; Muller, C. Y.; et al. Olaparib With or Without Cediranib Versus Platinum-Based Chemotherapy in Recurrent Platinum-Sensitive Ovarian Cancer (NRG-GY004): A Randomized, Open-Label, Phase III Trial. *J Clin Oncol* **2022**, *40* (19), 2138-2147. DOI: 10.1200/JCO.21.02011 From NLM Medline.
- (154) Dellomo, A. J.; Baer, M. R.; Rassool, F. V. Partnering with PARP inhibitors in acute myeloid leukemia with FLT3-ITD. *Cancer Lett* **2019**, *454*, 171-178. DOI: 10.1016/j.canlet.2019.03.048 From NLM Medline.
- (155) Sun, C.; Fang, Y.; Yin, J.; Chen, J.; Ju, Z.; Zhang, D.; Chen, X.; Vellano, C. P.; Jeong, K. J.; Ng, P. K.; et al. Rational combination therapy with PARP and MEK inhibitors capitalizes on therapeutic liabilities in RAS mutant cancers. *Sci Transl Med* **2017**, *9* (392). DOI: 10.1126/scitranslmed.aal5148 From NLM Medline.
- (156) Juvekar, A.; Burga, L. N.; Hu, H.; Lunsford, E. P.; Ibrahim, Y. H.; Balmana, J.; Rajendran, A.; Papa, A.; Spencer, K.; Lyssiotis, C. A.; et al. Combining a PI3K inhibitor with a PARP inhibitor provides an effective therapy for BRCA1-related breast cancer. *Cancer Discov* **2012**, *2* (11), 1048-1063. DOI: 10.1158/2159-8290.CD-11-0336 From NLM Medline.
- (157) Sun, C.; Yin, J.; Fang, Y.; Chen, J.; Jeong, K. J.; Chen, X.; Vellano, C. P.; Ju, Z.; Zhao, W.; Zhang, D.; et al. BRD4 Inhibition Is Synthetic Lethal with PARP Inhibitors through the Induction of Homologous Recombination Deficiency. *Cancer Cell* **2018**, *33* (3), 401-416 e408. DOI: 10.1016/j.ccell.2018.01.019 From NLM Medline.
- (158) Nam, A. R.; Yoon, J.; Jin, M. H.; Bang, J. H.; Oh, K. S.; Seo, H. R.; Kim, J. M.; Kim, T. Y.; Oh, D. Y. ATR inhibition amplifies antitumor effects of olaparib in biliary tract cancer. *Cancer Lett* **2021**, *516*, 38-47. DOI: 10.1016/j.canlet.2021.05.029 From NLM Medline.
- (159) Pismataro, M. C.; Astolfi, A.; Barreca, M. L.; Pacetti, M.; Schenone, S.; Bandiera, T.; Carbone, A.; Massari, S. Small Molecules Targeting DNA Polymerase Theta (POLtheta) as Promising Synthetic Lethal Agents for Precision Cancer Therapy. *J Med Chem* **2023**, *66* (10), 6498-6522. DOI: 10.1021/acs.jmedchem.2c02101 From NLM Medline.
- (160) Garcia-Santisteban, I.; Peters, G. J.; Giovannetti, E.; Rodriguez, J. A. USP1 deubiquitinase: cellular functions, regulatory mechanisms and emerging potential as target in cancer therapy. *Mol Cancer* **2013**, *12*, 91. DOI: 10.1186/1476-4598-12-91 From NLM Medline.
- (161) Ray-Coquard, I.; Pautier, P.; Pignata, S.; Perol, D.; Gonzalez-Martin, A.; Berger, R.; Fujiwara, K.; Vergote, I.; Colombo, N.; Maenpaa, J.; et al. Olaparib plus Bevacizumab as First-Line Maintenance in Ovarian Cancer. *N Engl J Med* **2019**, *381* (25), 2416-2428. DOI: 10.1056/NEJMoa1911361 From NLM Medline.
- (162) Hardesty, M. M.; Krivak, T. C.; Wright, G. S.; Hamilton, E.; Fleming, E. L.; Belotte, J.; Keeton, E. K.; Wang, P.; Gupta, D.; Clements, A.; et al. OVARIO phase II trial of combination niraparib plus bevacizumab maintenance therapy in advanced ovarian cancer following first-line platinum-based chemotherapy with bevacizumab. *Gynecol Oncol* **2022**, *166* (2), 219-229. DOI: 10.1016/j.ygyno.2022.05.020 From NLM Medline.
- (163) Westin, S. N.; Labrie, M.; Litton, J. K.; Blucher, A.; Fang, Y.; Vellano, C. P.; Marszalek, J. R.; Feng, N.; Ma, X.; Creason, A.; et al. Phase Ib Dose Expansion and Translational Analyses of Olaparib in Combination with Capivasertib in Recurrent Endometrial, Triple-Negative Breast, and Ovarian Cancer. *Clin Cancer Res* **2021**, *27* (23), 6354-6365. DOI: 10.1158/1078-0432.CCR-21-1656 From NLM Medline.
- (164) Stringer-Reasor, E. M.; May, J. E.; Olariu, E.; Caterinicchia, V.; Li, Y.; Chen, D.; Della Manna, D. L.; Rocque, G. B.; Vaklavas, C.; Falkson, C. I.; et al. An open-label, pilot study of veliparib and lapatinib in patients with metastatic, triple-negative breast cancer. *Breast Cancer Res* **2021**, *23* (1), 30. DOI: 10.1186/s13058-021-01408-9 From NLM Medline.
- (165) Kurnit KC, Meric-Bernstam F, Hess K, Coleman RL, Bhosale P, Savelieva K, et al. Abstract CT020: Phase I dose escalation of olaparib (PARP inhibitor) and selumetinib (MEK Inhibitor) combination in solid tumors with Ras pathway alterations. *Cancer Res*. 2019;79:CT020.
- (166) Shah, P. D.; Wethington, S. L.; Pagan, C.; Latif, N.; Tanyi, J.; Martin, L. P.; Morgan, M.; Burger, R. A.; Haggerty, A.; Zarrin, H.; et al. Combination ATR and PARP Inhibitor (CAPRI): A phase 2 study of

ceralasertib plus olaparib in patients with recurrent, platinum-resistant epithelial ovarian cancer. *Gynecol Oncol* **2021**, *163* (2), 246-253. DOI: 10.1016/j.ygyno.2021.08.024 From NLM Medline.

(167) Yap TA, Ngoi N, Dumbrava EE, Karp DD, Ahnert JR, Fu S, et al. NCI10329: phase Ib sequential trial of agents against DNA repair (STAR) study to investigate the sequential combination of the poly (ADP-ribose) polymerase inhibitor (PARPi) olaparib (ola) and WEE1 inhibitor (WEE1i) adavosertib (ada) in patients (pts) with DNA damage response (DDR)-aberrant advanced tumors, enriched for BRCA1/2 mutated and CCNE1 amplified cancers. *Eur J Cancer*. 2022;174:S7.

(168) *Tango Therapeutics Corporate Presentation, April 2023*. <https://ir.tangotx.com/news-events/events-presentations> (accessed 2023-05-04) (accessed).

(169) Cadzow, L.; Brenneman, J.; Sullivan, P.; Liu, H.; Shenker, S.; McGuire, M.; Grasberger, P.; Sinkevicius, K.; Hafeez, N.; Histén, G.; et al. Development of KSQ-4279 as a first-in-class USP1 inhibitor for the treatment of BRCA-deficient cancers. *European Journal of Cancer* **2020**, *138*, S52. DOI: 10.1016/S0959-8049(20)31215-6 (accessed 2023/05/04).

(170) <https://www.targetedonc.com/view/phase-2-trial-of-art4215-and-talazoparib-initiated-in-brca-deficient-breast-cancer>. (accessed).

(171) Konstantinopoulos, P. A.; Waggoner, S.; Vidal, G. A.; Mita, M.; Moroney, J. W.; Holloway, R.; Van Le, L.; Sachdev, J. C.; Chapman-Davis, E.; Colon-Otero, G.; et al. Single-Arm Phases 1 and 2 Trial of Niraparib in Combination With Pembrolizumab in Patients With Recurrent Platinum-Resistant Ovarian Carcinoma. *JAMA Oncol* **2019**, *5* (8), 1141-1149. DOI: 10.1001/jamaoncol.2019.1048 From NLM PubMed-not-MEDLINE.

(172) Vinayak, S.; Tolaney, S. M.; Schwartzberg, L.; Mita, M.; McCann, G.; Tan, A. R.; Wahner-Hendrickson, A. E.; Forero, A.; Anders, C.; Wulf, G. M.; et al. Open-label Clinical Trial of Niraparib Combined With Pembrolizumab for Treatment of Advanced or Metastatic Triple-Negative Breast Cancer. *JAMA Oncol* **2019**, *5* (8), 1132-1140. DOI: 10.1001/jamaoncol.2019.1029 From NLM PubMed-not-MEDLINE.

(173) Reiss, K. A.; Mick, R.; Teitelbaum, U.; O'Hara, M.; Schneider, C.; Massa, R.; Karasic, T.; Tondon, R.; Onyiah, C.; Gosselin, M. K.; et al. Niraparib plus nivolumab or niraparib plus ipilimumab in patients with platinum-sensitive advanced pancreatic cancer: a randomised, phase 1b/2 trial. *Lancet Oncol* **2022**, *23* (8), 1009-1020. DOI: 10.1016/S1470-2045(22)00369-2 From NLM Medline.

(174) Falchi, F.; Giacomini, E.; Masini, T.; Boutard, N.; Di Ianni, L.; Manerba, M.; Farabegoli, F.; Rossini, L.; Robertson, J.; Minucci, S.; et al. Synthetic Lethality Triggered by Combining Olaparib with BRCA2-Rad51 Disruptors. *ACS Chem Biol* **2017**, *12* (10), 2491-2497. DOI: 10.1021/acscchembio.7b00707 From NLM Medline.

(175) Bagnolini, G.; Milano, D.; Manerba, M.; Schipani, F.; Ortega, J. A.; Gioia, D.; Falchi, F.; Balboni, A.; Farabegoli, F.; De Franco, F.; et al. Synthetic Lethality in Pancreatic Cancer: Discovery of a New RAD51-BRCA2 Small Molecule Disruptor That Inhibits Homologous Recombination and Synergizes with Olaparib. *J Med Chem* **2020**, *63* (5), 2588-2619. DOI: 10.1021/acs.jmedchem.9b01526 From NLM Medline.

(176) Roberti, M.; Schipani, F.; Bagnolini, G.; Milano, D.; Giacomini, E.; Falchi, F.; Balboni, A.; Manerba, M.; Farabegoli, F.; De Franco, F.; et al. Rad51/BRCA2 disruptors inhibit homologous recombination and synergize with olaparib in pancreatic cancer cells. *Eur J Med Chem* **2019**, *165*, 80-92. DOI: 10.1016/j.ejmech.2019.01.008 From NLM Medline.

(177) McCabe, N.; Turner, N. C.; Lord, C. J.; Kluzek, K.; Bialkowska, A.; Swift, S.; Giavara, S.; O'Connor, M. J.; Tutt, A. N.; Zdzienicka, M. Z.; et al. Deficiency in the repair of DNA damage by homologous recombination and sensitivity to poly(ADP-ribose) polymerase inhibition. *Cancer Res* **2006**, *66* (16), 8109-8115. DOI: 10.1158/0008-5472.CAN-06-0140 From NLM Medline.

(178) Grundy, M. K.; Buckanovich, R. J.; Bernstein, K. A. Regulation and pharmacological targeting of RAD51 in cancer. *NAR Cancer* **2020**, *2* (3), zcaa024. DOI: 10.1093/narcan/zcaa024 From NLM PubMed-not-MEDLINE.

(179) [https://ascopubs.org/doi/10.1200/JCO.2023.41.16\\_suppl.3099](https://ascopubs.org/doi/10.1200/JCO.2023.41.16_suppl.3099). (accessed).



- (180) Xu, J.; Zhao, L.; Xu, Y.; Zhao, W.; Sung, P.; Wang, H. W. Cryo-EM structures of human RAD51 recombinase filaments during catalysis of DNA-strand exchange. *Nat Struct Mol Biol* **2017**, *24* (1), 40-46. DOI: 10.1038/nsmb.3336 From NLM Medline.
- (181) Tomblin, G.; Fishel, R. Biochemical characterization of the human RAD51 protein. I. ATP hydrolysis. *J Biol Chem* **2002**, *277* (17), 14417-14425. DOI: 10.1074/jbc.M109915200 From NLM Medline.
- (182) Brouwer, I.; Moschetti, T.; Candelli, A.; Garcin, E. B.; Modesti, M.; Pellegrini, L.; Wuite, G. J.; Peterman, E. J. Two distinct conformational states define the interaction of human RAD51-ATP with single-stranded DNA. *EMBO J* **2018**, *37* (7). DOI: 10.15252/embj.201798162 From NLM Medline.
- (183) <https://www.rcsb.org/structure/7EJC>. (accessed).
- (184) <https://www.rcsb.org/structure/1n0w>. (accessed).
- (185) Zhang, X.; Ma, N.; Yao, W.; Li, S.; Ren, Z. RAD51 is a potential marker for prognosis and regulates cell proliferation in pancreatic cancer. *Cancer Cell Int* **2019**, *19*, 356. DOI: 10.1186/s12935-019-1077-6 From NLM PubMed-not-MEDLINE.
- (186) Qiao, G. B.; Wu, Y. L.; Yang, X. N.; Zhong, W. Z.; Xie, D.; Guan, X. Y.; Fischer, D.; Kolberg, H. C.; Kruger, S.; Stuerzbecher, H. W. High-level expression of Rad51 is an independent prognostic marker of survival in non-small-cell lung cancer patients. *Br J Cancer* **2005**, *93* (1), 137-143. DOI: 10.1038/sj.bjc.6602665 From NLM Medline.
- (187) Mitra, A.; Jameson, C.; Barbachano, Y.; Sanchez, L.; Kote-Jarai, Z.; Peock, S.; Sodha, N.; Bancroft, E.; Fletcher, A.; Cooper, C.; et al. Overexpression of RAD51 occurs in aggressive prostatic cancer. *Histopathology* **2009**, *55* (6), 696-704. DOI: 10.1111/j.1365-2559.2009.03448.x From NLM Medline.
- (188) Klein, H. L. The consequences of Rad51 overexpression for normal and tumor cells. *DNA Repair (Amst)* **2008**, *7* (5), 686-693. DOI: 10.1016/j.dnarep.2007.12.008 From NLM Medline.
- (189) Richardson, C.; Stark, J. M.; Ommundsen, M.; Jasin, M. Rad51 overexpression promotes alternative double-strand break repair pathways and genome instability. *Oncogene* **2004**, *23* (2), 546-553. DOI: 10.1038/sj.onc.1207098 From NLM Medline.
- (190) Kelm, J. M.; Samarbakhsh, A.; Pillai, A.; VanderVere-Carozza, P. S.; Aruri, H.; Pandey, D. S.; Pawelczak, K. S.; Turchi, J. J.; Gavande, N. S. Recent Advances in the Development of Non-PIKKs Targeting Small Molecule Inhibitors of DNA Double-Strand Break Repair. *Front Oncol* **2022**, *12*, 850883. DOI: 10.3389/fonc.2022.850883 From NLM PubMed-not-MEDLINE.
- (191) Pan, M.; Sha, Y.; Qiu, J.; Chen, Y.; Liu, L.; Luo, M.; Huang, A.; Xia, J. RAD51 Inhibition Shows Antitumor Activity in Hepatocellular Carcinoma. *Int J Mol Sci* **2023**, *24* (9). DOI: 10.3390/ijms24097905 From NLM Medline.
- (192) Axelle Renodon-Cornière, P. W., Magali Le Breton, Fabrice Fleury. New Potential Therapeutic Approaches by Targeting Rad51-Dependent Homologous Recombination. *New Research Directions in DNA Repair*, 467-, doi:10.5772/53973 (2013).
- (193) Takaku, M.; Kainuma, T.; Ishida-Takaku, T.; Ishigami, S.; Suzuki, H.; Tashiro, S.; van Soest, R. W.; Nakao, Y.; Kurumizaka, H. Halenaquinone, a chemical compound that specifically inhibits the secondary DNA binding of RAD51. *Genes Cells* **2011**, *16* (4), 427-436. DOI: 10.1111/j.1365-2443.2011.01494.x From NLM Medline.
- (194) Normand, A.; Riviere, E.; Renodon-Corniere, A. Identification and characterization of human Rad51 inhibitors by screening of an existing drug library. *Biochem Pharmacol* **2014**, *91* (3), 293-300. DOI: 10.1016/j.bcp.2014.07.033 From NLM Medline.
- (195) Huang, F.; Mazin, A. V. A small molecule inhibitor of human RAD51 potentiates breast cancer cell killing by therapeutic agents in mouse xenografts. *PLoS One* **2014**, *9* (6), e100993. DOI: 10.1371/journal.pone.0100993 From NLM Medline.
- (196) Budke, B.; Logan, H. L.; Kalin, J. H.; Zelivianskaia, A. S.; Cameron McGuire, W.; Miller, L. L.; Stark, J. M.; Kozikowski, A. P.; Bishop, D. K.; Connell, P. P. RI-1: a chemical inhibitor of RAD51 that disrupts homologous recombination in human cells. *Nucleic Acids Res* **2012**, *40* (15), 7347-7357. DOI: 10.1093/nar/gks353 From NLM Medline.

- (197) Budke, B.; Kalin, J. H.; Pawlowski, M.; Zelivianskaia, A. S.; Wu, M.; Kozikowski, A. P.; Connell, P. P. An optimized RAD51 inhibitor that disrupts homologous recombination without requiring Michael acceptor reactivity. *J Med Chem* **2013**, *56* (1), 254-263. DOI: 10.1021/jm301565b From NLM Medline.
- (198) Budke, B.; Lv, W.; Kozikowski, A. P.; Connell, P. P. Recent Developments Using Small Molecules to Target RAD51: How to Best Modulate RAD51 for Anticancer Therapy? *ChemMedChem* **2016**, *11* (22), 2468-2473. DOI: 10.1002/cmdc.201600426 From NLM Medline.
- (199) Du, L. Q.; Du, X. Q.; Bai, J. Q.; Wang, Y.; Yang, Q. S.; Wang, X. C.; Zhao, P.; Wang, H.; Liu, Q.; Fan, F. Y. Methotrexate-mediated inhibition of RAD51 expression and homologous recombination in cancer cells. *J Cancer Res Clin Oncol* **2012**, *138* (5), 811-818. DOI: 10.1007/s00432-011-1132-8 From NLM Medline.
- (200) Adimoolam, S.; Sirisawad, M.; Chen, J.; Thiemann, P.; Ford, J. M.; Buggy, J. J. HDAC inhibitor PCI-24781 decreases RAD51 expression and inhibits homologous recombination. *Proc Natl Acad Sci U S A* **2007**, *104* (49), 19482-19487. DOI: 10.1073/pnas.0707828104 From NLM Medline.
- (201) Lu, C. H.; Lin, S. C.; Yang, S. Y.; Pan, M. Y.; Lin, Y. W.; Hsu, C. Y.; Wei, Y. H.; Chang, J. S.; Chang, C. C. Prodigiosin-induced cytotoxicity involves RAD51 down-regulation through the JNK and p38 MAPK pathways in human breast carcinoma cell lines. *Toxicol Lett* **2012**, *212* (1), 83-89. DOI: 10.1016/j.toxlet.2012.05.002 From NLM Medline.
- (202) Tsang, E. S.; Munster, P. N. Targeting RAD51-Mediated Homologous Recombination as a Treatment for Advanced Solid and Hematologic Malignancies: Opportunities and Challenges Ahead. *Onco Targets Ther* **2022**, *15*, 1509-1518. DOI: 10.2147/OTT.S322297 From NLM PubMed-not-MEDLINE.
- (203) Davies, A. A.; Masson, J. Y.; McIlwraith, M. J.; Stasiak, A. Z.; Stasiak, A.; Venkitaraman, A. R.; West, S. C. Role of BRCA2 in control of the RAD51 recombination and DNA repair protein. *Mol Cell* **2001**, *7* (2), 273-282. DOI: 10.1016/s1097-2765(01)00175-7 From NLM Medline.
- (204) Carreira, A.; Kowalczykowski, S. C. Two classes of BRC repeats in BRCA2 promote RAD51 nucleoprotein filament function by distinct mechanisms. *Proc Natl Acad Sci U S A* **2011**, *108* (26), 10448-10453. DOI: 10.1073/pnas.1106971108 From NLM Medline.
- (205) Schipani, F.; Manerba, M.; Marotta, R.; Poppi, L.; Gennari, A.; Rinaldi, F.; Armirotti, A.; Farabegoli, F.; Roberti, M.; Di Stefano, G.; et al. The Mechanistic Understanding of RAD51 Defibrillation: A Critical Step in BRCA2-Mediated DNA Repair by Homologous Recombination. *Int J Mol Sci* **2022**, *23* (15). DOI: 10.3390/ijms23158338 From NLM Medline.
- (206) Rinaldi, F.; Schipani, F.; Balboni, B.; Catalano, F.; Marotta, R.; Myers, S. H.; Previtali, V.; Veronesi, M.; Scietti, L.; Cecatiello, V.; et al. Isolation and Characterization of Monomeric Human RAD51: A Novel Tool for Investigating Homologous Recombination in Cancer. *Angew Chem Int Ed Engl* **2023**, *62* (51), e202312517. DOI: 10.1002/anie.202312517 From NLM Medline.
- (207) Rajendra, E.; Venkitaraman, A. R. Two modules in the BRC repeats of BRCA2 mediate structural and functional interactions with the RAD51 recombinase. *Nucleic Acids Res* **2010**, *38* (1), 82-96. DOI: 10.1093/nar/gkp873 From NLM Medline.
- (208) Zhu, J.; Zhou, L.; Wu, G.; Konig, H.; Lin, X.; Li, G.; Qiu, X. L.; Chen, C. F.; Hu, C. M.; Goldblatt, E.; et al. A novel small molecule RAD51 inactivator overcomes imatinib-resistance in chronic myeloid leukaemia. *EMBO Mol Med* **2013**, *5* (3), 353-365. DOI: 10.1002/emmm.201201760 From NLM Medline.
- (209) Lee, W.-H.; Chen, P.-L.; Zhou, L.; and Zhu, J. . Compositions and methods related to Rad51 inactivation in the treatment of neoplastic diseases and especially CML. . USA 2009.
- (210) Scott, D. E.; Francis-Newton, N. J.; Marsh, M. E.; Coyne, A. G.; Fischer, G.; Moschetti, T.; Bayly, A. R.; Sharpe, T. D.; Haas, K. T.; Barber, L.; et al. A small-molecule inhibitor of the BRCA2-RAD51 interaction modulates RAD51 assembly and potentiates DNA damage-induced cell death. *Cell Chem Biol* **2021**, *28* (6), 835-847 e835. DOI: 10.1016/j.chembiol.2021.02.006 From NLM Medline.
- (211) Myers, S. H.; Poppi, L.; Rinaldi, F.; Veronesi, M.; Ciamarone, A.; Previtali, V.; Bagnolini, G.; Schipani, F.; Ortega Martinez, J. A.; Giroto, S.; et al. An (19)F NMR fragment-based approach for the discovery and development of BRCA2-RAD51 inhibitors to pursuit synthetic lethality in combination with PARP inhibition in pancreatic cancer. *Eur J Med Chem* **2024**, *265*, 116114. DOI: 10.1016/j.ejmech.2023.116114 From NLM Medline.

- (212) Sullivan-Reed, K.; Bolton-Gillespie, E.; Dasgupta, Y.; Langer, S.; Siciliano, M.; Nieborowska-Skorska, M.; Hanamshet, K.; Belyaeva, E. A.; Bernhardt, A. J.; Lee, J.; et al. Simultaneous Targeting of PARP1 and RAD52 Triggers Dual Synthetic Lethality in BRCA-Deficient Tumor Cells. *Cell Rep* **2018**, *23* (11), 3127-3136. DOI: 10.1016/j.celrep.2018.05.034 From NLM Medline.
- (213) Jalan, M.; Olsen, K. S.; Powell, S. N. Emerging Roles of RAD52 in Genome Maintenance. *Cancers (Basel)* **2019**, *11* (7). DOI: 10.3390/cancers11071038 From NLM PubMed-not-MEDLINE.
- (214) Lok, B. H.; Carley, A. C.; Tchang, B.; Powell, S. N. RAD52 inactivation is synthetically lethal with deficiencies in BRCA1 and PALB2 in addition to BRCA2 through RAD51-mediated homologous recombination. *Oncogene* **2013**, *32* (30), 3552-3558. DOI: 10.1038/onc.2012.391 From NLM Medline.
- (215) Rossi, M. J.; DiDomenico, S. F.; Patel, M.; Mazin, A. V. RAD52: Paradigm of Synthetic Lethality and New Developments. *Front Genet* **2021**, *12*, 780293. DOI: 10.3389/fgene.2021.780293 From NLM PubMed-not-MEDLINE.
- (216) Feng, Z.; Scott, S. P.; Bussen, W.; Sharma, G. G.; Guo, G.; Pandita, T. K.; Powell, S. N. Rad52 inactivation is synthetically lethal with BRCA2 deficiency. *Proc Natl Acad Sci U S A* **2011**, *108* (2), 686-691. DOI: 10.1073/pnas.1010959107 From NLM Medline.
- (217) Mahajan, S.; Raina, K.; Verma, S.; Rao, B. J. Human RAD52 protein regulates homologous recombination and checkpoint function in BRCA2 deficient cells. *Int J Biochem Cell Biol* **2019**, *107*, 128-139. DOI: 10.1016/j.biocel.2018.12.013 From NLM Medline.
- (218) McIlwraith, M. J.; West, S. C. DNA repair synthesis facilitates RAD52-mediated second-end capture during DSB repair. *Mol Cell* **2008**, *29* (4), 510-516. DOI: 10.1016/j.molcel.2007.11.037 From NLM Medline.
- (219) Motycka, T. A.; Bessho, T.; Post, S. M.; Sung, P.; Tomkinson, A. E. Physical and functional interaction between the XPF/ERCC1 endonuclease and hRad52. *J Biol Chem* **2004**, *279* (14), 13634-13639. DOI: 10.1074/jbc.M313779200 From NLM Medline.
- (220) Zeman, M. K.; Cimprich, K. A. Causes and consequences of replication stress. *Nat Cell Biol* **2014**, *16* (1), 2-9. DOI: 10.1038/ncb2897 From NLM Medline.
- (221) Malacaria, E.; Pugliese, G. M.; Honda, M.; Marabitti, V.; Aiello, F. A.; Spies, M.; Franchitto, A.; Pichierri, P. Rad52 prevents excessive replication fork reversal and protects from nascent strand degradation. *Nat Commun* **2019**, *10* (1), 1412. DOI: 10.1038/s41467-019-09196-9 From NLM Medline.
- (222) Kondratieck, C. M.; Washington, M. T.; Spies, M. Making Choices: DNA Replication Fork Recovery Mechanisms. *Semin Cell Dev Biol* **2021**, *113*, 27-37. DOI: 10.1016/j.semcdb.2020.10.001 From NLM Medline.
- (223) Keskin, H.; Shen, Y.; Huang, F.; Patel, M.; Yang, T.; Ashley, K.; Mazin, A. V.; Storici, F. Transcript-RNA-templated DNA recombination and repair. *Nature* **2014**, *515* (7527), 436-439. DOI: 10.1038/nature13682 From NLM Medline.
- (224) Teng, Y.; Yadav, T.; Duan, M.; Tan, J.; Xiang, Y.; Gao, B.; Xu, J.; Liang, Z.; Liu, Y.; Nakajima, S.; et al. ROS-induced R loops trigger a transcription-coupled but BRCA1/2-independent homologous recombination pathway through CSB. *Nat Commun* **2018**, *9* (1), 4115. DOI: 10.1038/s41467-018-06586-3 From NLM Medline.
- (225) Wang, J.; Oh, Y. T.; Li, Z.; Dou, J.; Tang, S.; Wang, X.; Wang, H.; Takeda, S.; Wang, Y. RAD52 Adjusts Repair of Single-Strand Breaks via Reducing DNA-Damage-Promoted XRCC1/LIG3alpha Co-localization. *Cell Rep* **2021**, *34* (2), 108625. DOI: 10.1016/j.celrep.2020.108625 From NLM Medline.
- (226) Kagawa, W.; Kurumizaka, H.; Ishitani, R.; Fukai, S.; Nureki, O.; Shibata, T.; Yokoyama, S. Crystal structure of the homologous-pairing domain from the human Rad52 recombinase in the undecameric form. *Mol Cell* **2002**, *10* (2), 359-371. DOI: 10.1016/s1097-2765(02)00587-7 From NLM Medline.
- (227) Shen, Z.; Cloud, K. G.; Chen, D. J.; Park, M. S. Specific interactions between the human RAD51 and RAD52 proteins. *J Biol Chem* **1996**, *271* (1), 148-152. DOI: 10.1074/jbc.271.1.148 From NLM Medline.
- (228) Kinoshita, C.; Takizawa, Y.; Saotome, M.; Ogino, S.; Kurumizaka, H.; Kagawa, W. The cryo-EM structure of full-length RAD52 protein contains an undecameric ring. *FEBS Open Bio* **2023**, *13* (3), 408-418. DOI: 10.1002/2211-5463.13565 From NLM Medline.

- (229) Van Dyck, E.; Hajibagheri, N. M.; Stasiak, A.; West, S. C. Visualisation of human rad52 protein and its complexes with hRad51 and DNA. *J Mol Biol* **1998**, *284* (4), 1027-1038. DOI: 10.1006/jmbi.1998.2203 From NLM Medline.
- (230) Saotome, M.; Saito, K.; Yasuda, T.; Ohtomo, H.; Sugiyama, S.; Nishimura, Y.; Kurumizaka, H.; Kagawa, W. Structural Basis of Homology-Directed DNA Repair Mediated by RAD52. *iScience* **2018**, *3*, 50-62. DOI: 10.1016/j.isci.2018.04.005 From NLM PubMed-not-MEDLINE.
- (231) Ranatunga, W.; Jackson, D.; Flowers, I. R., 2nd; Borgstahl, G. E. Human RAD52 protein has extreme thermal stability. *Biochemistry* **2001**, *40* (29), 8557-8562. DOI: 10.1021/bi0155089 From NLM Medline.
- (232) Ranatunga, W.; Jackson, D.; Lloyd, J. A.; Forget, A. L.; Knight, K. L.; Borgstahl, G. E. Human RAD52 exhibits two modes of self-association. *J Biol Chem* **2001**, *276* (19), 15876-15880. DOI: 10.1074/jbc.M011747200 From NLM Medline.
- (233) <https://www.rcsb.org/structure/8BJM>.
- (234) Cramer-Morales, K.; Nieborowska-Skorska, M.; Scheibner, K.; Padget, M.; Irvine, D. A.; Sliwinski, T.; Haas, K.; Lee, J.; Geng, H.; Roy, D.; et al. Personalized synthetic lethality induced by targeting RAD52 in leukemias identified by gene mutation and expression profile. *Blood* **2013**, *122* (7), 1293-1304. DOI: 10.1182/blood-2013-05-501072 From NLM Medline.
- (235) Chandramouly, G.; McDevitt, S.; Sullivan, K.; Kent, T.; Luz, A.; Glickman, J. F.; Andrade, M.; Skorski, T.; Pomerantz, R. T. Small-Molecule Disruption of RAD52 Rings as a Mechanism for Precision Medicine in BRCA-Deficient Cancers. *Chem Biol* **2015**, *22* (11), 1491-1504. DOI: 10.1016/j.chembiol.2015.10.003 From NLM Medline.
- (236) Olney, J. W.; Zorumski, C. F.; Stewart, G. R.; Price, M. T.; Wang, G. J.; Labruyere, J. Excitotoxicity of L-dopa and 6-OH-dopa: implications for Parkinson's and Huntington's diseases. *Exp Neurol* **1990**, *108* (3), 269-272. DOI: 10.1016/0014-4886(90)90134-e From NLM Medline.
- (237) Huang, F.; Goyal, N.; Sullivan, K.; Hanamshet, K.; Patel, M.; Mazina, O. M.; Wang, C. X.; An, W. F.; Spoonamore, J.; Metkar, S.; et al. Targeting BRCA1- and BRCA2-deficient cells with RAD52 small molecule inhibitors. *Nucleic Acids Res* **2016**, *44* (9), 4189-4199. DOI: 10.1093/nar/gkw087 From NLM Medline.
- (238) Ronchetti, R.; Moroni, G.; Carotti, A.; Gioiello, A.; Camaioni, E. Recent advances in urea- and thiourea-containing compounds: focus on innovative approaches in medicinal chemistry and organic synthesis. *RSC Med Chem* **2021**, *12* (7), 1046-1064. DOI: 10.1039/d1md00058f From NLM PubMed-not-MEDLINE.
- (239) Hengel, S. R.; Malacaria, E.; Folly da Silva Constantino, L.; Bain, F. E.; Diaz, A.; Koch, B. G.; Yu, L.; Wu, M.; Pichierri, P.; Spies, M. A.; et al. Small-molecule inhibitors identify the RAD52-ssDNA interaction as critical for recovery from replication stress and for survival of BRCA2 deficient cells. *Elife* **2016**, *5*. DOI: 10.7554/eLife.14740 From NLM Medline.
- (240) Andreu-Fernandez, V.; Almeida Toledano, L.; Pizarro, N.; Navarro-Tapia, E.; Gomez-Roig, M. D.; de la Torre, R.; Garcia-Algar, O. Bioavailability of Epigallocatechin Gallate Administered With Different Nutritional Strategies in Healthy Volunteers. *Antioxidants (Basel)* **2020**, *9* (5). DOI: 10.3390/antiox9050440 From NLM PubMed-not-MEDLINE.
- (241) Bhat, D. S.; Malacaria, E.; Biagi, L. D.; Razzaghi, M.; Honda, M.; Hobbs, K. F.; Hengel, S. R.; Pichierri, P.; Spies, M. A.; Spies, M. Therapeutic disruption of RAD52-ssDNA complexation via novel drug-like inhibitors. *NAR Cancer* **2023**, *5* (2), zcad018. DOI: 10.1093/narcan/zcad018 From NLM PubMed-not-MEDLINE.
- (242) Yang, Q.; Li, Y.; Sun, R.; Li, J. Identification of a RAD52 Inhibitor Inducing Synthetic Lethality in BRCA2-Deficient Cancer Cells. *Front Pharmacol* **2021**, *12*, 637825. DOI: 10.3389/fphar.2021.637825 From NLM PubMed-not-MEDLINE.
- (243) Al-Mugotir, M.; Lovelace, J. J.; George, J.; Bessho, M.; Pal, D.; Struble, L.; Kolar, C.; Rana, S.; Natarajan, A.; Bessho, T.; et al. Selective killing of homologous recombination-deficient cancer cell lines by inhibitors of the RPA:RAD52 protein-protein interaction. *PLoS One* **2021**, *16* (3), e0248941. DOI: 10.1371/journal.pone.0248941 From NLM Medline.

- (244) Devico Marciano, N.; Kroening, G.; Dayyani, F.; Zell, J. A.; Lee, F. C.; Cho, M.; Valerin, J. G. BRCA-Mutated Pancreatic Cancer: From Discovery to Novel Treatment Paradigms. *Cancers (Basel)* **2022**, *14* (10). DOI: 10.3390/cancers14102453 From NLM PubMed-not-MEDLINE.
- (245) Rawla, P.; Sunkara, T.; Gaduputi, V. Epidemiology of Pancreatic Cancer: Global Trends, Etiology and Risk Factors. *World J Oncol* **2019**, *10* (1), 10-27. DOI: 10.14740/wjon1166 From NLM PubMed-not-MEDLINE.
- (246) Habeshian, S.; Merz, M. L.; Sangouard, G.; Mothukuri, G. K.; Schuttel, M.; Bogнар, Z.; Diaz-Perlas, C.; Vesin, J.; Bortoli Chapalay, J.; Turcatti, G.; et al. Synthesis and direct assay of large macrocycle diversities by combinatorial late-stage modification at picomole scale. *Nat Commun* **2022**, *13* (1), 3823. DOI: 10.1038/s41467-022-31428-8 From NLM Medline.
- (247) Nielsen, A. L.; Bogнар, Z.; Mothukuri, G. K.; Zarda, A.; Schuttel, M.; Merz, M. L.; Ji, X.; Will, E. J.; Chinellato, M.; Bartling, C. R. O.; et al. Large Libraries of Structurally Diverse Macrocycles Suitable for Membrane Permeation. *Angew Chem Int Ed Engl* **2024**, *63* (26), e202400350. DOI: 10.1002/anie.202400350 From NLM Medline.
- (248) Merz, M. L.; Habeshian, S.; Li, B.; David, J. G. L.; Nielsen, A. L.; Ji, X.; Il Khwildy, K.; Duany Benitez, M. M.; Phothirath, P.; Heinis, C. De novo development of small cyclic peptides that are orally bioavailable. *Nat Chem Biol* **2024**, *20* (5), 624-633. DOI: 10.1038/s41589-023-01496-y From NLM Medline.
- (249) Perot, S.; Sperandio, O.; Miteva, M. A.; Camproux, A. C.; Villoutreix, B. O. Druggable pockets and binding site centric chemical space: a paradigm shift in drug discovery. *Drug Discov Today* **2010**, *15* (15-16), 656-667. DOI: 10.1016/j.drudis.2010.05.015 From NLM Medline.
- (250) Lloyd, J. A.; Forget, A. L.; Knight, K. L. Correlation of biochemical properties with the oligomeric state of human rad52 protein. *J Biol Chem* **2002**, *277* (48), 46172-46178. DOI: 10.1074/jbc.M207262200 From NLM Medline.
- (251) Horak, Yu. I.; Matiichuk, V. S.; Obushak, M. D.; Kutsik, R. V.; Litvin, R. Z.; Kurovets, L. M., 2-(5-Aryl-2-furyl)quinolin-4-carboxylic acids and their antimicrobial activity. *Ukrainica Bioorganica Acta* **2008**, *6*, 49- 54.
- (252) Bai, X.; Huang, L.; Qing, B.; Zuo, Z.; Feng, H. Catalyst-Free Hydrogen Proton Transfer Reduction of Nitrobenzamides to Aminobenzamides with i PrOH/KOH System. *Asian J. Org. Chem.* **2021**, *10*, 2892–2894, DOI: 10.1002/ajoc.202100511.
- (253) Doebner, O. *Ann.* **1887**, 242 & 265.
- (254) Luo Y., S. H., Zhang W., Wang X., Xu S., Zhang G., Jian Y., G. Z. Triple zirconocene/brønsted acid/CuO cooperative and relay catalysis system for tandem Mannich addition/C–C formative cyclization/oxidation. *RSC Adv.*, **2017**, *7*, 28616.
- (255) Shigeyama T., S. T., Komatsu H., Nishiyama H. Production method of quinolinecarboxamide derivative of production intermediate thereof. Japan **2022**.
- (256) Komatsu, H.; Shigeyama, T.; Sugimoto, T.; Nishiyama, H. Correction to “Three-Component Synthesis of Quinoline-4-carboxylic Acids Based on Doebner Hydrogen-Transfer Reaction”. *The Journal of Organic Chemistry* **2023**, *88* (19), 14255-14255. DOI: 10.1021/acs.joc.3c01967.
- (257) Ismail, M. A.; Brun, R.; Wenzler, T.; Tanious, F. A.; Wilson, W. D.; Boykin, D. W. Novel dicationic imidazo[1,2-a]pyridines and 5,6,7,8-tetrahydro-imidazo[1,2-a]pyridines as antiprotozoal agents. *J Med Chem* **2004**, *47* (14), 3658-3664. DOI: 10.1021/jm0400092 From NLM Medline.
- (258) McClure, M. S.; Glover, B.; McSorley, E.; Millar, A.; Osterhout, M. H.; Roschangar, F. Regioselective palladium-catalyzed arylation of 2-furaldehyde. *Org Lett* **2001**, *3* (11), 1677-1680. DOI: 10.1021/ol0158866 From NLM Medline.
- (259) Fischel, J. L.; Formento, P.; Milano, G. Epidermal growth factor receptor double targeting by a tyrosine kinase inhibitor (Iressa) and a monoclonal antibody (Cetuximab). Impact on cell growth and molecular factors. *Br J Cancer* **2005**, *92* (6), 1063-1068. DOI: 10.1038/sj.bjc.6602428 From NLM Medline.

- (260) Moynahan, M. E.; Jasin, M. Mitotic homologous recombination maintains genomic stability and suppresses tumorigenesis. *Nat Rev Mol Cell Biol* **2010**, *11* (3), 196-207. DOI: 10.1038/nrm2851 From NLM Medline.
- (261) Fenech, M.; Knasmueller, S.; Bolognesi, C.; Holland, N.; Bonassi, S.; Kirsch-Volders, M. Micronuclei as biomarkers of DNA damage, aneuploidy, inducers of chromosomal hypermutation and as sources of pro-inflammatory DNA in humans. *Mutat Res Rev Mutat Res* **2020**, *786*, 108342. DOI: 10.1016/j.mrrev.2020.108342 From NLM Medline.
- (262) Longati, P.; Jia, X.; Eimer, J.; Wagman, A.; Witt, M. R.; Rehnmark, S.; Verbeke, C.; Toftgard, R.; Lohr, M.; Heuchel, R. L. 3D pancreatic carcinoma spheroids induce a matrix-rich, chemoresistant phenotype offering a better model for drug testing. *BMC Cancer* **2013**, *13*, 95. DOI: 10.1186/1471-2407-13-95 From NLM Medline.
- (263) Kota, S.; Hou, S.; Guerrant, W.; Madoux, F.; Troutman, S.; Fernandez-Vega, V.; Alekseeva, N.; Madala, N.; Scampavia, L.; Kissil, J.; et al. A novel three-dimensional high-throughput screening approach identifies inducers of a mutant KRAS selective lethal phenotype. *Oncogene* **2018**, *37* (32), 4372-4384. DOI: 10.1038/s41388-018-0257-5 From NLM Medline.
- (264) Balboni, B. Structural and biophysical characterization of RAD52 as novel pharmacological target for synthetic lethality. Bologna, 2022. <https://amsdottorato.unibo.it/10268/>.
- (265) Masi, M.; Garattini, E.; Bolis, M.; Di Marino, D.; Maraccani, L.; Morelli, E.; Grolla, A. A.; Fagiani, F.; Corsini, E.; Travelli, C.; et al. OXER1 and RACK1-associated pathway: a promising drug target for breast cancer progression. *Oncogenesis* **2020**, *9* (12), 105. DOI: 10.1038/s41389-020-00291-x From NLM PubMed-not-MEDLINE.
- (266) Bresciani, G.; Hofland, L. J.; Dogan, F.; Giamas, G.; Gagliano, T.; Zatelli, M. C. Evaluation of Spheroid 3D Culture Methods to Study a Pancreatic Neuroendocrine Neoplasm Cell Line. *Front Endocrinol (Lausanne)* **2019**, *10*, 682. DOI: 10.3389/fendo.2019.00682 From NLM PubMed-not-MEDLINE.

## *Ringraziamenti*

Vorrei ringraziare i miei supervisors, prof. Andrea Cavalli e prof.ssa Marinella Roberti per avermi dato l'opportunità di far parte di un gruppo di ricerca esperto e collaborativo. L'esperienza del dottorato mi ha fornito le conoscenze e le capacità necessarie per affrontare i problemi, consapevole del fatto che anche il fallimento è un mezzo per far chiarezza ed andare avanti. Ringrazio tutti i collaboratori dell'Unibo e dell'IIT per essere stati sempre disponibili e per aver sopportato la mia vivace curiosità. In particolare vorrei ringraziare Greta e Laura per il sostegno nei lavori e i chiarimenti.

Ringrazio la prof.ssa Maria Laura Bolognesi, coordinatrice del dottorato che mi ha mostrato che il mondo accademico è impegnativo, ma fatto anche di momenti di confronto e divertimento, quando opportuni. Ringrazio i miei colleghi del dottorato che spero di aver rappresentato durante i miei tre anni da rappresentante e di essere stato da supporto nei momenti del bisogno anche fuori dall'università. Grazie soprattutto a Bianca per i funghi porcini e a Viviana per i taralli baresi.

Ringrazio il professor Heinis e l'amministratrice Béatrice per avermi ospitato all'interno del suo laboratorio a Losanna e per avermi fatto conoscere una realtà stupenda con ricercatori da tutto il mondo, come Ed, Thomas, Jonathan, Nathan e Alex che ringrazio per tutte le preziose nozioni che mi hanno fornito in lab e davanti a una birra.

Grazie alle mie amiche Eleonora e Federica per non avermi fatto annoiare durante le domeniche svizzere e a Nico per avermi ospitato nella sua casa.

Grazie ai colleghi del dipartimento FaBiT che sono stati sempre disponibili nonostante i vari problemi di burocrazia e tecnici.

Vorrei mostrare una profonda gratitudine ai miei amici di Bologna con cui ho passato gli anni più belli della mia vita per ora e che mi porterò sempre vicino. Avere degli amici preziosi come voi che ti possono sostenere nei momenti di stanchezza e di sconforto mi ha dato l'energia per andare avanti anche qui.

Un ringraziamento speciale va alla mia fonte di energia primaria che sa che su un foglio non riuscirei mai ad esprimere la mia riconoscenza del rispetto e dell'amore che riesce a darmi e trasmettere ogni giorno.

Grazie ai miei genitori per tutto ciò che hanno fatto per me e per avermi insegnato il rispetto, il dovere e il lono ammargelluto. Grazie a mia sorella per la sua vivacità e la sua gioia di vivere. Grazie a Greg, amico fedele anche se un po' silenzioso.

Grazie ai miei amici di Santa Maria che so che anche se lontani sono un porto sicuro nel quale posso rifugiarmi, anche con un crociato rotto.

Grazie agli amici del PmB, per avermi fatto scoprire che c'è qualcuno più matto di me e per avermi dato da mangiare e da bere una volta uscito stanco dal laboratorio.

Grazie a tutti, anche a chi mi sono scordato di menzionare che ha sicuramente contribuito al mio percorso accademico e personale.